# ENDOPLASMIC RETICULUM-PLASMA MEMBRANE JUNCTIONS: NOVEL SITES FOR PHOSPHOINOSITIDE REGULATION

A Dissertation

Presented to the Faculty of the Graduate School

of Cornell University

In Partial Fulfillment of the Requirements for the Degree of

Doctor of Philosophy

by

Andrew Manford

January 2014

# ENDOPLASMIC RETICULUM-PLASMA MEMBRANE JUNCTIONS: NOVEL SITES FOR PHOSPHOINOSITIDE REGULATION

Andrew Manford, Ph. D.

Cornell University 2014

Endoplasmic reticulum-plasma membrane (ER-PM) contact sites are specialized stable regions of the ER that are tightly apposed to the PM. These conserved organelle junctions are thought to function as rapid and direct avenues for inter-organelle communication between the ER and PM. However, a major obstacle in the study of ER-PM contacts has been the identification of the factors that form and stabilize these structures. By trying to understand how Sac1, an ER anchored phosphoinositide phosphatase, regulates the phosphoinositide lipid phosphatidylinositol-4-phosphate (PI4P) on the PM, we have gained critical insight into ER-PM contact site formation and function.

Here I present work that demonstrates Sac1 functions at ER-PM contacts to dephosphorylate PI4P on the PM. In the first part of my thesis, I uncovered a role for the yeast *o*xy*s*terol binding protein *h*omolog (Osh) family as critical regulators of PI4P metabolism. The Osh proteins are known PI4P effectors that localize to ER-organelle contact sites, including ER-PM. We found that the entire Osh family regulates PI4P metabolism *in vivo*, through Sac1, and the Osh proteins stimulate Sac1 phosphatase activity *in vitro*. We propose that the Osh proteins serve as sensors of PI4P and activators of Sac1 at ER-PM contacts. In the second part of my thesis, I identified the tricalbin proteins (orthologs of the extended synaptotagmins), Ist2 (a member of the TMEM16 family of ion channels), and the yeast VAP proteins, Scs2/22 as ER-PM tethering proteins. Strikingly, cells lacking all three families of tethering proteins display a

dramatic retraction of the ER from the PM and an accumulation of cytoplasmic ER structures. These mutants also exhibit large accumulation of PI4P on the PM, consistent with a critical role for ER-PM contacts in regulating Sac1 function. Importantly, the generation of a strain lacking ER-PM junctions allowed us the opportunity to investigate novel functions for these structures. In addition to the defect in PI4P turnover, the unfolded protein response (UPR) was constitutively activated in cells lacking ER-PM junctions. This work provides a molecular mechanism for ER-PM contact site formation and identifies PI4P metabolism and ER homeostasis as new ER-PM contact site functions.

# BIOGRAPHICAL SKETCH

Andrew Manford was born in a Sonora California and grew up northern California mountain town of Twain Harte. In 2002, Andrew graduated from Summerville Union High School and started his undergraduate education at the University of California Davis, majoring in Biochemistry and Molecular Biology. While at Davis he worked in the laboratory of Dr. Kermit Carraway and Dr. Colleen Sweeney studying the regulation of receptor tyrosine kinases. Andrew completed his undergrad in 2006, and in 2007 was accepted into the Biochemistry Molecular, and Cell biology graduate program at Cornell University. He joined Dr. Scott Emr's lab in 2008 and began his Ph.D. began his thesis work on understanding phosphoinositide lipid signaling and regulation at endoplasmic reticulum-plasma membrane junctions.

This work is dedicated to my wife Cheng

# ACKNOWLEDGMENTS

I've thoroughly enjoyed my time at Cornell and have been fortunate to work and interact with many incredibly gifted and helpful people. Without those who have offered their support, advice, and expertise none of this work would have been possible.

First I want to thank my advisor, Dr. Scott Emr. Scott has provided me the perfect balance of direction and freedom, allowing me to run with ideas and try something new, but always helped me focus in on the important questions. He has been a terrific mentor whose guidance, encouragement, and insight have been instrumental in my scientific development. Scott's constant enthusiasm and motivation for science is contagious and I hope I can retain some of that energy and drive in the next step of my career.

I'm grateful to my committee members and would like to thank Dr. Bill Brown, Dr. Tom Fox, Dr. Tony Bretscher, and though not an official committee member, Dr. Yuxin Mao for taking the time to learn about my project, offer suggestions, and importantly give me other viewpoints on my work. Some of the questions and suggestions I received at my A exam and at committee meetings directly translated to important experiments in my projects.

I want to especially thank Chris Stefan, who has been an integral part of my scientific training at the bench, in my writing, and in presenting. Chris provided a wealth of knowledge and experience not just to me, but to everyone in the lab. His insight made a lot of this work possible and I feel privileged to have worked with him.

In addition I want to acknowledge all of the people in the Emr lab for the amazing work environment. I've appreciated all of the debates, conversations, and help. Many important ideas were hashed out from conversation at the bench or at lab meetings. Their generosity with time, reagents, and knowledge makes the lab a special place to work.

I'd also like to thank my family who always encourage and help me. Their constant support is a foundation for me and I am extremely grateful for all they have done for me through out my life and especially in graduate school.

Finally I want to thank my amazing wife, Cheng, whose love, support, and humor I rely on.

TABLE OF CONTENTS

LIST OF FIGURES

LIST OF TABLES

# Chapter I

## Introduction

### Phosphoinositide signaling

Lipids not only function as structural membrane barriers for the different compartments of the cell, they are also intimately involved in many aspects of cell physiology. Of the many lipid species found in eukaryotic cells, the phospholipid phosphatidylinositol (PI) and its phosphorylated derivatives, phosphoinositides (PIPs), are of particular importance in regulating an incredibly diverse array of critical cellular processes. These include cell signaling, cytoskeleton regulation, transcription, and membrane trafficking. Phosphoinositides are generated by phosphorylation of three accessible hydroxyl groups on the inositol sugar of phosphatidylinositol by PI-Kinases (Figure 1A). Phosphoinositides are turned over though dephosphorylation by PI-phosphatases. Through the interconversion of phosphoinositide isoforms by PI-kinases and phosphatases, phosphoinositides serve as highly versatile signaling molecules with 7 possible isoforms. Eukaryotes have evolved to use the versatile phosphoinositides to control a diverse array of membrane signaling events. Notably, mammals encode a large number of PI-Kinases (19) and phosphatases (at least 28)(Sasaki et al., 2009). Phosphoinositides mediate signaling though the membrane recruitment and activation of proteins with phosphoinositide binding domains, such as the pleckstrin homolog domain (PH), phox homology domain (PX), and FYVE domain (Fab1, YOTB, Vac1, and EEA1 domain)(Figure 1A; Harlan et al., 1994; Moravcevic et al., 2012; Vicinanza et al., 2008; Yu and Lemmon, 2001). In addition, there are several examples of phosphoinositide binding proteins that do not contain

established domains, interacting with phosphoinositides through basic patches or other motifs (Di Paolo and De Camilli, 2006; Dippold et al., 2009; Moravcevic et al., 2012). The number of proteins with phosphoinositide binding domains highlights the immensity of the phosphoinositide regulated signaling networks within eukaryotic cells. For example, in yeast at least 30 proteins contain PH domains (Yu et al. 2004). While in mammalian cells there are over 250 PH domain containing proteins (Vicinanza et al., 2008) .

Phosphoinositide recruitment and activation of proteins frequently occurs in concert with an additional protein component, such as a small GTPase, a small protein motif, or ubiquitin (Di Paolo and De Camilli, 2006). The coordinated recruitment and binding of a phosphoinositide and a protein by phosphoinositide effector proteins has been termed coincidence detection and allows for multiple signaling inputs to be integrated at a specific membrane in the cell (Figure 1B). For example, $PI(4,5)P_2$ on the plasma membrane (PM) along with ubiquitinated PM cargo proteins or sorting signals on the cargo proteins themselves serve as coincidence detection for clathrin adaptors that initiate clathrin mediate endocytosis (Ford et al., 2001; Gaidarov and Keen, 1999; Honing et al., 2005; Itoh et al., 2001; Traub, 2003). Phosphoinositides can also signal as soluble secondary messengers and one of the earliest examples of phosphoinositide signaling studied was the soluble messenger inositol-(1,4,5)-triphosphate ($InsP_3$). $InsP_3$, generated by the triggered hydrolysis of $PI(4,5)P_2$ by PLC, binds to the $InsP_3$ receptor in the endoplasmic reticulum (ER) to trigger release calcium ($Ca^{2+}$) stores (Berridge and Irvine, 1984; Clapham, 2007). Subsequently, additional soluble inositol phosphates are emerging as important signaling molecules in many systems (Tsui and York, 2010).

While phosphoinositides are involved in numerous cellular signaling processes, one of the most important and extensively studied roles for phosphoinositides is in the regulation of

Figure 1

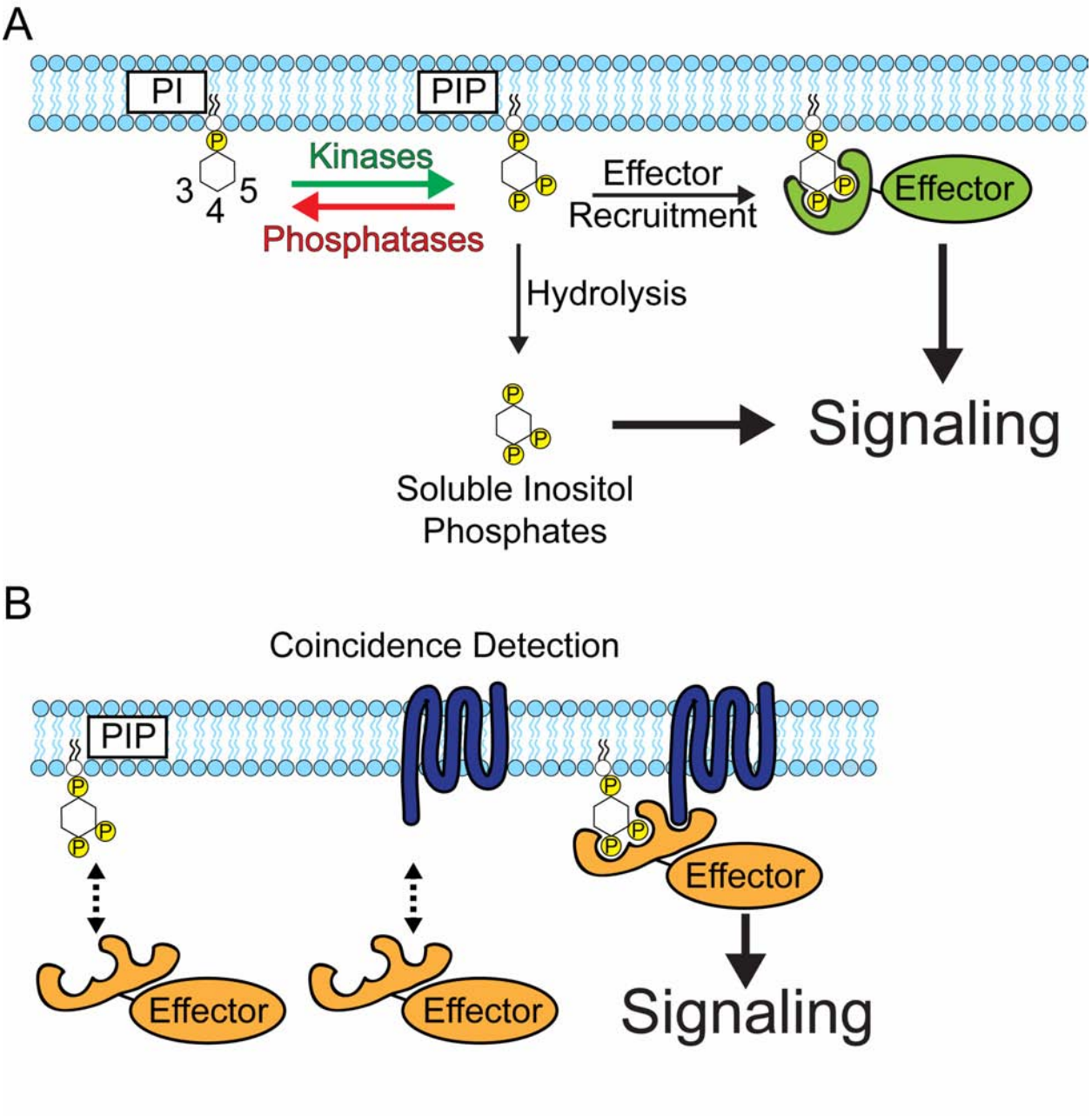
A
PI
PIP
3
4
5
Kinases
Phosphatases
Effector
Recruitment
Effector
Hydrolysis
Signaling
Soluble Inositol
Phosphates
B
Coincidence Detection
PIP
Effector
Effector
Effector
Signaling

**Figure 1.1. Phosphoinositide signaling**

(A) Phosphoinositide cycle. Phosphatidylinositol can be phosphorylated at the D3, D4, and D5 position of the inositol sugar to generate phosphatidylinositol phosphates (PIP). Phosphoinositides can be dephosphorylated by phosphatases that interconvert different phosphoinositide isoforms or shut down signaling. Phosphoinositides mediate signaling by recruiting and activating effector proteins with phosphoinositide binding domain to the membrane, or through hydrolysis by lipases to generated soluble inositol phosphates and diacylglycerol (not shown).

(B) Phosphoinositide signaling often requires an additional protein component on the membrane for effector recruitment. This type of dual targeting is called coincidence detection and adds an important layer of regulation to phosphoinositide signaling. Coincidence detection ensures the effector recruitment takes place at the right time and location. The protein or the phosphoinositide alone is not sufficient for recruitment of the effector, but when both are present, effector proteins are recruited and the effector is activated.

membrane trafficking between organelles. In addition to the example of endocytosis highlighted above, phosphoinositides are important for recruiting the machinery for nearly every trafficking step though the secretory and endocytic pathways (Vicinanza et al., 2008). Specific phosphoinositides are compartmentalized on organelles: PI4P and $PI(4,5)P_2$ on the PM, PI4P at the Golgi, PI3P at endosomes, and $PI(3,5)P_2$ on vacuoles/lysosomes (Di Paolo and De Camilli, 2006). The compartmentalization of specific phosphoinositide species along with a similar partitioning of small GTPases plays an important role in determining organelle identity, as well as coordinating trafficking reactions between organelles (Audhya et al., 2000; Desrivieres et al., 1998; Di Paolo and De Camilli, 2006; Hammond et al., 2012; Homma, 1998; Santiago-Tirado and Bretscher, 2011; Varnai et al., 2006; Vicinanza et al., 2008; Zoncu et al., 2007). This compartmentalization of phosphoinositides is tightly regulated to ensure that both phosphoinositides are generated and signaling takes place at the proper location and time. If phosphoinositides are misregulated, membrane trafficking events are either not initiated, when phosphoinositide generation is blocked, or potentially impaired when phosphoinositides are not turned over. Continuing with endocytosis as an example, $PI(4,5)P_2$ is required for the initiation and maturation of clathrin coated endocytic events, and when not present, greatly disrupts endocytosis (Desrivieres et al., 1998; Homma, 1998; Varnai et al., 2006; Zoncu et al., 2007). Importantly, $PI(4,5)P_2$ must also be hydrolyzed by PI-phosphatases during the completion of clathrin-mediated endocytosis to recycle the endocytic machinery that binds $PI(4,5)P_2$ and allow for the maturation of the endocytic vesicle to a PI3P rich endosome (Clague et al., 2009; Zoncu et al., 2009). Without this turnover of $PI(4,5)P_2$, the vesicle cannot progress to the endosome and the endocytic machinery remains trapped on the vesicle, unable to participate in new rounds of endocytosis (Cremona et al., 1999; Kim et al., 2002; Stefan et al., 2005; 2002). Not surprisingly,

defects in phosphoinositide regulation, through mutations in PI-kinases and phosphatases, can lead to several diseases. These include cancer, through inappropriate accumulation of $PI(3,4,5)P_3$, which drives proliferation signaling pathways, and several severe neurological diseases (Liu and Bankaitis, 2010). Therefore, studying the regulation and function of phosphoinositides is important to understanding and potentially intervening in human diseases.

**PI4P regulates essential Golgi and plasma membrane processes**

Of the many phosphoinositide isoforms, PI4P is unique in being found at relatively high abundance, relative to other phosphoinositide isoforms, at two distinct organelles in the cell. PI4P is a crucial regulator of essential and conserved processes at both the PM and Golgi (Figure 2A). The Golgi pool of PI4P regulates trafficking from the Golgi and is important for the Golgi targeting of cytoplasmic proteins (D'Angelo et al., 2008; Santiago-Tirado and Bretscher, 2011). In yeast the type III PI4-kinase, Pik1, generates the Golgi pool of PI4P. Pik1 is essential and temperature sensitive alleles of Pik1 lead to trafficking defects of both vacuole and secretory cargo (Audhya et al., 2000; Hama et al., 1999; Walch-Solimena and Novick, 1999). The Golgi PI4P effectors that cause this lethal block in secretory trafficking in *pik1* mutants are not completely clear, but it is at least in part due to the targeting of Myo2, a type 5 myosin that transports secretory vesicles to sites of growth (Santiago-Tirado et al., 2011). However Myo2 is not the only essential Golgi PI4P effector since *pik1* mutant phenotypes are distinct from *myo2* mutants; *pik1* mutants generate Berkeley bodies, which are seen in several secretory mutants, while *myo2* alleles accumulate secretory vesicles (Govindan et al., 1995; Johnston et al., 1991; Novick et al., 1980; Walch-Solimena and Novick, 1999). Similar to yeast, in mammalian cells PI4P is a critical regulator of trafficking from the Golgi. Knock down or kinase dead mutants of

mammalian Golgi PI-4 Kinases result in trafficking defects and disrupted Golgi morphology, indicating a conserved role for PI4P in Golgi function (Balla et al., 2005; Bruns et al., 2002; Wang et al., 2003). Many Golgi targeted proteins also require PI4P for targeting in mammalian cells, including AP-1**,** GGAs, FAPPs, OSBP, and GOLPH3 (Balla et al., 2005; Dippold et al., 2009; Levine and Munro, 2002; Wang et al., 2007; 2003).

In yeast, the type III PI-4kinase, Stt4, localizes to the PM and generates a PM pool of PI4P (Audhya et al., 2000; Audhya and Emr, 2002; Baird et al., 2008). This PM pool of PI4P regulates vacuole morphology, the actin cytoskeleton, cell wall integrity, and is a precursor for $PI(4,5)P_2$, which is critical regulator of many PM processes (Figure 2A; Audhya et al., 2000; Audhya and Emr, 2002; Clague et al., 2009; Desrivieres et al., 1998; Homma, 1998; Suh et al., 2006; Varnai et al., 2006; Zoncu et al., 2007). Despite some specific phenotypes of PI-4kinase mutants, the PM pool PI4P was thought to serve only as a precursor for $PI(4,5)P_2$ synthesis. However, recent work in mammalian cells using targeted PI-phosphatases demonstrated that many PM process thought to be regulated solely by $PI(4,5)P_2$ can also be regulated by PI4P as well (Hammond et al., 2012). Knockout of the mammalian homolog of the Stt4, PI 4-kinase III alpha, in mice is lethal (Nakatsu et al., 2012). Embryonic fibroblasts from a conditional knockout mouse of PI 4-kinase III alpha display a substantial decrease of cellular PI4P levels and a loss of PI4P reporter specifically from the PM. In addition these conditional knock out cells had disruption of many PM PI4P and $PI(4,5)P_2$ dependent cellular processes, including recruitment of STIM1 for store operated calcium entry and altered clathrin endocytic structure morphology and dynamics. Surprisingly only a small reduction of total $PI(4,5)P_2$ levels was observed in the knockout cells, but the distribution of $PI(4,5)P_2$ was greatly altered from the normal PM localization to aberrant internal structures within the cytoplasm. Taken together, this work has

demonstrated that PI4P generated at both at the Golgi and the PM control several conserved and essential membrane trafficking and signaling pathways within eukaryotic cells.

**PI4P regulation by the ER localized PI-Phosphatase Sac1**

PI4P levels within cells is tightly regulated by dephosphorylation mediated by the Sac1 domain containing phosphatases: Sac1, and the synaptojanin homologs Sjl2/Inp52, and Sjl3/Inp53 (Foti et al., 2001; Guo et al., 1999). Yeast mutants of *sac1* alone cause a large increase in cellular PI4P levels, while *sjl2* and *sjl3* single or double mutants have no change in PI4P. However *sjl3*/*sac1* double mutants display a greater increase in PI4P over *sac1* mutants alone and are inviable, indicating that although Sac1 is the primary phosphatase in PI4P turnover (Figure 2A), Sjl3 can compensate for loss of Sac1 (Foti et al., 2001).

Sac1, Suppressor of ACtin 1, was initially discovered as a bypass suppressor of certain actin alleles (Novick et al., 1989). Shortly after, *sac1* mutants were also found to be a suppressor of the yeast secretory mutant and phosphoinositide lipid transfer protein, Sec14 (Cleves et al., 1989). Sec14 was subsequently determined to be required for PI4P production at the Golgi (Hama et al., 1999). How Sac1 impacts both the actin cytoskeleton and secretion remained unclear until it was uncovered that the Sac1 domain was a polyphosphoinositide phosphatase capable of dephosphorylating PI4P, PI3P, and $PI(3,5)P_2$ and possessed a conserved $CX_5R$ motif found in several phosphoinositide phosphatases (Guo et al., 1999). As phosphoinositides regulate both membrane trafficking at the Golgi and the cytoskeleton, a role for Sac1 in these distinct processes is possible.

Although Sac1 is genetically linked to PI4P turnover at the Golgi, labeling experiments in PI4-kinase/*sac1* double mutants indicated that the major substrate of Sac1 is generated by the

Figure 2

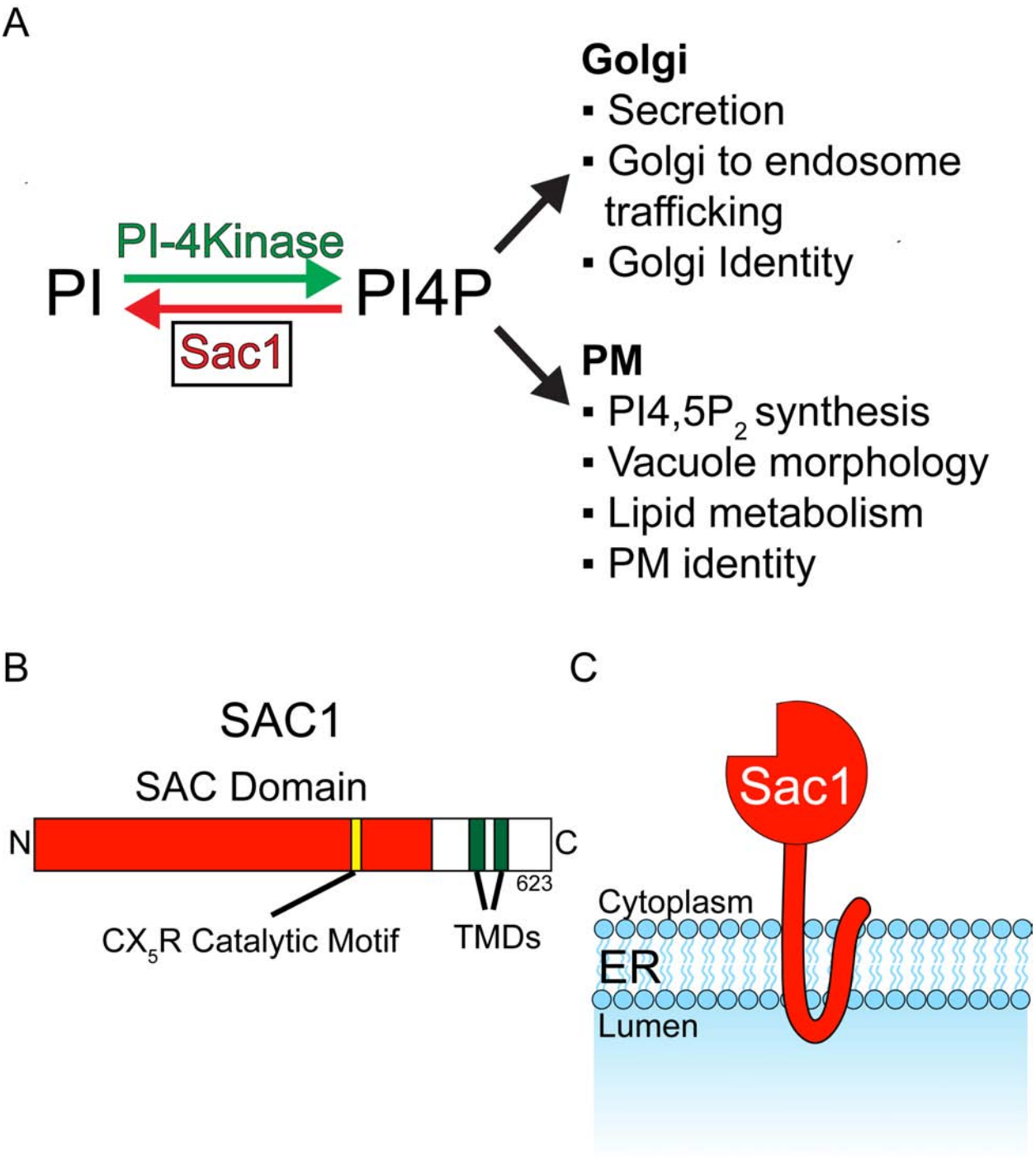
A
Golgi
▪ Secretion
▪ Golgi to endosome trafficking
▪ Golgi Identity
PI-4Kinase
PI
PI4P
Sac1
PM
▪ PI4,5P2 synthesis
▪ Vacuole morphology
▪ Lipid metabolism
▪ PM identity
B
SAC1
SAC Domain
N
C
623
CX5R Catalytic Motif
TMDs
C
Sac1
Cytoplasm
ER
Lumen

**Figure 1.2. PI4P regulation**

(A) PI4P is generated by multiple PI-4Kinases, but primarily is regulated by the phosphatase Sac1. PI4P serves as essential regulators at both the Golgi and PM. Examples of the processes controlled by PI4P in yeast on each organelle are listed.

(B) Yeast Sac1 domain organization. Sac1 is a 623 amino acid protein. TMDs = transmembrane domain.

(C) Cartoon schematic of Sac1 in the ER membrane. Topology of domains relative to the cytoplasm and lumen of the ER are indicated.

PM localized PI4-Kinase Stt4, and not the Golgi PI4-kinase Pik1 (Audhya and Emr, 2002; Foti et al., 2001). In addition, deletion of *sac1* can rescue the inviability of *stt4* mutants, but not *pik1* (Foti et al., 2001). Consistent with this, the PI4P reporter, $2xPH^{Osh2}$, shifts it localization from primarily Golgi with weak PM signal that is enriched in the bud, to strong uniform localization at the PM in *sac1* mutants (Roy and Levine, 2004). These results suggest that the major location of Sac1 PI4P turnover is the PM pool of PI4P, with a minor influence on Golgi pool of PI4P.

Sac1 is an integral membrane protein with its N-terminal Sac1 phosphatase domain exposed to the cytoplasm and two transmembrane domains at the C-terminus (Figure 2B and 2C; Konrad et al., 2002; Whitters et al., 1993). Yeast Sac1 chiefly localizes to the endoplasmic reticulum with a small pool that traffics between the ER and the Golgi (Foti et al., 2001; Whitters et al., 1993). Sac1 requires ER localization and membrane anchorage for function as a truncation of Sac1 that removes the C-terminal transmembrane domains was not functional unless greatly overexpressed (Foti et al., 2001). Golgi trafficking of Sac1 is regulated by the nutrient condition in yeast, where in rich growth conditions Sac1 is retained in the ER by an interaction with Dpm1, a glycosylation enzyme in the ER. Upon starvation Sac1 traffics to and remains at the Golgi (Faulhammer et al., 2005). This regulated shuttling of Sac1 from the ER to the Golgi has been proposed to deplete PI4P at the Golgi, resulting in decreased Golgi trafficking in starvation conditions. However, the PI-Kinase at the Golgi, Pik1, also delocalizes from the Golgi in these conditions (Faulhammer et al., 2007). It has not yet been demonstrated that this nutrient triggered attenuation of PI4P signaling at the Golgi is important for yeast survival during starvation.

In yeast, *sac1* mutants display many phenotypes, highlighting the importance of maintaining proper PI4P levels and spatial distribution. Examples of *sac1* mutant phenotypes include: inositol auxotrophy, constitutive unfolded protein signaling, disrupted protein

glycosylation, changes to vacuole morphology, and over 800 unique synthetic genetic relationships (Costanzo et al., 2010; Faulhammer et al., 2005; Foti et al., 2001; Jonikas et al., 2009; Whitters et al., 1993). Though the mechanism of how Sac1 or increased PI4P levels are linked to *sac1* mutant phenotypes is not known, it is likely that the overproduction of PI4P leads to improper targeting and activation of proteins to PI4P rich membranes. Interestingly, there is strong evidence that Sac1 has a potential direct role in sphingolipid regulation. Sac1 interacts with and is a stoichiometric member of the *s*erine *p*alymitoyltransferase, *O*rm1/2, *T*sc3, and *S*ac1 (SPOTS) complex, which regulates sphingolipid synthesis and includes the enzyme that catalyzes the first step in the sphingolipid biosynthetic pathway in the ER (Breslow et al., 2010). Sac1 is not required for SPOTS complex formation and its role in the SPOTS complex is unclear; however *sac1* mutants do have altered sphingolipid levels (Breslow et al., 2010; Brice et al., 2009). All of the phenotypes that we are aware of require Sac1 catalytic activity, however it is possible that some phenotypes may not be linked to PI4P turnover and may require Sac1 in additional roles.

Although Sac1 has been primarily studied in yeast, Sac1 is conserved in higher eukaryotes. Throughout evolution Sac1 retains the same domain architecture, a cytoplasmic N-terminal Sac1 domain linked to two transmembrane domains in the C-terminus, and like in yeast, primarily localizes to the ER with a pool that traffics to the Golgi (Nemoto et al., 2000; Rohde et al., 2003). Although *sac1* mutants in yeast are viable, mutants in higher eukaryotes display more severe phenotypes. Sac1 mutants in *Drosophila* exhibit accumulation of cellular PI4P levels, critical development defects, and embryonic lethality (Wei et al., 2003; Yavari et al., 2010). These developmental detriments are caused by the improper activation of key and conserved developmental signaling processes, including JNK MAPK signaling, and Hedgehog signaling

(Wei et al., 2003; Yavari et al., 2010). Sac1 has critical roles in mammals as Sac1 knockout mice are preimplantation lethal and siRNA knock down of Sac1 in cell culture results in loss of cell viability (Liu et al., 2008). siRNA knock down of Sac1 in mammalian cells also has pleiotropic effects including altered PI4P distribution, mitotic spindle defects, and Golgi fragmentation (Liu et al., 2008; Rohde et al., 2003). These studies highlight the important role of Sac1 in maintain proper PI4P levels to ensure normal developmental signaling and also demonstrate a key role for PI4P signaling in development in higher eukaryotes.

**How does the ER localized phosphatase, Sac1, regulate PI4P on the PM?**

Due to Sac1's ER localization and its primary substrate, PI4P, residing on the PM, the mechanism of how Sac1 hydrolyzes PI4P on the PM has remained a paradox. There are three major hypotheses or models to explain this conundrum. First Sac1 traffics through the secretory pathway to the PM where Sac1 would easily have access to PI4P *in cis* (Figure 3). Second, PI4P is transferred from the PM to the ER for hydrolysis by Sac1. Lastly, Sac1 reaches from the ER to the PI4P on the PM *in trans* at regions where the ER and PM are close together. Additional hypotheses, or a combination of the three above cannot be ruled out. There have been several studies that have either directly or indirectly tested these models and they are discussed below.

Sac1 trafficking to the PM may be simplest solution for how Sac1 reaches its substrate. Indeed Sac1 is found to traffic to the Golgi during certain starvation conditions in both yeast and metazoans (Blagoveshchenskaya et al., 2008; Faulhammer et al., 2005) However several lines of evidence discount this model. Critically, Sac1 has not been observed on the PM and its localization has been demonstrated by fluorescence microscopy to be primarily in the ER in both yeast (Faulhammer et al., 2005; Foti et al., 2001) and mammalian cells (Nemoto et al., 2000). In

addition, Sac1 has been shown to co-sediment with ER markers by sucrose gradient sedimentation (Faulhammer et al., 2005). Yeast Sac1 also doesn't accumulate on the PM in a strong endocytosis mutant (Tahirovic et al., 2004), ruling out small pools of Sac1 trafficking through the secretory system past the Golgi. Furthermore, mammalian Sac1 has a putative COP1 recognition signal and was found to bind COP1 coat components, providing a mechanism for retrieval of Sac1 from the Golgi back to the ER (Rohde et al., 2003). This study also found that Sac1 lacking this retrieval signal accumulates in the Golgi and does not progress to the PM. Finally, yeast strains expressing Sac1 fused to an ER retention signal have lower PI4P levels than wild type Sac1 cells, indicating normal PI4P metabolism does not require Sac1 to leave the ER (Konrad et al., 2002). Taken together, these results strongly favor a mechanism for Sac1 mediated PI4P turnover in which Sac1 resides in the ER.

The second model for the mechanism of Sac1 turnover is the transport of PI4P from the PM to the ER. There are two possible routes for the transport of PM PI4P to the ER: retrograde vesicular trafficking or non-vesicular lipid transport. Retrograde transport of PI4P from the PM to the ER is an unlikely mechanism of PI4P turnover due to the tight spatial regulation of phosphoinositides along the trafficking steps from the PM back to the ER. PI4P that is endocytosed would likely be turned over by the synaptojanin phosphatases that are recruited to endocytic sites to turn over PI(4,5)$P_2$ and PI4P through their 5-phosphatase and Sac1 domains (Stefan et al., 2002). The non-vesicular transport of PI4P from the PM to the ER is an intriguing alternative possibility. A growing amount of research has uncovered several families of lipid transfer proteins that are thought to transfer lipids between organelles (Lev, 2010; Toulmay and Prinz, 2011). One of the best studied examples is the phosphatidylinositol/phosphatidylcholine transfer protein Sec14, which is thought to be essential for the lipid composition of the Golgi and

by transferring PI to the Golgi for PI4P synthesis (Mousley et al., 2012). However recent work has argued that Sec14 function is not merely to transfer PI to the Golgi, but to present PI to Pik1 for efficient phosphorylation for the generation of PI4P (Mousley et al., 2012; Schaaf et al., 2008). In addition, while several proteins have been shown to transfer lipids between membranes *in vitro*, it is still contended whether some of these proteins do so *in vivo* (Georgiev et al., 2011). Nonetheless, for both the vesicular and non-vesicular transport, PI4P would be predicted to greatly accumulate on the ER in the absence of Sac1 due to PI4P's continual transfer to the ER without turnover. However as mentioned above, *sac1* mutants accumulate the PI4P reporter, $2xPH^{OSH2}$, on the plasma membrane and not in the ER (Roy and Levine, 2004; Stefan et al., 2011). Although some PI4P binding domains with a bias for the Golgi pool of PI4P (PH domains of FAPP1, Osh1, and OSBP all bind the small Golgi GTPase Arf1 in addition to PI4P) do show some weak ER localization in *sac1* mutants, they are still primarily Golgi localized (Godi et al., 2004; Levine and Munro, 2002; Roy and Levine, 2004). This small increase in PI4P detected at the ER is likely due to the PI4P generated at the Golgi trafficking back to the ER during normal retrograde transport, and not from the PM.

The third model for Sac1 hydrolysis of PM PI4P proposes that Sac1 regulate PM PI4P *in trans* from regions of the ER that are in close proximity to the PM. Based on the published research discussed above this is the favored model for Sac1 PI4P regulation. Sites where the ER is associated with the PM are termed ER-PM contact sites and will be the focus of the rest of the introduction.

Figure 3

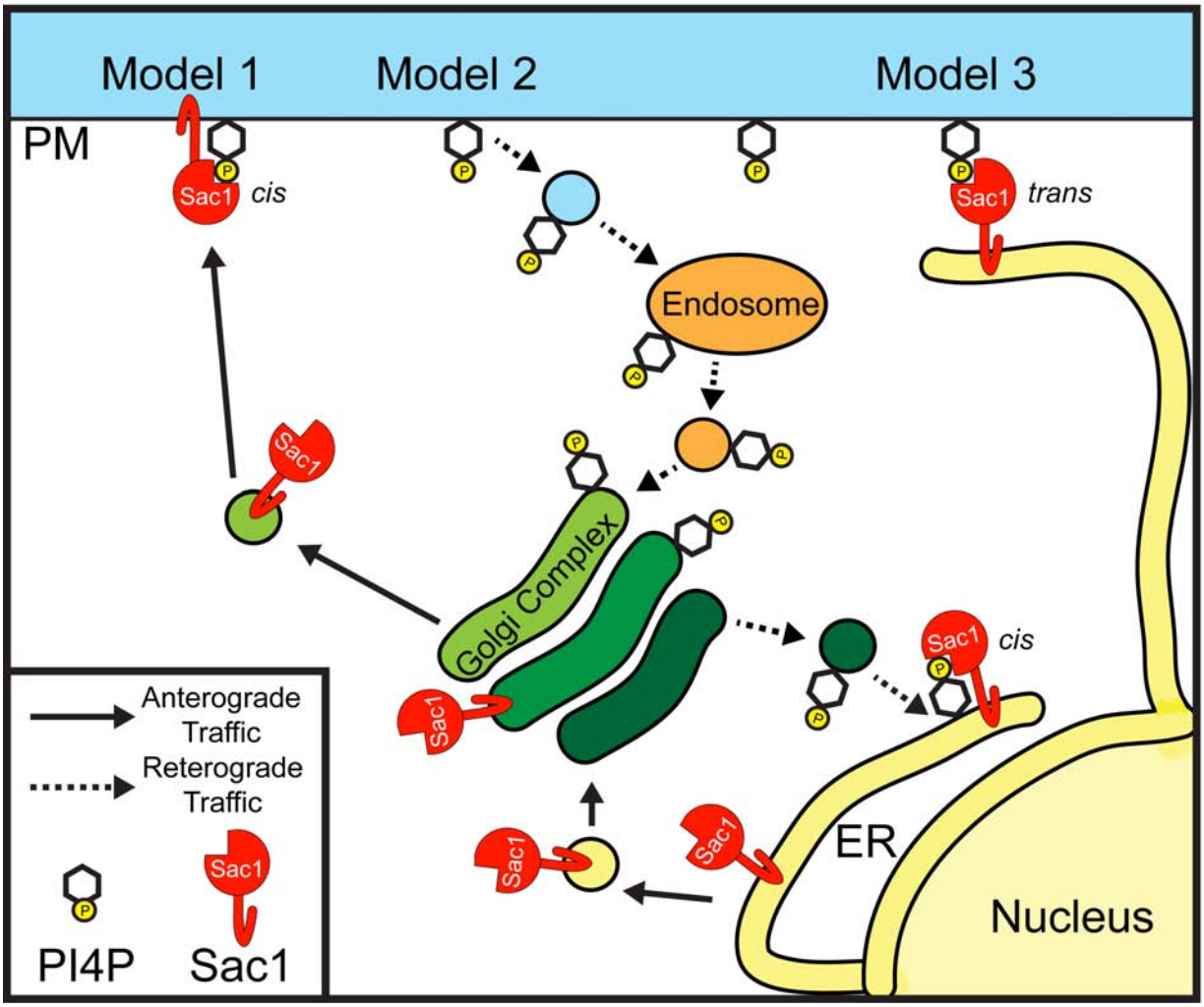


**Figure 1.3. Three potential models for ER localized Sac1 regulation of PM PI4P.**

Model 1. Sac1 traffics to the PM to turn over PI4P *in cis*.

Model 2. PI4P traffics back to the ER from the PM either through retrograde vesicular trafficking or through non-vesicular transport (Not shown).

Model 3. Sac1 regulated PI4P *in trans* at sites where the ER and PM are close together.

**ER-PM membrane contact sites**

Organelle contact sites, also known as membrane contact sites or organelle junctions, are ubiquitous structures in eukaryotes that are frequently seen in electron microscopy studies on various organisms and tissues (Elbaz and Schuldiner, 2011; Toulmay and Prinz, 2011). Organelle contacts sites have been defined as regions where two organelles come in very close proximity (10-30nm) and appear to be physically interacting, but do not fuse. Although overlap between organelles by fluorescence microscopy is relatively common, membrane contacts are generally characterized and quantitated by electron microscopy, due to the small dimensions that define these contacts. Despite being first described many decades ago (Copeland and Dalton, 1959; Porter and Palade, 1957), there is still a lot that is not known about organelle contacts. With some exceptions, the factors that mediate many of these contacts are undiscovered. In addition, the functions for several organelle contacts are poorly characterized or unknown. However, organelle contacts are intriguing structures as potential platforms for direct communication between organelles. Inter-organelle communication at organelle contacts would allow a more direct and rapid route for the transfer of signals and coordination between organelles than membrane trafficking. Indeed most of the known and proposed functions for these sites involve signaling and metabolite transport processes (Toulmay and Prinz, 2011).

The ER is the most frequent organelle that participates in organelle contacts and has been observed to form junctions with virtually all organelles in the cell, including the PM, mitochondria, and every compartment along the endocytic and secretory pathway (Friedman and Voeltz, 2011). The morphology of the ER in mammalian cells could explain this promiscuous association with many organelles, as the ER in most cells types consists of a continual network that emanates from the nucleus to every region of the cell (Friedman and Voeltz, 2011; Shibata

et al., 2006). However even in yeast, where the ER network is predominately sequestered to the cortex of the cell, contacts are still frequently seen with all organelles (West et al., 2011). One of the most striking examples of this has been observed between the ER and the mitochondria. By serial electron microscopy tomography studies with yeast, ER tubules emanating from the normal peripheral network appear to reach out and grasp tubules of the mitochondria in a process that is likely important for mitochondrial fission (Friedman et al., 2011). These observations, along with several others, indicate that organelle contacts are indeed directed and regulated structures, and are not formed as a result of spontaneous contact between organelles.

Of the ER-organelle contacts identified, ER-PM contacts are perhaps the most intriguing because they link the major biosynthetic organelle in the cell, the ER, with one of the primary destinations of the biosynthetic products, the PM. This potentially allows for a tight coordination of ER processes with the PM and vice versa. In addition the PM is the major signaling platform in the cell and direct cooperation between the ER and PM in response to extracellular signaling is an exciting possibility. Junctions between the ER and the PM were first described by electron microscopy of muscle cells during the 1950s (Porter and Palade, 1957). In the subsequent decades, ER-PM contacts have been observed by electron microscopy in various cell types and organisms. Like the diversity of ER morphologies that are seen in different organisms and cell types, ER-PM contacts very greatly in abundance and magnitude. The budding yeast *Saccharomyces cerevisiae* has served as an excellent model system for studying ER morphology, ER-organelle contacts, and in particular ER-PM contacts. In yeast the ER makes extensive contact with the PM; a large percentage of the non-nuclear ER is tethered to the PM at an average distance of 30nm, ranging from 10-50nm (Pichler et al., 2001; West et al., 2011). This ER associated with the PM has been termed cortical ER (cER) and forms a network of sheets and

tubules similar to the ER morphology of mammalian cells, except instead of spanning the cytoplasm, the network is adhered to the PM (Figure 4A). This network of both ER tubules and sheets can be easily seen by fluorescence microscopy by focusing on a focal plane at the periphery of yeast cells (Figure 4B; Prinz et al., 2000). This cortical ER network is tethered to about 40% of the PM surface, representing a significant domain on the plasma membrane of yeast cells (Pichler et al., 2001; West et al., 2011). The side of the cER facing the PM is completely devoid of ribosomes, indicating either a close enough connection that ribosomes are excluded or the enrichment of proteins between these organelles that preclude ribosome binding. The absence of ribosomes is a common feature of ER-organelle contacts and these ER regions likely have specialized functions distinct from protein synthesis and translocation (Figure 4C).

In most cultured mammalian cells, ER-PM contacts have not been extensively studied beyond their role in calcium signaling, which will be discussed below. This is primarily due to the very small percentage of the PM that is occupied by the ER. In Hela cells, less than .5% of PM has associated ER (Orci et al., 2009; Wu et al., 2006) and unlike yeast, the ER is evenly distributed throughout the entire cell, with only small contacts with the PM (Figure 4D). However close association between the ER and PM in cultured cells can be observed by total internal fluorescence microscopy despite the very small percentage of the PM in contact with the ER under normal conditions (Wu, 2006). However, in certain cell types ER-PM contacts are more prevalent. In muscle cells, where ER-PM associations were first observed, there are extensive ER-PM connections that are important for calcium release during muscle contraction (Porter and Palade, 1957). In addition, neuronal cells have more substantial ER-PM contacts, some greater than 5μm, in the cell body and several smaller sized contacts have been observed in the synapse (Hayashi et al., 2008; Rosenbluth, 1962). In plants the ER forms a cortical network

Figure 4

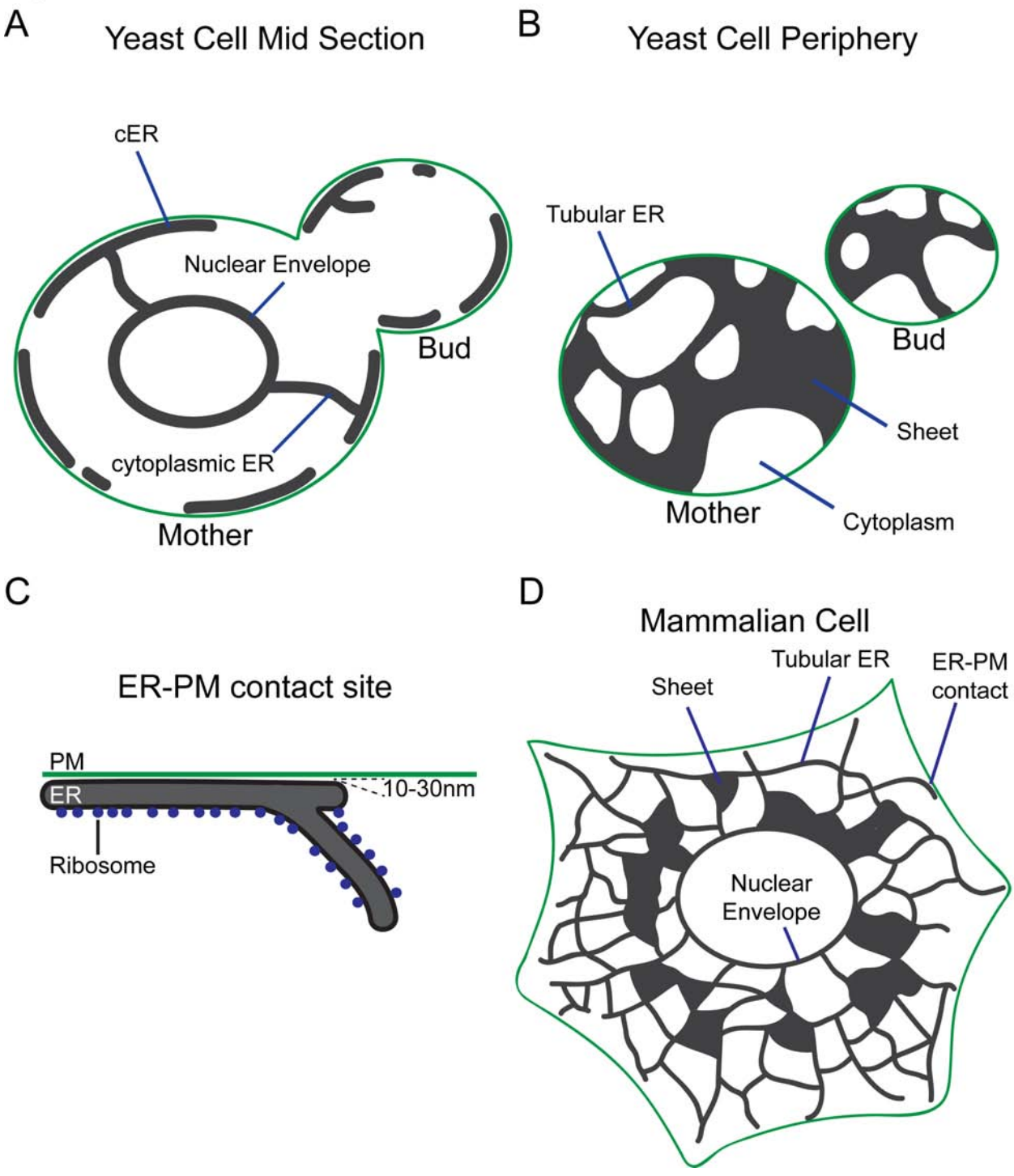
A
Yeast Cell Mid Section
cER
Nuclear Envelope
Bud
cytoplasmic ER
Mother
B
Yeast Cell Periphery
Tubular ER
Bud
Sheet
Mother
Cytoplasm
C
ER-PM contact site
PM
ER
10-30nm
Ribosome
D
Mammalian Cell
Sheet
Tubular ER
ER-PM contact
Nuclear Envelope

**Figure 1.4. ER morphology and ER-PM contacts**.

(A) Cartoon of the ER network in a midsection view of a yeast cell. The majority of the non-nuclear ER is associated with the PM.

(B) Cartoon of the ER network at the yeast periphery, the network sheets and tubules adhered to the PM is similar to the mammalian ER, but the network is only seen from this peripheral viewpoint.

(C) Diagram of an ER-PM contact site the spacing between the organelles range from 10-30nm and ribosomes (Blue dots) are excluded from this surface.

(D) Cartoon representation of the ER in a mammalian cell. Green represents the PM and black, the ER. ER forms of network of sheets and tubules through out the cell. Very little of the total ER is in contact with the PM, but stable structures are present.

tightly apposed to the PM, similar to the ER morphology seen in yeast (Staehelin, 1997). The cER network in plant cells is very tightly associated with the PM and can still be observed attached to the PM when cells are lysed and the cytoplasm is washed away (Hepler et al., 1990). In addition to the general association of the cER with the PM in plants, the ER is a component of more specialized PM structures. These include cER juxtaposed to large PM invaginations, that may play a role in membrane trafficking, and the plasmodesmata, a specialized ER, PM, and cell wall structure that connects two adjacent cells (Maule et al., 2011; Staehelin, 1997). Plasmodesmata are especially interesting ER-PM contacts as they are the major routes of intercellular communication and transport in plants and important hubs for several signaling pathways.

**Functions for ER-PM contacts**

Although ER-PM contacts are ubiquitous and conserved structures, they have mostly been appreciated for their roles in $Ca^{2+}$ signaling in muscle cells and lipid transport in the fly photoreceptor cells. However in recent years, a renewed interest in ER-PM contacts has uncovered additional functions for ER-PM contacts. Interestingly, for several of the functions that will be described in the following sections, ER-PM contacts have provided an important mechanistic insight for previously unclear observations. In addition, as research of ER-PM contacts has expanded, an intimate link between PM phosphoinositide signaling and ER-PM contacts has been uncovered and will be highlighted in the following sections on ER-PM contacts.

**Calcium signaling**

The best-characterized function of ER-PM contacts is $Ca^{2+}$ signaling in higher eukaryotes. In muscle cells there are abundant specialized ER-PM junctions critical for mobilizing calcium to induce muscle contractions. These muscle specific ER-PM structures are formed by the sarcoplasmic reticulum (muscle ER) engaging closely with the transverse tubules or T-tubule, a specialized invagination of the sarcolemma (muscle PM) (Rossi and Dirksen, 2006). These contacts form two types of junctions: a diad or triad. If a T-tubule is in contact with only one sarcoplasmic reticulum terminal cisterna, the structure is termed a diad (found in cardiac muscles) and if two on each side of the tubule, a triad (abundant in skeletal muscle) (Bootman, 2006; Carrasco and Meyer, 2011). At triad and diad junctions, the voltage gated $Ca^{2+}$ channel is enriched on the PM and the Ryanodine receptors (Ryr), a $Ca^{2+}$ channel, is enriched on the closely apposed sarcoplasmic reticulum. During depolarization of skeletal muscle cells, the voltage gated calcium channels (VGCC) on the PM open, causing an influx of extracellular $Ca^{2+}$ and triggering the closely apposed Ryr to open and release the store of calcium from the sarcoplasmic reticulum (Endo, 2009). This large increase in cytoplasmic $Ca^{2+}$ levels induces muscle contraction. Although the VGCC and Ryr receptors are major components of muscle ER-PM junctions, in cells lacking Ryr receptor, triads structures still persist (Franzini-Armstrong et al., 1991; Ikemoto et al., 1997). One family of proteins implicated in tethering these membranes together are the junctophilins, proteins that were found to be enriched in muscle cells and localize to triad and diad junctions (Takeshima et al., 2000). Exogenous expression of Junctophilin induces ER-PM contacts in non-muscle cells and loss of a junctophilin-2 results in a decrease in tight contacts at heart muscle diads in the mouse cardiomyocytes, suggesting a role for maintaining these ER-PM contacts in heart muscle (Takeshima et al., 2000). Junctophilin is anchored in the ER by a single transmembrane domain and contains several tandem cytoplasmic

MORN (membrane occupation and recognition nexus) motifs. MORN motifs have been shown to bind phosphoinositides (Ma et al., 2006) and full length junctophilin 2 can bind acidic phospholipids including phosphatidylserine and the phosphoinositide $PI(3,4,5)P_3$ (Bennett et al., 2013). Thus the junctophilins likely mediate sarcoplasmic reticulum tethering to the PM by binding to PM phosphoinositides.

Beyond the highly dedicated function in muscles, ER-PM contacts are also a central component in calcium signaling and transport in other cell types. Upon activation of phospholipase C (PLC) isoforms by several signaling pathways, PLC hydrolyzes the phosphoinositide $PI(4,5)P_2$ to generate two important signaling molecules (Kadamur and Ross, 2013). The lipid product of hydrolysis is diacylglycerol, which has important signaling functions at the PM. The released head group is inositol-(1,4,5)-trisphosphate $InsP_3$, a soluble inositol secondary messenger that binds to the $InsP_3$ receptor (a calcium channel in the ER) causing the release of the $Ca^{2+}$ stores in the ER and triggering calcium regulated signaling (Clapham, 2007). When the ER stores of $Ca^{2+}$ are depleted, the influx of extracellular $Ca^{2+}$ from the PM through calcium release activated channels (CRAC) is induced to refill $Ca^{2+}$ stores in the ER and to maintain a high cytoplasmic $Ca^{2+}$ concentrations for continued signaling (Carrasco and Meyer, 2011). The mechanism of this ER store regulated entry of extracellular $Ca^{2+}$ has been termed store operated calcium entry (SOCE) and had remained a mystery until the identification of stromal interacting molecule 1 and 2 (STIM). The STIM proteins were discovered to be ER integral membrane proteins that are the ER components required for SOCE and shortly after, ORAI1 was identified as the PM CRAC channel (Feske et al., 2006; Liou et al., 2005; Roos et al., 2005; Vig et al., 2006; Zhang et al., 2006; 2005). Subsequent work has revealed an elegant mechanism of how STIM and ORAI1 mediate SOCE at ER-PM contacts. STIM proteins contain

a luminal EF-hand and SAM calcium-binding motif that serves as the calcium sensor for the luminal concentration of $Ca^{2+}$, a single transmembrane domain, a CRAC activation domain (CAD), and a polybasic domain that can bind $PI(4,5)P_2$. Upon store depletion and the loss of $Ca^{2+}$ binding, the EF-hand motif triggers a conformational change that induces oligomerization of STIM proteins resulting in translocation to existing ER-PM junctions (Figure 5A; Liou et al., 2005; 2007; Wu et al., 2006). This recruitment to ER-PM contacts depends on the polybasic domain interacting with $PI(4,5)P_2$ on the PM (Korzeniowski et al., 2009; Liou et al., 2007). Once at these sites the STIM protein binds to, oligomerizes, and activates ORAI by direct interaction of the CRAC activation domain of the STIMs to ORAI (Park et al., 2009; Yuan et al., 2009). Interestingly, phosphoinositides play important roles in both the initial signaling response to generate $IP_3$ and in the later step for recruitment of the STIM proteins to ER-PM contacts sites for ORAI activation.

**Lipid transfer**

In addition to $Ca^{2+}$ signaling, lipid transfer has been a major focus of research for organelle contacts. The ER is the major site of synthesis for the three types of lipids found in eukaryotic cells: sphingolipids, phospholipids, and sterols. Although vesicular trafficking is the most obvious route to move lipids from the ER to other organelles, non-vesicular lipid transfer is required for several organelles. For example, non-vesicular transport must occur from the ER to the mitochondria, since there is no vesicular trafficking between these organelles (Voelker, 2003). In addition to the mitochondria, there is evidence that non-vesicular lipid transfer occurs between many other organelles and the ER, including between the ER and PM (Kaplan and Simoni, 1985; Vance et al., 1991). Due to the observed association of the ER with many

organelles, non-vesicular transport has been suggested to take place at organelle contact sites. Transfer of lipids between organelles is likely to be energetically unfavorable, even if the two membranes are in close proximity. Thus, protein factors are needed to mediate lipid transfer. Consistent with this, several families of lipid transfer proteins have been identified that can bind and transfer a wide variety of lipid substrates, including all three lipid classes (Holthuis and Levine, 2005).

One of the first and best-characterized lipid transfer protein that functions at ER-PM contacts is the *Drosophila* phosphatidylinositol transfer protein, retinal degeneration B (rdgB). As the name implies, rdgB mutants have retinal degeneration phenotypes caused by the loss of microvilli in the photoreceptor cells. rdgB was found by sequence homology to be related to the phosphatidylinositol transfer protein Sec14 and facilitated the transfer phosphatidylinositol *in vitro* (Bankaitis et al., 1989; Hotta and Benzer, 1970; Rubinstein et al., 1989; Vihtelic et al., 1993). rdgB is highly enriched at specialized ER-PM contacts near the microvilli of photoreceptors and its likely function is to transfer phosphatidylinositol from the ER to the PM at these contacts (Suzuki and Hirosawa, 1994; Vihtelic et al., 1993). This is an important process for *Drosophila* photoreceptor cells since a large amount of PI is lost by the hydrolysis of $PI(4,5)P_2$ to DAG and $InsP_3$ by PLC during light induced signaling (Hardie, 2001). Replenishment of PI on the PM from its site of synthesis in the ER by rdgB is needed to regenerate $PI(4,5)P_2$ for additional rounds of signaling. This process highlights another important function for ER-PM contact sites, as well as provides another link between PM phosphoinositides and the function of ER-PM contact sites. In addition, this particular example punctuates why an organelle contact site is a more direct and rapid route of transfer than

vesicular trafficking, which would require transport progression through the secretory pathway to reach the PM.

In addition to rdgB, the yeast *o*xy*s*terol-binding *h*omology (OSH) family of lipid transfer proteins is thought to function at ER-PM contacts. The Osh proteins are a seven-member family that all contain a conserved *o*xysterol binding protein *r*elated *d*omain (ORD). The domain architecture of the Osh proteins divides the family into short Osh proteins (Osh4, Osh5, Osh6, and Osh7) that consist of only an ORD domain, and the long Osh proteins, that in addition to the ORD domain contain an extended N-terminal region with protein and lipid interaction domains (Osh1, Osh2, Osh3). These long Osh proteins all contain a Pleckstrin homology (PH) domain and an FFAT ER-targeting motif (diphenylalanine in an acidic tract, consensus EFFDAxE) that is recognized by the ER *v*esicle associated membrane protein (VAMP) *a*ssociated *p*rotein (VAP) (Scs2 and Scs22 in yeast) (Loewen et al., 2003). The PH domain of the long Osh proteins can bind to phosphoinositides, including PI4P (Yu et al., 2004). A tandem PH domain of Osh2 is used as a PI4P reporter in yeast and the PH domain of Osh1 is used as a Golgi specific PI4P reporter since this PH domain also interacts with the small Golgi GTPase Arf1 (Levine and Munro, 2002; Roy and Levine, 2004). Four of the Osh proteins (Osh2, Osh3, Osh6, and Osh7) are enriched at ER-PM contacts, while Osh1 localizes to the Golgi and another ER-organelle contact, the nuclear vacuole junction (Levine and Munro, 2001; Schulz et al., 2009). Interestingly, nearly all (9/12) of the mammalian oxysterol-binding protein (OSBP)–related proteins (ORPs) contain the extended N-terminus with an ER targeting FFAT motif and a PH domain. Many of the mammalian ORP proteins localize to various ER-organelle contacts (reviewed in (Olkkonen and Li, 2013; Yan and Olkkonen, 2008)). Interestingly, other lipid protein families contain a similar domain architecture. The ceramide transfer protein (CERT)

also shares the same architecture of a PH domain and an FFAT motif in its long N-terminus that precedes the lipid transfer domain and Nir2, the mammalian ortholog of rdgB, contains an FFAT motif (Hanada et al., 2003; Kawano et al, 2006). Moreover, both Nir2 and CERT require these targeting motifs to localize to ER-Golgi contacts for efficient lipid transfer (Kawano, 2006; Perreti et al., 2008). This shared architecture of lipid transfer proteins likely serves as a coincidence detection mechanism for ER-organelle contacts, where the FFAT motif localizes the protein to the ER, and the PH domain specifies the other organelle by binding to a specific phosphoinositide (Figure 5B).

The yeast Osh family share a common redundant function, as deletion of all seven genes is inviable, with only one is required to maintain viability (Beh et al., 2001). The function for the Osh proteins has been assumed to involve sterol binding and transport as they are related to the mammalian oxysterol binding protein. In strong support of this, the Osh4 protein crystal structure has been solved bound to a variety of sterol molecules in a conserved pocket of the ORD that all of the Osh proteins contain (Im et al., 2005). However, when assayed *in vitro* only the ORD domain of Osh2, Osh4, and Osh5 can extract and transfer sterols *in vitro*, while the other Osh proteins had weak or no sterol transfer activity (Schulz et al., 2009). Despite both the *in vitro* and structural data, the *in vivo* function for these proteins is unclear and the shared essential function has yet to be identified. Specifically testing for sterol transport *in vivo*, *osh* mutants display PM to ER transport defects (Raychaudhuri et al., 2006), but when tested by different approaches, *osh* mutants are near wild type in non vesicular sterol transport either to or from the ER (Georgiev et al., 2011). In addition, the Osh proteins have been linked to many other phenotypes, including the regulation of cell polarity (Kozminski et al., 2006) and Osh4 in Golgi PI4P regulation (Fairn et al., 2007).

Figure 5

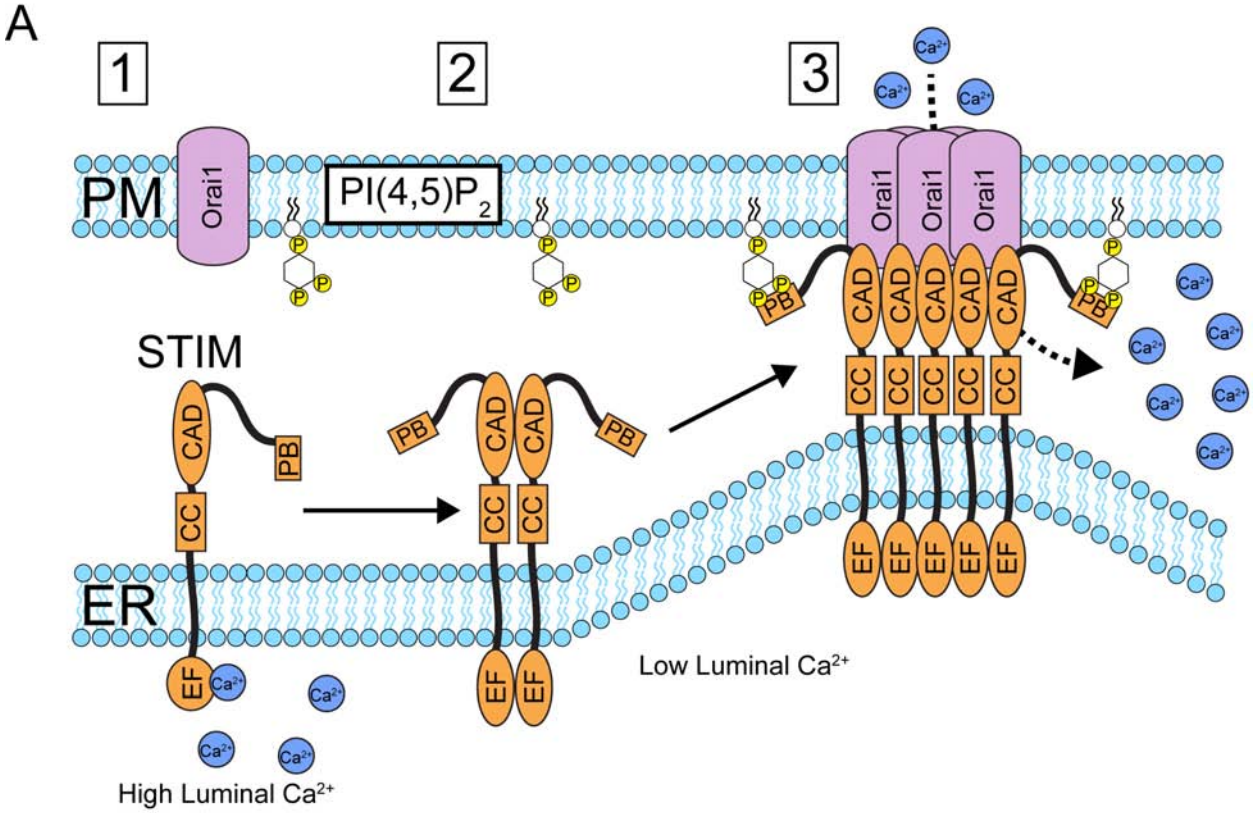
A
1
2
3
PM
Orai1
PI(4,5)P2
STIM
CAD
PB
CC
EF
ER
Ca2+
High Luminal Ca2+
Low Luminal Ca2+

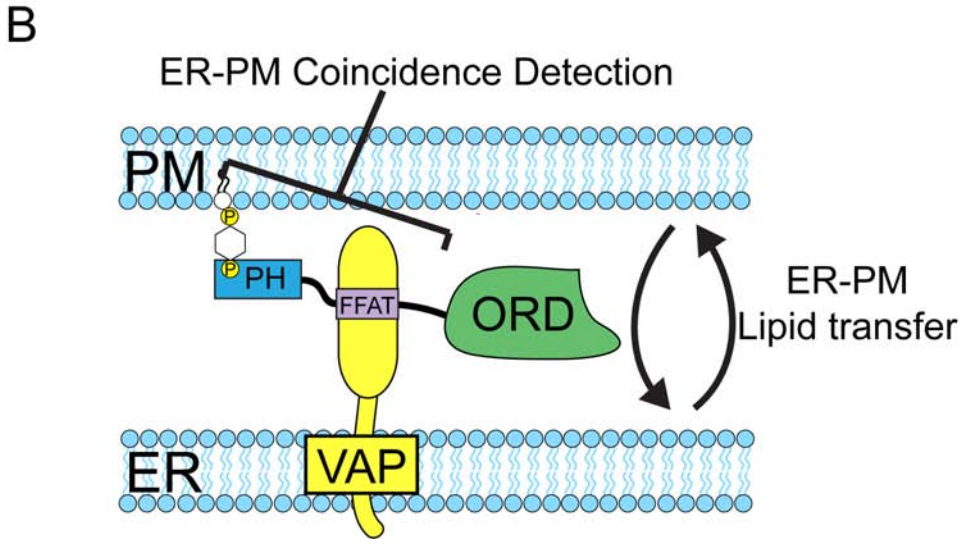
B
ER-PM Coincidence Detection
PM
PH
FFAT
ORD
ER-PM
Lipid transfer
ER
VAP

**Figure 1.5. Functions for ER-PM contacts**

(A) Store operated Calcium entry. CC=coiled coil, CAD CRAC activation domain, PB=Poly Basic domain, EF-hand calcium binding domain.

When ER lumen $Ca^{2+}$ levels are high the EF-hand of STIM1 binds calcium and is monomeric (1). Upon release of $Ca^{2+}$ stores in the ER, the EF hand confirmation changes resulting in oligomerization of the STIM proteins (2). STIM oligomerization increases its affinity for PM $PI4,5P_2$, resulting in translocation of STIM to existing ER-PM contacts. At ER-PM contacts the STIM proteins cluster and activate the Orai1 channels, inducing Calcium influx for sustained signaling and reloading of ER stores (3).

(B) The long Osh proteins in yeast and the mammalian Orp family contain a protein architecture that serves as a coincidence detector for ER-PM (or other ER-organelle contacts). The PH domain specifies binding to phosphoinositides on the target organelle and the FFAT motif binds the ER protein VAP proteins (Scs2/22 in yeast). The ORD domain is proposed to transfer sterols between organelles. Similar architectures are found in other lipid transfer protein families (see text).

In mammalian cells, the functions ascribed to the ORP proteins are even more varied and include sterol transport between the ER and various organelles, membrane trafficking, microtubule motor regulation, and cell signaling (Jansen et al., 2010; Lev, 2010; Peretti et al., 2008; Rocha et al., 2009; Wang et al., 2005). Although diverse in function, and unclear in their shared essential function in yeast, nearly all the ORP protein family localize to, and likely function at various ER-organelle contacts, including ER-PM.

**PM signaling regulation**

Another proposed function for ER-PM contacts is the regulation of receptor tyrosine kinase signaling. Ptp1b is a tyrosine phosphatase that dephosphorylates many signaling proteins that reside on the PM (Tonks, 2003). However Ptp1b, in a situation similar to Sac1, is an ER resident protein that regulates substrates on a different organelle. Ptp1b doesn't contain a transmembrane domain, but associates with the ER via its hydrophobic C-terminus (Anderie et al., 2007a; Frangioni et al., 1992; Woodford-Thomas et al., 1992). Ptp1b dephosphorylation of proteins has been proposed to take place at ER-PM structures, and interactions between Ptp1b and its substrates have been observed at the cell periphery (Anderie et al., 2007b). These *trans* interactions have been detected with PKCδ, insulin receptor, epidermal growth factor receptor, and EphA3 receptor (Anderie et al., 2007b; Nievergall et al., 2010). Alternatively, it has also been suggested that ER-endosome contacts are a platform for Ptp1b dephosphorylation for receptors that have been endocytosed (Eden et al., 2010; Haj et al., 2002). It is possible that Ptp1b can function at both ER-PM and ER-endosome contacts, but in the case for insulin receptor signaling, Ptp1b has been shown not to require endocytosis (Shi et al., 2004). In addition, ER associated Ptp1b is enriched at specialized ER-PM structures at cell-matrix

adhesions and cell-cell contacts, indicating that at least for some substrates, ER-PM contacts are the likely site for Ptp1b regulation (Haj et al., 2012; Hernández et al., 2006). Thus, the ER-resident Ptp1b likely acts *in trans* from the ER to dephosphorylate signaling proteins on the PM.

**PI4P regulation by Sac1 and ER-PM contacts**

Sac1 functioning at ER-PM contacts is an attractive mechanism for PM PI4P turnover. Are ER-PM junctions required for Sac1 function and if so, is Sac1 regulated at these sites? In addition to these specific questions related to Sac1, little is known on how ER-PM contacts are formed and maintained. Not knowing the identity of the factors that hold or tether the ER and PM together has proved a major hurdle in the study of ER-PM contacts. In addition, as these structures are conserved, and in some systems incredibly extensive, there are likely additional important functions for ER-PM contact that have not yet been discovered.

In the following chapters, my work (in addition to the exceptional work of my colleagues and collaborators) on understanding the mechanism of Sac1 function has led to many important insights into PI4P regulation and ER-PM contacts. We have found that Sac1 contains a long flexible linker that can span the distance of membrane contact sites found at ER-PM junctions, suggesting that an *in trans* mechanism for Sac1 function is possible. In addition, we discovered that PI4P regulation in yeast requires a family of lipid transfer proteins, the yeast oxysterol binding protein homologs. Osh proteins, as mentioned above, localize to ER-PM contacts sites, and *osh* mutants display *sac1* mutant phenotypes, including large accumulations of PI4P. In addition, Osh proteins can stimulate Sac1 activity *in vitro*. Finally, we uncover the mechanism for ER-PM tethering in yeast and importantly demonstrate that Sac1 requires these contacts for function. This work has provided others with the foundation to study these contacts in other

systems and has identified exciting additional functions for these structures that were not previously known. Some of this recent work from the field will be highlighted in the conclusion and future directions chapter.

**References**


Anderie, I., Schulz, I., and Schmid, A. (2007a). Characterization of the C-terminal ER membrane anchor of PTP1B. Experimental Cell Research *313*, 3189–3197.

Anderie, I., Schulz, I., and Schmid, A. (2007b). Direct interaction between ER membrane-bound PTP1B and its plasma membrane-anchored targets. Cellular Signalling *19*, 582–592.

Audhya, A., Foti, M., and Emr, S.D. (2000). Distinct roles for the yeast phosphatidylinositol 4-kinases, Stt4p and Pik1p, in secretion, cell growth, and organelle membrane dynamics. Molecular Biology of the Cell *11*, 2673–2689.

Audhya, A., and Emr, S.D. (2002). Stt4 PI 4-kinase localizes to the plasma membrane and functions in the Pkc1-mediated MAP kinase cascade. Developmental Cell *2*, 593–605.

Baird, D., Stefan, C., Audhya, A., Weys, S., and Emr, S.D. (2008). Assembly of the PI 4-kinase Stt4 complex at the plasma membrane requires Ypp1 and Efr3. The Journal of Cell Biology *183*, 1061–1074.

Balla, A., Tuymetova, G., Tsiomenko, A., Varnai, P., and Balla, T. (2005). A plasma membrane pool of phosphatidylinositol 4-phosphate is generated by phosphatidylinositol 4-kinase type-III alpha: studies with the PH domains of the oxysterol binding protein and FAPP1. Molecular Biology of the Cell *16*, 1282–1295.

Bankaitis, V.A., Malehorn, D.E., Emr, S.D., and Greene, R. (1989). The Saccharomyces cerevisiae SEC14 gene encodes a cytosolic factor that is required for transport of secretory proteins from the yeast Golgi complex. The Journal of Cell Biology *108*, 1271–1281.

Beh, C.T., Cool, L., Phillips, J., and Rine, J. (2001). Overlapping functions of the yeast oxysterol-binding protein homologues. Genetics *157*, 1117–1140.

Bennett, H.J., Davenport, J.B., Collins, R.F., Trafford, A.W., Pinali, C., and Kitmitto, A. (2013). Human junctophilin-2 undergoes a structural rearrangement upon binding PI(3,4,5)$P_3$ and the S101R mutation identified in hypertrophic cardiomyopathy obviates this response. Biochem. J. *456*, 205–217.

Berridge, M.J., and Irvine, R.F. (1984). Inositol trisphosphate, a novel second messenger in cellular signal transduction. Nature *312*, 315–321.

Blagoveshchenskaya, A., Cheong, F.Y., Rohde, H.M., Glover, G., Knodler, A., Nicolson, T.,

Boehmelt, G., and Mayinger, P. (2008). Integration of Golgi trafficking and growth factor signaling by the lipid phosphatase SAC1. The Journal of Cell Biology *180*, 803–812.

Bootman, M.D. (2006). Calcium signalling during excitation-contraction coupling in mammalian atrial myocytes. Journal of Cell Science *119*, 3915–3925.

Breslow, D.K., Collins, S.R., Bodenmiller, B., Aebersold, R., Simons, K., Shevchenko, A., Ejsing, C.S., and Weissman, J.S. (2010). Orm family proteins mediate sphingolipid homeostasis. Nature *463*, 1048–1053.

Brice, S.E., Alford, C.W., and Cowart, L.A. (2009). Modulation of Sphingolipid Metabolism by the Phosphatidylinositol-4-phosphate Phosphatase Sac1p through Regulation of Phosphatidylinositol in Saccharomyces cerevisiae. Journal of Biological Chemistry *284*, 7588–7596.

Bruns, J.R., Ellis, M.A., Jeromin, A., and Weisz, O.A. (2002). Multiple roles for phosphatidylinositol 4-kinase in biosynthetic transport in polarized Madin-Darby canine kidney cells. J. Biol. Chem. *277*, 2012–2018.

Carrasco, S., and Meyer, T. (2011). STIM Proteins and the Endoplasmic Reticulum-Plasma Membrane Junctions. Annu. Rev. Biochem. *80*, 973–1000.

Clague, M.J., Urbé, S., and de Lartigue, J. (2009). Phosphoinositides and the endocytic pathway. Experimental Cell Research *315*, 1627–1631.

Clapham, D.E. (2007). Calcium Signaling. Cell *131*, 1047–1058.

Cleves, A.E., Novick, P.J., and Bankaitis, V.A. (1989). Mutations in the SAC1 gene suppress defects in yeast Golgi and yeast actin function. The Journal of Cell Biology *109*, 2939–2950.

Copeland, Dalton (1959). An association between mitochondria and the endoplasmic reticulum in cells of the pseudobranch gland of a teleost. J Biophys Biochem Cytol *5*, 393–396.

Costanzo, M., Baryshnikova, A., Bellay, J., Kim, Y., Spear, E.D., Sevier, C.S., Ding, H., Koh, J.L.Y., Toufighi, K., Mostafavi, S., et al. (2010). The Genetic Landscape of a Cell. Science *327*, 425–431.

Cremona, O., Di Paolo, G., Wenk, M.R., Lüthi, A., Kim, W.T., Takei, K., Daniell, L., Nemoto, Y., Shears, S.B., Flavell, R.A., et al. (1999). Essential role of phosphoinositide metabolism in synaptic vesicle recycling. Cell *99*, 179–188.

D'Angelo, G., Vicinanza, M., Di Campli, A., and De Matteis, M.A. (2008). The multiple roles of PI(4)P - not just the precursor of PI(4,5)P2. Journal of Cell Science *121*, 1955–1963.

Desrivieres, S., Cooke, F.T., Parker, P.J., and Hall, M.N. (1998). MSS4, a phosphatidylinositol-4-phosphate 5-kinase required for organization of the actin cytoskeleton in Saccharomyces cerevisiae. J. Biol. Chem. *273*, 15787–15793.

Di Paolo, G., and De Camilli, P. (2006). Phosphoinositides in cell regulation and membrane dynamics. Nature *443*, 651–657.

Dippold, H.C., Ng, M.M., Farber-Katz, S.E., Lee, S.-K., Kerr, M.L., Peterman, M.C., Sim, R., Wiharto, P.A., Galbraith, K.A., Madhavarapu, S., et al. (2009). GOLPH3 Bridges Phosphatidylinositol-4- Phosphate and Actomyosin to Stretch and Shape the Golgi to Promote Budding. Cell *139*, 337–351.

Eden, E.R., White, I.J., Tsapara, A., and Futter, C.E. (2010). Membrane contacts between endosomes and ER provide sites for PTP1B-epidermal growth factor receptor interaction. Nat. Cell Biol. *12*, 267–272.

Elbaz, Y., and Schuldiner, M. (2011). Staying in touch: the molecular era of organelle contact sites. Trends in Biochemical Sciences *36*, 616–623.

Endo, M. (2009). Calcium-induced calcium release in skeletal muscle. Physiological Reviews *89*, 1153–1176.

Fairn, G.D., Curwin, A.J., Stefan, C.J., and McMaster, C.R. (2007). The oxysterol binding protein Kes1p regulates Golgi apparatus phosphatidylinositol-4-phosphate function. Proc. Natl. Acad. Sci. U.S.A. *104*, 15352–15357.

Faulhammer, F., Kanjilal-Kolar, S., Knödler, A., Lo, J., Lee, Y., Konrad, G., and Mayinger, P. (2007). Growth Control of Golgi Phosphoinositides by Reciprocal Localization of Sac1 Lipid Phosphatase and Pik1 4-Kinase. Traffic *8*, 1554–1567.

Faulhammer, F., Konrad, G., Brankatschk, B., Tahirovic, S., Knödler, A., and Mayinger, P. (2005). Cell growth-dependent coordination of lipid signaling and glycosylation is mediated by interactions between Sac1p and Dpm1p. The Journal of Cell Biology *168*, 185–191.

Feske, S., Gwack, Y., Prakriya, M., Srikanth, S., Puppel, S.-H., Tanasa, B., Hogan, P.G., Lewis, R.S., Daly, M., and Rao, A. (2006). A mutation in Orai1 causes immune deficiency by abrogating CRAC channel function. Nature *441*, 179–185.

Ford, M.G., Pearse, B.M., Higgins, M.K., Vallis, Y., Owen, D.J., Gibson, A., Hopkins, C.R., Evans, P.R., and McMahon, H.T. (2001). Simultaneous binding of PI(4,5)P2 and clathrin by AP180 in the nucleation of clathrin lattices on membranes. Science *291*, 1051–1055.

Foti, M., Audhya, A., and Emr, S.D. (2001). Sac1 lipid phosphatase and Stt4 phosphatidylinositol 4-kinase regulate a pool of phosphatidylinositol 4-phosphate that functions in the control of the actin cytoskeleton and vacuole morphology. Molecular Biology of the Cell *12*, 2396–2411.

Frangioni, J.V., Beahm, P.H., Shifrin, V., Jost, C.A., and Neel, B.G. (1992). The nontransmembrane tyrosine phosphatase PTP-1B localizes to the endoplasmic reticulum via its 35 amino acid C-terminal sequence. Cell *68*, 545–560.

Franzini-Armstrong, C., Pincon-Raymond, M., and Rieger, F. (1991). Muscle fibers from

dysgenic mouse in vivo lack a surface component of peripheral couplings. Dev. Biol. *146*, 364–376.

Friedman, J.R., Lackner, L.L., West, M., DiBenedetto, J.R., Nunnari, J., and Voeltz, G.K. (2011). ER Tubules Mark Sites of Mitochondrial Division. Science *334*, 358–362.

Friedman, J.R., and Voeltz, G.K. (2011). The ER in 3D: a multifunctional dynamic membrane network. Trends in Cell Biology *21*, 709–717.

Gaidarov, I., and Keen, J.H. (1999). Phosphoinositide-AP-2 interactions required for targeting to plasma membrane clathrin-coated pits. The Journal of Cell Biology *146*, 755–764.

Georgiev, A.G., Sullivan, D.P., Kersting, M.C., Dittman, J.S., Beh, C.T., and Menon, A.K. (2011). Osh Proteins Regulate Membrane Sterol Organization but Are Not Required for Sterol Movement Between the ER and PM. Traffic *12*, 1341–1355.

Godi, A., Di Campli, A., Konstantakopoulos, A., Di Tullio, G., Alessi, D.R., Kular, G.S., Daniele, T., Marra, P., Lucocq, J.M., and De Matteis, M.A. (2004). FAPPs control Golgi-to-cell-surface membrane traffic by binding to ARF and PtdIns(4)P. Nat. Cell Biol. *6*, 393–404.

Govindan, B., Bowser, R., and Novick, P. (1995). The role of Myo2, a yeast class V myosin, in vesicular transport. The Journal of Cell Biology *128*, 1055–1068.

Guo, S., Stolz, L.E., Lemrow, S.M., and York, J.D. (1999). SAC1-like domains of yeast SAC1, INP52, and INP53 and of human synaptojanin encode polyphosphoinositide phosphatases. J. Biol. Chem. *274*, 12990–12995.

Haj, F.G., Sabet, O., Kinkhabwala, A., Wimmer-Kleikamp, S., Roukos, V., Han, H.-M., Grabenbauer, M., Bierbaum, M., Antony, C., Neel, B.G., et al. (2012). Regulation of Signaling at Regions of Cell-Cell Contact by Endoplasmic Reticulum-Bound Protein-Tyrosine Phosphatase 1B. PLoS ONE *7*, e36633.

Haj, F.G., Verveer, P.J., Squire, A., Neel, B.G., and Bastiaens, P.I.H. (2002). Imaging sites of receptor dephosphorylation by PTP1B on the surface of the endoplasmic reticulum. Science *295*, 1708–1711.

Hama, H., Schnieders, E.A., Thorner, J., Takemoto, J.Y., and DeWald, D.B. (1999). Direct involvement of phosphatidylinositol 4-phosphate in secretion in the yeast Saccharomyces cerevisiae. J. Biol. Chem. *274*, 34294–34300.

Hammond, G.R.V., Fischer, M.J., Anderson, K.E., Holdich, J., Koteci, A., Balla, T., and Irvine, R.F. (2012). PI4P and PI(4,5)P2 Are Essential But Independent Lipid Determinants of Membrane Identity. Science *337*, 727–730.

Hanada, K., Kumagai, K., Yasuda, S., Miura, Y., Kawano, M., Fukasawa, M., and Nishijima, M. (2003). Molecular machinery for non-vesicular trafficking of ceramide. Nature *426*, 803–809.

Hardie, R.C. (2001). Phototransduction in Drosophila melanogaster. J. Exp. Biol. *204*, 3403–

3409.

Harlan, J.E., Hajduk, P.J., Yoon, H.S., and Fesik, S.W. (1994). Pleckstrin homology domains bind to phosphatidylinositol-4,5-bisphosphate. Nature *371*, 168–170.

Hayashi, M., Raimondi, A., O'Toole, E., Paradise, S., Collesi, C., Cremona, O., Ferguson, S.M., and De Camilli, P. (2008). Cell- and stimulus-dependent heterogeneity of synaptic vesicle endocytic recycling mechanisms revealed by studies of dynamin 1-null neurons. Proc. Natl. Acad. Sci. U.S.A. *105*, 2175–2180.

Hepler, P.K., Palevitz, B.A., Lancelle, S.A., McCauley, M.M., and Lichtschidl, L. (1990). Cortical endoplasmic reticulum in plants. Journal of Cell Science *96*, 355–373.

Hernández, M.V., Sala, M.G.D., Balsamo, J., Lilien, J., and Arregui, C.O. (2006). ER-bound PTP1B is targeted to newly forming cell-matrix adhesions. Journal of Cell Science *119*, 1233–1243.

Holthuis, J.C.M., and Levine, T.P. (2005). Lipid traffic: floppy drives and a superhighway. Nat Rev Mol Cell Biol *6*, 209–220.

Homma, K. (1998). Phosphatidylinositol-4-phosphate 5-Kinase Localized on the Plasma Membrane Is Essential for Yeast Cell Morphogenesis. Journal of Biological Chemistry *273*, 15779–15786.

Höning, S., Ricotta, D., Krauss, M., Späte, K., Spolaore, B., Motley, A., Robinson, M., Robinson, C., Haucke, V., and Owen, D.J. (2005). Phosphatidylinositol-(4,5)-bisphosphate regulates sorting signal recognition by the clathrin-associated adaptor complex AP2. Molecular Cell *18*, 519–531.

Hotta, Y., and Benzer, S. (1970). Genetic dissection of the Drosophila nervous system by means of mosaics. Proc. Natl. Acad. Sci. U.S.A. *67*, 1156–1163.

Ikemoto, T., Komazaki, S., Takeshima, H., Nishi, M., Noda, T., Iino, M., and Endo, M. (1997). Functional and morphological features of skeletal muscle from mutant mice lacking both type 1 and type 3 ryanodine receptors. J. Physiol. (Lond.) *501 ( Pt 2)*, 305–312.

Im, Y.J., Raychaudhuri, S., Prinz, W.A., and Hurley, J.H. (2005). Structural mechanism for sterol sensing and transport by OSBP-related proteins. Nature *437*, 154–158.

Itoh, T., Koshiba, S., Kigawa, T., Kikuchi, A., Yokoyama, S., and Takenawa, T. (2001). Role of the ENTH domain in phosphatidylinositol-4,5-bisphosphate binding and endocytosis. Science *291*, 1047–1051.

Jansen, M., Ohsaki, Y., Rita Rega, L., Bittman, R., Olkkonen, V.M., and Ikonen, E. (2010). Role of ORPs in Sterol Transport from Plasma Membrane to ER and Lipid Droplets in Mammalian Cells. Traffic *12*, 218–231.

Johnston, G.C., Prendergast, J.A., and Singer, R.A. (1991). The Saccharomyces cerevisiae

MYO2 gene encodes an essential myosin for vectorial transport of vesicles. The Journal of Cell Biology *113*, 539–551.

Jonikas, M.C., Collins, S.R., Denic, V., Oh, E., Quan, E.M., Schmid, V., Weibezahn, J., Schwappach, B., Walter, P., Weissman, J.S., et al. (2009). Comprehensive characterization of genes required for protein folding in the endoplasmic reticulum. Science *323*, 1693–1697.

Kadamur, G., and Ross, E.M. (2013). Mammalian Phospholipase C. Annu. Rev. Physiol. *75*, 127–154.

Kaplan, M.R., and Simoni, R.D. (1985). Intracellular transport of phosphatidylcholine to the plasma membrane. The Journal of Cell Biology *101*, 441–445.

Kawano, M. (2006). Efficient Trafficking of Ceramide from the Endoplasmic Reticulum to the Golgi Apparatus Requires a VAMP-associated Protein-interacting FFAT Motif of CERT. Journal of Biological Chemistry *281*, 30279–30288.

Kim, W.T., Chang, S., Daniell, L., Cremona, O., Di Paolo, G., and De Camilli, P. (2002). Delayed reentry of recycling vesicles into the fusion-competent synaptic vesicle pool in synaptojanin 1 knockout mice. Proc. Natl. Acad. Sci. U.S.A. *99*, 17143–17148.

Konrad, G., Schlecker, T., Faulhammer, F., and Mayinger, P. (2002). Retention of the yeast Sac1p phosphatase in the endoplasmic reticulum causes distinct changes in cellular phosphoinositide levels and stimulates microsomal ATP transport. J. Biol. Chem. *277*, 10547–10554.

Korzeniowski, M.K., Popovic, M.A., Szentpetery, Z., Varnai, P., Stojilkovic, S.S., and Balla, T. (2009). Dependence of STIM1/Orai1-mediated Calcium Entry on Plasma Membrane Phosphoinositides. Journal of Biological Chemistry *284*, 21027–21035.

Kozminski, K.G., Alfaro, G., Dighe, S., and Beh, C.T. (2006). Homologues of Oxysterol-Binding Proteins Affect Cdc42p- and Rho1p-Mediated Cell Polarization in Saccharomyces cerevisiae. Traffic *7*, 1224–1242.

Lev, S. (2010). Non-vesicular lipid transport by lipid-transfer proteins and beyond. Nat Rev Mol Cell Biol *11*, 739–750.

Levine, T.P., and Munro, S. (2001). Dual targeting of Osh1p, a yeast homologue of oxysterol-binding protein, to both the Golgi and the nucleus-vacuole junction. Molecular Biology of the Cell *12*, 1633–1644.

Levine, T.P., and Munro, S. (2002). Targeting of Golgi-specific pleckstrin homology domains involves both PI 4-kinase-dependent and -independent components. Curr. Biol. *12*, 695–704.

Liou, J., Fivaz, M., Inoue, T., and Meyer, T. (2007). Live-cell imaging reveals sequential oligomerization and local plasma membrane targeting of stromal interaction molecule 1 after Ca2+ store depletion. Proc. Natl. Acad. Sci. U.S.A. *104*, 9301–9306.

Liou, J., Kim, M.L., Do Heo, W., Jones, J.T., Myers, J.W., Ferrell, J.E., Jr., and Meyer, T. (2005). STIM Is a Ca2+ Sensor Essential for Ca2+-Store-Depletion-Triggered Ca2+ Influx. Current Biology *15*, 1235–1241.

Liu, Y., Boukhelifa, M., Tribble, E., Morin-Kensicki, E., Uetrecht, A., Bear, J.E., and Bankaitis, V.A. (2008). The Sac1 Phosphoinositide Phosphatase Regulates Golgi Membrane Morphology and Mitotic Spindle Organization in Mammals. Molecular Biology of the Cell *19*, 3080–3096.

Liu, Y., and Bankaitis, V.A. (2010). Phosphoinositide phosphatases in cell biology and disease. Progress in Lipid Research *49*, 201–217.

Loewen, C.J.R., Roy, A., and Levine, T.P. (2003). A conserved ER targeting motif in three families of lipid binding proteins and in Opi1p binds VAP. Embo J *22*, 2025–2035.

Ma, H., Lou, Y., Lin, W.H., and Xue, H.W. (2006). MORN motifs in plant PIPKs are involved in the regulation of subcellular localization and phospholipid binding. Cell Res *16*, 466–478.

Maule, A.J., Benitez-Alfonso, Y., and Faulkner, C. (2011). Plasmodesmata - membrane tunnels with attitude. Curr. Opin. Plant Biol. *14*, 683–690.

Moravcevic, K., Oxley, C.L., and Lemmon, M.A. (2012). Conditional peripheral membrane proteins: facing up to limited specificity. Structure *20*, 15–27.

Mousley, C.J., Davison, J.M., and Bankaitis, V.A. (2012). Sec14 Like PITPs Couple Lipid Metabolism with Phosphoinositide Synthesis to Regulate Golgi Functionality. In Subcellular Biochemistry, (Dordrecht: Springer Netherlands), pp. 271–287.

Nakatsu, F., Baskin, J.M., Chung, J., Tanner, L.B., Shui, G., Lee, S.Y., Pirruccello, M., Hao, M., Ingolia, N.T., Wenk, M.R., et al. (2012). PI4P synthesis by PI4KIII  at the plasma membrane and its impact on plasma membrane identity. The Journal of Cell Biology *199*, 1003–1016.

Nemoto, Y., Kearns, B.G., Wenk, M.R., Chen, H., Mori, K., Alb, J.G., De Camilli, P., and Bankaitis, V.A. (2000). Functional characterization of a mammalian Sac1 and mutants exhibiting substrate-specific defects in phosphoinositide phosphatase activity. J. Biol. Chem. *275*, 34293–34305.

Nievergall, E., Janes, P.W., Stegmayer, C., Vail, M.E., Haj, F.G., Teng, S.W., Neel, B.G., Bastiaens, P.I., and Lackmann, M. (2010). PTP1B regulates Eph receptor function and trafficking. The Journal of Cell Biology *191*, 1189–1203.

Novick, P., Field, C., and Schekman, R. (1980). Identification of 23 complementation groups required for post-translational events in the yeast secretory pathway. Cell *21*, 205–215.

Novick, P., Osmond, B.C., and Botstein, D. (1989). Suppressors of yeast actin mutations. Genetics *121*, 659–674.

Olkkonen, V.M., and Li, S. (2013). Oxysterol-binding proteins: Sterol and phosphoinositide sensors coordinating transport, signaling and metabolism. Progress in Lipid Research *52*, 529–

538.

Orci, L., Ravazzola, M., Le Coadic, M., Shen, W.-W., Demaurex, N., and Cosson, P. (2009). From the Cover: STIM1-induced precortical and cortical subdomains of the endoplasmic reticulum. Proc. Natl. Acad. Sci. U.S.A. *106*, 19358–19362.

Park, C.Y., Hoover, P.J., Mullins, F.M., Bachhawat, P., Covington, E.D., Raunser, S., Walz, T., Garcia, K.C., Dolmetsch, R.E., and Lewis, R.S. (2009). STIM1 Clusters and Activates CRAC Channels via Direct Binding of a Cytosolic Domain to Orai1. Cell *136*, 876–890.

Peretti, D., Dahan, N., Shimoni, E., Hirschberg, K., and Lev, S. (2008). Coordinated lipid transfer between the endoplasmic reticulum and the Golgi complex requires the VAP proteins and is essential for Golgi-mediated transport. Molecular Biology of the Cell *19*, 3871–3884.

Pichler, H., Gaigg, B., Hrastnik, C., Achleitner, G., Kohlwein, S.D., Zellnig, G., Perktold, A., and Daum, G. (2001). A subfraction of the yeast endoplasmic reticulum associates with the plasma membrane and has a high capacity to synthesize lipids. Eur. J. Biochem. *268*, 2351–2361.

Porter, K.R., and Palade, G.E. (1957). Studies on the endoplasmic reticulum. III. Its form and distribution in striated muscle cells. J Biophys Biochem Cytol *3*, 269–300.

Prinz, W.A., Grzyb, L., Veenhuis, M., Kahana, J.A., Silver, P.A., and Rapoport, T.A. (2000). Mutants affecting the structure of the cortical endoplasmic reticulum in Saccharomyces cerevisiae. The Journal of Cell Biology *150*, 461–474.

Raychaudhuri, S., Im, Y.J., Hurley, J.H., and Prinz, W.A. (2006). Nonvesicular sterol movement from plasma membrane to ER requires oxysterol-binding protein-related proteins and phosphoinositides. The Journal of Cell Biology *173*, 107–119.

Rocha, N., Kuijl, C., van der Kant, R., Janssen, L., Houben, D., Janssen, H., Zwart, W., and Neefjes, J. (2009). Cholesterol sensor ORP1L contacts the ER protein VAP to control Rab7-RILP-p150Glued and late endosome positioning. The Journal of Cell Biology *185*, 1209–1225.

Rohde, H.M., Cheong, F.Y., Konrad, G., Paiha, K., Mayinger, P., and Boehmelt, G. (2003). The human phosphatidylinositol phosphatase SAC1 interacts with the coatomer I complex. J. Biol. Chem. *278*, 52689–52699.

Roos, J., DiGregorio, P.J., Yeromin, A.V., Ohlsen, K., Lioudyno, M., Zhang, S., Safrina, O., Kozak, J.A., Wagner, S.L., Cahalan, M.D., et al. (2005). STIM1, an essential and conserved component of store-operated Ca2+ channel function. The Journal of Cell Biology *169*, 435–445.

Rosenbluth, J. (1962). Subsurface cisterns and their relationship to the neuronal plasma membrane. The Journal of Cell Biology *13*, 405–421.

Rossi, A.E., and Dirksen, R.T. (2006). Sarcoplasmic reticulum: The dynamic calcium governor of muscle. Muscle Nerve *33*, 715–731.

Roy, A., and Levine, T.P. (2004). Multiple pools of phosphatidylinositol 4-phosphate detected

using the pleckstrin homology domain of Osh2p. J. Biol. Chem. *279*, 44683–44689.

Rubinstein, C.T., Bar-Nachum, S., Selinger, Z., and Minke, B. (1989). Light-induced retinal degeneration in rdgB (retinal degeneration B) mutant of Drosophila: electrophysiological and morphological manifestations of degeneration. Vis. Neurosci. *2*, 529–539.

Santiago-Tirado, F.H., and Bretscher, A. (2011). Membrane-trafficking sorting hubs: cooperation between PI4P and small GTPases at the trans-Golgi network. Trends in Cell Biology *21*, 515–525.

Santiago-Tirado, F.H., Legesse-Miller, A., Schott, D., and Bretscher, A. (2011). PI4P and Rab inputs collaborate in myosin-V-dependent transport of secretory compartments in yeast. Developmental Cell *20*, 47–59.

Sasaki, T., Takasuga, S., Sasaki, J., Kofuji, S., Eguchi, S., Yamazaki, M., and Suzuki, A. (2009). Mammalian phosphoinositide kinases and phosphatases. Progress in Lipid Research *48*, 307–343.

Schaaf, G., Ortlund, E.A., Tyeryar, K.R., Mousley, C.J., Ile, K.E., Garrett, T.A., Ren, J., Woolls, M.J., Raetz, C.R.H., Redinbo, M.R., et al. (2008). Functional Anatomy of Phospholipid Binding and Regulation of Phosphoinositide Homeostasis by Proteins of the Sec14 Superfamily. Molecular Cell *29*, 191–206.

Schulz, T.A., Choi, M.G., Raychaudhuri, S., Mears, J.A., Ghirlando, R., Hinshaw, J.E., and Prinz, W.A. (2009). Lipid-regulated sterol transfer between closely apposed membranes by oxysterol-binding protein homologues. The Journal of Cell Biology *187*, 889–903.

Shi, K., Egawa, K., Maegawa, H., Nakamura, T., Ugi, S., Nishio, Y., and Kashiwagi, A. (2004). Protein-tyrosine phosphatase 1B associates with insulin receptor and negatively regulates insulin signaling without receptor internalization. J. Biochem. *136*, 89–96.

Shibata, Y., Voeltz, G.K., and Rapoport, T.A. (2006). Rough Sheets and Smooth Tubules. Cell *126*, 435–439.

Staehelin, L.A. (1997). The plant ER: a dynamic organelle composed of a large number of discrete functional domains. Plant J. *11*, 1151–1165.

Stefan, C.J., Padilla, S.M., Audhya, A., and Emr, S.D. (2005). The Phosphoinositide Phosphatase Sjl2 Is Recruited to Cortical Actin Patches in the Control of Vesicle Formation and Fission during Endocytosis. Molecular and Cellular Biology *25*, 2910–2923.

Stefan, C.J., Audhya, A., and Emr, S.D. (2002). The yeast synaptojanin-like proteins control the cellular distribution of phosphatidylinositol (4,5)-bisphosphate. Molecular Biology of the Cell *13*, 542–557.

Stefan, C.J., Manford, A.G., Baird, D., Yamada-Hanff, J., Mao, Y., and Emr, S.D. (2011). Osh proteins regulate phosphoinositide metabolism at ER-plasma membrane contact sites. Cell *144*, 389–401.

Suh, B.C., Inoue, T., Meyer, T., and Hille, B. (2006). Rapid Chemically Induced Changes of PI(4,5)P2 Gate KCNQ Ion Channels. Science *314*, 1454–1457.

Suzuki, E., and Hirosawa, K. (1994). Immunolocalization of a Drosophila phosphatidylinositol transfer protein (rdgB) in normal and rdgA mutant photoreceptor cells with special reference to the subrhabdomeric cisternae. J Electron Microsc (Tokyo) *43*, 183–189.

Tahirovic, S., Schorr, M., and Mayinger, P. (2004). Regulation of Intracellular Phosphatidylinositol-4-Phosphate by the Sac1 Lipid Phosphatase. Traffic *6*, 116–130.

Takeshima, H., Komazaki, S., Nishi, M., Iino, M., and Kangawa, K. (2000). Junctophilins: a novel family of junctional membrane complex proteins. Molecular Cell *6*, 11–22.

Tonks, N.K. (2003). PTP1B: From the sidelines to the front lines! FEBS Letters *546*, 140–148.

Toulmay, A., and Prinz, W.A. (2011). Lipid transfer and signaling at organelle contact sites: the tip of the iceberg. Curr. Opin. Cell Biol. *23*, 458–463.

Traub, L.M. (2003). Sorting it out: AP-2 and alternate clathrin adaptors in endocytic cargo selection. The Journal of Cell Biology *163*, 203–208.

Tsui, M.M., and York, J.D. (2010). Roles of inositol phosphates and inositol pyrophosphates in development, cell signaling and nuclear processes. Advances in Enzyme Regulation *50*, 324–337.

Vance, J.E., Aasman, E.J., and Szarka, R. (1991). Brefeldin A does not inhibit the movement of phosphatidylethanolamine from its sites for synthesis to the cell surface. J. Biol. Chem. *266*, 8241–8247.

Varnai, P., Thyagarajan, B., Rohacs, T., and Balla, T. (2006). Rapidly inducible changes in phosphatidylinositol 4,5-bisphosphate levels influence multiple regulatory functions of the lipid in intact living cells. The Journal of Cell Biology *175*, 377–382.

Vicinanza, M., D'Angelo, G., Di Campli, A., and De Matteis, M.A. (2008). Function and dysfunction of the PI system in membrane trafficking. Embo J *27*, 2457–2470.

Vig, M., Peinelt, C., Beck, A., Koomoa, D.L., Rabah, D., Koblan-Huberson, M., Kraft, S., Turner, H., Fleig, A., Penner, R., et al. (2006). CRACM1 is a plasma membrane protein essential for store-operated Ca2+ entry. Science *312*, 1220–1223.

Vihtelic, T.S., Goebl, M., Milligan, S., O'Tousa, J.E., and Hyde, D.R. (1993). Localization of Drosophila retinal degeneration B, a membrane-associated phosphatidylinositol transfer protein. The Journal of Cell Biology *122*, 1013–1022.

Voelker, D.R. (2003). New perspectives on the regulation of intermembrane glycerophospholipid traffic. The Journal of Lipid Research *44*, 441–449.

Walch-Solimena, C., and Novick, P. (1999). The yeast phosphatidylinositol-4-OH kinase pik1

regulates secretion at the Golgi. Nat. Cell Biol. *1*, 523–525.

Wang, J., Sun, H.-Q., Macia, E., Kirchhausen, T., Watson, H., Bonifacino, J.S., and Yin, H.L. (2007). PI4P promotes the recruitment of the GGA adaptor proteins to the trans-Golgi network and regulates their recognition of the ubiquitin sorting signal. Molecular Biology of the Cell *18*, 2646–2655.

Wang, P.-Y., Weng, J., and Anderson, R.G.W. (2005). OSBP is a cholesterol-regulated scaffolding protein in control of ERK 1/2 activation. Science *307*, 1472–1476.

Wang, Y.J., Wang, J., Sun, H.-Q., Martinez, M., Sun, Y.X., Macia, E., Kirchhausen, T., Albanesi, J.P., Roth, M.G., and Yin, H.L. (2003). Phosphatidylinositol 4 Phosphate Regulates Targeting of Clathrin Adaptor AP-1 Complexes to the Golgi. Cell *114*, 299–310.

Wei, H.-C., Sanny, J., Shu, H., Baillie, D.L., Brill, J.A., Price, J.V., and Harden, N. (2003). The Sac1 Lipid Phosphatase Regulates Cell Shape Change and the JNK Cascade during Dorsal Closure in Drosophila. Current Biology *13*, 1882–1887.

West, M., Zurek, N., Hoenger, A., and Voeltz, G.K. (2011). A 3D analysis of yeast ER structure reveals how ER domains are organized by membrane curvature. The Journal of Cell Biology *193*, 333–346.

Whitters, E.A., Cleves, A.E., McGee, T.P., Skinner, H.B., and Bankaitis, V.A. (1993). SAC1p is an integral membrane protein that influences the cellular requirement for phospholipid transfer protein function and inositol in yeast. The Journal of Cell Biology *122*, 79–94.

Woodford-Thomas, T.A., Rhodes, J.D., and Dixon, J.E. (1992). Expression of a protein tyrosine phosphatase in normal and v-src-transformed mouse 3T3 fibroblasts. The Journal of Cell Biology *117*, 401–414.

Wu, M.M. (2006). Ca2+ store depletion causes STIM1 to accumulate in ER regions closely associated with the plasma membrane. The Journal of Cell Biology *174*, 803–813.

Wu, M.M., Buchanan, J., Luik, R.M., and Lewis, R.S. (2006). Ca2+ store depletion causes STIM1 to accumulate in ER regions closely associated with the plasma membrane. The Journal of Cell Biology *174*, 803–813.

Yan, D., and Olkkonen, V.M. (2008). Characteristics of Oxysterol Binding Proteins. In International Review of Cytology, pp. 253–285.

Yavari, A., Nagaraj, R., Owusu-Ansah, E., Folick, A., Ngo, K., Hillman, T., Call, G., Rohatgi, R., Scott, M.P., and Banerjee, U. (2010). Role of Lipid Metabolism in Smoothened Derepression in Hedgehog Signaling. Developmental Cell *19*, 54–65.

Yu, J.W., and Lemmon, M.A. (2001). All phox homology (PX) domains from Saccharomyces cerevisiae specifically recognize phosphatidylinositol 3-phosphate. J. Biol. Chem. *276*, 44179–44184.

Yu, J.W., Mendrola, J.M., Audhya, A., Singh, S., Keleti, D., DeWald, D.B., Murray, D., Emr, S.D., and Lemmon, M.A. (2004). Genome-wide analysis of membrane targeting by S. cerevisiae pleckstrin homology domains. Molecular Cell *13*, 677–688.

Yuan, J.P., Zeng, W., Dorwart, M.R., Choi, Y.-J., Worley, P.F., and Muallem, S. (2009). SOAR and the polybasic STIM1 domains gate and regulate Orai channels. Nat. Cell Biol. *11*, 337–343.

Zhang, S.L., Yeromin, A.V., Zhang, X.H.-F., Yu, Y., Safrina, O., Penna, A., Roos, J., Stauderman, K.A., and Cahalan, M.D. (2006). Genome-wide RNAi screen of Ca(2+) influx identifies genes that regulate Ca(2+) release-activated Ca(2+) channel activity. Proc. Natl. Acad. Sci. U.S.A. *103*, 9357–9362.

Zhang, S.L., Yu, Y., Roos, J., Kozak, J.A., Deerinck, T.J., Ellisman, M.H., Stauderman, K.A., and Cahalan, M.D. (2005). STIM1 is a Ca2+ sensor that activates CRAC channels and migrates from the Ca2+ store to the plasma membrane. Nature Publishing Group *437*, 902–905.

Zoncu, R., Perera, R.M., Balkin, D.M., Pirruccello, M., Toomre, D., and Pietro De Camilli (2009). A Phosphoinositide Switch Controls the Maturation and Signaling Properties of APPL Endosomes. Cell *136*, 1110–1121.

Zoncu, R., Perera, R.M., Sebastian, R., Nakatsu, F., Chen, H., Balla, T., Ayala, G., Toomre, D., and De Camilli, P.V. (2007). Loss of endocytic clathrin-coated pits upon acute depletion of phosphatidylinositol 4,5-bisphosphate. Proc. Natl. Acad. Sci. U.S.A. *104*, 3793–3798.

# Chapter II

## Osh Proteins Regulate Phosphoinositide Metabolism at ER-Plasma Membrane Contact Sites

Christopher J. Stefan*[1], Andrew G. Manford*[1], Daniel Baird[1,2], Jason Yamada-Hanff[1,3], Yuxin Mao[1], and Scott D. Emr[1]

[1]Weill Institute for Cell & Molecular Biology, Department of Molecular Biology & Genetics, Cornell University, Ithaca, NY, 14853

[2]Current address: Novartis Institutes for Biomedical Research, 250 Massachusetts Ave, Cambridge, MA, 02139

[3]Current address: Program in Neuroscience, Harvard Medical School, 220 Longwood Ave, Boston, MA 02215

*These authors contributed equally to this work.

Andrew Manford contributed data for figures 2.1-2.4, 2.6, 2.13, and 2.14 and assisted in designing experiments and preparation of the manuscript.

Chapter II was originally published in Cell 144, 389–401, (2011)

## Abstract

Sac1 phosphoinositide (PI) phosphatases are essential regulators of PI signaling networks. Yeast Sac1, an integral endoplasmic reticulum (ER) membrane protein, controls PI4P levels at the ER, Golgi, and plasma membrane (PM). Whether Sac1 can act *in trans* and turnover PI4P at the Golgi and PM from the ER remains a paradox. We find that Sac1-mediated PI4P metabolism requires the oxysterol-binding homology (Osh) proteins. The PH domain-containing family member, Osh3, localizes to PM/ER membrane contact sites dependent upon PM PI4P levels. We reconstitute Osh protein-stimulated Sac1 PI phosphatase activity *in vitro*. We also show that the ER membrane VAP proteins, Scs2/Scs22, control PM PI4P levels and Sac1 activity *in vitro*. We propose that Osh3 functions at ER/PM contact sites as both a sensor of PM PI4P and an activator of the ER Sac1 phosphatase. Our findings further suggest that the conserved Osh proteins control PI metabolism at additional membrane contact sites.

## Introduction

Phosphatidylinositol 4-phosphate, PI4P, serves as an essential signaling molecule at the plasma membrane and Golgi in the control of membrane trafficking, cytoskeletal organization, lipid metabolism, and signal transduction pathways (D'Angelo et al., 2008). Maintaining the proper balance of PI4P levels through the regulation of phosphoinositide (PI) kinases and phosphatases is critical. Sac1-like PI phosphatases are important regulators of PI4P turnover and are implicated in disease (Liu and Bankaitis, 2010). Yeast cells lacking Sac1 display elevated PI4P levels resulting in impaired membrane trafficking, abnormal vacuolar morphology, altered lipid metabolism, and growth defects (Foti et al., 2001; Guo et al., 1999; Rivas et al., 1999). Inactivation of Sac1 PI phosphatase activity provided by Sac1 and the synaptojanin-like proteins, Sjl2 and Sjl3, results in massive PI4P accumulation, secretory defects, and lethality (Foti et al., 2001). In mammalian cells, depletion of Sac1 leads to elevated cellular PI4P levels, Golgi fragmentation, and defects in mitotic spindle organization (Liu et al., 2008). Loss of Sac1 in the mouse and *Drosophila* results in embryonic lethality (Liu et al., 2008; Wei et al., 2003). Thus, Sac1 PI phosphatases are essential for multiple, conserved cellular functions.

While Sac1 PI phosphatases are key modulators of PI4P metabolism, little is known about their regulation. Both yeast and mammalian Sac1 are integral membrane proteins localized to the endoplasmic reticulum (ER) and Golgi (Faulhammer et al., 2007; Foti et al., 2001; Nemoto et al., 2000). Upon starvation in yeast, or in the absence of growth factors in mammalian cells, Sac1 traffics from the ER to the Golgi where it antagonizes PI4P synthesis and Golgi function (Blagoveshchenskaya et al., 2008; Faulhammer et al., 2007). While roles for Sac1 in the control of PI4P at the ER and Golgi PI4P are known, less is understood about how Sac1 regulates PI4P levels at the plasma membrane (PM). Previous studies indicate that *sac1*Δ mutant yeast cells

accumulate PI4P at the PM generated by the PI 4-kinase Stt4 (Baird et al., 2008; Foti et al., 2001; Roy and Levine, 2004). Yet, Sac1 is not known to traffic to the PM, nor is it known if Sac1 regulates PM PI4P pools from the ER. A recent study describing the molecular structure of the Sac1 catalytic domain suggests that Sac1 may act *in trans* from the ER to turnover PI4P at the PM (Manford et al., 2010). However, factors that link Sac1 PI phosphatase activity to PI4P at the PM are unknown.

We find that PI4P metabolism and Sac1 function require the oxysterol-binding homology (Osh) protein family. In particular, Osh3 assembles at cortical ER structures in response to PM PI4P levels. We reconstitute Osh protein-stimulated Sac1 PI phosphatase activity against PI4P-containing liposomes *in vitro*. In addition, the ER membrane VAP proteins, Scs2 and Scs22, control PM PI4P levels *in vivo* and Sac1 activity *in vitro*. We propose that the Osh and VAP proteins regulate Sac1 PI phosphatase activity at PM/ER membrane contact sites. We also discuss potential roles for these proteins in the control of PI metabolism at additional membrane contact sites. Membrane junctions between the ER and other organelles are sites for lipid transfer and metabolism, $Ca^{2+}$ transport and signaling, and the down-regulation of insulin and growth factor receptors (reviewed in Lev, 2010). Thus, modulation of PI levels at membrane contact sites may provide a fundamental mechanism for signaling between cellular membrane compartments.

## Materials and Methods

### Yeast Strains, Plasmids, and Media

Descriptions of strains and plasmids used in this study are in Tables 2.1 and 2.2. Gene deletions and epitope tags were introduced into yeast by homologous recombination (Longtine et

al., 1998). The pGO-GFP expression vectors were used to create GFP-Sac1 and GFP-2xPH$^{Osh2}$ fusion constructs. The pRS vector series have been described previously (Christianson et al., 1992; Sikorski and Hieter, 1989). Coding sequences were amplified by PCR using ExTaq (Takara Mirus Bio). Plasmids were sequenced to ensure that no mutations were introduced due to manipulations. Mutant constructs were generated by site directed mutagenesis (Quickchange, Stratagene) and confirmed by sequencing. Standard techniques and media were used for yeast and bacterial growth.

**Fluorescence Microscopy**

Fluorescence microscopy experiments were performed on mid-log yeast cultures in synthetic media at the indicated temperatures. To visualize the plasma membrane, cells were stained with filipin (10 mg/ml) that binds ergosterol. Images were obtained using a DeltaVision RT microscopy system (Applied Precision) equipped with an IX71 Olympus microscope, a PlanApo 100X objective (1.35 NA, Olympus), DAPI, FITC, and rhodamine filters, and a Cool Snap HQ digital camera (Photometrics). Images were deconvolved using soft-WoRx 3.5.0 software (Applied Precision, LLC). All results are based on observations of > 100 cells.

**Electron Microscopy**

For ultrastructural analysis, 50 $OD_{600}$ units of log-phase cells incubated at the appropriate temperature were harvested from YPD medium and fixed in 3% glutaraldehyde, 0.1 M Na cacodylate (pH 7.4), 5 mM $CaCl_2$, 5 mM $MgCl_2$, and 2.5% sucrose for 1 h. Cells were further processed for electron microscopy as described previously (Rieder et al., 1996).

**Phosphoinositide Analysis**

Cellular phosphoinositide levels were measured as described (Baird et al., 2008; Stefan et al., 2002). Briefly, yeast were grown to mid-log phase ($OD_{600}$=0.5-0.8), harvested, washed in media lacking inositol, preshifted to the indicated temperature for 10 minutes, and labeled with *myo*-[2-$^{3}$H]inositol for 1 hour. Cells were precipitated in 4.5% perchloric acid (PCA) and mechanically lysed using glass beads. Lysates were washed in 100 mM EDTA, phospholipids were deacylated, and the resulting gro-PI species were separated by HPLC (Shimadzu) using a Partisphere SAX column (GE Healthcare) and detected with a 610TR radiomatic detector (PerkinElmer).

**Protein Expression Levels**

5 $OD_{600}$ equivalents of mid-log cells pretreated at the indicated temperatures were harvested by precipitation in 10% trichloroacidic acid (TCA). Precipitates were washed in acetone, aspirated, resuspended in lysis buffer (150 mM NaCl, 50mM Tris pH 7.5, 1mM EDTA, 1% SDS), and mechanically lysed with glass beads. Sample buffer (150 mM Tris pH 6.8, 6M Urea, 6%SDS, 10% b-mercaptoethanol, 20% Glycerol) was added and extracts were analyzed by SDS PAGE and immunoblotting with the following antibodies: α-Myc (9E10, Abcam), α-HA (12CA5, Roche), α-Pep12 (Invitrogen), α-Dpm1 (Invitrogen), and α-GFP (Santa Cruz Biotechnology).

**Protein Binding Assays**

For Scs2-3xHA and GST-Osh$^{1-613}$ binding, GST alone or GST-Osh$^{1-613}$ was immobilized on glutathione sepharose 4B (GE Healthcare) and incubated with Scs2-3xHA yeast cell lysates

solubilized in PBS containing 0.5% Tween 20, 0.1 mM EDTA, 0.1 mM AEBSF, 1 μM pepstatin A, and a protease inhibitor cocktail (Complete EDTA-free; Roche). Beads were extensively washed with lysis buffer and bound material was subsequently analyzed by SDS-PAGE and immunoblotting.

For Sac1-13xmyc crosslinking to 3xHA-Osh3 and Osh7-3xHA, 30 $OD_{600}$ cell equivalents were spheroplasted, and disrupted in a dounce homogenizer in lysis buffer (20 mM HEPES pH 7.4, 50 mM potassium acetate, 2mM EDTA, 0.2M sorbitol, 0.1 mM AEBSF, 1 μM pepstatin A, and a protease inhibitor cocktail, Complete EDTA-free). Lysates were precleared for 5 min at 500 x *g* and were then centrifuged at 13,000 x *g* for 10 min at 4°C to generate pellet (P13) fractions. P13 fractions were incubated with 2mM DSP and 2mM DTBP in crosslinking buffer (same as lysis buffer, but no AEBSF) and prepared for denaturing immunoprecipitation conditions as previously described (Seaman et al., 1998). 3xHA-Osh3 and Osh7-3xHA complexes were immunoisolated with Ezview$^{TM}$ Red anti-HA affinity gel (Sigma), incubated in sample buffer containing 10% b-mercaptoethanol to cleave crosslinkers, and analyzed by SDS-PAGE and immunoblotting.

**Recombinant Protein Expression and Purification**

The bacterial expression vectors pGEX6P-1 (GE healthcare) and pRSET-B (Invitrogen) were used to generate recombinant fusion proteins. BL21 (DE3)pLys cells (EMD) transformed with protein expression plasmids were grown at 37 °C to an $OD_{600}$ of 0.4. The bacteria were then shifted to 25°C for 1 h and protein expression was induced by the addition of 0.1 mM IPTG for 16 hours. GST and $his_6$ fusion proteins were purified from BL21 cells with glutathione sepharose 4B (GE Healthcare) and Ni-NTA agarose (Qiagen) respectively according to the manufactures

instructions. Protein concentrations were determined by the Bradford assay (BioRad). Purified proteins were stored at -20$^{o}$C in storage buffer (50mM Tris pH 6.8, 150mM NaCl, 2mM DTT, 50% glycerol) until use. The GST-Osh$^{1-613}$ fusion was stored at -80$^{o}$C in phosphate buffered saline (PBS) until further use.

### *In vitro* Sac1 Phosphatase Assays

For the microsome phosphatase assays, P13 fractions were isolated from mechanically disrupted spheroplasts in lysis buffer (50mM Tris pH 6.8, 150mM NaCl, 2mM DTT, 1 mM EDTA) lacking protease inhibitors. P13 pellets were extensively washed in lysis buffer and sonicated to form microsomes. Protein concentrations were determined with Pierce® protein assay reagent (Thermo) and adjusted to 0.8 mg/ml and aliquots were stored at -80$^{o}$C until further use. High salt washed microsomes were prepared by incubation on ice in RB containing 2 M NaCl for 30 minutes. Salt treated microsomes were recovered by centrifugation at 13,000 x *g* and the resulting P13 membrane pellets were resuspended by sonication to reform microsomes.

Phospholipids (1-palmitoyl-2-oleoyl-*sn*-glycero-3-phosphocholine, POPC; 1-palmitoyl-2-oleoyl-*sn*-glycero-3-phosphoserine, POPS; bovine brain phosphatidylinositol, PtdIns; and cholesterol) were purchased from Avanti and stock solutions were stored in chloroform at -20$^{o}$C. Both diC16 PI4P and soluble diC8 PI4P were purchased from Echelon or Cell Signals. PI4P-containing liposomes (0.6 mM POPC:0.2 mM POPS:0.2 mM diC16 PI4P, 1mM total lipid) were prepared by hydrating dried lipid pellets in reaction buffer (50mM Tris pH 6.8, 150mM NaCl, 2mM DTT) and subsequent sonication. PtdIns-containing liposomes (0.6 mM POPC:0.2 mM POPS:0.2 mM PtdIns, 1mM total lipid) were prepared similarly. Microsomes were incubated with liposomes of indicated composition or soluble diC8 PI4P (60 mM) at 37$^{o}$C and reaction

aliquots (50 ml) were stopped at indicated time points reactions with 50 mM *N*-ethylmaleimide (NEM). Phosphate release was measured by the addition of Biomol Green™ (Enzo) and measured at $OD_{620}$, as described previously (Maehama et al., 2000)

For *in vitro* phosphatase assays using recombinant $Sac1^{1-522}$ and Osh proteins, purified proteins were added at indicated concentrations to liposomes or soluble diC8 PI4P in reaction buffer at the indicated temperatures. Cholesterol-containing liposomes (0.6 mM POPC:0.2 mM POPS:0.2 mM PI4P: 0.2 mM cholesterol) were prepared as described above. Reactions (50 ml) were stopped at the indicated times with NEM and detection of phosphate release was assayed as described above.

**Preparation of $^3$H-PI Liposomes and Lipid Transfer/Fusion Assays**

Liposomes containing $^3$H-PI isoforms were initially prepared as described above, except consisting of 0.6 mM POPC, 0.2 mM POPS, and 15 Ci/mmol $^3$H-PI(4,5)$P_2$ (American Radiolabeled Chemicals). The resulting liposomes containing $^3$H-PI(4,5)$P_2$ were incubated with recombinant SHIP2 PI 5-phosphatase (Echelon) to dephorylate $^3$H-PI(4,5)$P_2$ and thus generate liposomes containing $^3$H-PI4P. The presence of both $^3$H-PI(4,5)$P_2$ and $^3$H-PI4P was confirmed by HPLC analysis.

Liposomes containing $^3$H-PI(4,5)$P_2$ and $^3$H-PI4P ($^3$H-PI) were mixed with Sac1-GFP microsomes in RB buffer and incubated at 37$^o$C for 30 minutes either in the absence or presence of 0.2 mM GST-$Osh3^{588-996}$. Following this incubation, anti-GFP antibodies were added and Sac1-GFP microsomes were immuno-isolated using protein A-coupled magnetic Dynabeads. Liposomes in the unbound fraction were then sedimented by centrifugation at 100,000 x *g*. The amount of $^3$H-PI present in the resulting immuno-isolated microsome fraction, sedimented

liposome pellet fraction, and supernatant fraction was determined by liquid scintillation counting.

**Lipid Overlay and Sedimentation Assays**

The lipid overlay assays were performed essentially as described (Audhya and Emr, 2002). Briefly, two-fold dilutions of lipids solubilized in chloroform were spotted onto reinforced nitrocellulose (Whatman) as indicated. Membranes were blocked with 5% non-fat milk in PBS containing 0.1 % Tween 20 and incubated overnight with 4 mg/ml $his_6$-Osh4 constructs in PBS containing 0.1 % Tween 20 and 2% fatty acid-free albumin. Membranes were extensively washed with PBS containing 0.1 % Tween 20 and bound protein was detected by immunoblotting using α-T7-Tag (Novagen) against the T7 tag in the fusion proteins.

For the liposome sedimentation assays in Figure 2.10A, PI4P and PI-containing liposomes were prepared as described above, incubated with 2 mM recombinant $his_6$-Osh4, GST-$Osh3^{588-996}$, or $his_6$-$Sac1^{C392S,C395S}$ for 30min at 25°C, and centrifuged at 100,000 x *g* for 15 minutes at 4°C. Liposomes consisted of PC:PS:PI4P (3:1:1, 1 mM total lipid). The resulting supernatant and pellet fractions were prepared for SDS-PAGE analysis and Coomassie-stained to detect recombinant proteins. For the experiments in Figure 2.14D, liposomes consisted of PC:PS:PI4P (3:1:1, 0.1 mM total lipid) and were incubated with 0.4 mM $his_6$-Osh4 and 0.4 mM $his_6$-$Sac1^{C341NBD}$ for 30min at 25°C, and centrifuged at 100,000 x *g* for 15 minutes at 4°C. The resulting supernatant and pellet fractions were prepared for SDS-PAGE analysis and proteins were detected by immunoblotting using α-T7-Tag (Novagen) against the T7 tag in the fusion proteins. The relative amounts of $his_6$-$Sac1^{C341NBD}$ in supernatant and pellet fractions were determined using ImageJ analysis software.

**NBD Protein Labeling and Fluorescence Spectroscopy**

Purified $his_6$-$Sac1^{C392S,C395S}$ protein was labeled with IANBD [*N,N'*-dimethyl-*N*-(iodoacetyl)-*N'*-(7-nitrobenz-2-oxa-1,3-diazolyl)ethylenediamine] (GE Healthcare) essentially using the same technique as described earlier (Saksena et al., 2009). The labeled protein was extensively dialyzed in 150 mM NaCl, 50 mM Tris pH 7.5, 0.1% b-mercaptoethanol to quench and remove excess IANBD. The concentration of NBD-labeled Sac1 was determined by the Bradford assay (BioRad). All intensity measurements were carried out in RB buffer at 22°C. Emission spectra for NBD-labeled $his_6$-$Sac1^{C341NBD}$ were recorded in quartz cuvettes in 150 ml final volume, either in the absence or presence of liposomes (PC:PS:PI4P, 3:1:1, 0.1 mM lipid total). NBD was excited at 468 nm, and emission was scanned at 500-590 nm.

## Results

### The Oxysterol-Binding Homology Proteins Regulate PI4P Metabolism

Yeast Sac1 is an integral membrane protein that localizes to nuclear and peripheral ER compartments (Figure 2.1A; Foti et al., 2001). Yet, PI4P is generated by the PI 4-kinases Stt4 and Pik1 at the PM and the Golgi, respectively (Figure 2.1E; Audhya et al., 2000). It is not known how ER-embedded Sac1 turns over these distinct PI4P pools. Sac1 traffics between the ER and Golgi to regulate PI4P levels at these membrane compartments (Faulhammer et al., 2007). However, Sac1 has not been found at the PM. We reasoned that ER-localized Sac1 might control PM PI4P pools at PM/ER membrane contact sites where the peripheral ER closely apposes the PM (within 10 nm; Figure 2.1B). While Sac1 localizes to the peripheral ER (Figure 2.1A), no proteins that regulate Sac1 activity at PM/ER membrane contact sites are known.

We hypothesized that a PI4P effector might link PI4P at the PM to Sac1 at the ER (Figure 2.1B). For this, we focused on the PI4P-binding proteins Osh1, Osh2, and Osh3,

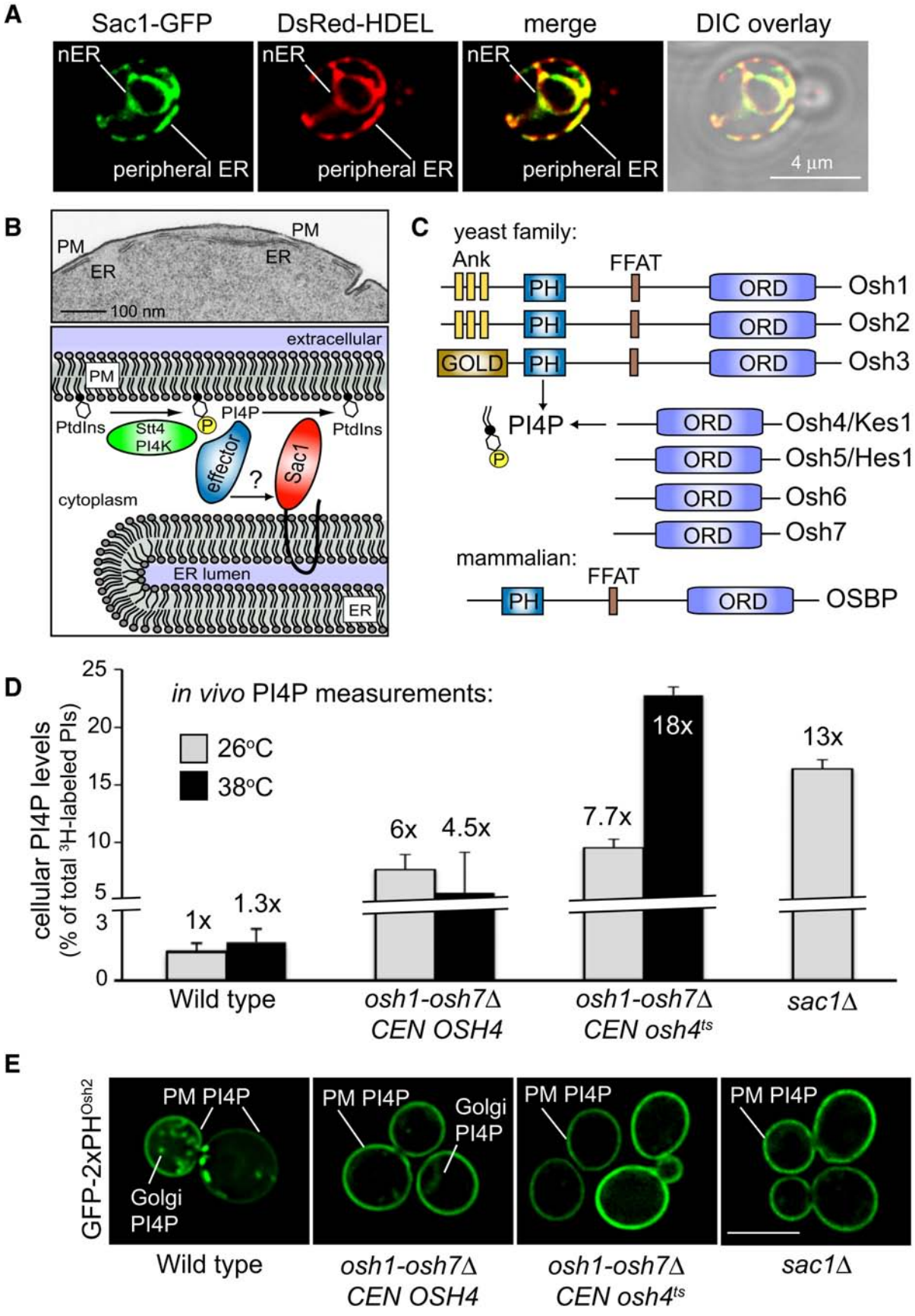
A
Sac1-GFP
DsRed-HDEL
merge
DIC overlay
nER
peripheral ER
4 μm
B
PM
ER
100 nm
extracellular
PtdIns
Stt4 PI4K
PI4P
effector
Sac1
cytoplasm
ER lumen
C
yeast family:
Ank
FFAT
PH
ORD
GOLD
Osh1
Osh2
Osh3
Osh4/Kes1
Osh5/Hes1
Osh6
Osh7
mammalian:
OSBP
D
in vivo PI4P measurements:
26°C
38°C
cellular PI4P levels
(% of total 3H-labeled PIs)
1x
1.3x
6x
4.5x
7.7x
18x
13x
Wild type
osh1-osh7Δ CEN OSH4
osh1-osh7Δ CEN osh4ts
sac1Δ
E
GFP-2xPHOsh2
PM PI4P
Golgi PI4P
Wild type
osh1-osh7Δ CEN OSH4
osh1-osh7Δ CEN osh4ts
sac1Δ

**Figure 2.1. The yeast oxysterol-binding proteins control PI4P metabolism.**

(A) Sac1-GFP localizes to the ER (marked by DsRed-HDEL). Peripheral ER and nuclear ER (nER) compartments are labeled. Scale bar = 4μm. See also Figure 2.2B.

(B) Electron microscopy of a region of a yeast spheroplast showing proximity between cortical ER and the PM (top, scale bar = 100nm). Model for PI4P metabolism at PM/ER membrane contact sites (bottom).

(C) Diagram of the oxysterol binding homology (Osh) proteins and OSBP. ORD, OSBP-related sterol binding domain; FFAT, di-phenalanines within an acidic track; PH, pleckstrin homology domain; GOLD, Golgi localization domain; Ank, ankyrin repeats

(D) Cellular PI4P levels measured by $^{3}$H-inositol labeling and HPLC analysis for wild type, *osh*Δ [*CEN OSH4*], *osh*Δ [*CEN osh4$^{ts}$*], and *sac1*Δ cells at 26$^{o}$C (grey) and 38$^{o}$C (black). Error bars are the SD of three experiments. See also Figure 2.2C and Table 2.3.

(E) PI4P localization in wild type, *osh*Δ [*CEN OSH4*], *osh*Δ [*CEN osh4$^{ts}$*], and *sac1*Δ cells. Wild type, *osh*Δ [*CEN OSH4*], and *osh*Δ [*CEN osh4$^{ts}$*] cells carrying GFP-2xPH$^{Osh2}$ were shifted to 38°C for 1 hour; *sac1*Δ cells were observed at 26$^{o}$C. Scale bar = 4μm.

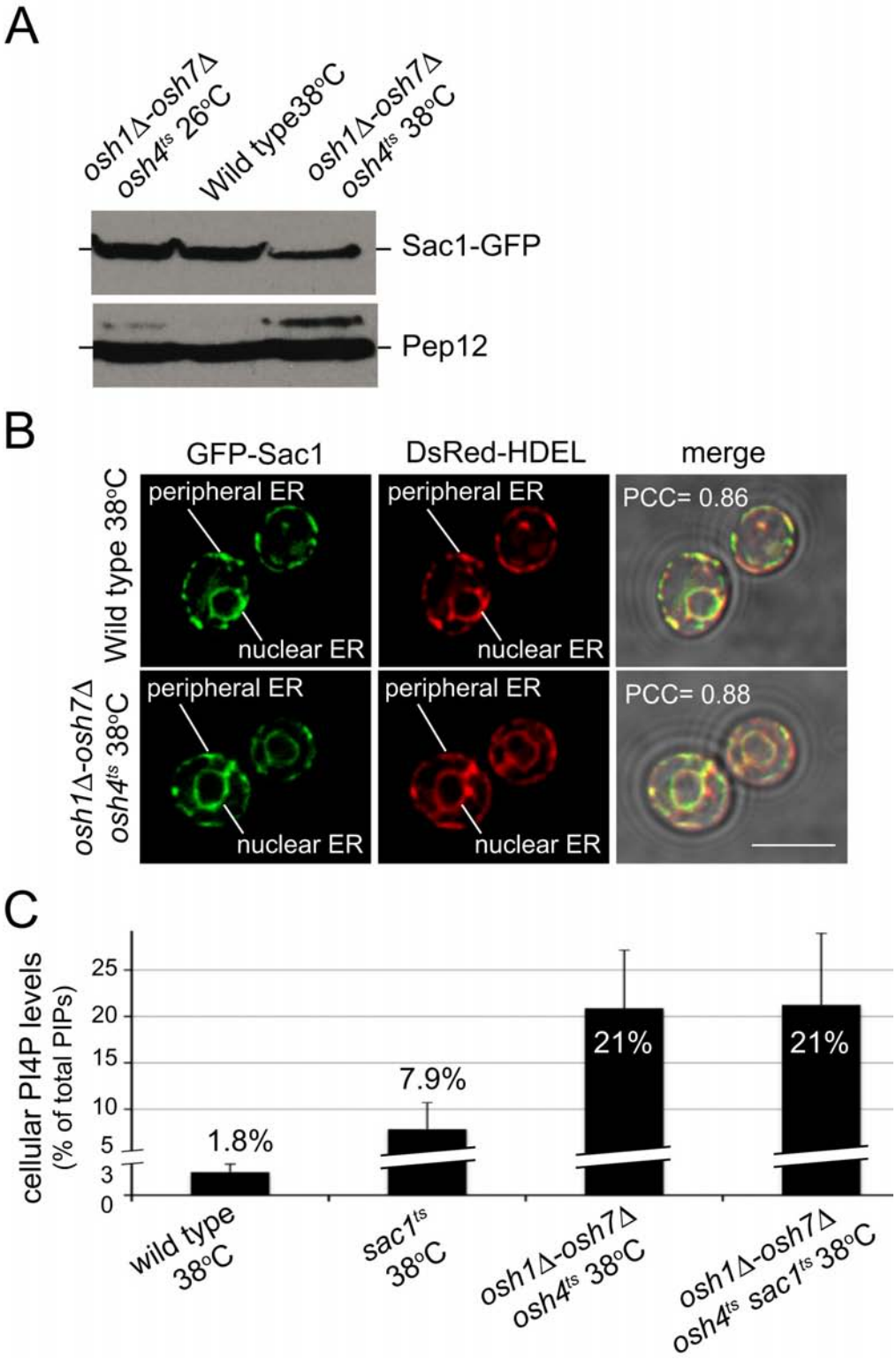
A
osh1Δ-osh7Δ osh4ts 26°C
Wild type38°C
osh1Δ-osh7Δ osh4ts 38°C
Sac1-GFP
Pep12
B
GFP-Sac1
DsRed-HDEL
merge
Wild type 38°C
osh1Δ-osh7Δ osh4ts 38°C
peripheral ER
nuclear ER
PCC= 0.86
PCC= 0.88
C
cellular PI4P levels (% of total PIPs)
25
20
15
10
5
3
0
1.8%
7.9%
21%
21%
wild type 38°C
sac1ts 38°C
osh1Δ-osh7Δ osh4ts 38°C
osh1Δ-osh7Δ osh4ts sac1ts 38°C

**Figure 2.2. Sac1 expression, localization, and function in cells lacking Osh protein function.**

(A) Steady-state Sac1-GFP expression levels in *osh1-7*Δ *osh4*$^{ts}$ cells at 26°C, wild type cells at 38°C, and *osh1-7*Δ *osh4*$^{ts}$ cells at 38°C. Pep12 was followed as a loading control. Cultures were incubated at the indicated temperature for 90 minutes.

(B) GFP-Sac1 localizes to the ER (marked with DsRed-HDEL) in wild type and *osh1-7*Δ *osh4*$^{ts}$ cells at 38°C. Peripheral ER and nuclear ER are labeled. Pearson correlation coefficients (PCC) between GFP-Sac1 and DsRed-HDEL are shown for each cell. Scale bar = 4μm.

(C) Sac1 and the Osh proteins function in a common pathway. Cellular PI4P levels were measured by $^{3}$H-inositol labeling and HPLC analysis for wild type, *sac1*$^{ts}$, *osh1-osh7*Δ [*CEN osh4*$^{ts}$], and *osh1-osh7Δ sac1*Δ [*CEN osh4*$^{ts}$ *sac1*$^{ts}$] cells. Cells were pre-shifted 38°C for 10 minutes and prior to labeling for 1 hour at 38$^{o}$C. Error bars represent SD of four independent experiments.

members of the oxysterol-binding protein homology family (Figure 2.1C). Osh2 and Osh3 possess PH domains that bind PI4P and localize to cortical, punctate structures (Figures 2.1C, 2.3A, 2.4; Levine and Munro, 2001; Roy and Levine, 2004). Osh1 also contains a PH domain, but localizes to the Golgi and nuclear-vacuolar membrane junction sites (Levine and Munro, 2001). Osh1, Osh2, and Osh3 are similar to mammalian oxysterol-binding protein (OSBP) that contains a PI4P-binding PH domain (Figure 2.1C). These proteins are members of the OSBP-related protein (ORP) family that contain sterol-binding OSBP-related domains (ORD; Figure 2.1C). Among the ORP family, Osh4/Kes1 does not possess a PH domain, but also binds PI lipids (Figure 2.1C; Li et al., 2002). Osh4/Kes1 is also known to regulate PI4P levels at the Golgi (Fairn et al., 2007; Li et al., 2002). Given the properties of the Osh protein family to bind PI4P, regulate PI4P (in the case of Osh4/Kes1), and to localize to membrane contact sites, we further examined the role of the Osh proteins in PI4P metabolism.

First, we measured PI4P levels in cells lacking Osh protein function. For this, we utilized strains that lack the *OSH1-OSH7* genes and carry wild type *OSH4* or a temperature sensitive allele, *osh4-1*, on a plasmid, as loss of all Osh proteins is lethal (*osh*Δ:*CEN OSH4* or *osh*Δ:*CEN* $osh4^{ts}$ cells; Beh and Rine, 2004). In $^{3}$H-inositol labeling experiments, PI4P levels were 6 to 7-fold higher than wild type cells in *osh*Δ:*CEN OSH4* and *osh*Δ:*CEN* $osh4^{ts}$ cells at the permissive temperature (26$^{o}$C, Figure 2.1D), suggesting that Osh proteins (other than Osh4) control PI4P levels *in vivo*. At the restrictive temperature for *osh*Δ:*CEN* $osh4^{ts}$ cells, PI4P levels were elevated 18-fold above wild type levels (38$^{o}$C, Figure 2.1D) and were greater than PI4P levels in *sac1*Δ mutant cells (13-fold above wild type; Figure 2.1D). Expression levels of a Sac1-GFP fusion were slightly reduced in *osh*Δ:*CEN* $osh4^{ts}$ mutant cells at 38$^{o}$C (approximately three-fold; Figure 2.2A). This did not account for the 18-fold increase in PI4P in *osh*Δ:*CEN* $osh4^{ts}$ cells, as

complete loss of Sac1 resulted in only a 13-fold increase in PI4P (*sac1*Δ cells; Figure 2.1D). Moreover, GFP-Sac1 localized to both nuclear and peripheral ER compartments in wild type and *osh*Δ:*CEN osh4*$^{ts}$ cells at 38$^{o}$C (Figure 2.2B). The 18-fold increase in PI4P levels in *osh*Δ:*CEN osh4*$^{ts}$ mutant cells resembled levels previously reported for triple mutant *sac1*$^{ts}$ *sjl2*Δ *sjl3*Δ cells (Foti et al., 2001), suggesting that the Osh proteins may regulate multiple Sac1-like PI phosphatase activities. We also examined PI4P levels in cells lacking both Sac1 and Osh protein function to test for additive effects. PI4P levels were not further elevated in *sac1*$^{ts}$ *osh*Δ:*CEN osh4*$^{ts}$ cells compared to *osh*Δ:*CEN osh4*$^{ts}$ cells at 38$^{o}$C (Figure 2.2C, Table 2.3) suggesting that Sac1 and the Osh proteins act in a common pathway. Together, these results implicate the Osh proteins in PI4P metabolism and Sac1 phosphatase function.

Using the PI4P FLARE (fluorescent lipid-associated reporter) GFP-2xPH$^{Osh2}$, PI4P is found, in wild type cells, at Golgi compartments and the PM via Pik1 and Stt4 PI 4-kinase activities, respectively (Figure 2.1E; Roy and Levine, 2004). In contrast, the PI4P FLARE was stabilized at the PM in *osh*Δ:*CEN OSH4* and *osh*Δ:*CEN osh4*$^{ts}$ cells, although weak fluorescence at intracellular puncta was detected (Figure 2.1E). The PI4P FLARE was also increased at the PM in *sac1*Δ cells, consistent with elevated levels of Stt4-generated PI4P at the PM (Figure 2.1E; Baird et al., 2008; Foti et al., 2001; Roy and Levine, 2004). While previous studies have implicated one Osh family member, Osh4/Kes, in PI4P regulation at the Golgi (Fairn et al., 2007; Li et al., 2002), our results suggested that additional Osh proteins control PI4P metabolism at the PM.

**Osh2 and Osh3 Localize to PM/ER Contact Sites in a PI4P-Dependent Manner**

Several lines implicated Osh2 and Osh3 in the control of PI4P metabolism at the PM. First, both bind PI4P and localize to cortical structures (Figures 2.1C, 2.3A, 2.4A; Levine and Munro, 2001; Roy and Levine, 2004; Schulz et al., 2009). Second, expression of *OSH2* or *OSH3* from a plasmid partially rescued the increased PI4P levels in *osh*Δ:*CEN osh4*$^{ts}$ mutant cells at 38$^{o}$C (from 18-fold above wild type to 5 and 8-fold, respectively; Table 2.3). Third, *osh2*Δ *osh3*Δ double mutant cells displayed elevated PI4P levels as measured by $^{3}$H-inositol labeling experiments (2.7-fold above wild type; Figure 2.3B, Table 2.3). Lastly, the PI4P FLARE was stabilized at the PM in *osh2*Δ *osh3*Δ double mutant cells (particularly in mother cells), compared to wild type cells (Figure 2.3B).

We examined if Osh3 localized to PM/ER membrane contact sites in order to regulate PI4P at the PM. Osh3-GFP localized to cortical patches often associated with cortical ER (cER) compartments marked with DsRed-HDEL (Figure 2.3A, arrows), as well as the PM stained with filipin (Figure 2.4A). To confirm that Osh3 patches associated with cER, we examined Osh3-GFP localization in cells lacking the reticulons Rtn1, Rtn2, and Yop1, as the cER displays expanded sheet-like structures in these mutant cells (Voeltz et al., 2006). Osh3-GFP patches clustered at cER compartments (marked with DsRed-HDEL) adjacent to the PM (stained with filipin) in *rtn1*Δ *rtn2*Δ *yop1*Δ triple mutant cells and was absent from regions lacking cER structures (Figure 2.4A). Together, our results suggested that Osh3 localizes to PM/ER membrane contact sites and modulates PM PI4P levels, possibly by regulation of cER-localized Sac1.

Osh3 localization did not always coincide with cER compartments (Figure 2.3A, asterisk), suggesting that its assembly at PM/ER membrane contact sites may be dynamic and progress in regulated stages. Thus, we tested if Osh3 localization and function required PM PI4P.

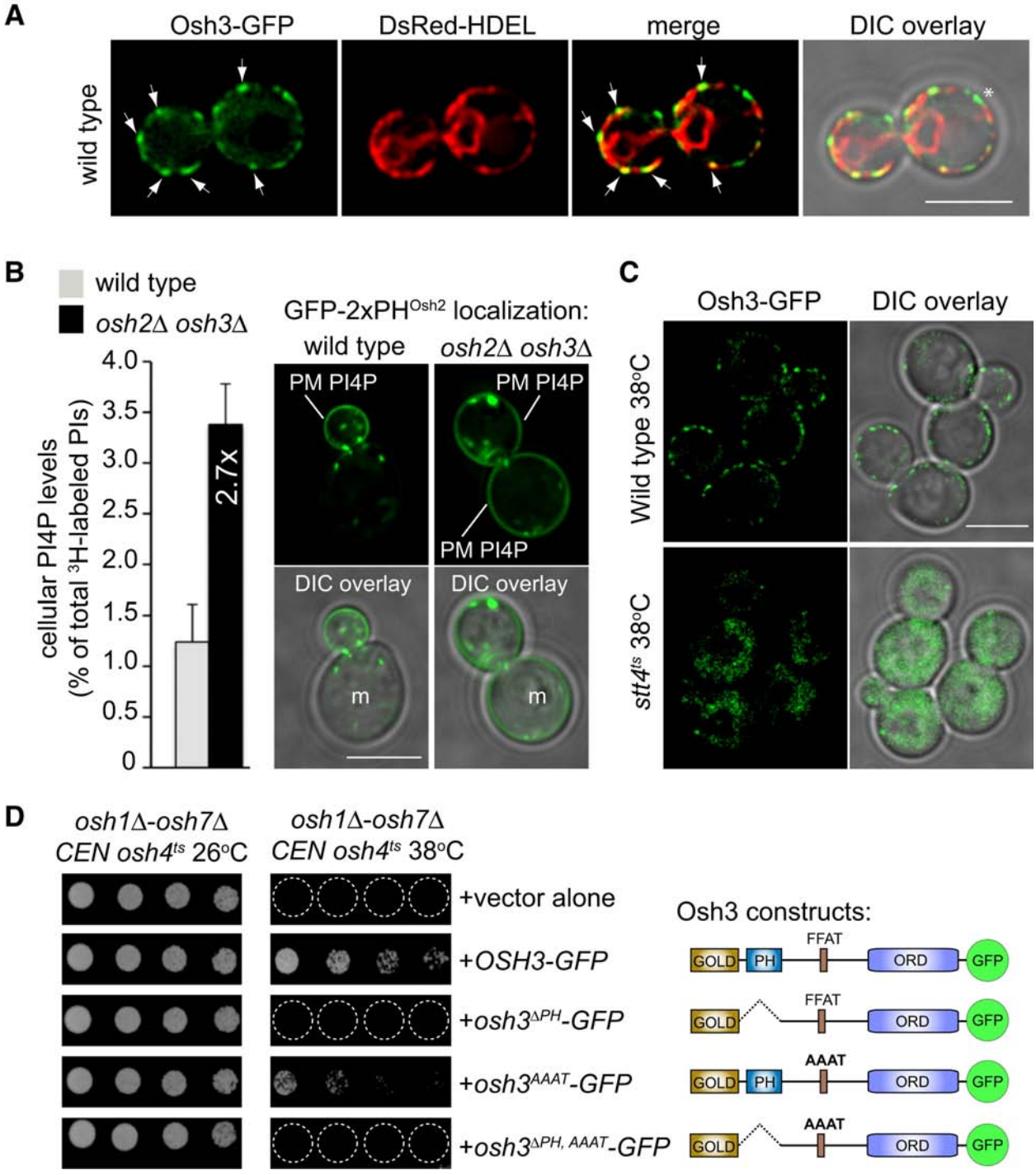
A
Osh3-GFP
DsRed-HDEL
merge
DIC overlay
wild type
B
wild type
osh2Δ osh3Δ
cellular PI4P levels
(% of total 3H-labeled PIs)
4.0
3.5
3.0
2.5
2.0
1.5
1.0
0.5
0
2.7x
GFP-2xPHOsh2 localization:
wild type
osh2Δ osh3Δ
PM PI4P
PM PI4P
PM PI4P
DIC overlay
DIC overlay
m
m
C
Osh3-GFP
DIC overlay
Wild type 38°C
stt4ts 38°C
D
osh1Δ-osh7Δ
CEN osh4ts 26°C
osh1Δ-osh7Δ
CEN osh4ts 38°C
+vector alone
+OSH3-GFP
+osh3ΔPH-GFP
+osh3AAAT-GFP
+osh3ΔPH, AAAT-GFP
Osh3 constructs:
GOLD
PH
FFAT
ORD
GFP
AAAT

**Figure 2.3. Osh2 and Osh3 localize to PM/ER contact sites and control PM PI4P.**

(A) Osh3-GFP localization in wild type cells coexpressing the DsRed-HDEL ER marker. Arrows show Osh3-GFP puncta associated with cortical ER. The asterisk shows an Osh3-GFP patch not associated with the cortical ER. See also Figure 2.4A.

(B) Cellular PI4P levels in wild type and *osh2*Δ *osh3*Δ mutant cells measured by $^{3}$H-inositol labeling and HPLC analysis (left). Error bars are the SD of three experiments. See also Table 2.3. GFP-2xPH$^{Osh2}$ (PI4P) localization in wild type or *osh2*Δ *osh3*Δ mutant cells (right). Mother cells are indicated (m).

(C) Osh3-GFP localization in wild type or *stt4*$^{ts}$ cells at 38°C. Levels were enhanced using Adobe Photoshop in the DIC overlay image for *stt4* mutant cells (lower left). See also Figure 2.4B.

(D) Growth of *osh*Δ [*CEN osh4*$^{ts}$] cells coexpressing *OSH3* alleles. Serial dilutions of cells carrying empty vector or Osh3-GFP constructs were incubated at 26°C and 38°C. Osh3-GFP mutant constructs: AAAT, substitution of phenylalanines in the FFAT motif with alanine, DPH, deletion of the PH domain. See also Figure 2.4C.

Scale bars = 4μm.

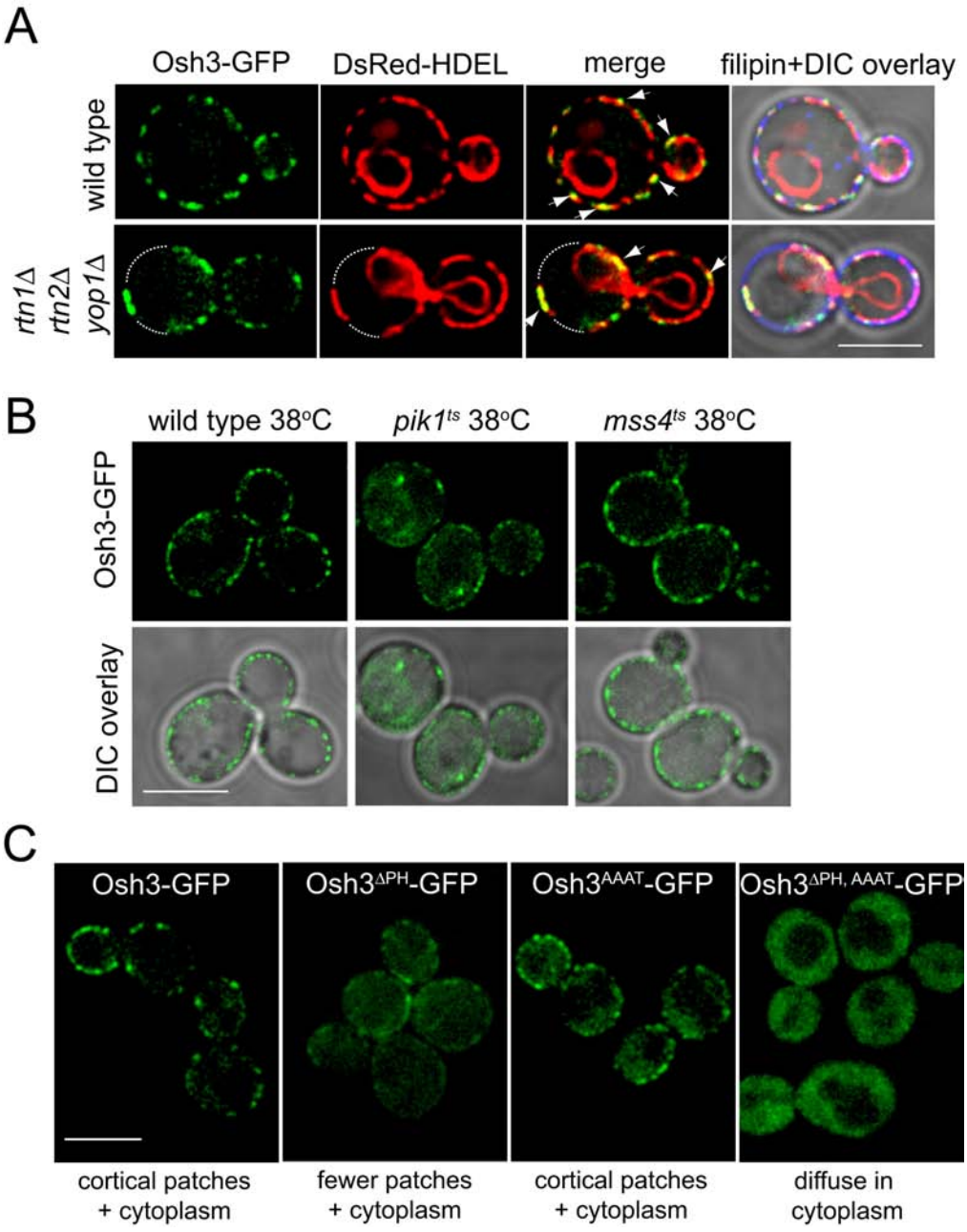
A
Osh3-GFP
DsRed-HDEL
merge
filipin+DIC overlay
wild type
rtn1Δ rtn2Δ yop1Δ
B
wild type 38°C
pik1ts 38°C
mss4ts 38°C
Osh3-GFP
DIC overlay
C
Osh3-GFP
Osh3ΔPH-GFP
Osh3AAAT-GFP
Osh3ΔPH, AAAT-GFP
cortical patches + cytoplasm
fewer patches + cytoplasm
cortical patches + cytoplasm
diffuse in cytoplasm

**Figure 2.4. Osh3 localizes to PM/ER contact sites.**

(A) Osh3-GFP localization in wild type cells co-expressing the DsRed-HDEL ER marker (top). Arrows show Osh3-GFP puncta associated with cortical ER structures. The PM was stained with the sterol-binding dye filipin. Osh3-GFP and DsRed-HDEL localization in cells lacking the reticulons Rtn1, Rtn2, and Yop1 (bottom). Arrows indicate overlap between Osh3-GFP, DsRed-HDEL, and the PM stained with filipin. Peripheral regions devoid of cortical ER and Osh3-GFP are highlighted by dashed lines.

(B) Osh3 localization to cortical patches is independent of $PI(4,5)P_2$ and Golgi PI4P pools. Osh3-GFP in wild-type, *pik1*$^{ts}$, or *mss4*$^{ts}$ cells at 38°C. Cells were shifted to 38°C for one hour prior to being observed.

(C) Osh3 localization depends on its PH domain and FFAT motif. Localization of wild type Osh3-GFP and various Osh3-GFP mutants expressed from a plasmid in *osh3*Δ cells is shown. Scale bars = 4μm.

Osh3-GFP localized diffusely in the cytoplasm in cells with impaired Stt4 PI 4-kinase activity (*stt4*$^{ts}$ cells; Figure 2.3C), showing that Osh3 localization required PM PI4P synthesis. In contrast, Osh3-GFP was present at the PM in *pik1*$^{ts}$ mutant cells impaired in PI4P synthesis at the Golgi, although Osh3 was observed at intracellular structures in these cells (Figure 2.4B). Likewise, Osh3-GFP localized to cortical patches in cells with reduced PI(4,5)$P_2$ levels (*mss4*$^{ts}$ cells; Figure 2.4B). A form of Osh3 lacking its PH domain (Osh3 $^{\Delta PH}$-GFP) did not rescue the growth defects of *osh*Δ:*CEN osh4*$^{ts}$ mutant cells at 38$^{o}$C (Figure 2.3D). In addition, Osh3 $^{\Delta PH}$-GFP displayed increased cytoplasmic localization, compared to wild type Osh3-GFP (Figure 2.4C). Thus, the assembly of Osh3 at cortical patches required PM PI4P synthesis, consistent with its ability to bind PI4P and control PM PI4P levels.

Next we asked if other regions in Osh3 play a role in its function. Osh3 contains an FFAT motif (di-phenyalanines within an acidic track; Figures 2.1C, 2.3D, 2.5A). FFAT motifs bind the MSP domains of the yeast ER membrane proteins Scs2 and Scs22, orthologs of the mammalian ER membrane VAP proteins (Figure 2.5A; Kaiser et al., 2005; Loewen et al., 2003). A form of Osh3 bearing substitutions in the FFAT motif (Osh3$^{AAAT}$-GFP) partially rescued the growth defects of *osh*Δ:*CEN osh4*$^{ts}$ cells at 38$^{o}$C (Figure 2.3D) and assembled at cortical patches (Figure 2.4C). A previous study reported that a mutant form of Osh3 with substitutions in the FFAT motif was mislocalized from the cortical ER (Loewen et al., 2003). However, this study used a GFP-Osh3 fusion that required Scs2 overexpression to target to the cortical ER. Consistent with this previous study, we found that Osh3-GFP targeting to the cortical ER was impaired in *scs2*Δ *scs22*Δ double mutant cells (see Figure 2.6D). As expected, substitution of the FFAT motif in combination with deletion of the PH domain (GFP-Osh3 $^{\Delta PH, AAAT}$; Figure 2.3D) resulted in inactivation of Osh3, as this mutant protein did not rescue the growth defect of *osh*Δ:*CEN osh4*$^{ts}$

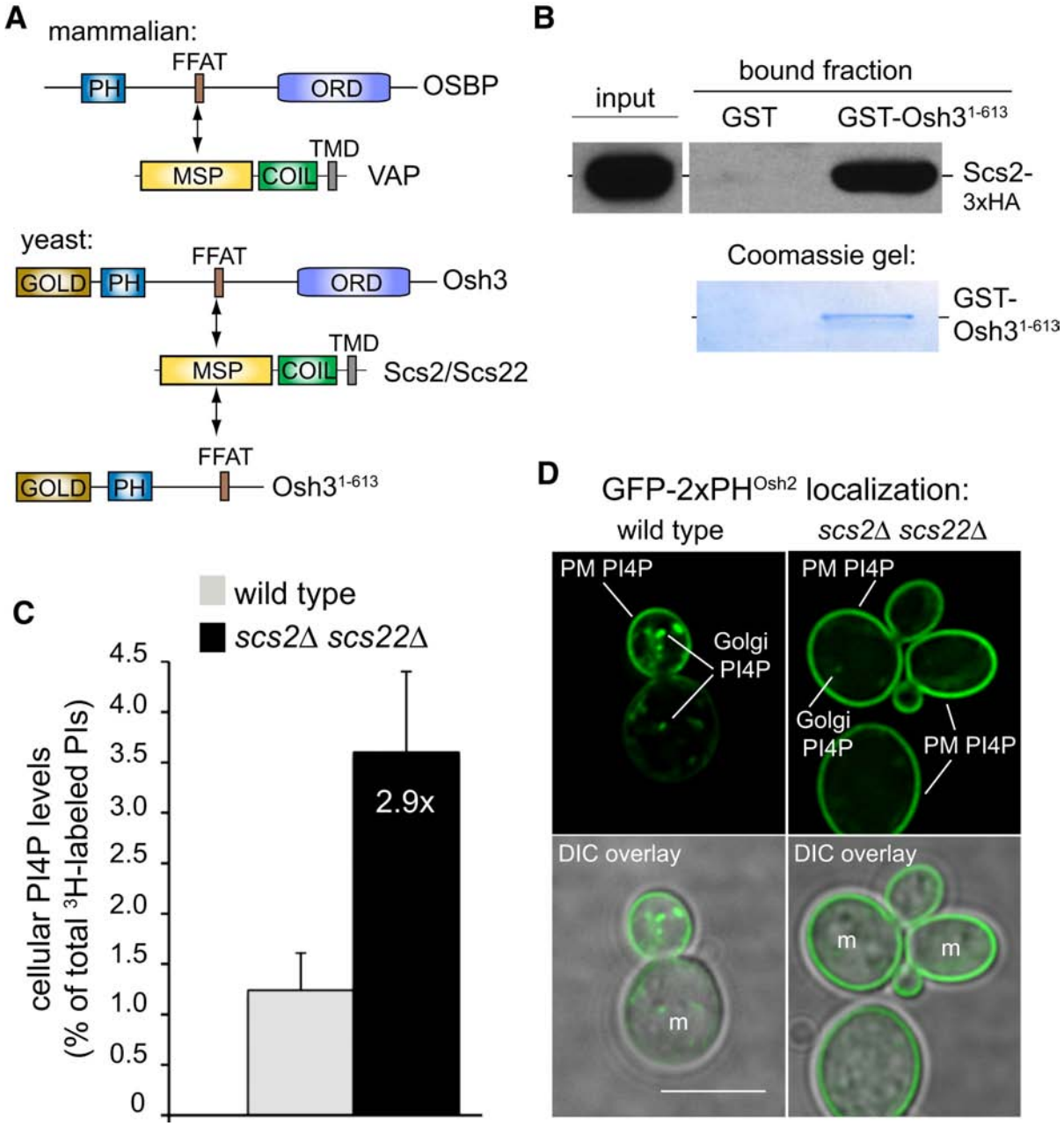
A
mammalian:
FFAT
PH
ORD
OSBP
TMD
MSP
COIL
VAP
yeast:
FFAT
GOLD
PH
ORD
Osh3
TMD
MSP
COIL
Scs2/Scs22
FFAT
GOLD
PH
Osh3^1-613
B
bound fraction
input
GST
GST-Osh3^1-613
Scs2-
3xHA
Coomassie gel:
GST-
Osh3^1-613
C
wild type
scs2Δ scs22Δ
cellular PI4P levels
(% of total ³H-labeled PIs)
4.5
4.0
3.5
3.0
2.5
2.0
1.5
1.0
0.5
0
2.9x
D
GFP-2xPH^Osh2 localization:
wild type
scs2Δ scs22Δ
PM PI4P
Golgi
PI4P
PM PI4P
Golgi
PI4P
PM PI4P
DIC overlay
DIC overlay
m
m
m

**Figure 2.5. The VAP proteins Scs2 and Scs22 control PM PI4P metabolism.**

(A) Diagrams of mammalian VAP, yeast Scs2/Scs22, OSBP, and Osh3. VAP proteins possess a major sperm protein domain (MSP), a coiled-coil, and a transmembrane domain (TMD).

(B) The GST-Osh3$^{1\text{-}613}$ fusion binds Scs2-3xHA from solubilized yeast lysates. GST alone does not bind Scs2-3xHA. Total input and bound fractions are shown.

(C) Cellular PI4P levels in wild type and *scs2*Δ *scs22*Δ cells measured by $^{3}$H-inositol labeling and HPLC analysis. Error bars show SD of three independent experiments. See also Table 2.3.

(D) Localization of GFP-2xPH$^{Osh2}$ (PI4P) in wild type and *scs2*Δ*scs22*Δ cells. Mother cells are indicated (m). Scale bar = 4μm. See also Figure 2.6.

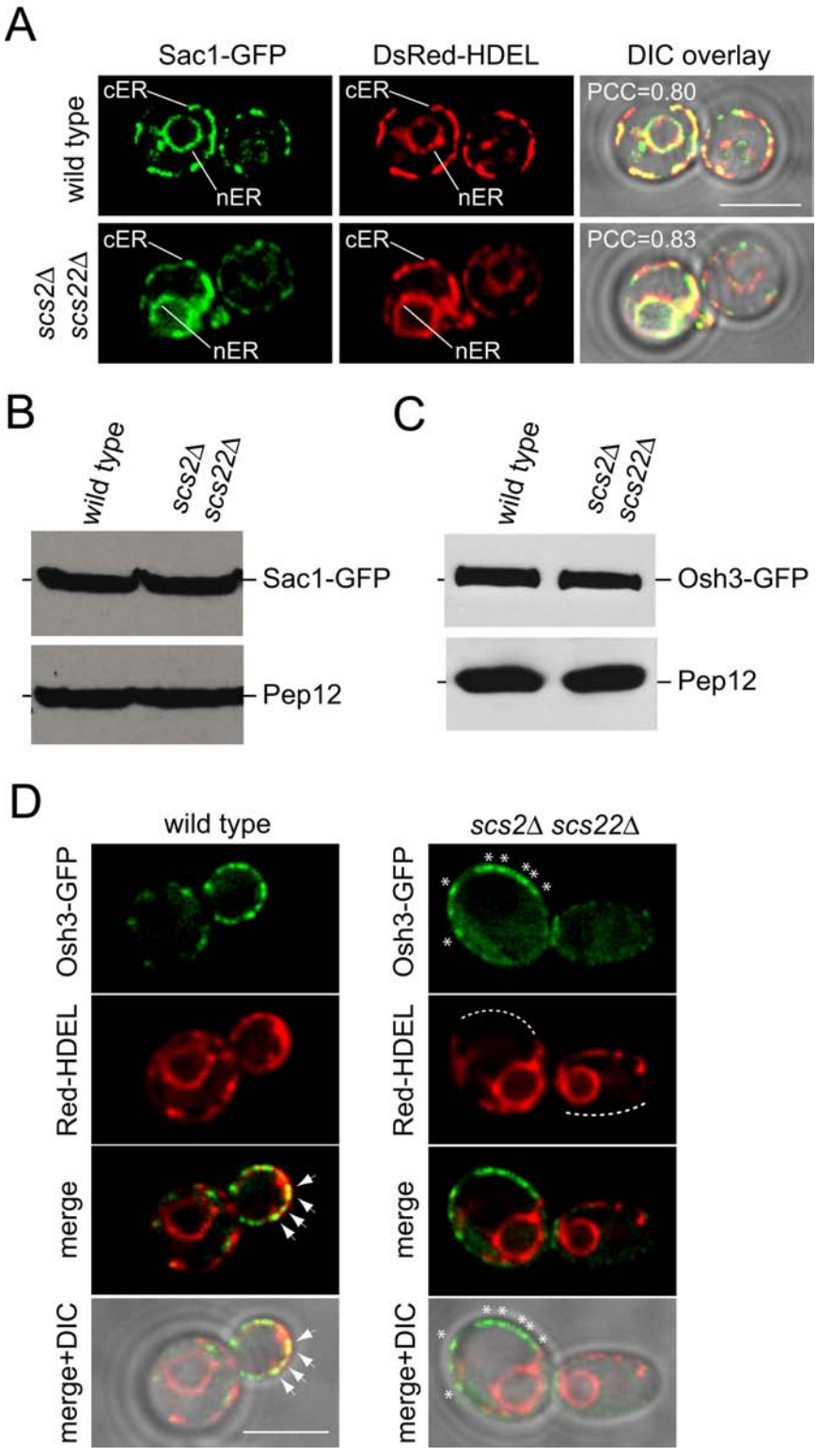
A
Sac1-GFP
DsRed-HDEL
DIC overlay
wild type
scs2Δ scs22Δ
cER
nER
PCC=0.80
PCC=0.83
B
wild type
scs2Δ scs22Δ
Sac1-GFP
Pep12
C
wild type
scs2Δ scs22Δ
Osh3-GFP
Pep12
D
wild type
scs2Δ scs22Δ
Osh3-GFP
Red-HDEL
merge
merge+DIC

**Figure 2.6. Sac1 and Osh3 expression and localization in cells lacking the VAP proteins.**

(A) Sac1-GFP localizes to the ER (marked with DsRed-HDEL) in wild type and *scs2*Δ *scs22*Δ cells. Peripheral ER and nuclear ER are labeled. Pearson correlation coefficients (PCC) between GFP-Sac1 and DsRed-HDEL are shown for each cell.

(B) Sac1-GFP expression levels are similar in lysates from wild type and *scs2*Δ *scs22*Δ cells as analyzed by immunoblotting using GFP antibodies. Pep12 is used as a loading control.

(C) Osh3-GFP expression levels are similar in lysates from wild type and *scs2*Δ *scs22*Δ cells as analyzed by immunoblotting using GFP antibodies. Pep12 is used as a loading control.

(D) Osh3-GFP localizes to cortical patches in wild type and *scs2*Δ *scs22*Δ cells. Osh3-GFP localization in wild type cells co-expressing the DsRed-HDEL ER marker (left). Arrows show Osh3-GFP puncta associated with cortical ER structures. Osh3-GFP and DsRed-HDEL localization in cells lacking the VAP proteins Scs2 and Scs22 (right). Osh3-GFP cortical puncta not localized with the cortical ER are indicated by asterisks. Peripheral regions devoid of cortical ER are highlighted by dashed lines.

Scale bars = 4μm.

cells (Figure 2.3D). Moreover, Osh3 $^{\Delta PH,AAAT}$-GFP localized diffusely in the cytoplasm, and not at cortical patches (Figure 2.4C). Thus, Osh3 undergoes multiple interactions involving at least PI4P and the Scs2/Scs22 VAP proteins to assemble and function at PM/ER membrane contact sites.

**The VAP Proteins Scs2 and Scs22 Regulate PI4P Metabolism**

We then addressed if the ER membrane VAP proteins Scs2/Scs22 control Osh3 function and PI4P metabolism. As FFAT motifs from OSBP and Osh proteins bind VAP proteins (Figure 2.5A; Kaiser et al., 2005; Loewen et al., 2003), we specifically confirmed interactions for Osh3 and Scs2. A GST-Osh3 N-terminal fragment containing the FFAT motif (GST-Osh3$^{1-613}$; Figure 2.5A) bound to glutathione-sepharose beads efficiently isolated an Scs2-3xHA fusion from solubilized cell extracts (Figure 2.5B). GST alone was unable to bind Scs2-3xHA (Figure 2.5B). We then tested if the VAP proteins Scs2/Scs22 impact PI4P metabolism. PI4P levels were elevated 2.9-fold above wild type in *scs2*Δ *scs22*Δ double mutant cells, as assessed by $^{3}$H-inositol labeling (Figure 2.5C; Table 2.3). The PI4P FLARE was also stabilized at the PM in *scs2*Δ *scs22*Δ double mutant cells, particularly in mother cells (the PI4P FLARE was also weakly observed at intracellular puncta; Figure 2.5D). Thus, Osh3 and Scs2 interact and the VAP proteins Scs2/Scs22 control PI4P levels at the PM.

We performed additional tests to address how the VAP proteins Scs2/Scs22 might control PI4P metabolism. Sac1-GFP localized to nuclear and cortical ER membrane compartments in *scs2*Δ *scs22*Δ double mutant cells (Figure 2.6A). Steady-state expression of Sac1-GFP and Osh3-GFP were unaffected in *scs2*Δ *scs22*Δ mutant cells, compared to wild type cells (Figures 2.6B, 2.6C). Thus while Sac1, Osh3, and the VAP proteins Scs2/Scs22 act in common to control

PI4P metabolism, the VAP proteins are not required for Sac1 or Osh3 stability. Similar to the cortical localization of Osh3$^{AAAT}$-GFP (Figure 2.4C), Osh3-GFP localized to cortical structures in *scs2*Δ *scs22*Δ mutant cells (Figure 2.6D). However, Osh3-GFP cortical patches did not appear to be associated with the peripheral ER in *scs2*Δ *scs22*Δ mutant cells (Figure 2.6D), consistent with a previous study (Loewen et al., 2003). These findings suggest that PI4P metabolism at PM/ER junctions may occur in regulated stages. Osh3 may initially assemble at the PM, possibly as a PI4P sensor via its PH domain. Subsequent interactions between Osh3 and the VAP proteins may lead to stimulation of Sac1 PI phosphatase activity at PM/ER junctions.

**The Osh and VAP Proteins Control Sac1 Phosphatase Activity**

To test if the VAP and Osh proteins regulate Sac1 activity, we set up an *in vitro* phosphatase assay using PI4P-containing liposomes (PC:PS:PI4P) and microsomes containing integral Sac1-GFP prepared from cellular membranes (Figures 2.7A, 2.8A). PI4P phosphatase activity was readily detected with wild type microsomes (145 pmol/mg total protein/min, at 10 min, Figure 2.7A) and was specifically due to Sac1-GFP, as microsomes prepared from *sac1*Δ cells lacked activity (Figure 2.7A). We also did not detect significant phosphatase activity using Sac1-GFP microsomal preps against liposomes lacking PI4P (PC:PS:PtdIns liposomes; Figure 2.8B). Thus, this *in vitro* assay followed microsome-embedded Sac1 activity against PI4P presented on liposomes, rather than PI species that might be present in the microsomes.

To confirm that liposomes did not fuse with Sac1-GFP microsomes or that PI4P did not transfer from liposomes to microsomes, we incubated Sac1-GFP microsomes with liposomes containing $^{3}$H-labeled PI4P and PI(4,5)$P_2$ (Figure 2.8C). Following a 30-minute incubation at 37$^{o}$C (the course of the phosphatase assays; Figures 2.7A, 2.8B), Sac1-GFP microsomes were

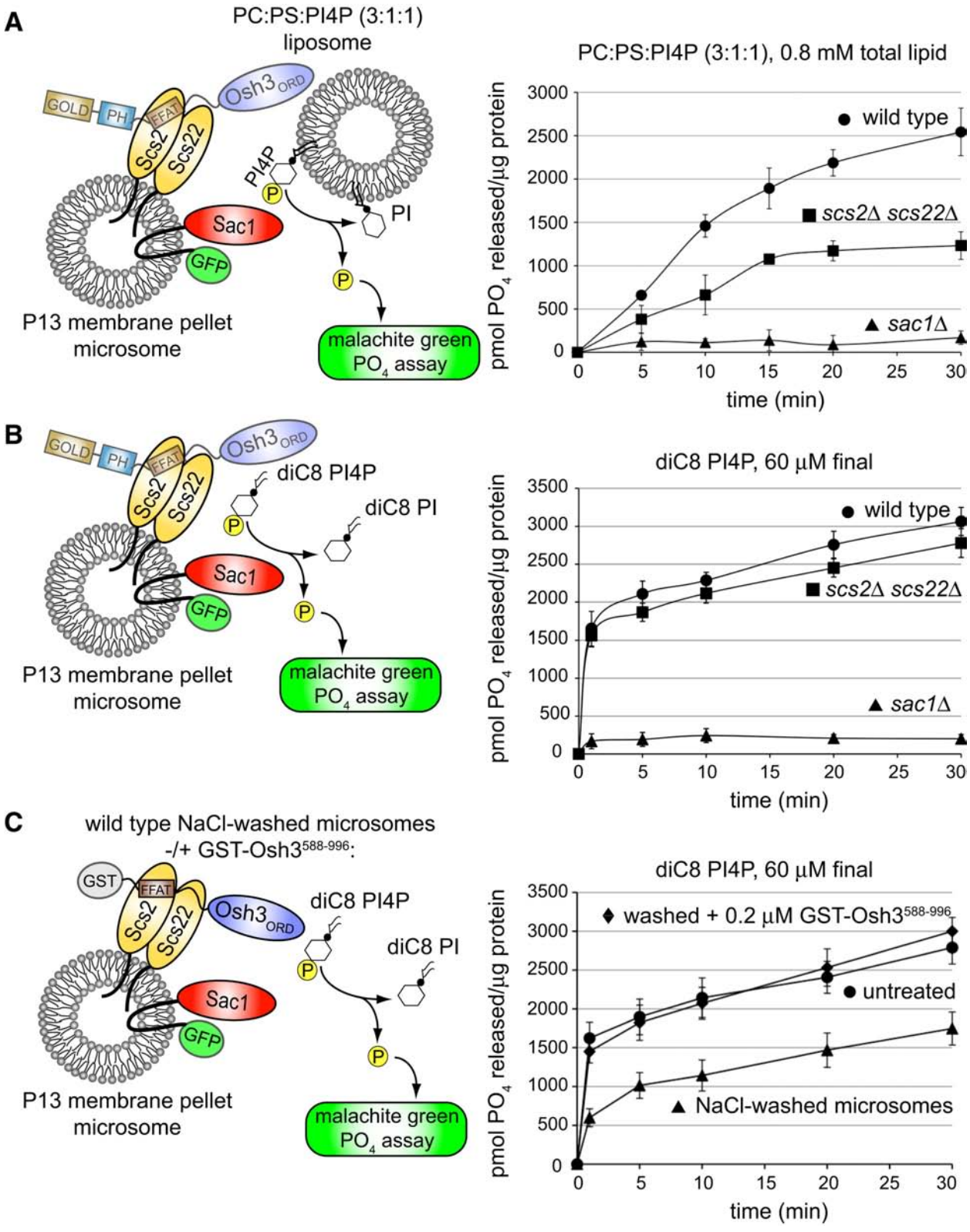
A
PC:PS:PI4P (3:1:1)
liposome
GOLD
PH
FFAT
Scs2
Scs22
Osh3 ORD
PI4P
P
PI
Sac1
GFP
P13 membrane pellet
microsome
malachite green
PO4 assay
PC:PS:PI4P (3:1:1), 0.8 mM total lipid
pmol PO4 released/µg protein
wild type
scs2Δ scs22Δ
sac1Δ
time (min)
B
diC8 PI4P
diC8 PI
diC8 PI4P, 60 µM final
C
wild type NaCl-washed microsomes
-/+ GST-Osh3588-996:
GST
washed + 0.2 µM GST-Osh3588-996
untreated
NaCl-washed microsomes

**Figure 2.7. The VAP proteins Scs2/Scs22 control Sac1 PI phosphatase activity *in vitro*.**

(A) PI4P-containing liposomes were incubated with wild-type (circles), *scs2*Δ *scs22*Δ (squares), or *sac1*Δ (triangles) microsomes for the indicated times. Phosphate release was measured by a malachite green assay. Error bars show the SD of two experiments measured in duplicate. See also Figure 2.8.

(B) Short acyl chain diC8 PI4P was incubated with wild-type (circles), *scs2*Δ *scs22*Δ (squares), or *sac1*Δ (triangles) microsomes for the indicated times. Error bars show the SD of two experiments measured in duplicate.

(C) Short acyl chain diC8 PI4P was incubated with untreated (circles), NaCl-washed (triangles), or NaCl-washed microsomes in the presence of GST-Osh3$^{588\text{-}996}$ (diamonds) for the indicated times. Error bars show the SD of two experiments measured in duplicate. See also Figure 2.10A.

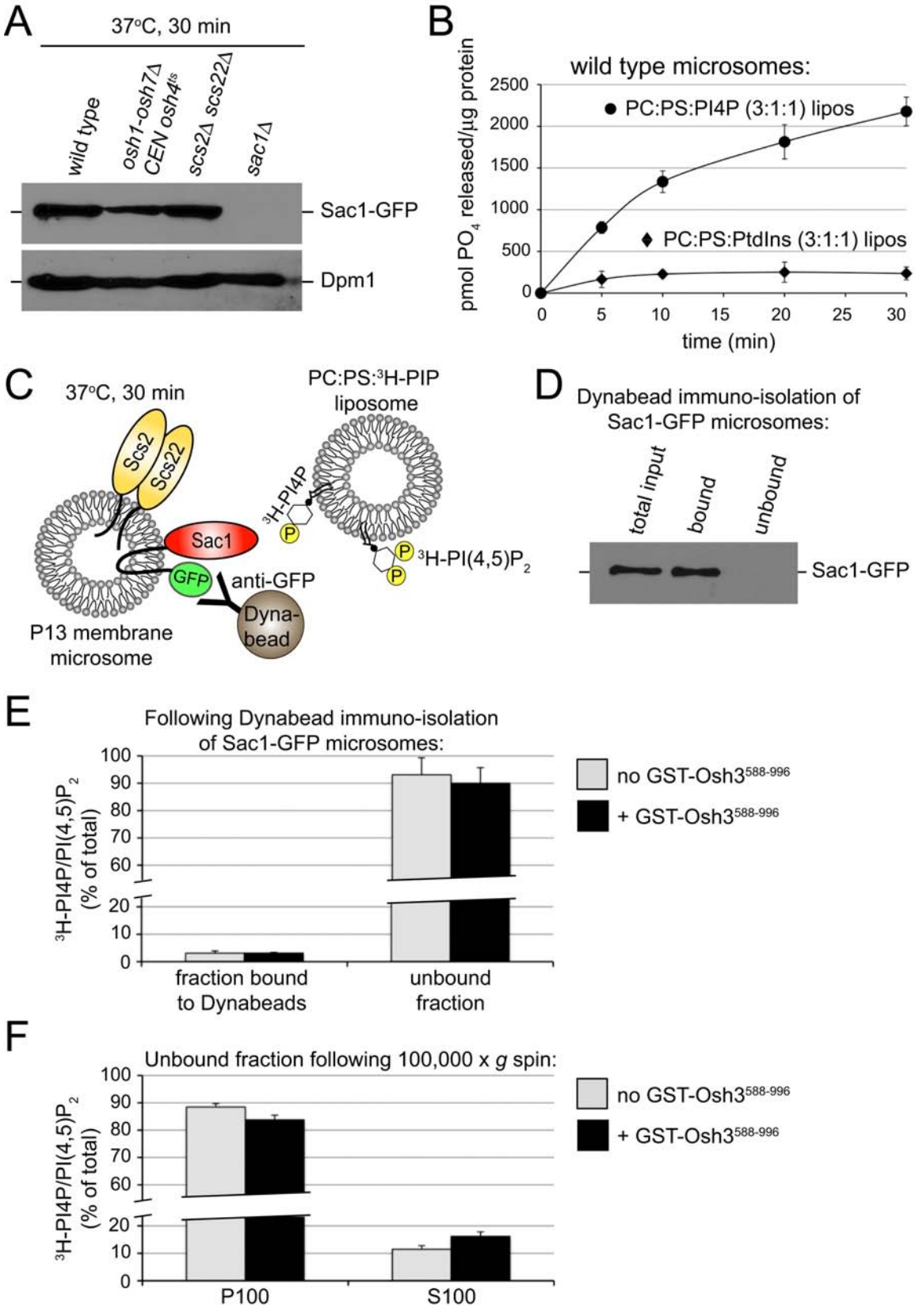
A
37°C, 30 min
wild type
osh1-osh7Δ CEN osh4ts
scs2Δ scs22Δ
sac1Δ
Sac1-GFP
Dpm1
B
wild type microsomes:
PC:PS:PI4P (3:1:1) lipos
PC:PS:PtdIns (3:1:1) lipos
pmol PO4 released/µg protein
time (min)
C
37°C, 30 min
PC:PS:3H-PIP liposome
Scs2
Scs22
Sac1
GFP
anti-GFP
Dyna-bead
3H-PI4P
3H-PI(4,5)P2
P13 membrane microsome
D
Dynabead immuno-isolation of Sac1-GFP microsomes:
total input
bound
unbound
Sac1-GFP
E
Following Dynabead immuno-isolation of Sac1-GFP microsomes:
3H-PI4P/PI(4,5)P2 (% of total)
no GST-Osh3588-996
+ GST-Osh3588-996
fraction bound to Dynabeads
unbound fraction
F
Unbound fraction following 100,000 x g spin:
3H-PI4P/PI(4,5)P2 (% of total)
no GST-Osh3588-996
+ GST-Osh3588-996
P100
S100

**Figure 2.8. The Osh3 ORD domain does not stimulate PI4P extraction or transfer *in vitro*.**

(A) Sac1-GFP levels in P13 microsomes isolated from wild type, *osh1-osh7*Δ [*CEN osh4*$^{ts}$], *scs2*Δ *scs22*Δ, and *sac1*Δ cells. Samples were incubated at 37˚C for 30 minutes (phosphatase reaction conditions) prior to immunoblotting. The ER membrane protein Dpm1 is used as a loading control.

(B) Liposomes containing PI4P (PC:PS:PI4P, circles) or liposomes without PI4P (PC:PS:PtdIns, diamonds) were incubated with P13 membrane fraction microsomes from wild type cells. Phosphate release was measure by a malachite green assay (Maehama et al., 2000). Liposomes lacking PI4P (PC:PS:PtdIns) show background phosphatase activity (diamonds). Error bars show SD of two independent experiments each performed in duplicate.

(C) Schematic diagram of the Sac1-GFP microsome/liposome fusion and lipid transfer control assay. Liposomes containing $^{3}$H-PI4P and $^{3}$H-PI(4,5)$P_2$ (PC:PS:$^{3}$H-PIP liposome) were incubated with P13 membrane fraction microsomes from wild type cells. Samples were incubated at 37˚C for 30 minutes (phosphatase reaction conditions) prior to immuno-isolation of Sac1-GFP microsomes using GFP antibodies and protein A-coupled magnetic Dynabeads.

(D) Examination of Sac1-GFP microsome immuno-isolation. Fractions shown are the total input, the fraction bound to magnetic Dynabeads, and the unbound fraction depleted of Sac1-GFP microsomes.

(E) Measurements of $^{3}$H-PI4P and $^{3}$H-PI(4,5)$P_2$ present in isolated Sac1-GFP microsome fractions and the fractions unbound to Dynabeads by scintillation counting. Sac1-GFP microsomes were incubated with PC:PS:$^{3}$H-PIP liposomes either in the absence (grey bars) or presence of 0.2 mM GST-Osh3$^{588\text{-}996}$ (black bars).

(F) Measurements of $^{3}$H-PI4P and $^{3}$H-PI(4,5)$P_2$ from the ubound fraction present in liposome pellet (P100), and supernatant fractions (S100) by liquid scintillation counting. Sac1-GFP microsomes were incubated with PC:PS:$^{3}$H-PIP liposomes either in the absence (grey bars) or presence of 0.2 mM GST-Osh3$^{588-996}$ (black bars).

immuno-isolated using anti-GFP antibodies and protein A-coupled magnetic Dynabeads (Figure 2.8D). Unbound liposomes (and microsomes not containing Sac1-GFP) were subsequently sedimented by high-speed centrifugation. The amount of $^{3}$H-PI species in isolated Sac1-GFP microsomes, sedimented liposomes, and the resulting supernatant fraction was determined by liquid scintillation counting. Only a minor portion, 3.1±0.9% of the total $^{3}$H-PI, associated with isolated Sac1-GFP microsomes (Figure 2.8E, bound fraction). The bulk of $^{3}$H-PI, 93.1±6.2%, remained in the unbound fraction (Figure 2.8E). 88.5±1.3% of $^{3}$H-PI in the unbound fraction sedimented upon high-speed centrifugation (Figure 2.8F, P100 fraction), indicating that the majority of $^{3}$H-PI in the unbound fraction remained in a membrane bilayer. A small amount of the unbound fraction, 11.5±1.2%, was found in the supernatant fraction, perhaps due to micelles that did not sediment (Figure 2.8F, S100 fraction). Thus, liposomes did not fuse with Sac1-GFP microsomes and $^{3}$H-PI species were not efficiently transferred from liposomes to Sac1-GFP microsomes, under conditions that resulted in efficient dephosphorylation of PI4P in liposomes (Figures 2.7A, 2.8B). We also performed experiments in the presence of recombinant Osh3 (GST-Osh3$^{588\text{-}996}$ including the FFAT and ORD domain, see Figure 2.9A). However, the distribution of $^{3}$H-PI species was not significantly affected by the addition of GST-Osh3$^{588\text{-}996}$ (Figures 2.8E and 2.8F). Similarly, purified his$_6$-Osh4 (see Figure 2.9A) did not significantly alter the distribution of $^{3}$H-PI species in analogous experiments (our unpublished results). Thus, Osh3 and Osh4 did not enhance membrane fusion or $^{3}$H-PI transfer between liposomes and Sac1-GFP microsomes.

Following these control experiments, we addressed whether the VAP proteins controlled Sac1 PI phosphatase activity. Microsomes lacking Scs2 and Scs22 were impaired in the initial rate of PI4P turnover (more than two-fold: 66 pmol/mg total protein/min, at 10 min; as compared

to wild type, Figure 2.7A). In addition, *scs2*Δ *scs22*Δ microsomes were impaired in maximal Sac1 phosphatase activity as compared to wild type microsomes (1232±159 pmol $PO_4$ released versus 2543±274 pmol, respectively; Figure 2.7A). Levels of Sac1-GFP and the ER protein Dpm1 were similar in both wild type and *scs2*Δ *scs22*Δ microsomal preparations (Figure 2.8A). Thus, while Sac1-GFP levels were similar, Sac1 activity was impaired in *scs2*Δ *scs22*Δ microsomes. Importantly, these experiments provide the first *in vitro* demonstration of Sac1 activity *in trans* and indicate that the yeast VAP proteins promote this activity.

Wild type and *scs2*Δ *scs22*Δ microsomes demonstrated similar activity against a soluble substrate, short acyl chain diC8 PI4P (in the absence of other lipids; Figure 2.7B), indicating that both microsomal preps contained similar intrinsic Sac1 activity. As in the PI4P liposome assay, microsomes isolated from *sac1*Δ cells did not display activity against diC8 PI4P (Figure 2.7B). Notably, both wild type and *scs2*Δ *scs22*Δ microsomes displayed increased activity for the soluble diC8 PI4P substrate (approximately 1500 pmol $PO_4$ released/mg total protein/min, after 1 minute; Figure 2.7B). At later time points both preps continued to display similar turnover rates, although slower likely due to reduced substrate concentrations. Thus, the VAP proteins Scs2/Scs22 may act to link Sac1 to substrates on opposing membranes, possibly through the FFAT-containing Osh proteins, Osh2 and Osh3.

We then tested if the Osh proteins stimulate Sac1 activity *in vitro*. As Sac1 levels were reduced in *osh*Δ:*CEN osh4*$^{ts}$ cell lysates (Figures 2.2B, 2.8A), we did not use microsomes prepared from these mutant cells. However, we found that Osh3 was depleted from membrane fractions by incubation in high salt (our unpublished results). Sac1-GFP microsomes were then subjected to a high salt wash to deplete peripherally associated membrane proteins, such as Osh3. Sac1-containing microsomes were not active against PI4P-containing liposomes following

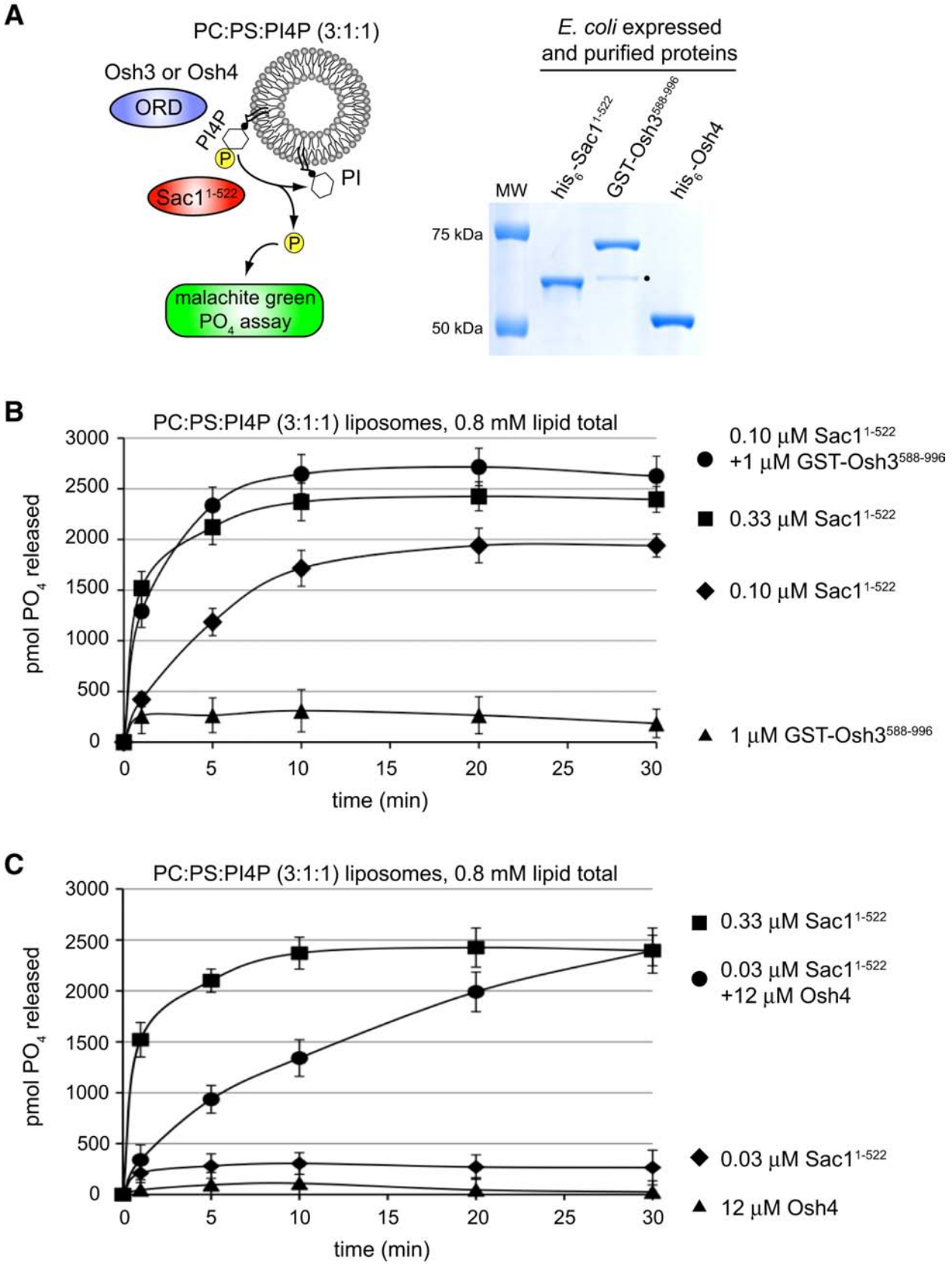
A
PC:PS:PI4P (3:1:1)
Osh3 or Osh4
ORD
PI4P
P
PI
Sac1^1-522
malachite green
PO4 assay
E. coli expressed
and purified proteins
MW
his6-Sac1^1-522
GST-Osh3^588-996
his6-Osh4
75 kDa
50 kDa
B
PC:PS:PI4P (3:1:1) liposomes, 0.8 mM lipid total
pmol PO4 released
time (min)
0.10 μM Sac1^1-522
+1 μM GST-Osh3^588-996
0.33 μM Sac1^1-522
0.10 μM Sac1^1-522
1 μM GST-Osh3^588-996
C
PC:PS:PI4P (3:1:1) liposomes, 0.8 mM lipid total
pmol PO4 released
time (min)
0.33 μM Sac1^1-522
0.03 μM Sac1^1-522
+12 μM Osh4
0.03 μM Sac1^1-522
12 μM Osh4

**Figure 2.9. The ORD domains stimulate Sac1 activity *in vitro*.**

(A) Schematic of the reconstituted Sac1 phosphatase assay. PI4P-containing liposomes were incubated with $his_6$-$Sac1^{1-522}$, GST-$Osh3^{588-996}$ or $his_6$-Osh4. Phosphate release was measured by a malachite green assay. The Coomassie-stained gel shows the recombinant proteins used in the *in vitro* assays. The dot indicates a GST-$Osh3^{588-996}$ degradation product.

(B) GST-$Osh3^{588-996}$ stimulates Sac1 *in vitro*. Results from *in vitro* phosphatase assays including 0.33 mM $his_6$-$Sac1^{1-522}$ (squares), 0.1 mM $his_6$-$Sac1^{1-522}$ (diamonds), 1 mM GST-$Osh3^{588-996}$ and 0.1 mM $Sac1^{1-522}$ (circles), and background levels in the presence of 1 mM GST-$Osh3^{588-996}$ alone (triangles). Error bars show SD of two experiments measured in duplicate. See also Figure 2.10B.

(C) Osh4 stimulates Sac1 *in vitro*. Results from *in vitro* phosphatase assays with 0.33 mM $his_6$-$Sac1^{1-522}$ (squares), 0.03 mM $his_6$-$Sac1^{1-522}$ (diamonds), 0.03 mM $his_6$-$Sac1^{1-522}$ and 12 mM $his_6$-Osh4 (circles), and 12 mM $his_6$-Osh4 alone (triangles). Error bars show SD of two experiments measured in duplicate.

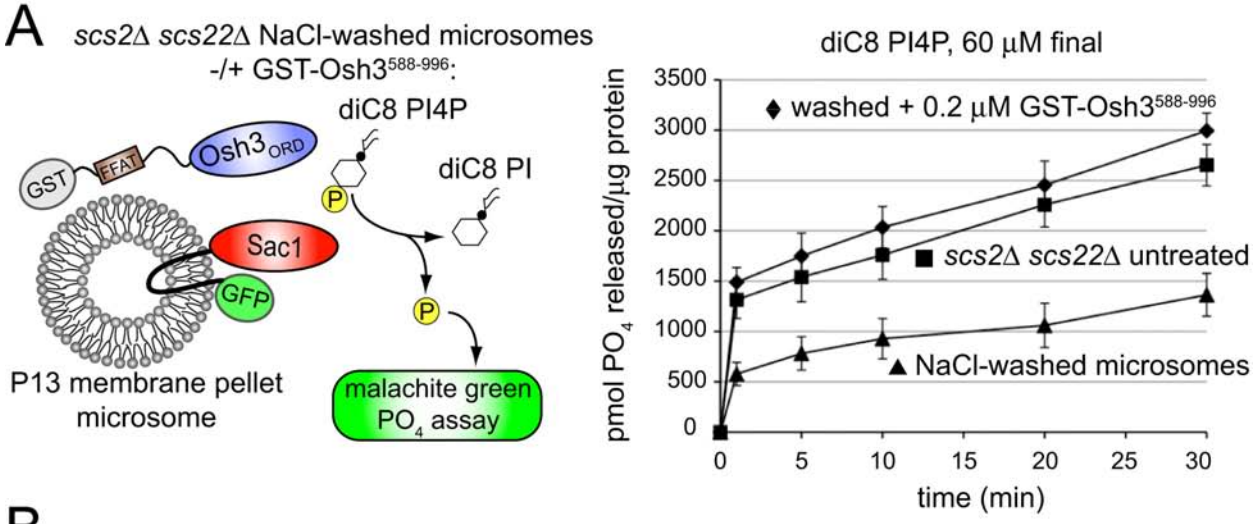
A
scs2Δ scs22Δ NaCl-washed microsomes
-/+ GST-Osh3588-996:
diC8 PI4P
diC8 PI
GST
FFAT
Osh3ORD
Sac1
GFP
P
P13 membrane pellet
microsome
malachite green
PO4 assay
diC8 PI4P, 60 μM final
pmol PO4 released/μg protein
washed + 0.2 μM GST-Osh3588-996
scs2Δ scs22Δ untreated
NaCl-washed microsomes
time (min)

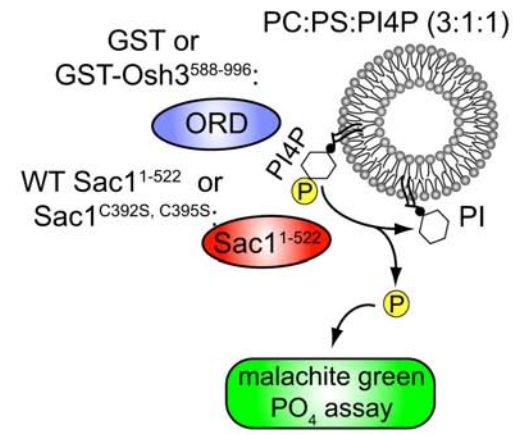
B
PC:PS:PI4P (3:1:1)
GST or
GST-Osh3588-996:
ORD
PI4P
WT Sac11-522 or
Sac1C392S, C395S:
Sac11-522
PI
P
malachite green
PO4 assay

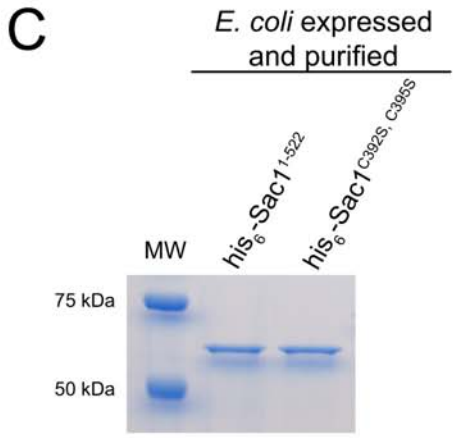
C
E. coli expressed
and purified
MW
his6-Sac11-522
his6-Sac1C392S, C395S
75 kDa
50 kDa

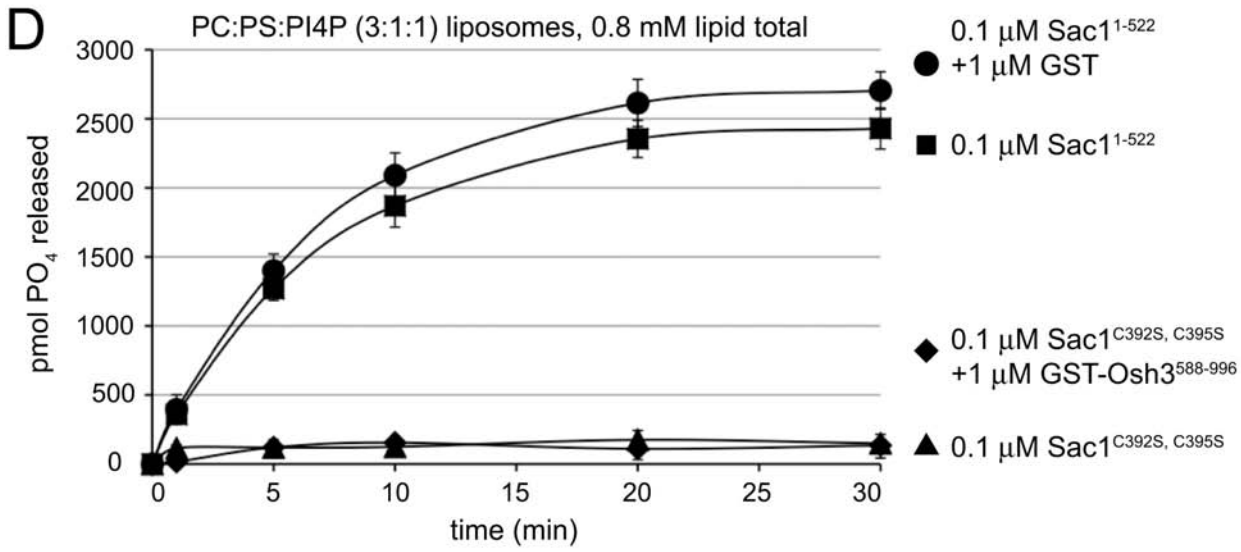
D
PC:PS:PI4P (3:1:1) liposomes, 0.8 mM lipid total
pmol PO4 released
0.1 μM Sac11-522
+1 μM GST
0.1 μM Sac11-522
0.1 μM Sac1C392S, C395S
+1 μM GST-Osh3588-996
0.1 μM Sac1C392S, C395S
time (min)

**Figure 2.10. The ORD domain stimulates Sac1 activity *in vitro*.**

(A) The Osh3 ORD domain activates Sac1 independently of the VAP proteins. Short acyl chain diC8 PI4P (60 mM) was incubated with untreated *scs2*Δ *scs22*Δ microsomes (squares), NaCl-washed *scs2*Δ *scs22*Δ microsomes (triangles), or NaCl-washed *scs2*Δ *scs22*Δ microsomes in the presence of 0.2 mM GST-Osh3$^{588\text{-}996}$ (diamonds) for the indicated times. Phosphate release was measured by the malachite green assay. Error bars show the SD of two experiments measured in duplicate.

(B) Scheme for the reconstituted Sac1 phosphatase assay. PI4P-containing liposomes were incubated with his$_6$-Sac1$^{1\text{-}522}$, his$_6$-Sac1$^{C392S,C395S}$, GST-Osh3$^{588\text{-}996}$ or GST. Phosphate release was measured by a malachite green assay.

(C) The Coomassie-stained gel shows purified, recombinant his$_6$-Sac1$^{1\text{-}522}$ and catalytically inactive his$_6$-Sac1$^{1\text{-}522,\ C392S,\ C395}$ proteins.

(D) GST does not stimulate his$_6$-Sac1$^{1\text{-}522}$ activity *in vitro* and GST-Osh3$^{588\text{-}996}$ does not activate his$_6$-Sac1$^{C392S,\ C395S}$. The results of control *in vitro* phosphatase assay experiments are shown: 0.1 mM inactive his$_6$-Sac1$^{C392S,C395S}$ (triangles), 0.1 mM inactive his$_6$-Sac1$^{C392S,\ C395S}$ and 1 mM GST-Osh3$^{588\text{-}996}$ (diamonds), 0.1 mM his$_6$-Sac1$^{1\text{-}522}$ (squares), and 0.1 mM his$_6$-Sac1$^{1\text{-}522}$ and 1 mM GST (circles).

the high salt wash. Thus, we were not able to test whether recombinant Osh3 stimulated Sac1 *in trans* activity (our unpublished results). However, NaCl-washed microsomes displayed a reduced rate of diC8 PI4P turnover (more than two-fold: 600±115 pmol/mg total protein/min, after 1 min, as compared to untreated microsomes at 1600±206 pmol/mg total protein/min, after 1 min, Figure 2.7C) and maximal Sac1 phosphatase activity compared to untreated microsomes (1746±213 pmol $PO_4$ released versus 2789±211 pmol, respectively after 30 min; Figure 2.7C). To test if impaired Sac1 activity in NaCl-washed microsomes was due to the loss of Osh proteins, purified GST-Osh3$^{588\text{-}996}$ (see Figure 2.9B) was added back to the reaction. Strikingly, 0.2 mM GST-Osh3$^{588\text{-}996}$ restored activity in salt-washed microsomes to levels nearly identical to untreated Sac1-GFP microsomes (1450±155 pmol/mg total protein/min after 1 min, and 3000±176 pmol $PO_4$ released after 30 min, Figure 2.7C). Thus, recombinant Osh3 stimulated full-length Sac1 in microsomes, providing the first evidence that ORP proteins control Sac1 PI phosphatase activity *in vitro*.

To test if GST-Osh3$^{588\text{-}996}$ required the VAP proteins to stimulate Sac1, Sac1-GFP microsomes prepared from *scs2*Δ *scs22*Δ mutant cells were washed with high salt to deplete peripheral membrane proteins. As expected, NaCl-washed *scs2*Δ *scs22*Δ microsomes displayed impaired rates of diC8 PI4P turnover, compared to untreated *scs2*Δ *scs22*Δ microsomes (more than two-fold: 577±151 pmol/mg total protein/min, after 1 min, as compared to untreated *scs2*Δ *scs22*Δ microsomes at 1315±186 pmol/mg total protein/min, after 1 min, Figure 2.10A). Salt-washed *scs2*Δ *scs22*Δ microsomes also displayed reduced maximal Sac1 phosphatase activity, compared to untreated *scs2*Δ *scs22*Δ microsomes (1364±223 pmol $PO_4$ released versus 2652±206 pmol, respectively after 30 min; Figure 2.10A). Interestingly, 0.2 mM GST-Osh3$^{588\text{-}996}$ restored full activity in salt-washed *scs2*Δ *scs22*Δ microsomes (1489±145 pmol/mg total

protein/min after 1 min, and 2994±176 pmol $PO_4$ released after 30 min, Figure 2.10A). Thus, the Osh3 ORD domain stimulated Sac1 activity against diC8 PI4P independently of the VAP proteins Scs2 and Scs22.

**Reconstitution of Sac1 Phosphatase Activation by ORD Domains**

Since the Osh3 ORD domain stimulated Sac1 activity in microsomes, we tested whether Osh proteins directly stimulate Sac1. We reconstituted Sac1 phosphatase activity *in vitro* using purified components at known concentrations. Sac1 lacking its transmembrane domains was expressed and purified from bacteria ($his_6$-$Sac1^{1-522}$) and incubated with PI4P-containing liposomes (Figure 2.9A). Purified $his_6$-$Sac1^{1-522}$ dephosphorylated PI4P in a dose and time-dependent manner (400 pmol/min/mg protein for 0.33 mM $his_6$-$Sac1^{1-522}$ after 5 minutes; Figure 2.9B). At 0.1 mM $his_6$-$Sac1^{1-522}$, the turnover rate was reduced to approximately 250 pmol $PO_4$ released/min/mg protein after 5 minutes (Figures 2.9B, 2.10D). A mutant form of Sac1 bearing substitutions in both cysteine residues in the $CX_5R$ active site ($his_6$-$Sac1^{C392S, C395S}$, Figure 2.10C) did not display phosphatase activity against PI4P-containing liposomes (Figure 2.10D). Importantly, addition of the Osh3 ORD domain (GST-$Osh3^{588-996}$; Figure 2.9B) stimulated Sac1 phosphatase activity three-fold against PI4P-containing liposomes, as 0.1 mM $his_6$-$Sac1^{1-522}$ in the presence of 1 mM GST-$Osh3^{600-996}$ displayed a turnover rate similar to 0.33 mM $his_6$-$Sac1^{1-522}$ (Figure 2.9B). As a control, 1 mM GST alone did not increase Sac1 activity (Figure 2.10D). GST-$Osh3^{588-996}$ did not catalyze PI4P turnover in the absence of $his_6$-$Sac1^{1-522}$ (Figure 2.9B) or in the presence of inactive $his_6$-$Sac1^{C392S, C395S}$ (Figure 2.10D).

As the ORD domain is common to all ORP proteins, we addressed if Sac1 activation is a conserved function for the Osh proteins. We then tested if full-length Osh4/Kes1 stimulated Sac1

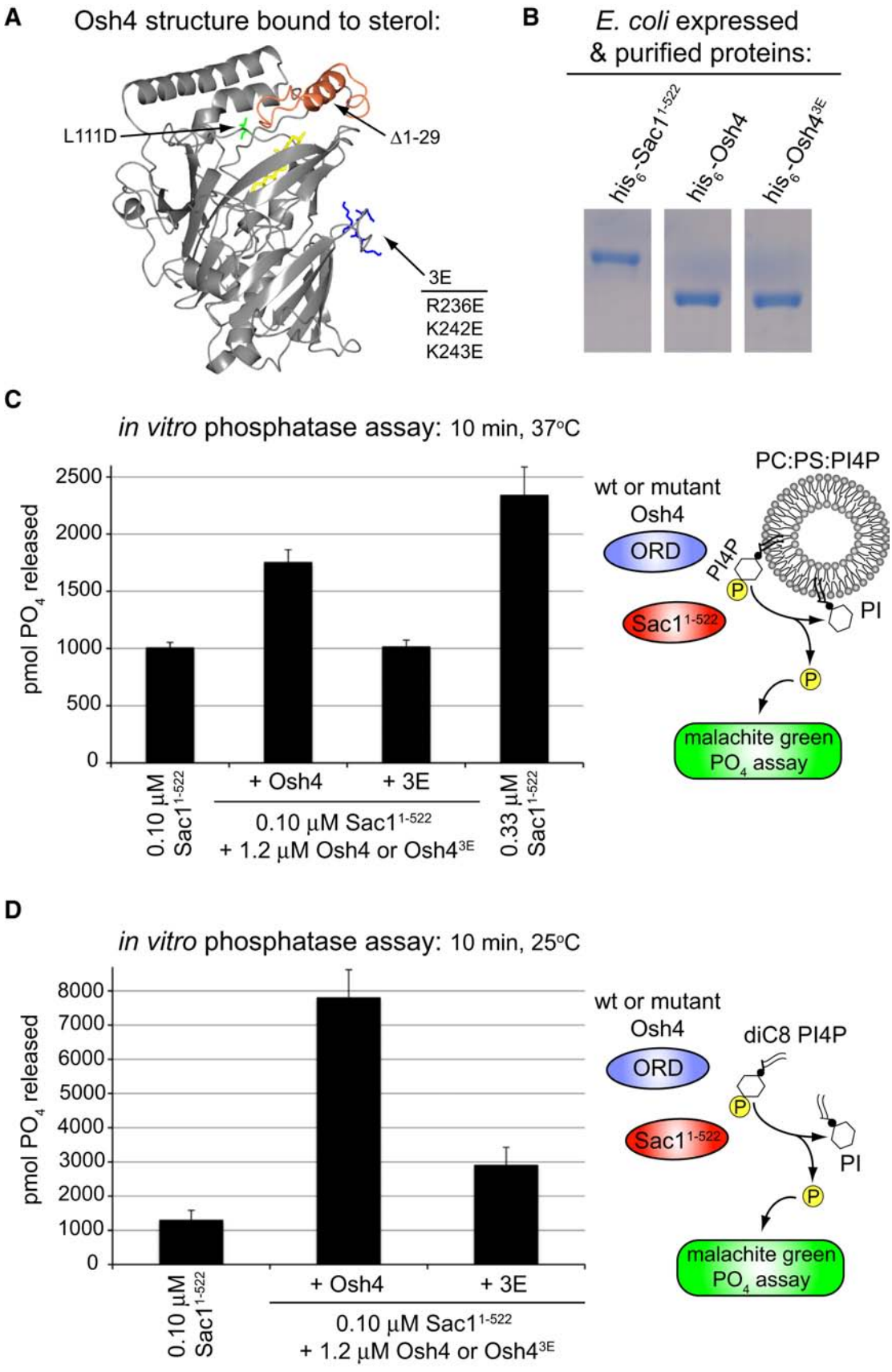
A
Osh4 structure bound to sterol:
L111D
Δ1-29
3E
R236E
K242E
K243E
B
E. coli expressed & purified proteins:
his6-Sac1 1-522
his6-Osh4
his6-Osh4 3E
C
in vitro phosphatase assay: 10 min, 37°C
pmol PO4 released
2500
2000
1500
1000
500
0
0.10 μM Sac1 1-522
+ Osh4
+ 3E
0.10 μM Sac1 1-522
+ 1.2 μM Osh4 or Osh4 3E
0.33 μM Sac1 1-522
wt or mutant Osh4
ORD
Sac1 1-522
PC:PS:PI4P
PI4P
PI
P
malachite green PO4 assay
D
in vitro phosphatase assay: 10 min, 25°C
pmol PO4 released
8000
7000
6000
5000
4000
3000
2000
1000
0
0.10 μM Sac1 1-522
+ Osh4
+ 3E
0.10 μM Sac1 1-522
+ 1.2 μM Osh4 or Osh4 3E
wt or mutant Osh4
ORD
Sac1 1-522
diC8 PI4P
PI
P
malachite green PO4 assay

**Figure 2.11. PI binding regulates Osh4 function.**

(A) The structure of Osh4/Kes1 (Im et al., 2005) is shown with mutants used in this study. Osh4$^{\Delta 1\text{-}29}$ (orange) and Osh4$^{L111D}$ (green) are defective in sterol binding (Im et al., 2005). Osh4$^{3E}$ (R236E, R242E, R243E; blue) is impaired in PI binding (see Figures 2.12A and B; Li et al., 2002). Cholesterol bound within the structure is shown in yellow.

(B) Coomassie-stained gel showing recombinant, purified his$_6$-Sac1$^{1\text{-}522}$ and wild type and mutant his$_6$-Osh4 proteins.

(C) *In vitro* phosphatase assays using 0.1 mM his$_6$-Sac1$^{1\text{-}522}$ and wild type and mutant Osh4$^{3E}$ proteins (1.2 mM). PI4P liposomes (PC:PS:PI, 3:1:1) were tested. Error bars show the SD of two experiments each measured in duplicate.

(D) *In vitro* phosphatase assays using 0.1 mM his$_6$-Sac1$^{1\text{-}522}$ and wild type and mutant Osh4$^{3E}$ proteins (1.2 mM) against short acyl chain diC8 PI4P. Error bars show the SD of two experiments each measured in duplicate. See also Figure 2.12C.

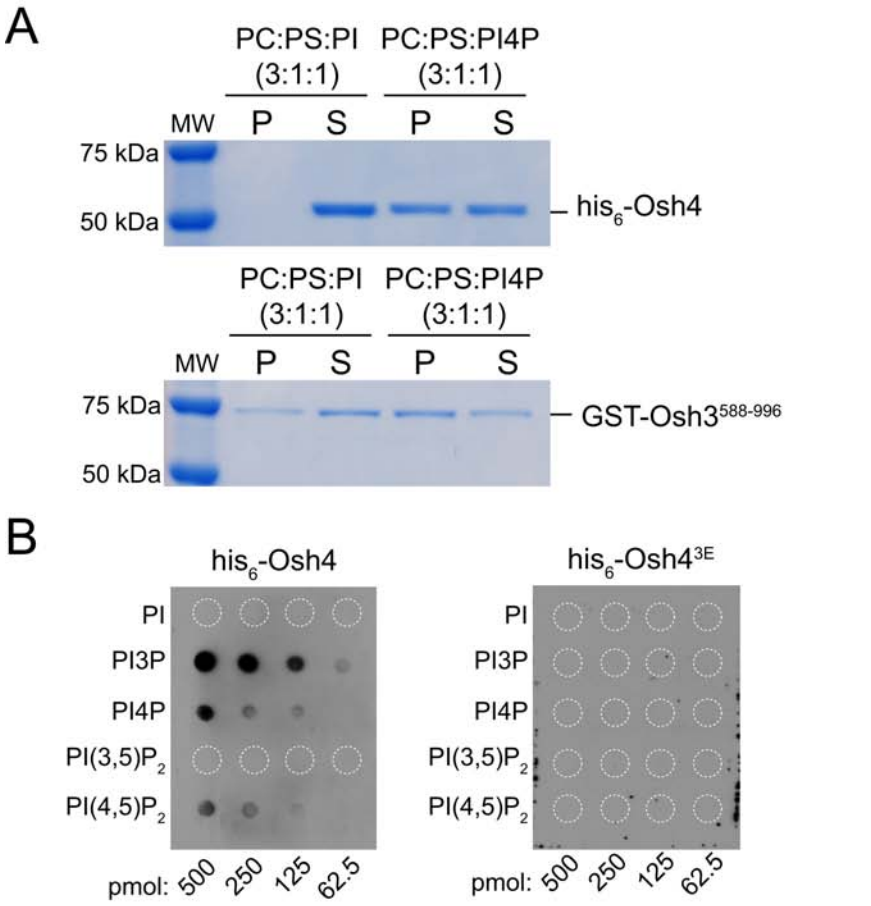
A
PC:PS:PI (3:1:1)
PC:PS:PI4P (3:1:1)
MW
P
S
P
S
75 kDa
50 kDa
his6-Osh4
GST-Osh3588-996
B
his6-Osh4
his6-Osh43E
PI
PI3P
PI4P
PI(3,5)P2
PI(4,5)P2
pmol: 500 250 125 62.5
C
in vitro phosphatase assay: 10 min, 25°C
pmol PO4 released
diC8 PI4P (μM)
0.1 μM Sac11-522 +1.2 μM Osh4
0.1 μM Sac11-522 +1.2 μM Osh4 +250 μM cholesterol
0.1 μM Sac11-522

**Figure 2.12. The ORD domains of Osh3 and Osh4 bind phosphoinositides.**

(A) The Osh3 and Osh4 ORD domains bind PI4P in liposome sedimentation assays. PI4P-containing liposomes (PC:PS:PI4P, 3:1:1, 1 mM total lipid) or PtdIns-containing liposomes (PC:PS:PI, 3:1:1, 1 mM total lipid) were incubated with recombinant $his_6$-Osh4 or GST-$Osh3^{588-996}$ proteins. Liposomes and bound proteins were sedimented by centrifugation at 100,000 x *g* and proteins were detected in Coomassie-stained SDS-PAGE gels.

(B) $his_6$-Osh4 binds phosphoinositides. PI lipid overlay binding assays (FAT blots) using $his_6$-Osh4 and the PI binding mutant $his_6$-$Osh4^{3E}$. Bound proteins were detected with antibodies against the T7 tag in the fusion proteins.

(C) Osh4 stimulates $Sac1^{1-522}$ activity *in vitro*: 0.1 mM $his_6$-$Sac1^{1-522}$ *in vitro* phosphatase activity against increasing concentrations of diC8 PI4P (circles), activity in the presence of 0.1 mM $his_6$-$Sac1^{1-522}$ and 1.2 mM $his_6$-Osh4 (squares). Osh4 stimulates $Sac1^{1-522}$ activity *in vitro* independently of cholesterol: activity in the presence of 0.1 mM $his_6$-$Sac1^{1-522}$,1.2 mM $his_6$-Osh4, and 250 mM cholesterol (triangles). Errors bars show the SD of two independent experiments measured in duplicate.

phosphatase activity *in vitro*. In these assays, we lowered the $his_6$-$Sac1^{1-522}$ concentration (to 0.033 mM with activity near background levels; Figure 2.9C). In the presence of 12 mM $his_6$-Osh4, 0.033 mM $his_6$-$Sac1^{1-522}$ activity increased ten-fold over the course of the experiment, reaching that of 0.33 mM $his_6$-$Sac1^{1-522}$ (Figure 2.9C). In addition, at high concentrations (300 mM) of short acyl chain diC8 PI4P, 1.2 mM $his_6$-Osh4 stimulated 0.1 mM $his_6$-$Sac1^{1-522}$ activity greater than six-fold (Figures 2.11D, 2.12C). Thus, the ORD domains from Osh3 and Osh4 directly activated Sac1 *in vitro*.

**PI and Sterol Binding Control Osh4 Function**

Osh4/Kes1 binds PI lipids *in vitro* (Li et al., 2002). Consistent with this, $his_6$-Osh4 sedimented more efficiently with PI4P-containing liposomes, compared to PtdIns-containing liposomes (Figure 2.12A). GST-$Osh3^{588-996}$ also sedimented more readily with PI4P-containing liposomes than it did with PtdIns-containing liposomes (Figure 2.12A). We tested if PI binding was necessary for Osh4 function *in vitro* and *in vivo*. Substitution of three basic residues (R236E, K242E, K243E; termed 3E, Figure 2.11A) impairs Osh4 PI binding (Li et al., 2002). The mutant $his_6$-$Osh4^{3E}$ protein was stably expressed and purified (Figure 2.11B). We confirmed that $his_6$-$Osh4^{3E}$ was defective in PI binding using an overlay assay (Figure 2.12B). In contrast, wild type $his_6$-Osh4 bound PI3P, PI4P, and $PI(4,5)P_2$ (in order of binding affinity; Figure 2.12B). Notably, $his_6$-$Osh4^{3E}$ did not stimulate Sac1 activity against PI4P in liposomes (Figure 2.11C). In addition, $his_6$-$Osh4^{3E}$ was impaired in Sac1 activation against short acyl chain diC8 PI4P, as compared to wild type $his_6$-Osh4 (two-fold *vs*. six-fold stimulation respectively, Figure 2.11D). Consistent with these *in vitro* results, cellular PI4P levels were 17-fold above wild type in

*osh*Δ:*CEN osh4*$^{ts}$ cells co-expressing Osh4$^{3E}$ at 38$^{o}$C (Table 2.3), indicating that PI binding is essential for Osh4 function.

As the Osh proteins bind sterol lipids *in vitro* (Im et al., 2005; Raychaudhuri et al., 2006), we tested if sterol lipids regulate Osh-stimulated Sac1 activity. Addition of 250 mM cholesterol (>800-fold above the $K_d$ of Osh4 for cholesterol; Im et al., 2005) did not significantly affect Osh4-stimulated Sac1 activity against diC8 PI4P (Figure 2.12C). We also measured *in vivo* PI levels in *osh*Δ:*CEN osh4*$^{ts}$ cells expressing wild type *OSH4* or the sterol-binding defective mutants, *osh4*Δ *1-29* or *osh4L111D* (see Figure 2.11A; Im et al., 2005). In *osh*Δ:*CEN osh4*$^{ts}$ cells co-expressing either Osh4 $^{\Delta 1\text{-}29}$ or Osh4$^{L111D}$, PI4P levels were 21- and 19-fold above wild type levels (Table 2.3). Thus, while cholesterol did not alter Sac1 activity *in vitro*, sterol binding was essential for Osh4-mediated PI4P metabolism *in vivo*.

**The Osh Proteins Interact with the Sac1 Catalytic Domain**

As the Osh3 and Osh4 ORD domains activated Sac1 *in vitro*, we examined if Osh proteins interact with Sac1. We initially used Osh7 for these experiments as it is expressed at higher levels than Osh3 (2350 Osh7 molecules/cell *vs.* 600 Osh3 molecules/cell; Ghaemmaghami et al., 2003). Osh7 localizes to the cortical ER even though it lacks a PH domain and FFAT motif (Schulz et al., 2009; Figure 2.1C). A membrane pellet fraction containing Osh7-3xHA and Sac1-13x*myc* was incubated with crosslinkers, solubilized, and processed for co-immunoprecipiation against the 3xHA tag on Osh7. A small fraction of Sac1-13x*myc* specifically isolated with Osh7-3xHA (Figure 2.13A), suggesting that this interaction was transient or possibly indirect since it required crosslinking. However, Sac1 is far more abundant in cells than Osh7 (48, 000 Sac1 molecules/cell; Ghaemmaghami et al., 2003); thus

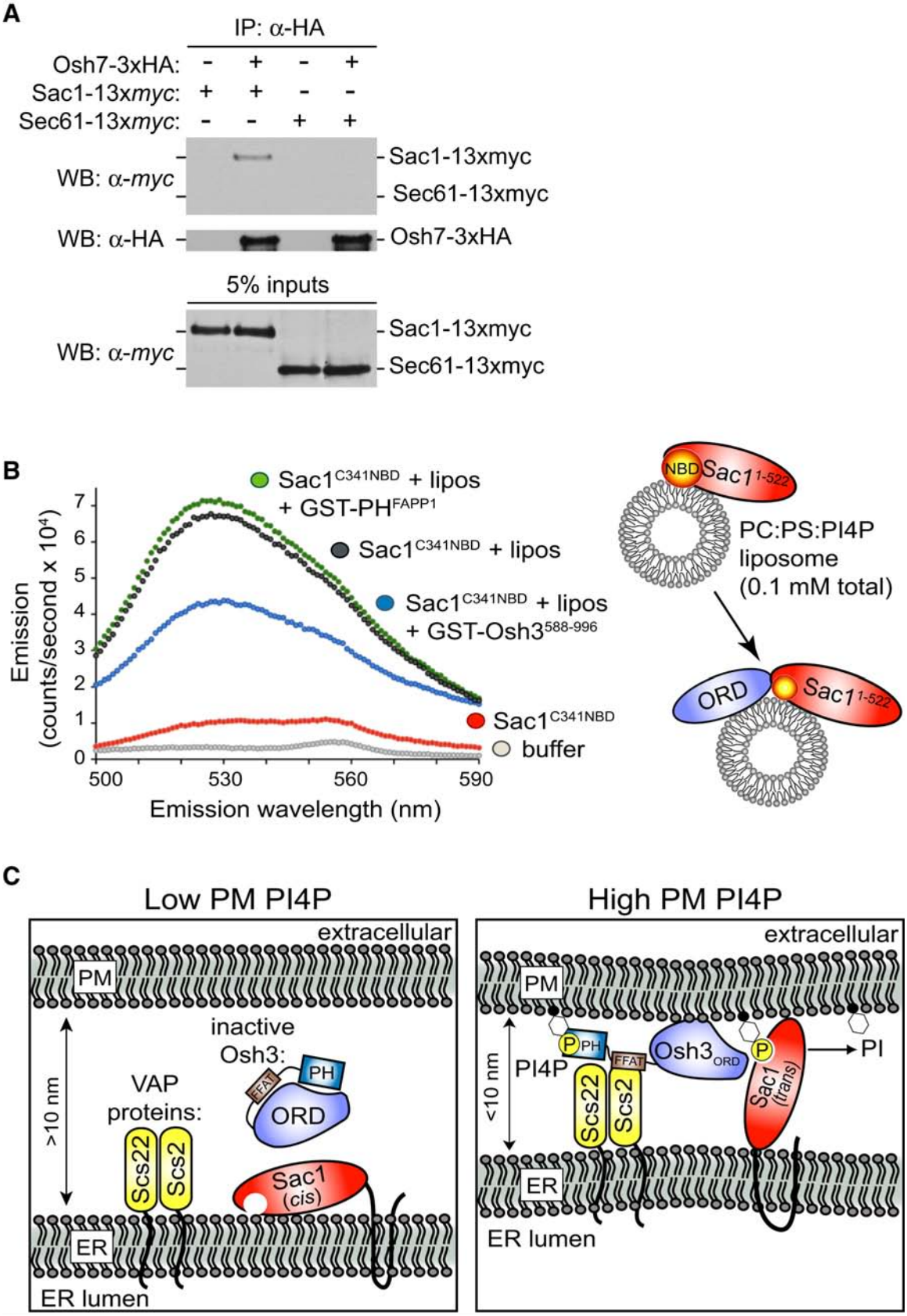
A
IP: α-HA
Osh7-3xHA: - + - +
Sac1-13xmyc: + + - -
Sec61-13xmyc: - - + +
WB: α-myc
Sac1-13xmyc
Sec61-13xmyc
WB: α-HA
Osh7-3xHA
5% inputs
WB: α-myc
Sac1-13xmyc
Sec61-13xmyc
B
Sac1C341NBD + lipos + GST-PHFAPP1
Sac1C341NBD + lipos
Sac1C341NBD + lipos + GST-Osh3588-996
Sac1C341NBD
buffer
Emission (counts/second x 10⁴)
Emission wavelength (nm)
NBD Sac1 1-522
PC:PS:PI4P liposome (0.1 mM total)
ORD
Sac1 1-522
C
Low PM PI4P
High PM PI4P
extracellular
PM
inactive Osh3:
PH
FFAT
ORD
VAP proteins:
Scs22
Scs2
Sac1 (cis)
>10 nm
ER
ER lumen
PI4P
<10 nm
Osh3ORD
Sac1 (trans)
PI

**Figure 2.13. The ORD domain interacts with Sac1 and model for regulation of PI4P metabolism by Osh3, Scs2/Scs22, and Sac1 at PM/ER Membrane Contact Sites.**

(A) Sac1-13x*myc* specifically interacts with Osh7-3xHA. Membrane fractions from cells expressing Osh7-3xHA and Sac1-13x*myc* or Sec61-13x*myc* were incubated with crosslinkers, solubilized, immunoprecipitated with anti-HA beads and analyzed by immunoblotting to detect Osh7-Sac1 complexes. See also Figure 2.14A.

(B) GST-Osh3$^{588\text{-}996}$ induces a conformational shift in the Sac1 catalytic domain. Emission scans of 0.06 mM Sac1$^{C341NBD}$ in buffer (red), in the presence of liposomes (PC:PS:PI4P, 3:1:1, 0.1 mM lipid total; dark grey), liposomes and 0.8 mM GST-Osh3$^{588\text{-}996}$ (blue), liposomes with 0.8 mM GST-PH$^{FAPP1}$ (green), and buffer alone (light grey). See also Figure 2.14.

(C) Model for PI4P turnover at PM/ER membrane contact sites. High PM PI4P levels recruit and activate Osh3 at ER/PM contact sites. Interactions between Osh3 and the VAP proteins Scs2/Sc22 activate ER-localized Sac1.

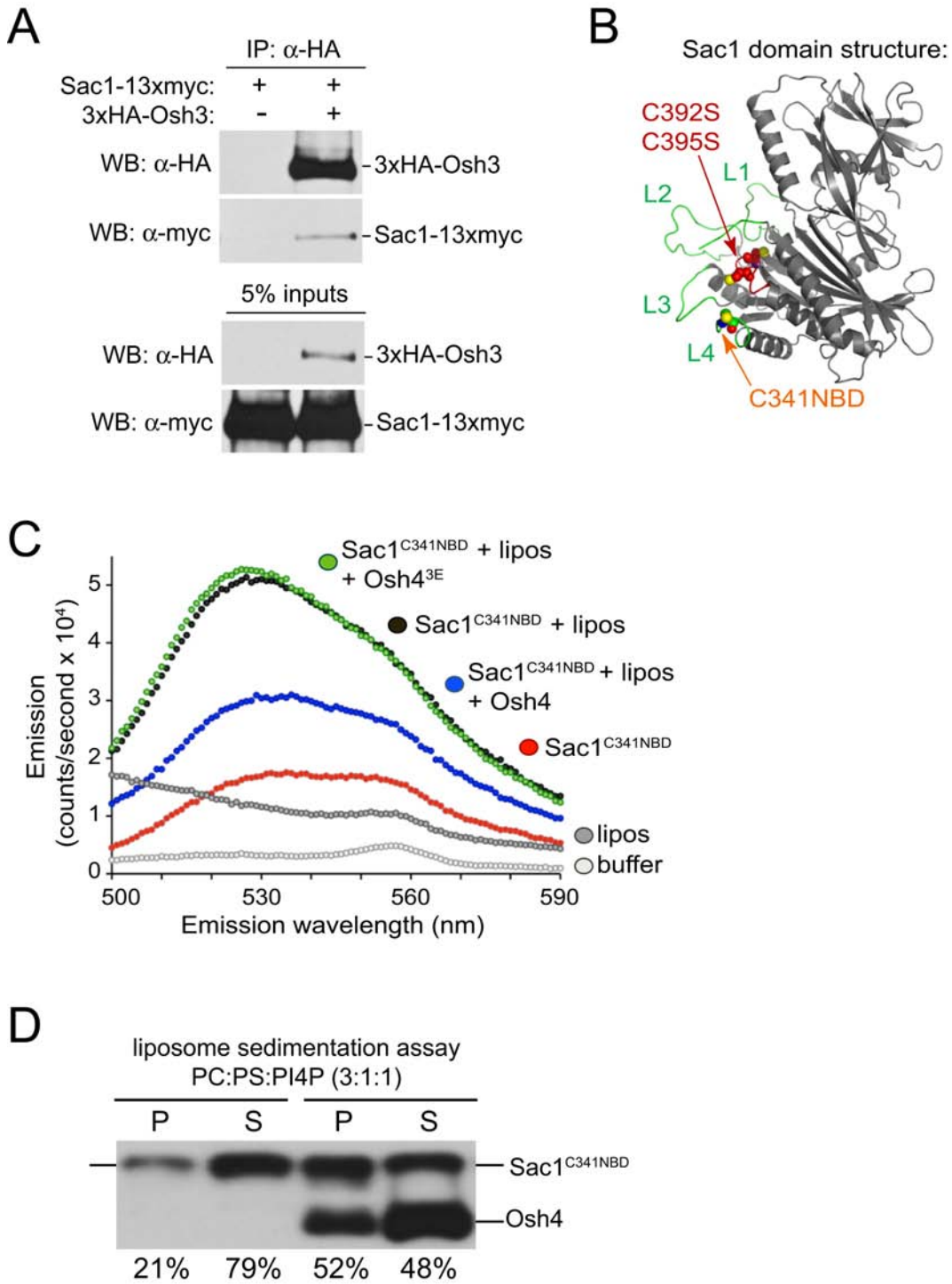
A
IP: α-HA
Sac1-13xmyc: + +
3xHA-Osh3: - +
WB: α-HA
3xHA-Osh3
WB: α-myc
Sac1-13xmyc
5% inputs
WB: α-HA
3xHA-Osh3
WB: α-myc
Sac1-13xmyc
B
Sac1 domain structure:
C392S
C395S
L1
L2
L3
L4
C341NBD
C
Sac1C341NBD + lipos + Osh43E
Sac1C341NBD + lipos
Sac1C341NBD + lipos + Osh4
Sac1C341NBD
lipos
buffer
Emission (counts/second x 10⁴)
0
1
2
3
4
5
500
530
560
590
Emission wavelength (nm)
D
liposome sedimentation assay
PC:PS:PI4P (3:1:1)
P
S
P
S
Sac1C341NBD
Osh4
21%
79%
52%
48%
(% of Sac1C341NBD in fractions)

**Figure 2.14. Osh3 and Osh4 interact with Sac1.**

(A) Sac1-13x*myc* interacts with 3xHA-Osh3. P13 membrane fractions from cells expressing 3xHA-Osh3 and Sac1-13x*myc* or Sac1-13x*myc* alone were incubated with crosslinkers, solubilized, immunoprecipitated with anti-HA beads and analyzed by SDS-PAGE and western analysis to detect Osh3-Sac1 complexes.

(B) The structure of the Sac1 domain (Manford et al., 2010) is shown. The purified $his_6$-$Sac1^{C392,C395S}$ protein was labeled with NBD at the only remaining cysteine residue, C341 (orange), residing in L4 of the loops (L1-L4, green) that surround the catalytic cysteine residues (C392 and C395, red).

(C) PI binding is required for the Osh-induced conformational shift in the Sac1 catalytic domain. Emission scans of 0.06 mM $Sac1^{C341NBD}$ in buffer (red), in the presence of liposomes (PC:PS:PI4P, 3:1:1, 0.1 mM lipid total; dark grey), liposomes and 0.4 mM $his_6$-Osh4 (blue), and liposomes with 0.4 mM PI binding-defective mutant $his_6$-$Osh4^{3E}$ (green). The control emission scans of liposomes in buffer and buffer alone are shown in grey and light grey, respectively.

(D) Osh4 increases membrane association of the Sac1 domain. PI4P-containing liposomes (PC:PS:PI4P, 3:1:1, 0.1 mM total lipid) were incubated with 0.4 mM $his_6$-Osh4 and 0.06 mM $his_6$-$Sac1^{C392S,C395S}$ proteins. Liposomes and bound proteins were sedimented by centrifugation at 100,000 x *g* and proteins were detected by immunoblotting against the T7 tag in the fusion proteins. Quantification of $his_6$-$Sac1^{C341NBD}$ for each fraction is shown underneath.

only a small fraction of Sac1 is expected to co-isolate with Osh7. Importantly, Osh7-3xHA did not crosslink to another abundant ER membrane protein, Sec61-13x*myc* (Figure 2.13A). We also observed cross-linking between 3xHA-Osh3 and Sac1-13x*myc* (Figure 2.14A). As a control, the ER transmembrane protein Wbp1 was not isolated with 3xHA-Osh3 (our unpublished observations). Together, these results suggested that multiple Osh proteins interact with Sac1 and that the ORD domain is responsible.

Next, we tested if the ORD and Sac1 domains physically interact *in vitro*. We were unable to detect a stable complex between the purified Sac1 domain and Osh3 or Osh4 ORD domains in solution (our unpublished results). For this reason, we developed assays to monitor Sac1 and ORD domain interactions on a membrane bilayer. The $Sac1^{1\text{-}522}$ domain contains three cysteine residues: C392 and C395 in the catalytic site and C341 in loop 4 (L4) that resides on the same surface as the catalytic site (Figure 2.14B; Manford et al., 2010). Purified $his_6$-$Sac1^{C392S,\ C395S}$ was covalently labeled with the fluorescent dye NBD at C341 ($Sac1^{C341NBD}$, Figure 2.14B). Movement of NBD from an aqueous environment to a more hydrophobic environment is accompanied by changes in its spectral properties (*e.g.* emission wavelength maximum, termed "blue shift", and intensity) and thus can be used as an indicator for conformational changes in a protein as well as membrane association. $Sac1^{C341NBD}$ underwent a significant increase in NBD fluorescence signal (6.6-fold) and a shift in the maximum emission wavelength (blue shift) upon addition of liposomes (Figure 2.13B), reflecting a membrane-induced change in the local environment of L4 in the Sac1 catalytic domain. Interestingly, addition of GST-$Osh3^{588\text{-}996}$ reduced $Sac1^{C341NBD}$ signal intensity in the presence of liposomes (1.7-fold), consistent with an Osh3-induced shift in L4 of Sac1 to a less hydrophobic environment (Figure 2.13B). As a control, GST fused to the PI4P-binding PH domain from FAPP1 did not alter the $Sac1^{C341NBD}$

fluorescence signal in the presence of liposomes (Figure 2.13B). Thus, the Osh3 ORD domain-induced reduction in Sac1$^{C341NBD}$ signal intensity was not simply due to competition for PI4P binding.

To address whether these effects were conferred by another ORD domain, we incubated Sac1$^{C341NBD}$ with liposomes either in the absence or presence of his$_6$-Osh4. Addition of his$_6$-Osh4 reduced Sac1$^{C341NBD}$ signal intensity in the presence of liposomes (1.7-fold, Figure 2.14C), similar to GST-Osh3$^{588-996}$. Interestingly, the Osh4$^{3E}$ mutant protein that is defective in PI binding and Sac1 stimulation did not affect Sac1$^{C341NBD}$ fluorescence intensity in the presence of liposomes (Figure 2.14C). As a change in NBD fluorescence can be due to effects in membrane association as well as protein conformational states, we examined the membrane binding status of Sac1$^{C341NBD}$ in the absence and presence of Osh4. Surprisingly, the ability of his$_6$-Sac1$^{C341NBD}$ to sediment with liposomes was increased in the presence of his$_6$-Osh4 (> two-fold; Figure 2.14D). Thus, the reduction in Sac1$^{C341NBD}$ fluorescence intensity by Osh4 was not due to decreased Sac1 domain membrane binding. Accordingly, the Osh-induced shift in Sac1$^{C341NBD}$ fluorescence intensity may reflect an Osh-induced conformational change in the Sac1 catalytic domain, consistent with Osh-stimulated Sac1 phosphatase activity *in vitro*. Moreover, an Osh-induced increase in membrane association may contribute to Sac1 activation.

## Discussion

Sac1-like phosphatases are essential regulators of PI signaling networks. We show that the oxysterol binding homology (Osh) proteins control Sac1 activity. Members of the ORP family are known to bind sterol and PI lipids and are implicated in disease (Ngo et al., 2010). We demonstrate a new role for this family: control of PI4P metabolism through Sac1 PI

phosphatases. Our results also explain how ER-localized Sac1 can regulate PM PI4P levels *in trans*: via the function of Osh proteins at PM/ER membrane contact sites as sensors of PI4P at the PM and activators of the Sac1 phosphatase in the ER.

**PM PI4P Metabolism Occurs at PM/ER Membrane Contact Sites**

Recent studies have proposed that Sac1 regulates PI4P *in cis* at the ER and Golgi, as well as *in trans* at the PM from the ER (Baird et al., 2008; Manford et al., 2010). In accord, Sac1 has been shown to regulate PI4P levels at the ER and Golgi (Faulhammer et al., 2007; Foti et al., 2001). Our findings and additional evidence indicate that ER-localized Sac1 controls PM PI4P pools. First, PI4P accumulates at the PM in cells lacking Sac1 (Figure 2.1E; Roy and Levine, 2004). Second, Sac1 does not traffic to the PM and was not stabilized at the PM in an endocytosis mutant (Tahirovic et al., 2005). Likewise, cells expressing a form of Sac1 that is retained in the ER do not display elevated PI4P levels (Konrad et al., 2002). Last, we demonstrate that full-length Sac1 in microsomes dephosphorylates PI4P *in trans* on distinct liposomes (Figure 2.7).

We propose that the Osh and VAP proteins function as regulators of Sac1 activity at membrane contact sites. Notably, Osh3 localization to PM/ER membrane sites was dependent on PI4P synthesis (Figure 2.3C) and a mutant form lacking the PH domain was destabilized from cortical patches (Figure 2.4C). We suggest that the PH domain-containing protein Osh3 acts as a sensor of PI4P levels at the PM and subsequently activates the Sac1 PI phosphatase at the ER (Figure 2.13C). Our study also highlights a role for Scs2 and Scs22 in PI4P metabolism. Cells lacking Scs2 and Scs22 display elevated PM PI4P levels (Figure 2.5). Moreover, Scs2 and Scs22 stimulate Sac1 activity against PI4P in liposomes (Figure 2.7A). Scs2 and Scs22 may activate

Osh3 at PM/ER membrane contact sites to control PM PI4P levels (Figure 2.13C). The yeast VAP proteins may also aid in the formation of membrane junctions. Scs2 and Scs22 have been implicated in PM/ER membrane contact site formation (Loewen et al., 2007). In addition, Scs2 binds anionic phospholipids, including PI4P, *in vitro* (Kagiwada and Hashimoto, 2007).

**Mechanisms for Regulation of Sac1 Activity by the Osh Proteins**

Multiple inputs control Osh protein function. We propose that PI4P binding to the Osh3 PH domain and Scs2 interactions via the FFAT motif activate Osh3 at PM/ER membrane contact sites (Figure 2.13C). These interactions may then facilitate interactions between the Osh3 ORD domain and downstream target proteins such as Sac1 (Figure 2.13C). Thus, Osh3 may serve as a 'co-incidence detector' of PI4P, the VAP proteins, and Sac1. We also found that PI and sterol binding control Osh4/Kes1 function (Figure 2.11, Table 2.3). The Osh proteins control sterol localization *in vivo* (Beh and Rine, 2004) and transfer sterol lipids *in vitro* (Raychaudhuri et al., 2006). Osh4/Kes1 function required sterol binding *in vivo* (Table 2.3), but was not affected by the addition of cholesterol *in vitro* (Figure 2.12C). The concentrations of Osh4 or PI4P in our *in vitro* studies may have bypassed a requirement for sterol binding. *In vivo*, the ability of the Osh proteins to extract sterol lipids may control membrane bilayer rigidity and curvature, and thus formation of membrane contact sites (Figure 2.13C). Notably, the Osh proteins can tether liposomes *in vitro* (Schulz et al., 2009). Alternatively, sterol binding may control Osh protein localization *in vivo*. Consistent with this idea, OSBP localizes to the ER when bound to cholesterol and to the Golgi when bound to 25-hydroxycholesterol (Peretti et al., 2008).

Osh4/Kes1 also binds PI lipids *in vitro* (Figure 2.12; Li et al., 2002). This may be a general feature of ORD domains, as Osh3 showed increased affinity for PI4P liposomes (Figure

2.12). A form of Osh4 impaired in PI binding (Figure 2.12) did not stimulate Sac1 activity *in vitro* (Figure 2.11). While our results did not indicate that Osh3 transfers PI lipids (Figure 2.8), the Osh proteins may bind PI lipids and present substrates to Sac1 at the membrane interface. Alternatively, PI binding may be necessary for productive interactions with Sac1. This idea is supported by our findings that Osh3 and Osh4 induced changes in $Sac1^{C341NBD}$ spectral properties in the presence of liposomes, but PI binding-defective $Osh4^{3E}$ was incapable of interacting with Sac1 (Figures 2.13, 2.14). The Osh-induced effects on $Sac1^{C341NBD}$ signal intensity may reflect a conformational change in Sac1 or a shift in the orientation of Sac1 with respect to the membrane bilayer. In addition PI binding may be necessary for Osh-stimulated Sac1 membrane association (Figure 2.14D).

**Conserved Functions for the Osh/ORP and VAP Proteins in PI Metabolism**

ORP and VAP proteins may share conserved roles in PI homeostasis. Each of the Osh proteins partially rescues the PI4P metabolism defects in *osh*Δ:*CEN osh4*$^{ts}$ cells (our unpublished observations). Both Osh3 and Osh4 stimulate Sac1 PI phosphatase activity *in vitro* (Figures 2.7, 2.9, 2.11). Osh6 and Osh7 localize to the peripheral ER (Schulz et al., 2009), and Osh7 interacts with Sac1 in crosslinking experiments (Figure 2.13A). Osh1 localizes to nuclear-vacuole junctions to participate in lipid metabolism (Levine and Munro, 2001). Osh4 regulates PI4P at the Golgi (Fairn et al., 2007; Li et al., 2002) where it may regulate Sac1 activity. Likewise, mammalian ORP and VAP proteins have been implicated at membrane contact sites. A recent study found ORP1L and VAP at ER/endosome membrane contact sites (Rocha et al., 2009). Mammalian VAP proteins control PI4P metabolism at ER/Golgi membrane contact sites (Peretti

et al., 2008). In addition, bound to 25-hydroxycholesterol, OSBP localizes to the Golgi and ER/Golgi contact sites (Peretti et al., 2008).

ORP and VAP proteins may then regulate additional PI signaling networks. Osh7 and Scs2 overexpression rescued the growth defects of mutant yeast cells with toxic levels of PI3P due to loss of the Sac1-like PI phosphatases Ymr1 and Sjl3, myotubularin and synaptojanin orthologs (Parrish et al., 2005). Cells lacking Osh or VAP protein function also display increased cellular PI3P levels (Table 2.3). It is unclear which Osh proteins regulate PI3P metabolism and if Osh and VAP proteins regulate other Sac1-like PI phosphatases, such as synaptojanins or myotubularin. Yet, cells lacking Osh function accumulate PI4P levels similar to *sac1 sjl2 sjl3* triple mutant cells (Figure1; Foti et al., 2001), suggesting they may control Sac1-like activity encoded by the yeast synaptojanins.

We propose that the Osh proteins act as sensors of PI levels and regulate the Sac1 PI phosphatase at membrane contact sites. By retaining Sac1 at the ER, cells can recruit Sac1 to distinct organelle contact sites as needed (*e.g.* ER/PM, ER/Golgi, ER/endosome, ER/lysosome). This would allow the cell to maintain a wide range of Sac1 phosphatase activity and permit use of a common phosphatase (Sac1) to regulate PI lipids at multiple sites in the cell. Membrane contact sites facilitate communication between organelles through lipid transfer and metabolism (Lev, 2010). This elegant system may allow cells to balance not only PI levels but also other lipids at ER membrane contact sites, as the ER is a major site of lipid synthesis. Thus, modulation of PI levels by Sac1, the Osh proteins, and VAP proteins may allow signaling between the ER and compartments along the secretory and endocytic systems, thus linking ER lipid biosynthesis to multiple membrane compartments in the cell. Interestingly, both Sac1 and the yeast VAP protein Scs2 are implicated in phospholipid metabolism (Loewen et al., 2004;

Rivas et al., 1999). In addition, Sac1 has recently been identified as a component of a protein complex at the ER involved in sphingolipid metabolism (Breslow et al., 2010). Thus, future studies on Sac1 may reveal new insights into the links between membrane homeostasis and PI signaling pathways.


## Acknowledgements

We thank C. Beh for strains and plasmids. We are grateful to S. Weys for technical assistance. We thank members of the Emr lab, C. McMaster, and S. Henry for discussions and A. Bretscher, C. Fromme, and D. Teis for comments on the manuscript. This work was supported by funds from the Weill Institute for Cell and Molecular Biology (S.D.E.).


## Tables

**Table 2.1. Strains used in this study**

| Strain | Genotype | Reference |
|---|---|---|
| SEY6210 | *MATa leu2-3,112 ura3-52 his3D200 trp1-D901 lys2-801 suc2D9* | (Robinson et al., 1988) |
| SEY6210.1 | *MAT**a** leu2-3,112 ura3-52 his3D200 trp1-D901 lys2-801 suc2D9* | (Robinson et al., 1988) |
| AAY102 | SEY6210 except *stt4*Δ*::HIS3* and harboring pRS415*stt4-4* | (Audhya et al., 2000) |
| AAY104 | SEY6210 except *pik1*Δ*::HIS3* and harboring pRS314*pik1-83* | (Audhya et al., 2000) |
| AAY202 | SEY6210 *mss4*Δ*::HIS3* and harboring YCp*lac*111*mss4$^{ts}$-102* | (Stefan et al., 2002) |
| MFY55 | SEY6210 *sac1*Δ*::TRP1* | (Foti et al., 2001) |
| JRY6203 | SEY6210 *osh2*Δ*::URA3* | (Beh et al., 2001) |
| JRY6202 | SEY6210 *osh3*Δ*::LYS2* | (Beh et al., 2001) |
| ANDY25 | SEY6210 *osh2*Δ*::URA3 osh3*Δ*::LYS2* | This study |
| CBY926 | SEY6210 *osh1*Δ*::KanMX4 osh2*Δ*::KanMX4 osh3*Δ*::LYS2 osh4*Δ*::HIS3 osh5D::LEU2 osh6D::LEU2 osh7D::HIS3* [*TRP1 CEN osh4-1*] | (Beh and Rine, 2004) |
| CBY924 | SEY6210 *osh1D::KanMX4 osh2D::KanMX4 osh3D::LYS2 osh4D::HIS3 osh5*Δ*::LEU2 osh6*Δ*::LEU2 osh7*Δ*::HIS3* [*TRP1 CEN OSH4*] | (Beh and Rine, 2004) |
| CBY886 | SEY6210 *osh1D::KanMX4 osh2D::KanMX4 osh3D::LYS2 osh4D::HIS3 osh5*Δ*::LEU2 osh6*Δ*::LEU2 osh7*Δ*::HIS3* [*URA3 CEN osh4-1*] | (Beh and Rine, 2004) |
| ANDY14 | SEY6210 *SCS2-mCherry::HISMX6* | This study |
| ANDY17 | SEY6210 *OSH3-GFP::HISMX6* | This study |
| ANDY34 | SEY6210 *OSH2-GFP::TRP1* | This study |
| YCS471 | CBY886 except SAC1-GFP::TRP1 | This study |
| DBY355 | SEY6210 *scs2*Δ*::TRP1 scs22*Δ*::HIS3MX6* | This study |

| | | |
|---|---|---|
| DBY337 | SEY6210 *SCS2-3xHA::HISMX6* | This study |
| DBY407 | SEY6210 *scs2Δ::TRP1 scs22Δ::HIS3MX6 SAC1-GFP::TRP1* | This study |
| DBY408 | SEY6210.1 *scs2Δ::TRP1 scs22Δ::HIS3MX6 sac1Δ::TRP1* | This study |
| DBY336 | SEY6210 *SCS2-GFP::HISMX6* | This study |
| MFY110 | SEY6210.1 *SAC1-GFP::TRP1* | (Foti et al., 2001) |
| ANDY57 | AAY102 except *OSH3-GFP::TRP1* | This study |
| ANDY70 | AAY202 except *OSH3-GFP::TRP1* | This study |
| ANDY144 | AAY104 except *OSH3-GFP:: KANMX6* | This study |
| ANDY89 | SEY6210 *SAC1-13xMYC::TRP1* | This study |
| ANDY90 | SEY6210 *SAC1-13xMYC::TRP1 osh3Δ::LYS2* and harboring (*URA3 CEN 3xHA-OSH3*) | This study |
| ANDY101 | MFY55 except harboring [*URA3 CEN sac1$^{ts}$ osh4$^{ts}$*] | This study |
| ANDY102 | CBY886 except harboring [*URA3 CEN sac1$^{ts}$ osh4$^{ts}$*] | This study |
| ANDY104 | CBY886 sac1Δ*::TRP1* and harboring [*URA3 CEN sac1$^{ts}$ osh4$^{ts}$*] | This study |
| ANDY105 | SEY6210 *rtn1Δ::TRP1 rtn2Δ::HISMX6 yop1Δ::TRP1 OSH3-GFP::KANMX6* | This study |
| ANDY145 | SEY6210 *SEC61-13xMYC::TRP1* | This study |
| ANDY142 | SEY6210 *OSH7-3xHA::HISMX6 SAC1-13xMYC::TRP1* | This study |
| ANDY146 | SEY6210 *OSH7-3xHA::HISMX6 SEC61-13xMYC::TRP1* | This study |

**Table 2.2. Plasmids used in this study**

| Plasmid | Description | Source |
|---|---|---|
| pCS276 | pRS426-p*PRC1*-GFP-2xPH$^{Osh2}$ | This study |
| pCS357 | pRS424-p*PRC1*-GFP-2xPH$^{Osh2}$ | This study |
| | pRS416-DsRed-HDEL | (Audhya and Emr, 2002) |
| pRH1585 | pKar2-DsRed-HDEL | (Bevis et al., 2002) |
| pCS355 | pRS424-p*PRC1*-GFP-*SAC1* | This study |
| pAM5 | pRS414-*OSH2* | This study |
| pAM6 | pRS414-*OSH3* | This study |
| pAM7 | pRS414-*OSH3*-GFP | This study |
| pAM8 | pRS414-*osh3$^{AAAT}$*-GFP | This study |
| pAM9 | pRS414-*osh3$^{PH\Delta}$*-GFP | This study |
| pAM10 | pRS414-*osh3$^{AAAT, PH\Delta}$*-GFP | This study |
| pAM12 | pRS416- p*PRC1*-3xHA-*OSH3* | This study |
| pCB254 | pRS314-*OSH4* | (Beh and Rine, 2004) |
| pCS388 | pRS314-*osh4$^{1-29\Delta}$* | This study |
| pCS381 | pRS314-*osh4$^{L111D}$* | This study |
| pCS384 | pRS314-*osh4$^{3E, R236E K242E k243E}$* | This study |
| pCB255 | pRS314-*osh4$^{ts}$-1* | (Beh and Rine, 2004) |
| pCB231 | pRS316-*OSH4* | (Beh and Rine, 2004) |
| | pRS316-*osh4$^{ts}$-1* | (Beh and Rine, 2004) |
| MFB65 | pRS416-*sac1$^{ts}$-23* | (Foti et al., 2001) |
| pAM11 | pRS416-*sac1$^{ts}$*-23 *osh4$^{ts}$*-1 | This study |
| pAM13 | pGEX6P-1-*OSH3*$^{588-996}$ | This study |
| pAM14 | pGEX6P-1-*OSH3*$^{1-613}$ | This study |
| pCS389 | pRSET-B-his$_6$-*OSH4* | This study |
| pCS397 | pRSET-B-his$_6$-*osh4$^{1-29\Delta}$* | This study |
| pCS390 | pRSET-B-his$_6$-*osh4$^{L111D}$* | This study |
| pCS393 | pRSET-B-his$_6$-*osh4$^{3E, R236E K242E k243E}$* | This study |
| pCS398 | pRSET-B-his$_6$-*SAC1$^{1-522}$* | This study |
| pCS399 | pRSET-B-his$_6$-*sac1$^{C392S C395S}$* | This study |

| | | |
|---|---|---|
| | pRS415-*stt4-4* | (Audhya et al., 2000) |
| | YC*plac*111-*mss4$^{ts}$-102* | (Stefan et al., 2002) |

| **Table 2.3. Phosphoinositide levels in wild type and mutant cells examined in this study** | | | | | |
|---|---|---|---|---|---|
| | **PI levels (% of total $^{3}$H-labeled PtdIns & PIPs)** | | | | |
| **Strain** | **PtdIns** | **PI3P** | **PI4P** | **PI(3,5)$P_2$** | **PI(4,5)$P_2$** |
| wild type 26°C | 95.7±1.81 | 1.24±0.37 | 1.24±0.36 | 0.13±0.07 | 1.06±0.38 |
| wild type 38°C | 93.1±2.21 | 1.15±0.58 | 1.61±0.35 | 0.13±0.02 | 1.66±0.24 |
| | | | | | |
| *osh1-osh7*Δ [*OSH4*] 26°C | 88.5±2.34 | 1.38±0.19 | 7.64±1.31 | 0.18±0.05 | 1.04±0.32 |
| *osh1-osh7*Δ [*OSH4*] 38°C | 90.3±3.74 | 1.27±0.87 | 5.63±3.51 | 0.10±0.11 | 1.29±0.57 |
| | | | | | |
| *osh1-osh7*Δ [*osh4$^{ts}$*] 26°C | 85.8±1.44 | 1.75±0.22 | 9.54±0.24 | 0.13±0.03 | 0.92±0.08 |
| *osh1-osh7*Δ [*osh4$^{ts}$*] 38°C | 72.5±0.61 | 2.01±0.16 | 22.8±0.72 | 0.30±0.16 | 0.44±0.12 |
| | | | | | |
| *sac1Δ* 26°C | 81.6±0.56 | 1.56±0.32 | 16.4±0.79 | 0.16±0.02 | 0.30±0.10 |
| | | | | | |
| *sac1$^{ts}$* 38°C | 88.2±4.21 | 2.21±0.80 | 7.85±2.86 | 0.13±0.08 | 1.58±0.55 |
| *sac1$^{ts}$ osh1-7*Δ [*osh4$^{ts}$*] 38°C | 76.3±8.43 | 1.74±0.50 | 21.2±7.71 | 0.13±0.06 | 0.62±0.30 |
| | | | | | |
| *osh2*Δ *osh3*Δ 26°C | 90.9±3.77 | 1.41±0.12 | 3.38±0.40 | 0.13±0.03 | 1.19±0.55 |
| | | | | | |
| *scs2*Δ *scs22*Δ 26°C | 92.8±2.32 | 2.18±0.73 | 3.60±0.80 | 0.23±0.07 | 1.61±0.59 |
| | | | | | |
| *osh1-osh7*Δ [*osh4$^{ts}$*] 38°C | | | | | |
| + [*CEN OSH2*] | 84.5±5.88 | 0.88±0.44 | 6.36±3.05 | 0.09±0.01 | 0.65±0.36 |
| + [*CEN OSH3*] | 86.5±4.95 | 1.67±1.36 | 9.82±3.30 | 0.14±0.10 | 0.62±0.38 |
| + [*CEN OSH4*] | 83.0±3.91 | 2.22±0.71 | 9.92±2.19 | 0.16±0.03 | 1.05±0.52 |
| + [*CEN osh4 $^{\Delta 1\text{-}29}$*] | 67.9±7.86 | 2.21±0.64 | 26.3±6.72 | 0.29±0.11 | 0.36±0.28 |
| + [*CEN osh4$^{L111D}$*] | 79.9±4.38 | 1.63±0.12 | 24.3±2.08 | 0.18±0.06 | 0.22±0.10 |
| + [*CEN osh4$^{R236E,\ K242E,\ K243E}$*] | 81.1±4.44 | 1.58±0.10 | 21.7±1.92 | 0.30±0.03 | 0.28±0.06 |
| + [empty vector] | 71.0±3.91 | 1.69±0.31 | 24.3±3.56 | 0.26±0.06 | 0.22±0.09 |

Yeast strains incubated at the indicated temperatures were labeled with $^{3}$H-*myo*-inositol. Lipids were extracted and deacylated for analysis by HPLC as described. The mean peak area (cpm) of PtdIns and each PI species is reported as a percentage of the total $^{3}$H-labeled lipids. The values reported are the mean (± standard deviation) of at least two independent experiments.

## References


Audhya, A., Foti, M., and Emr, S.D. (2000). Distinct roles for the yeast phosphatidylinositol 4-kinases, Stt4p and Pik1p, in secretion, cell growth, and organelle membrane dynamics. Mol Biol Cell *11*, 2673-2689.

Audhya, A., and Emr, S.D. (2002). Stt4 PI 4-kinase localizes to the plasma membrane and functions in the Pkc1-mediated MAP kinase cascade. Dev Cell *2*, 593-605.

Baird, D., Stefan, C., Audhya, A., Weys, S., and Emr, S.D. (2008). Assembly of the PtdIns 4-kinase Stt4 complex at the plasma membrane requires Ypp1 and Efr3. J Cell Biol *183*, 1061-1074.

Beh, C.T., Cool, L., Phillips, J., and Rine, J. (2001). Overlapping functions of the yeast oxysterol-binding protein homologues. Genetics *157*, 1117-1140.

Beh, C.T., and Rine, J. (2004). A role for yeast oxysterol-binding protein homologs in endocytosis and in the maintenance of intracellular sterol-lipid distribution. J Cell Sci *117*, 2983-2996.

Bevis, B.J., Hammond, A.T., Reinke, C.A., and Glick, B.S. (2002). De novo formation of transitional ER sites and Golgi structures in Pichia pastoris. Nat Cell Biol *4*, 750-756.

Blagoveshchenskaya, A., Cheong, F.Y., Rohde, H.M., Glover, G., Knodler, A., Nicolson, T., Boehmelt, G., and Mayinger, P. (2008). Integration of Golgi trafficking and growth factor signaling by the lipid phosphatase SAC1. J Cell Biol *180*, 803-812.

Breslow, D.K., Collins, S.R., Bodenmiller, B., Aebersold, R., Simons, K., Shevchenko, A., Ejsing, C.S., and Weissman, J.S. (2010). Orm family proteins mediate sphingolipid homeostasis. Nature *463*, 1048-1053.

Christianson, T.W., Sikorski, R.S., Dante, M., Shero, J.H., and Hieter, P. (1992). Multifunctional yeast high-copy-number shuttle vectors. Gene *110*, 119-122.

D'Angelo, G., Vicinanza, M., Di Campli, A., and De Matteis, M.A. (2008). The multiple roles of PtdIns(4)P -- not just the precursor of PtdIns(4,5)P2. J Cell Sci *121*, 1955-1963.

Fairn, G.D., Curwin, A.J., Stefan, C.J., and McMaster, C.R. (2007). The oxysterol binding protein Kes1p regulates Golgi apparatus phosphatidylinositol-4-phosphate function. Proc Natl Acad Sci U S A *104*, 15352-15357.

Faulhammer, F., Kanjilal-Kolar, S., Knodler, A., Lo, J., Lee, Y., Konrad, G., and Mayinger, P. (2007). Growth control of Golgi phosphoinositides by reciprocal localization of sac1 lipid phosphatase and pik1 4-kinase. Traffic *8*, 1554-1567.

Foti, M., Audhya, A., and Emr, S.D. (2001). Sac1 lipid phosphatase and Stt4 phosphatidylinositol 4-kinase regulate a pool of phosphatidylinositol 4-phosphate that functions in the control of the actin cytoskeleton and vacuole morphology. Mol Biol Cell *12*, 2396-2411.

Ghaemmaghami, S., Huh, W.K., Bower, K., Howson, R.W., Belle, A, Dephoure, N., O'Shea, E.K., and Weissman, J.S., (2003). Global analysis of protein expression in yeast. Nature *425*, 737-741.

Guo, S., Stolz, L.E., Lemrow, S.M., and York, J.D. (1999). SAC1-like domains of yeast SAC1, INP52, and INP53 and of human synaptojanin encode polyphosphoinositide phosphatases. J Biol Chem *274*, 12990-12995.

Im, Y.J., Raychaudhuri, S., Prinz, W.A., and Hurley, J.H. (2005). Structural mechanism for sterol sensing and transport by OSBP-related proteins. Nature *437*, 154-158.

Kagiwada, S., and Hashimoto, M. (2007). The yeast VAP homolog Scs2p has a phosphoinositide-binding ability that is correlated with its activity. Biochem Biophys Res Commun *364*, 870-876.

Kaiser, S.E., Brickner, J.H., Reilein, A.R., Fenn, T.D., Walter, P., and Brunger, A.T. (2005). Structural basis of FFAT motif-mediated ER targeting. Structure *13*, 1035-1045.

Konrad, G., Schlecker, T., Faulhammer, F., and Mayinger, P. (2002). Retention of the yeast Sac1p phosphatase in the endoplasmic reticulum causes distinct changes in cellular phosphoinositide levels and stimulates microsomal ATP transport. J Biol Chem *277*, 10547-10554.

Lev, S. (2010). Non-vesicular lipid transport by lipid-transfer proteins and beyond. Nat Rev Mol Cell Biol, *11*, 739-750.

Levine, T.P., and Munro, S. (2001). Dual targeting of Osh1p, a yeast homologue of oxysterol-binding protein, to both the Golgi and the nucleus-vacuole junction. Mol Biol Cell *12*, 1633-1644.

Li, X., Rivas, M.P., Fang, M., Marchena, J., Mehrotra, B., Chaudhary, A., Feng, L., Prestwich, G.D., and Bankaitis, V.A. (2002). Analysis of oxysterol binding protein homologue Kes1p function in regulation of Sec14p-dependent protein transport from the yeast Golgi complex. J Cell Biol *157*, 63-77.

Liu, Y., and Bankaitis, V.A. (2010). Phosphoinositide phosphatases in cell biology and disease. Prog Lipid Res *49*, 201-217.

Liu, Y., Boukhelifa, M., Tribble, E., Morin-Kensicki, E., Uetrecht, A., Bear, J.E., and Bankaitis, V.A. (2008). The Sac1 phosphoinositide phosphatase regulates Golgi membrane morphology and mitotic spindle organization in mammals. Mol Biol Cell *19*, 3080-3096.

Loewen, C.J., Gaspar, M.L., Jesch, S.A., Delon, C., Ktistakis, N.T., Henry, S.A., and Levine, T.P. (2004). Phospholipid metabolism regulated by a transcription factor sensing phosphatidic acid. Science *304*, 1644-1647.

Loewen, C.J., Roy, A., and Levine, T.P. (2003). A conserved ER targeting motif in three families of lipid binding proteins and in Opi1p binds VAP. EMBO J *22*, 2025-2035.

Loewen, C.J., Young, B.P., Tavassoli, S., and Levine, T.P. (2007). Inheritance of cortical ER in yeast is required for normal septin organization. J Cell Biol *179*, 467-483.

Longtine, M.S., McKenzie, A., 3rd, Demarini, D.J., Shah, N.G., Wach, A., Brachat, A., Philippsen, P., and Pringle, J.R. (1998). Additional modules for versatile and economical PCR-based gene deletion and modification in Saccharomyces cerevisiae. Yeast *14*, 953-961.

Maehama, T., Taylor, G.S., Slama, J.T., and Dixon, J.E. (2000). A sensitive assay for phosphoinositide phosphatases. Anal Biochem *279*, 248-250.

Manford, A., Xia, T., Saxena, A.K., Stefan, C., Hu, F., Emr, S.D., and Mao, Y. (2010). Crystal structure of the yeast Sac1: implications for its phosphoinositide phosphatase function. EMBO J.

Nemoto, Y., Kearns, B.G., Wenk, M.R., Chen, H., Mori, K., Alb, J.G., Jr., De Camilli, P., and Bankaitis, V.A. (2000). Functional characterization of a mammalian Sac1 and mutants exhibiting substrate-specific defects in phosphoinositide phosphatase activity. J Biol Chem *275*, 34293-34305.

Ngo, M.H., Colbourne, T.R., and Ridgway, N.D. (2010). Functional implications of sterol transport by the oxysterol-binding protein gene family. Biochem J *429*, 13-24.

Parrish, W.R., Stefan, C.J., and Emr, S.D. (2005). PtdIns(3)P accumulation in triple lipid-phosphatase-deletion mutants triggers lethal hyperactivation of the Rho1p/Pkc1p cell-integrity MAP kinase pathway. J Cell Sci *118*, 5589-5601.

Peretti, D., Dahan, N., Shimoni, E., Hirschberg, K., and Lev, S. (2008). Coordinated lipid transfer between the endoplasmic reticulum and the Golgi complex requires the VAP proteins and is essential for Golgi-mediated transport. Mol Biol Cell *19*, 3871-3884.

Raychaudhuri, S., Im, Y.J., Hurley, J.H., and Prinz, W.A. (2006). Nonvesicular sterol movement from plasma membrane to ER requires oxysterol-binding protein-related proteins and phosphoinositides. J Cell Biol *173*, 107-119.

Rieder, S.E., Banta, L.M., Kohrer, K., McCaffery, J.M., and Emr, S.D. (1996). Multilamellar endosome-like compartment accumulates in the yeast vps28 vacuolar protein sorting mutant. Mol Biol Cell *7*, 985-999.

Rivas, M.P., Kearns, B.G., Xie, Z., Guo, S., Sekar, M.C., Hosaka, K., Kagiwada, S., York, J.D., and Bankaitis, V.A. (1999). Pleiotropic alterations in lipid metabolism in yeast sac1 mutants: relationship to "bypass Sec14p" and inositol auxotrophy. Mol Biol Cell *10*, 2235-2250.

Robinson, J.S., Klionsky, D.J., Banta, L.M., and Emr, S.D. (1988). Protein sorting in Saccharomyces cerevisiae: isolation of mutants defective in the delivery and processing of multiple vacuolar hydrolases. Mol Cell Biol *8*, 4936-4948.

Roy, A., and Levine, T.P. (2004). Multiple pools of phosphatidylinositol 4-phosphate detected using the pleckstrin homology domain of Osh2p. J Biol Chem *279*, 44683-44689.

Saksena, S., Wahlman, J., Teis, D., Johnson, A.E., and Emr, S.D. (2009). Functional reconstitution of ESCRT-III assembly and disassembly. Cell *136*, 97-109.

Schulz, T.A., Choi, M.G., Raychaudhuri, S., Mears, J.A., Ghirlando, R., Hinshaw, J.E., and Prinz, W.A. (2009). Lipid-regulated sterol transfer between closely apposed membranes by oxysterol-binding protein homologues. J Cell Biol *187*, 889-903.

Seaman, M.N., McCaffery, J.M., and Emr, S.D. (1998). A membrane coat complex essential for endosome-to-Golgi retrograde transport in yeast. J Cell Biol *142*, 665-681.

Sikorski, R.S., and Hieter, P. (1989). A system of shuttle vectors and yeast host strains designed for efficient manipulation of DNA in Saccharomyces cerevisiae. Genetics *122*, 19-27.

Tahirovic, S., Schorr, M., and Mayinger, P. (2005). Regulation of intracellular phosphatidylinositol-4-phosphate by the Sac1 lipid phosphatase. Traffic *6*, 116-130.

Voeltz, G.K., Prinz, W.A., Shibata, Y., Rist, J.M., and Rapoport, T.A. (2006). A class of membrane proteins shaping the tubular endoplasmic reticulum. Cell *124*, 573-586.

Wei, H.C., Sanny, J., Shu, H., Baillie, D.L., Brill, J.A., Price, J.V., and Harden, N. (2003). The Sac1 lipid phosphatase regulates cell shape change and the JNK cascade during dorsal closure in Drosophila. Curr Biol *13*, 1882-1887.

# Chapter III

## ER-PM tethering proteins regulate cell signaling and ER morphology

Andrew G. Manford*[1], Christopher J. Stefan*[1], Helen L. Yuan[1], Jason A. MacGurn[1], and Scott D. Emr[1]

[1]Weill Institute for Cell & Molecular Biology, Department of Molecular Biology & Genetics, Cornell University, Ithaca, NY, 14853

* These authors contributed equally to this work.

Andrew Manford contributed significantly to all figures and wrote and prepared the manuscript.

Chapter III was originally published in Developmental Cell 23, 1129–1140, 2012

# Abstract

ER-PM junctions are conserved structures defined as regions of the ER that tightly associate with the PM. However, little is known about the mechanisms that tether these organelles together and why such connections are maintained. Using a quantitative proteomic approach, we identified three families of ER-PM tethering proteins in yeast: Ist2 (related to mammalian TMEM16 ion channels), the tricalbins (Tcb1/2/3, orthologs of the Extended Synaptogmins), and Scs2 and Scs22 (VAP proteins). Loss of all six tethering proteins results in the separation of the ER from the PM and the accumulation cytoplasmic ER. Importantly, we find that phosphoinositide signaling is mis-regulated at the PM and the unfolded protein response is constitutively activated in the ER in cells lacking ER-PM tether proteins. These results reveal critical roles for ER-PM contacts in cell signaling, organelle morphology, and ER function.

# Introduction

The endoplasmic reticulum (ER) is a vast membrane network of sheets and tubules with essential roles in protein modification and secretion, lipid synthesis, and calcium signaling. To execute its various functions, the ER is organized into distinct compartments, such as rough ER membranes studded with ribosomes and smooth ER enriched in lipid biosynthetic enzymes. In addition, the ER adopts diverse shapes and architectures in different organisms and specialized cell types (Shibata et al., 2006). For example, in cells dedicated to protein secretion such as pancreatic acinar cells, the ER is an expansive system compactly arranged into stacks of membrane sheets. In contrast, in excitable cells such as muscle cells, ER tubules form close associations with the plasma membrane (PM) that are important for calcium-inducible contractions (Carrasco and Meyer, 2011). Thus, cells have evolved multiple mechanisms for ER shape and architecture that support specialized functions performed in the ER.

The ER must coordinate each of its specialized functions with other organelles in the cell (*e.g.* the PM, Golgi, endosomes, lysosomes, and mitochondria). Vesicular trafficking between organelles has long been appreciated as a major mechanism for intracellular signaling and communication. However, recent studies have highlighted roles for membrane junctions between organelles– where two organelles are closely apposed without undergoing membrane fusion– as important sites for intracellular signaling (Carrasco and Meyer, 2011; Toulmay and Prinz, 2011). Although the ER is known to contact numerous organelles, ER-PM junctions are some of the most prominent. Since their initial discovery (Porter & Palade, 1957), ER-PM junctions have been observed in numerous organisms and cell types. One of the best-studied examples is the association of ER-localized STIM proteins with the PM calcium channel Orai at ER-PM junctions in the store-operated calcium entry pathway (Liou et al., 2005; Park et al., 2009).

Additional PM-ER junctions have been described in neurons, insect photoreceptor cells, and in plants (Hayashi et al., 2008; Hepler et al., 1990; Suzuki and Hirosawa, 1994).

In yeast cells, large regions of the plasma membrane have an underlying network of cortical ER (cER; Pichler et al., 2001; West et al., 2011). This network is associated with 20-45% of the PM, with an average distance of 33nm between the organelles (Pichler et al., 2001; West et al., 2011). Due to the close association of the PM and cER, ribosomes are excluded from the face of the cER adjacent to the PM (West et al., 2011), suggesting these structures have roles distinct from protein translocation into the ER. Consistent with this, a pathway has been described for the regulation of phosphoinositide (PI) lipid turnover at the PM by an ER-localized PI phosphatase (Stefan et al., 2011). In addition, the yeast oxysterol-binding protein homologs (Osh proteins) have been suggested to mediate sterol lipid transport at ER-PM contact sites (Schulz et al., 2009). Thus, junctions between the ER and the PM appear to be important sites for lipid metabolism and transport.

While ER-PM junctions have been known for several decades, our understanding of the mechanisms that tether the cortical ER to the PM and why such connections are established remains limited. The VAP orthologs Scs2 and Scs22 have been implicated in PM-ER contact formation and cortical ER inheritance in yeast (Loewen et al., 2007). However, we know relatively little about the architecture and the structural components of ER-PM junctions. In this study, we have uncovered the mechanism of ER-PM tethering in yeast. Using quantitative proteomics approaches, we identified additional ER-PM tethering factors: Ist2 (a member of the TMEM16 ion channel family) and the tricalbin proteins (Tcb1, Tcb2, and Tcb3–orthologs of the extended synaptotagmin family). These proteins have been suggested to localize to the cortical ER, but functions for these proteins have remained unknown (Fischer et al., 2009; Toulmay and

Prinz, 2011). We demonstrate that Ist2, the tricalbins, and the VAP orthologs Scs2/22 tether the cortical ER to the plasma membrane. Deletion of all six genes leads to a retraction of the ER away from the PM, and redistribution of ER into internal structures. This collapse of cortical ER leads to elevated levels of a phosphoinositide lipid at the PM and an unexpected induction of the unfolded protein response (UPR) in the ER. Moreover, cells lacking cER have impaired growth under cellular stress conditions and require an intact UPR for viability.

## Materials and Methods

### Yeast Strains, Plasmids, and Growth Assays

Chromosmal taggings and knock outs were performed as previously described (Longtine et al., 1998). To generate the *ire1*/Δtether double mutant, Δtether cells harboring a pRS416-*IRE1* (pAM36) plasmid were transformed with a NATMX knock out PCR for *IRE1* containing 500bp of 5' and 3' UTR. Transformants were screened by PCR and 3 positive candidates were struck on 5FOA 2x to select for loss of pAM36. A similar plasmid shuffle was performed for the *hac1*/Δtether double mutant. For all plating assays, cells were grown to mid-log, adjusted to 1 $OD_{600}$/ml and serial dilutions were plated on the indicated media. For liquid growth assays, cells were grown to midlog, adjusted to 0.1 $OD_{600}$/ml, and grown at 26°C. $OD_{600}$ measurements were taken at the indicated time points.

### Fluorescence Microscopy

All fluorescent microscopy was performed on mid-log cells. Images were aquired with a CSU-X spinning disk microscope (Yokogawa), with a 63x 1.4NA objective on an inverted microscope (DM16000B; Leica), a QuantEM EMCCD camera (Photometrics), and controlled by Slidebook

5.0 (Intelligent Imaging Innovations). The brightness and contrast of images were adjusted in Slidebook 5.0 and cropped in Photoshop (Adobe).

**Electron Microscopy**

Yeast cells were fixed with 2.5% (v/v) glutaradye for 1 hour and incubated in 1% potassium permanganate for 1 hour. Cells were dehydrated with 50%, 70%, 95%, and 100% ethanol. Samples were transitioned into 100% propylene oxide and embedded in Spurr's resin. Electron microscopy was performed on a Morgnani 268 transmission electron microscope (FEI) with a AMT digital camera and 80eV beam. The cER/PM ratios were measured using ImageJ. The brightness of EM images was adjusted with Photoshop (Adobe).

**Phosphoinositide Analysis**

To measuere cellular phosphoinositide levels, $5OD_{600}$ equivalents of mid-log cell grown in minimal media were harvested, washed in inositol free media, incubated for 10min in inositol free media at 26°C unless indicated, and labeled with myo-[2-$^{3}$H] inositol for 1 hour. Cells were then precipitated in 4.5% perchloric acid and lysed by vortexing with glass beads. Lysates were than washed in 100mM EDTA, phospholipids were deacylated, and head groups were isolated by extraction. Samples were dryed and resuspened in $H_2O$. 5million counts of each sample were were seperated by HPLC (Shimadzu) using a partisphere SAX column (GE healthcare) and measured by a 610TR radiomatic detector (PerkinElmer).

**Subcellular Fractionation**

Sucrose gradients were performed as described (Estrata et al., 2003) with modification. 75$OD_{600}$ equivalents of mid-log cells were harvested, washed in TE (10mM Tris-HCl pH 7.5, 1mM EDTA) and resuspened in STE10 buffer (10%[wt/wt] sucrose, 10mM EDTA, 10mM Tris-HCl pH7.5, Complete EDTA-free protease inhibitor cocktail [Roche], .1mM AEBSF, 1μM pepstatin A). Beads were added to the meniscus and vortexed for 2 min. 1ml of additional STE 10 buffer was added and lysates were cleared by 500g spin for 5min. .5mls of lysate (25$OD_{600}$ equivalents) were loaded on top of a 10ml 20-60% linear sucrose gradient and spun at 100000g's for 18 hours in a SW41TI rotor (Beckman). Twelve .875ul fractions were collected form the top and TCA precipitated. The fractions were washed 2x in Acetone, dryed, and resuspened in 6M urea sample buffer (150 mM Tris pH 6.8, 6 M Urea, 6% SDS, 10% β-mercaptoethanol, 20% Glycerol). All samples were heated at 42°C 20min and then analzyed by western blot.

**β-galactosidase assay**

Harvested cells were washed 1x in Z buffer (60mM $Na_2HPO_4$, 40mM $NaH_2PO_4$ 10mM KCl, 1mM $MgSO_4$) and $OD_{600}$ were measured. Samples were adjusted to 500ul in Z buffer, 50ul of .1% SDS was added, and samples were vortexed for 15 seconds. 50ul of chloroform was then added and samples were vortexed for 15 seconds. Reactions were started by the addion of 100ul of ONPG (4mg/ml). 500ul of 1M $Na_2CO_3$ was added to quench the reaction and samples were spun for 13000gs for 2min. $Abs_{420}$ of the supernatent was measured and the units of activity were calculated (1000 x $Abs_{420}$)/(time (min) x $OD_{600}$ equivelents).

**CPY sorting**

CPY sorting was performed as described (Foti et al.) Briefly mid-log cells were harvested, washed in synthetic media, and Easytag Express $^{35}S$ protein labeling mix(Perkin Elmer) was added for 10 min. Chase solution of cold Methionine and Cysteine was added, and samples were TCA precipitated at indicated time points. After 30 min of precipitation, extracts were generated, and carboxypeptidase Y (CPY) was immunopecipitated.

**SILAC experiment and quantitative mass spectrometry**

Cells were grown in the presence of heavy or light lysine and arginine isotopes, harvested at mid-log, washed in TE, and frozen. Cells were resupended in lysis buffer (50 mM Tris pH 7.5, 1% Tween20, 150 mM NaCl, 5 mM EDTA, 2X Complete EDTA-Free protease inhibitor tablets [Roche], 1X PhosStop [Roche]) and disrupted with glass beads for 30min. Cell lysates were cleared by 2x 16000g spin and incubated with M2 flag beads (Sigma) for 2 hours at 4°C. Beads were then washed 3 times and the protein was eluted with 100 mM Tris (pH 8.0), 1% SDS at 95°C for 5 min. Samples were processed for mass spectrometry as described (MacGurn et al., 2011).

**Cellular protien expression levels and antibodies**

$5OD_{600}$ equivelents of mid-log cells were harvested and precipitated with tricholoroacidic acid (TCA). Samples were washed 2x in acetone, dryed, and lysed by bead beating. Extracts were analyzed by Western blot using an Odyssey infared imaging system (LI-COR Biosciences). The following antibodies were used in this study: α-HA (12CA5, Roche), α-G6PDH (Sigma), α-Dpm1 (Invitrogen), and α-GFP (Santa Cruz Biotechnology), α-FLAG (M2, Sigma), α-CPY, and α-Pma1 (gift from Amy Chang, University of Michigan-Ann Arbor).

## Results

### Identification of candidate PM-ER tether proteins

The cortical ER (cER) and PM make extensive contacts, as observed in yeast cells by the close apposition of the ER protein Sec61-GFP and a PM marker (mCherry-2xPH$^{PLC\delta}$; Figure 3.1A). At these sites, levels of the lipid phosphatidylinositol-4-phosphate (PI4P) in the PM are regulated in *trans* by the ER-localized PI phosphatase Sac1 (Stefan et al., 2011). However, the mechanisms that link the cER and PM (within 15 nm) and allow Sac1 to catalyze PI4P turnover at the PM are not well understood. The VAP orthologs Scs2/Scs22 have been implicated in PM-ER membrane tethering and Sac1-mediated PI4P turnover (Loewen et al., 2007; Stefan et al., 2011). Scs2 and its homolog Scs22 contain a single transmembrane domain and a major sperm protein (MSP) domain that binds FFAT motifs (two phenylalanines in an acidic tract) in lipid transfer proteins (Figure1C; Loewen et al., 2003). However, cells lacking both Scs2 and Scs22 only accumulate a 2-fold increase in PI4P, while loss of Sac1 results in a nearly 10-fold increase (Foti et al., 2001; Stefan et al., 2011, Figure 3.8B). If Scs2/22 were the only cER-PM tethers, cells lacking these proteins should display a dramatic change in PI4P levels, similar to *sac1* mutants. Thus, additional tethering proteins that link the PM and ER likely exist.

Since Sac1 and Scs2 function at sites where the PM and ER are tightly apposed, we hypothesized that additional proteins involved in PM-ER tethering might interact with Sac1 and Scs2. We performed stable isotope labeling of amino acids in culture (SILAC) and identified Sac1 and Scs2-interacting proteins by quantitative mass spectrometry analysis (Figure 3.1B). We identified 26 and 32 high confidence interactions for Sac1 and Scs2 respectively (hits with greater then 10 peptides, a false positive rate <1%, and an Xpress Ratio above 20), and 17 proteins interacted with both Sac1 and Scs2, including each other (Tables 3.1, 3.2). We also

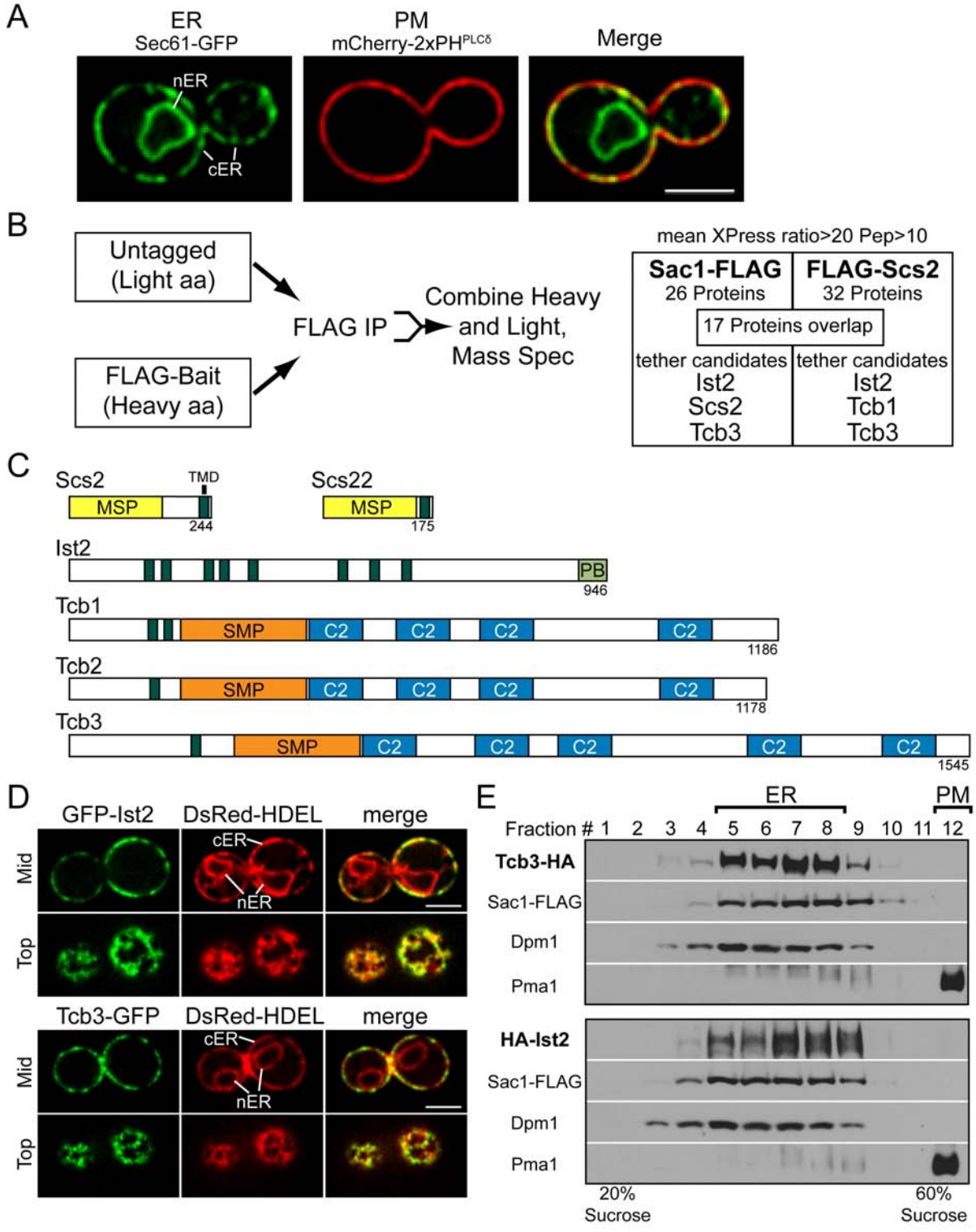
A
ER
Sec61-GFP
PM
mCherry-2xPH^PLCδ
Merge
nER
cER
B
Untagged
(Light aa)
FLAG-Bait
(Heavy aa)
FLAG IP
Combine Heavy
and Light,
Mass Spec
mean XPress ratio>20 Pep>10
Sac1-FLAG
26 Proteins
FLAG-Scs2
32 Proteins
17 Proteins overlap
tether candidates
Ist2
Scs2
Tcb3
tether candidates
Ist2
Tcb1
Tcb3
C
Scs2
TMD
MSP
244
Scs22
MSP
175
Ist2
PB
946
Tcb1
SMP
C2
1186
Tcb2
SMP
C2
1178
Tcb3
SMP
C2
1545
D
GFP-Ist2
DsRed-HDEL
merge
Mid
Top
cER
nER
Tcb3-GFP
DsRed-HDEL
merge
E
ER
PM
Fraction # 1 2 3 4 5 6 7 8 9 10 11 12
Tcb3-HA
Sac1-FLAG
Dpm1
Pma1
HA-Ist2
Sac1-FLAG
Dpm1
Pma1
20%
Sucrose
60%
Sucrose

**Figure 3.1. Identification of candidate PM-ER tethers.**

(A) ER marker Sec61-GFP (green) and PM marker mCherry-2xPH$^{PLC\delta}$ (red) expressed in wild type cells. Cortical ER and nuclear ER are labeled. Scale bar, 3μm.

(B) Schematic of Sac1 and Scs2 SILAC experiments followed by quantitative mass spectrometery. See Tables 3.1 and 3.2.

(C) Diagram of candidate tethering proteins. Amino acid length is indicated. MSP, major sperm protein domain; TMD, transmembrane domain; PB, poly-basic domain; SMP, synaptotagmin-like-mitochondrial lipid binding protein.

(D) GFP-Ist2 and Tcb3-GFP localize to the cER in wild type cells (ER is marked by DsRed-HDEL). Nuclear ER and cortical ER are indicated. Scale bar, 3 μm.

(E) Equilibrium density fractionation of cells expressing 3xHA-Ist2, Tcb3-3xHA, and Sac1-3xFLAG. Fractions were collected and analyzed by immunobotting for Sac1-3xFLAG (ER), Dpm1(ER), and Pma1(PM) as organelle markers.

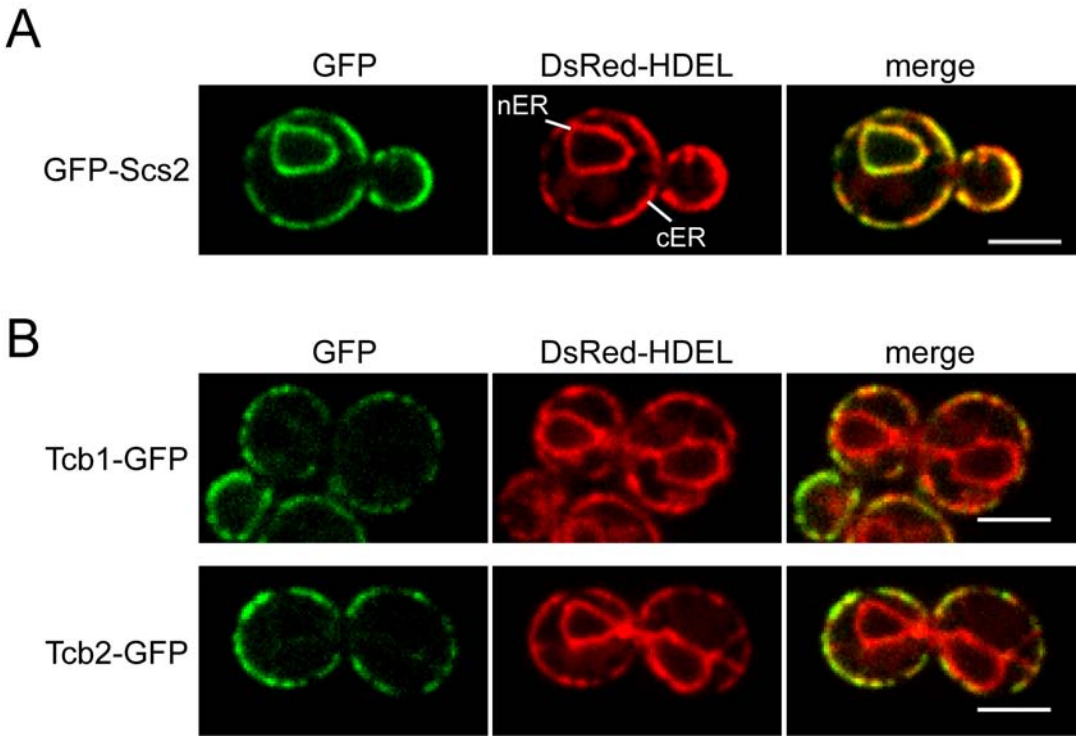


**Figure 3.2. GFP-Scs2 localizes to the ER, Tcb1-GFP and Tcb2-GFP are enriched in the cER.**

(A) GFP-Scs2 localization in wild type cells expressing the ER marked DsRed-HDEL. Scale bar, 3μm.

(B) Tcb1-GFP, and Tcb2-GFP localization in wild type cells expressing the ER marked DsRed-HDEL. Scale bar, 3μm.

identified three reported Sac1-interacting proteins, Lcb1, Lcb2, and Dpm1 (Table 3.1; Breslow et al., 2010; Faulhammer et al., 2005), and two known Scs2-interacting proteins, Osh1 and Yet1 (Table 3.2; Loewen et al., 2003; Wilson et al., 2011). Many of the Sac1 and Scs2-interacting proteins have known functions in lipid metabolism, protein trafficking, and protein glycosylation, while only a small subset had no previously annotated function (Tables 3.1, 3.2). Interestingly we identified the reticulons, Rtn1 and 2, and atlastin, Sey1, as Scs2-interacting proteins. These proteins have established roles in maintaining the structure of the ER (Hu et al., 2009; Voeltz et al., 2006). However loss of these proteins does not disrupt PM-ER contacts (Hu et al., 2009; West et al., 2011).

Among the proteins identified, we considered three as candidate PM-ER tethers: Scs2, Ist2, and the yeast tricalbin proteins Tcb1 and Tcb3 (Figure 3.1B). Ist2, Tcb1, and Tcb3, along with the other tricalbin Tcb2, were selected because they exhibit exclusively cortical ER localization (Toulmay and Prinz, 2012; Fischer et al., 2009; Figures 3.1D and 3.2B) and have no annotated functions. Ist2 and the tricalbins also have protein architectures that might be expected for an organelle-tethering protein: transmembrane domains and cytoplasmic lipid-binding domains. Ist2 is comprised of 8 transmembrane domains and a long cytoplasmic carboxyl-terminus that binds lipids and localizes to the cell cortex (Fischer et al., 2009; Figure 3.1C). The tricalbins contain transmembrane domains in their N-termini and lipid-binding C2 domains in their long cytoplasmic carboxyl-termini (Figure 3.1C, Schulz and Creutz, 2004). The tricalbins also possess a SMP domain that is found in other proteins localized to ER-organelle contact sites and is homologous to a domain found in lipid transfer proteins (Kopec et al., 2010; Toulmay and Prinz, 2012).

We next confirmed the localization of Ist2 and Tcb3 to the cER. At the midsection of yeast cells, GFP-tagged Ist2 and Tcb3 overlapped with the ER marker DsRed-HDEL, specifically at the cortical ER (Figure 3.1D). Significant co-localization of both Ist2 and Tcb3 was observed with the ER marker at the periphery of these cells (Figure 3.1D). Notably, regions devoid of ER lacked GFP signal. The other tricalbin family members, Tcb1 and Tcb2, also localize to the cER (Figure 3.2B; Toulmay and Prinz, 2012). However, both Ist2 and the tricalbins have been suggested to be PM proteins (Creutz et al., 2004; Juschke et al., 2005). To resolve these differing results, we performed equilibrium density gradient fractionations that efficiently separate ER and PM membranes. Consistent with our microscopy results that localized Ist2 and Tcb3 in the cER, both 3xHA-Ist2 and Tcb3-3xHA were present in fractions containing the ER markers Sac1-3xFLAG and Dpm1 and absent from the PM marker Pma1 fraction (Figure 3.1E).

**Deletion of tethers results in a loss of cER and accumulation of large cytoplasmic ER structures**

To determine if Ist2 and the tricalbin proteins function by tethering the cER to the PM, we constructed multiple deletion mutants of each of the tether candidates and scored Sec61-GFP localization as an ER marker. In wild type cells, the ER is organized into nuclear ER, a few cytoplasmic ER tubes and sheets, and cortical structures juxtaposed to the periphery of the cells (Figure 3.3A). Deletion of all six genes (*ist2, scs2/22, tcb1/2/3*) resulted in a striking phenotype– substantial reduction in cER, as large areas of the cell periphery have no associated ER (DIC/GFP merge, Figure 3.3A). Occasionally, small regions of the ER closely apposed to the cell cortex were observed (Figure 3.3A, arrow). In addition, collapsed ER structures accumulated

in the cytoplasm around the nucleus and in the emerging bud of mutant cells (Figure 3.3A). ER inheritance appeared to be normal in cells lacking the six genes, as non-nuclear ER was present in the bud before nuclear migration (Figure 3.4, asterisk). To verify our results with Sec61-GFP, we examined the morphology of the ER using another marker, GFP-HDEL, in multiple sections along the Z-axis in cells. In wild type cells, the ER network was clearly visible at the cell cortex and remained associated with the periphery through all Z sections observed (Figure 3.3B). However, in cells lacking the tether proteins the ER was no longer closely apposed to the PM, as GFP-HDEL was not observed at the periphery and mainly localized internally, (Figure 3.3B). Based on these results, we termed the strain lacking all six tethering proteins as Δtether cells and use this name throughout the study.

We observed a range of effects upon loss of the VAP proteins, Ist2, or tricalbins either alone or in combination. In *ist2* single mutant cells and *tcb1/2/3* triple mutant cells there was no significant loss of cER (marked by yellow arrows, Figure 3.4). Likewise, cER structures were readily observed in *ist2 tcb1/2/3* quadruple mutant cells, suggesting that the Scs2 and Scs22 VAP proteins were sufficient to form cER (Figure 3.4). In *scs2 scs22* mutant cells, cER structures were reduced compared to wild type cells–but not absent–consistent with roles for Ist2 and the tricalbins in cER formation (Figure 3.4). Accordingly, upon loss of Ist2 or the tricalbins in *scs2/22* cells (*ist2 scs2/22* and *scs2/scs22 tcb1/2/3* cells, Figure 3.4), we observed a further decrease in cER and an increase in enlarged cytoplasmic ER structures (red arrows, Figure 3.4) compared to *scs2/22* cells. We next confirmed that Ist2 and the tricalbins are sufficient for cER formation and localize to the remaining cER in cells expressing only one type of tether. In cells lacking all other tethers, both GFP-Ist2 (in *tcb1/2/3, scs2/22* cells) and Tcb3-GFP (in *ist2, scs2/22* cells) localized to the regions of remaining cortical ER, suggesting that the cortical ER

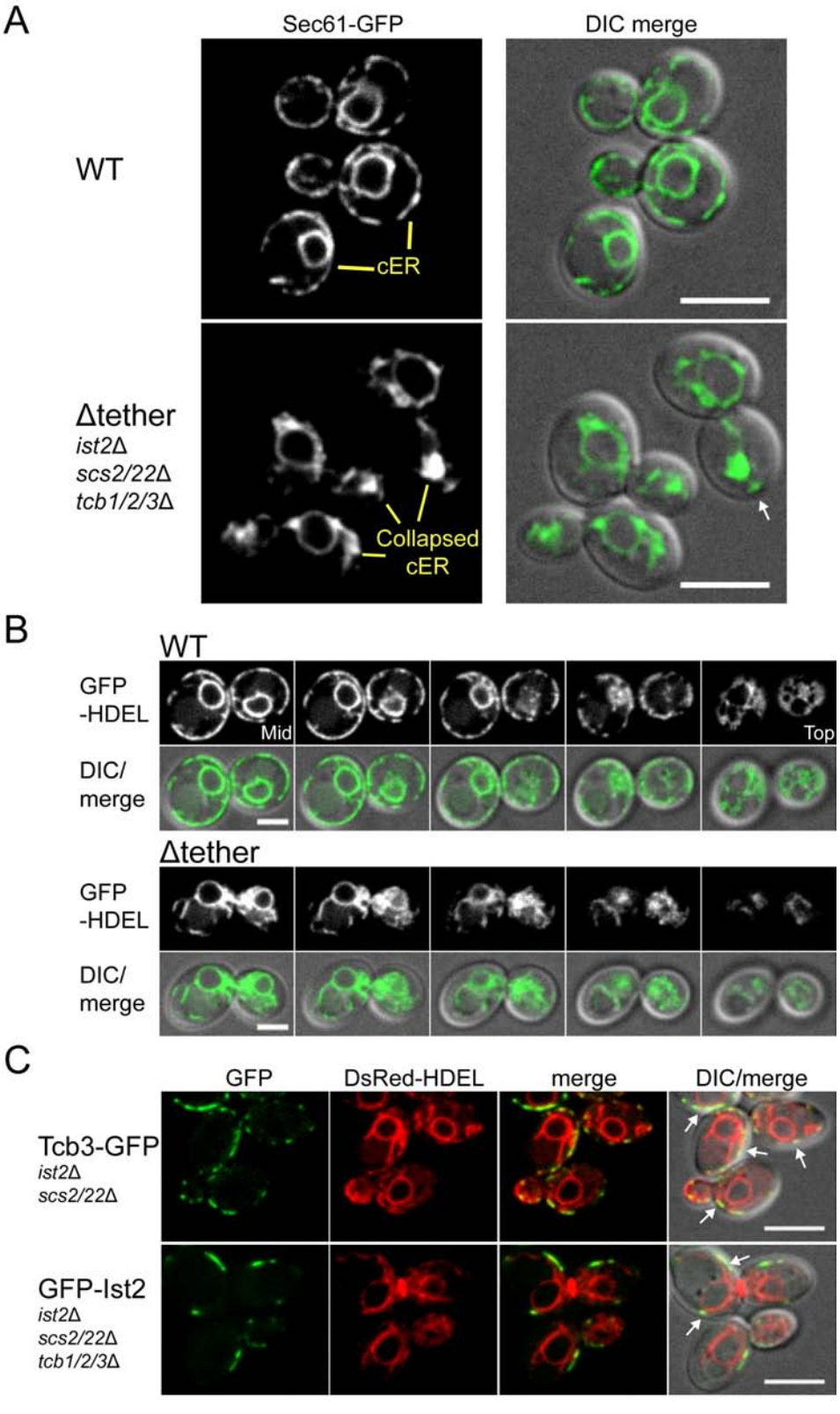
A
Sec61-GFP
DIC merge
WT
cER
Δtether
ist2Δ
scs2/22Δ
tcb1/2/3Δ
Collapsed
cER
B
WT
GFP
-HDEL
Mid
Top
DIC/
merge
Δtether
GFP
-HDEL
DIC/
merge
C
GFP
DsRed-HDEL
merge
DIC/merge
Tcb3-GFP
ist2Δ
scs2/22Δ
GFP-Ist2
ist2Δ
scs2/22Δ
tcb1/2/3Δ

**Figure 3.3. Scs2/22, Ist2, and the Tricalbins tether the cER to the PM in yeast.**

(A) Localization of the ER marker Sec61-GFP in wild type and Δtether cells (*ist2*Δ, *scs2/22*Δ, *tcb1/2/3*Δ). cER is indicated in wild type cells and collapsed ER in Δtether cells. Arrow indicates potential remaining cER in Δtether cell. Scale bar, 5 μm.

(B) Z stacks of wild type and Δtether cells expressing the ER marker GFP-HDEL. Each step is 0.4μm. Scale bar, 2.5 μm.

(C) Tcb3-GFP in *ist2*Δ, *scs2/22*Δ cells and GFP-Ist2 localization in *scs2/22*Δ, *tcb1/2/3*Δ cells expressing DsRed-HDEL. Arrow show regions labeled by the ER marker and Ist2 or Tcb3. Scale bar, 5 μm.

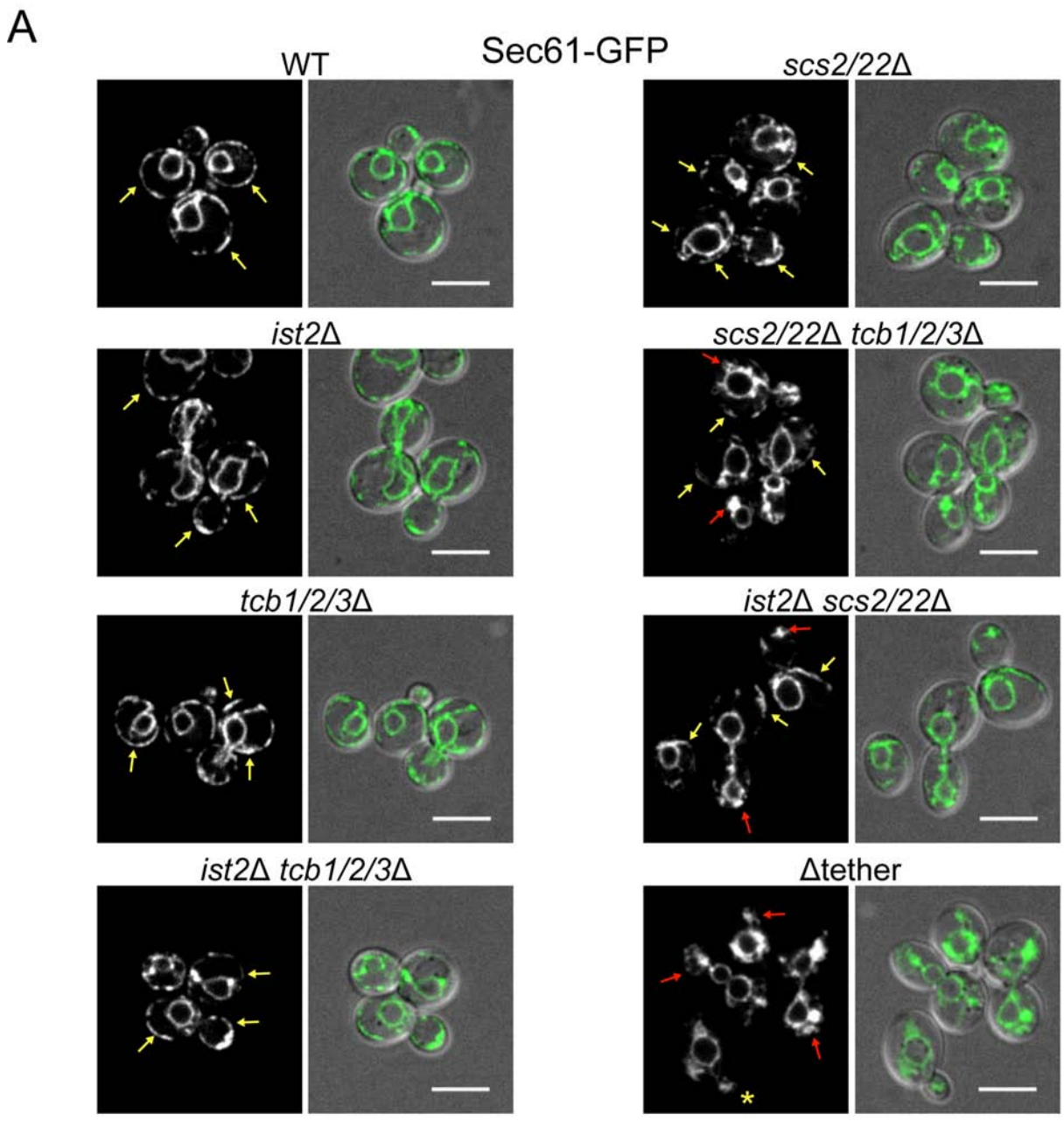


**Figure 3.4. Gradual loss of the cER and increase in cytoplasmic ER accumulations in tether mutants.**

(A) Fluorescent microscopy of Sec61-GFP in indicated strains. Yellow arrows are highlighting cER and red arrows ER accumulations within the cell. * indicates a small budded cell that contains ER in a Δtether cell. Scale bar, 5μm.

that is still present in an *scs2/22* mutant is tethered by Ist2 and the tricalbins (Figure 3.3C). These results also demonstrated that Ist2 and the tricalbins do not require the other tethers for their localization to PM-ER contacts or tethering function.

**Ultrastructural analysis of cER mutants**

Because we observed cytoplasmic ER accumulations in the Δtether mutant cells by fluorescence microscopy, we next examined the morphology of these structures at higher resolution using electron microscopy. In wild type cells, ER membranes appeared as dark stained structures at the periphery of the cell (cER) and as a discontinuous ring within the cell (nuclear ER, labeled in blue, Figure 3.5A). The cER (ER adjacent to the PM, labeled in purple) is the most abundant non-nuclear ER in wild type cells as very little cytoplasmic ER (green) was observed. In striking contrast to the ER morphology in wild type cells, the majority of the ER in Δtether mutant is not at the periphery. Instead, retracted masses of ER accumulated within the cytoplasm and likely account for the collapsed ER structures observed by fluorescence microscopy (Figure 3.5A). In addition to the cytoplasmic network, some Δtether cells also contained what appeared to be long ER tubules (Figure 3.6A). However, these structures are more likely extended ER sheets, as a tubule would not remain in the same plane of a thin EM section (~70nm) for such great distances (up to 5-7μm). Additional examples of Δtether mutant cells with collapsed ER structures and long cytoplasmic ER structures are shown in Figure 3.6B. Despite the large decrease in ER-PM contacts, mitochondria-ER junctions appear intact (Figure 3.5A).

Next, we quantified the loss of cER structures upon sequential deletion of the ER tether proteins. We decided to focus on mutants that had obvious cER morphology defects by

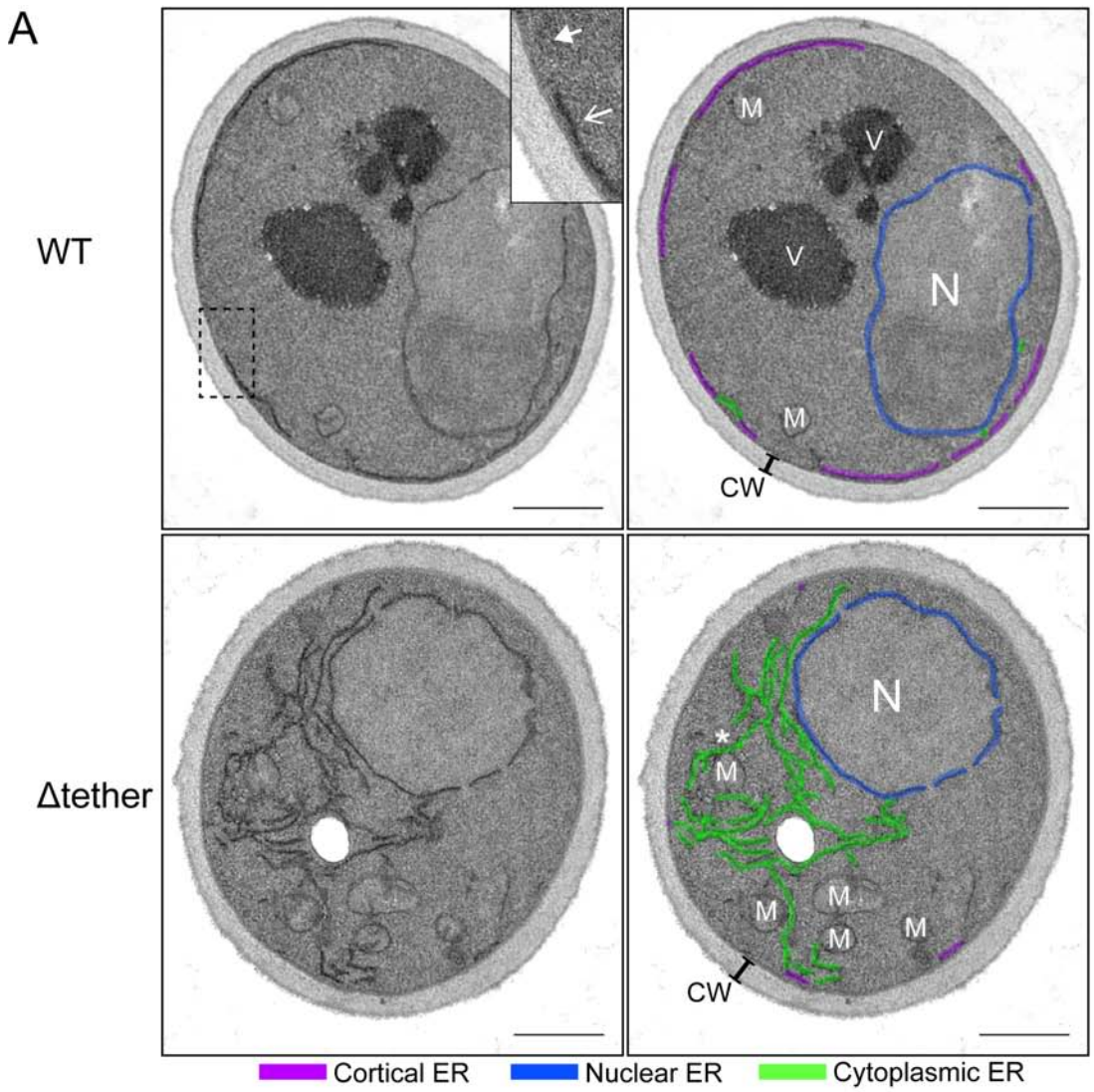
A
WT
Δtether
M
V
V
N
M
CW
N
*
M
M
M
M
M
CW
Cortical ER
Nuclear ER
Cytoplasmic ER

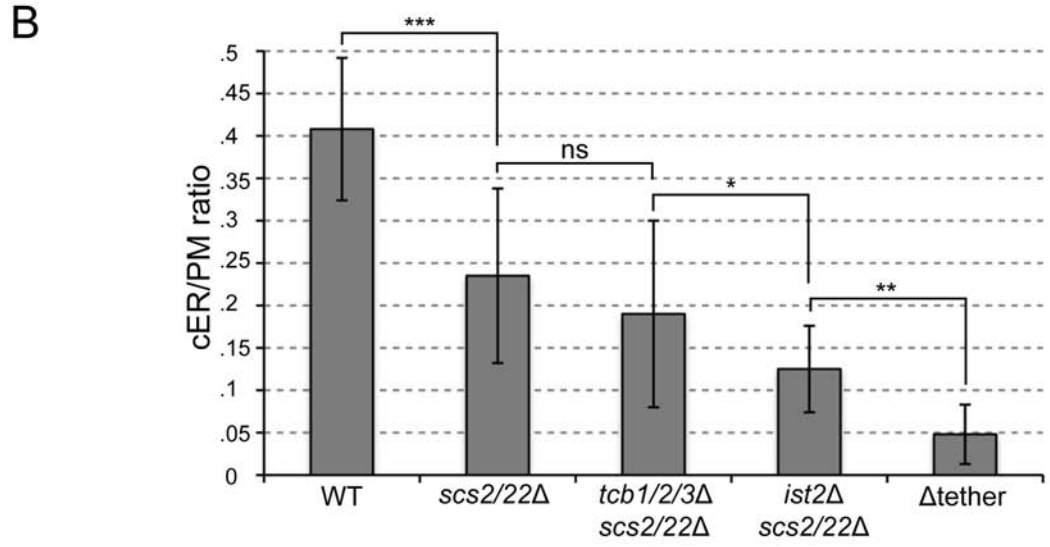
B
cER/PM ratio
.5
.45
.4
.35
.3
.25
.2
.15
.1
.05
0
***
ns
*
**
WT
scs2/22Δ
tcb1/2/3Δ scs2/22Δ
ist2Δ scs2/22Δ
Δtether

**Figure 3.5. Morphology of Δtether cells and quantification of cER in tether mutants**

(A) Electron microscopy of wild type and Δtether cells. Inset of wild type cell is an enlarged region showing PM associated with (open arrow) and without ER (closed arrow). Different ER structures are labeled in the right panels: cER in purple, nER in blue, and cytoplasmic ER in green. Mitochondria (M), nucleus (N), cell wall (CW) and vacuole (V) are also labeled. A mitochondrial-ER contact is shown by an asterisk. Scale bar, 500 nm.

(B) Quantification of cER expressed as a ratio of the length of cER/length of the PM in wild type and mutant cells. Error bars show StdDev (n=30 for each strain); significance was determined by one-way ANOVA with post-processing to correct for multple comparions (***P< 0.001; **P< 0.01; *P< 0.05; ns, not significant P >0.05).

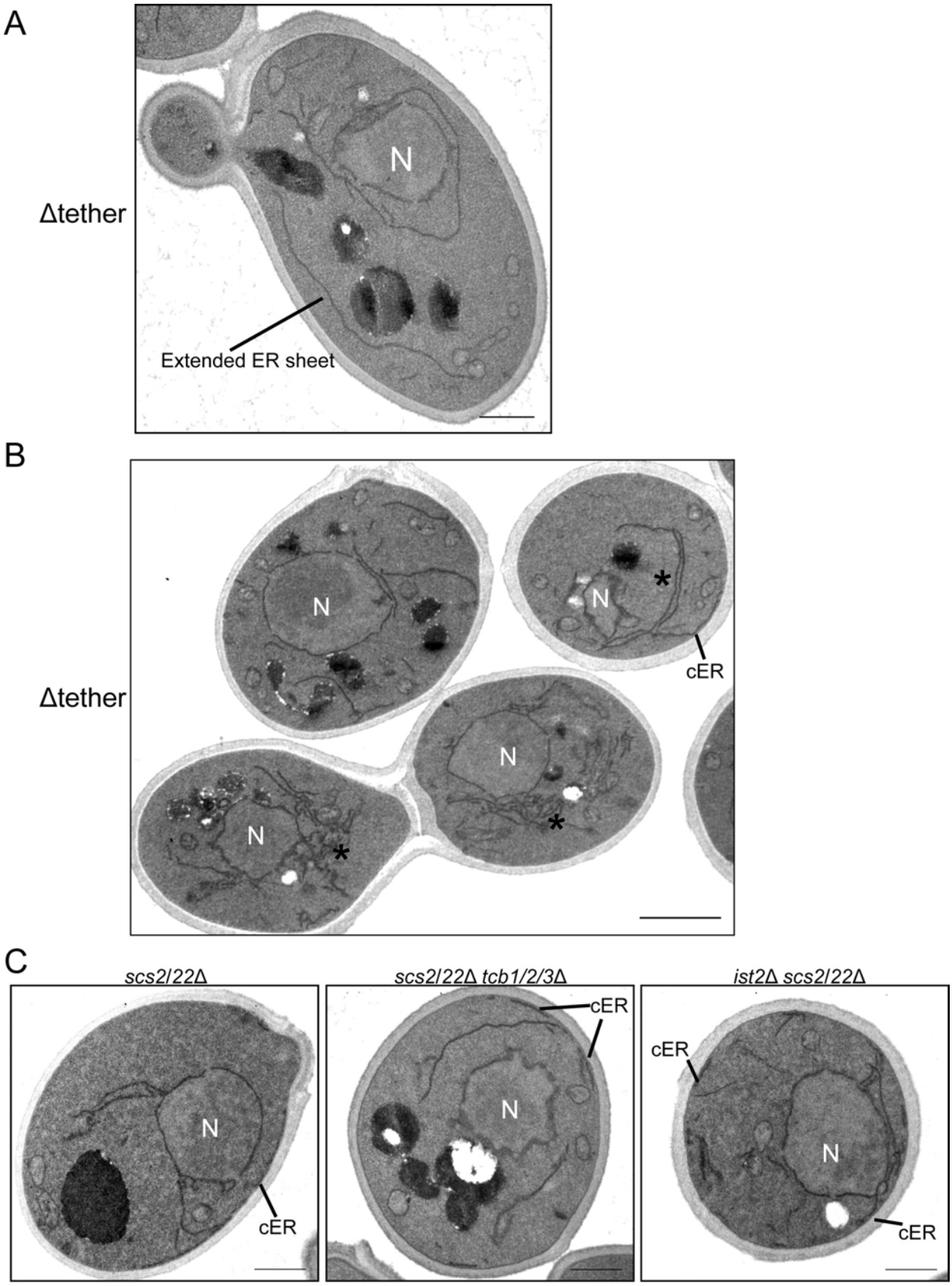
A
Δtether
N
Extended ER sheet
B
Δtether
N
N
cER
N
N
C
scs2/22Δ
scs2/22Δ tcb1/2/3Δ
ist2Δ scs2/22Δ
N
cER
N
cER
cER
N
cER

**Figure 3.6. Additional Δtether electron microscopy**

(A) Electron microscopy showing an extended ER sheet observed in Δtether cells. Scale bar, 500nm.

(B) Electron micscopy of a group of Δtether cells. * indicates abnormal ER structures. A region of potential cER is indicated. Scale bar, 1μm.

(C) Electron microscopy of *scs2/22*Δ, *scs2/22*Δ *tcb1/2/3*Δ, and *ist2*Δ *scs2/22*Δ cells. cER remaining in these mutants is indicated. Scale bar, 500nm.

Nucleus (N)

fluorescent microscopy, and thus we used *scs2/22* double mutant cells as a starting point. To quantitate the loss of cER in the mutants, we used a ratio of the sum length of cER segments (purple) over the circumference of the PM. Consistent with published results (West et al., 2011), in wild type cells approximately 40% of the PM was associated with cER structures (0.4 cER/PM ratio, Figure 3.5B). In *scs2/22* mutants the cER/PM ratio was decreased by nearly one-half (24% of the PM associated with cER; Figures 3.5B, 3.6C), consistent with previously published observations (Loewen et al., 2007). Upon further loss of Ist2, the cER/PM ratio decreased an additional two-fold (13% of the PM associated with cER structures in *ist2, scs2/22* triple mutant cells; Figures 3.5B, 3.6C). Upon deletion of all six genes (Δtether mutant cells), the cER/PM ratio decreased greater than 8-fold as compared to wild type cells (only 4.8% of the PM associated with cER, Figure 3.5B). Surprisingly, the cER/PM ratio for *tcb1/2/3*, *scs2/22* mutant cells was not significantly different than *scs2/22* mutants alone, and loss of the tricalbins only exhibited an effect when the other tethers (Scs2/22 and Ist2) were absent (compare *ist2 scs2 scs22* cells to Dtether cells; Figures 3.5B, 3.6C). Our results using both fluorescence and electron microscopy suggest a hierarchy amongst the PM-ER tethers where Scs2/22 provide a significant contribution, followed by Ist2, and then the tricalbins. It should be noted that in Δtether mutant cells, even though there is a large redistribution of cER to the cytoplasm, there appears to be small regions of cER present, suggesting the presence of additional unknown tethering proteins (Figures 3.5, 3.6B).

**PI4P accumulates at the PM in Δtether mutant cells**

The PI phosphatase Sac1 dephosphorylates PI4P on the PM in *trans* from the ER (Figure 3.7A; Stefan et al., 2011). In cells where PM-ER connections are disrupted, Sac1 should have

less access to its substrate at the PM and PI4P levels should increase. We first confirmed that Sac1 was mislocalized to intracellular ER structures in Δtether cells. Similar to other ER markers, GFP-Sac1 accumulated in the collapsed ER in Δtether cells (Figure 3.7B). Sac1 expression levels were not significantly different in whole cell lysates from wild type and Δtether mutant cells (Figure 3.8A). To monitor Sac1 function, we performed $^{3}$H-inositol labeling experiments and HPLC analysis to measure cellular PI levels in wild type and the tether mutant strains (Table 3.3). Consistent with a requirement for ER-localized Sac1 to be in close proximity to the PM, mutants with reduced cER displayed increased PI4P levels (Figure 3.7C). Increases in PI4P correlated with decreases in cER, as *scs2/22* and *scs2/22, tcb1/2/3* mutant cells had a modest increase in PI4P (greater than 2-fold), while *ist2*, *scs2/22* mutants with significantly reduced cER, accumulated higher PI4P levels (4-fold). In cells lacking only Ist2 (*ist2* mutant cells) or the tricalbins (*tcb1/2/3* cells), PI4P levels were similar to wild type (Table 3.3). In Δtether cells, in which the cER/PM ratio is reduced more than 8-fold (only 5% of the PM is associated with cER), PI4P levels increased greater than 7-fold (Figure 3.7C).

In addition to PI4P at the PM, the Sac1 PI phosphatase regulates pools of PI4P at the Golgi and ER (Faulhammer et al., 2005). We then addressed whether the ER tether proteins specifically regulate PI4P levels at the PM. For this, we visualized PI4P in wild type and Δtether cells using a fluorescent reporter that binds to PI4P (GFP-2xPH$^{Osh2}$; Roy and Levine, 2004). In wild type cells, the PI4P sensor was present at both Golgi compartments and the PM, with enriched PM localization in the bud (Figure 3.7D). However, similar to *sac1* mutant cells, the PI4P reporter was shifted to the PM in Δtether cells, with an even distribution in both mother and daughter cells (Figure 3.7D).

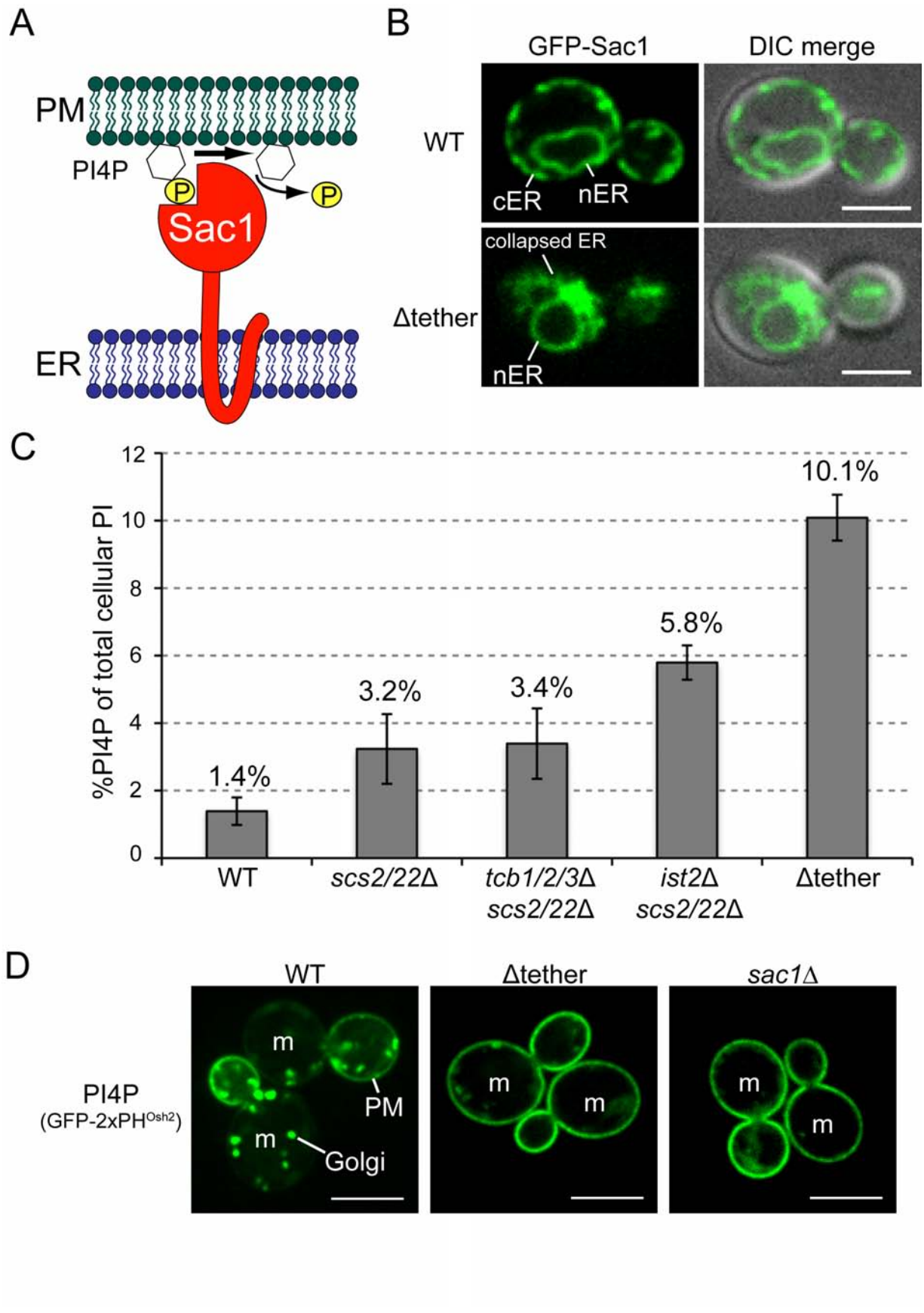
A
PM
PI4P
P
P
Sac1
ER
B
GFP-Sac1
DIC merge
WT
cER
nER
collapsed ER
Δtether
nER
C
%PI4P of total cellular PI
12
10
8
6
4
2
0
1.4%
3.2%
3.4%
5.8%
10.1%
WT
scs2/22Δ
tcb1/2/3Δ scs2/22Δ
ist2Δ scs2/22Δ
Δtether
D
WT
Δtether
sac1Δ
PI4P
(GFP-2xPH^Osh2)
m
PM
m
Golgi
m
m
m
m
m

**Figure 3.7. Loss of ER-PM contacts results in misregulation of PI4P at the PM.**

(A) Schematic for Sac1 phosphatase function. Sac1 is an integral ER membrane protein that dephosphorylates the lipid PI4P at the PM.

(B) Localization of GFP-Sac1 in wild type and Δtether cells. Scale bar, 5 μm.

C) Cellular PI4P levels in wild type and ER tether mutant cells, as measured by $^{3}$H-inositol labeling and HPLC analysis. Error bars show StdDev (n=3). See also Table 3.3.

(D) Localization of the PI4P reporter GFP-2xPH$^{Osh2}$ in wild type, Δtether, and *sac1*Δ cells. PM and Golgi pools of PI4P are indicated. Mother cells are labeled (m). Scale bar, 5 μm.

A

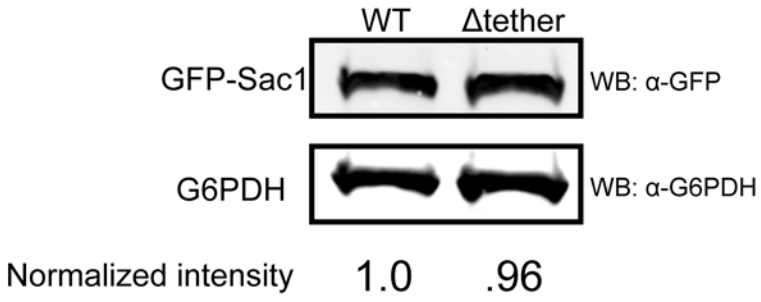
WT
Δtether
GFP-Sac1
WB: α-GFP
G6PDH
WB: α-G6PDH
Normalized intensity
1.0
.96

B

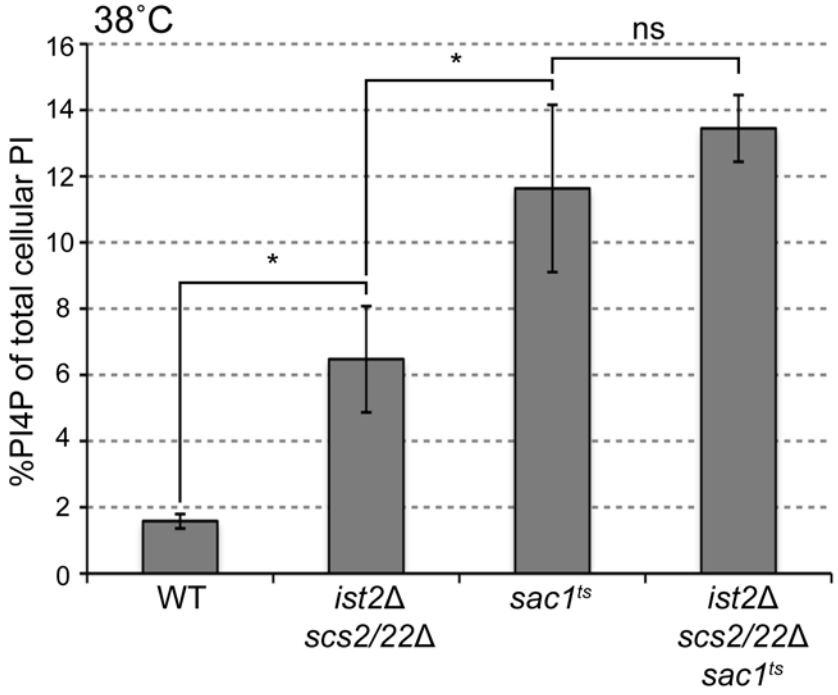
38˚C
%PI4P of total cellular PI
16
14
12
10
8
6
4
2
0
*
*
ns
WT
ist2Δ scs2/22Δ
sac1ts
ist2Δ scs2/22Δ sac1ts

**Figure 3.8. GFP-Sac1 levels do not change in Δtether strain and genetic test of tether/*sac1* double mutant.**

(A) Whole cell lysates of GFP-Sac1 expressed in wild type and Δtether cells. G6PDH is a loading control.

(B) Quantification of PI4P by $^{3}$H-inositol labeling and HPLC of wildtype, *ist2*Δ *scs2/22*Δ, *sac1*$^{ts}$, and *ist2*Δ *scs2/22*Δ *sac1*$^{ts}$ cells labeled at 38°C. Error bars are the StdDev (n=3). Significance determined by one-way ANOVA with post-processing to correct for multple comparions. (*P= .01-0.05; ns, not significant P >0.05).

If the ER tether proteins regulate PI4P metabolism through the Sac1 phosphatase, then loss of ER tether proteins should not result in a significant increase in PI4P in cells lacking Sac1 function. We measured PI4P levels in an *ist2*, *scs2/22*, *sac1*$^{ts}$ temperature conditional strain (*ist2*, *scs2/22*, *sac1* quadruple null mutants were inviable, our unpublished data) and *sac1*$^{ts}$ single mutant cells at the non-permissive temperature. PI4P levels in *ist2*, *scs2/22*, *sac1*$^{ts}$ quadruple mutant cells were not significantly increased as compared to PI4P in *sac1*$^{ts}$ single mutant cells (13.4% ±1 and 11.6% ±2.5 respectively; Figure 3.8B). Similar to our previous results, PI4P levels were increased (>3-fold) in *ist2*, *scs2/22* triple mutant cells as compared to wild type cells (Figure 3.8B). Taken together, our results indicate that the ER tether proteins facilitate Sac1 interactions with the PM to regulate PI4P.

**Identification of regions in Scs2, Ist2, and Tcb3 involved in ER-PM tethering and localization**

To better understand the mechanisms of ER-PM tethering, we identified domains in the ER tether proteins necessary for their function. We focused on Scs2 and Ist2, since our results implicated these proteins as key ER-PM tethers. Ist2 consists of eight transmembrane domains comprising a putative ion channel followed by a long cytoplasmic C-terminus containing a polybasic region rich in lysine and histidine residues necessary for cortical localization of Ist2 (Juschke et al., 2005). The Ist2 polybasic region also binds to PI(4,5)$P_2$-containing liposomes in *vitro* (Fischer et al., 2009). Similar to our previous results, expression of full-length Ist2 in Δtether cells was sufficient to restore some cER (Figures 3.3C, 3.9A, 3.10D). Interestingly the last two transmembrane domains and the extended C-terminus (GFP-Ist2$^{490\text{-}946}$) were sufficient to form cER when expressed in Δtether cells (Figures 3.9A, 3.10D). The C-terminal polybasic

domain was required for cER tethering, as the C-terminal truncated protein (GFP-Ist2$^{1-928}$) did not restore cER and instead localized to cytoplasmic ER structures in Δtether cells (Figures 3.9A, 3.10D). As an independent test for tethering function, we measured PI4P levels in Δtether mutant cells expressing the Ist2 constructs. Consistent with the ability to form cER, wild type GFP-Ist2 and the mutant protein consisting of the last two transmembrane domains and the C-terminus (GFP-Ist2$^{490-946}$) were able to reduce PI4P levels, but Ist2 lacking the polybasic domain (GFP-Ist2$^{1-928}$) was not (Figure 3.9B). Thus, the C-terminus was necessary for Ist2 tethering and the proposed ion channel of Ist2 was dispensable for ER-PM tethering.

Since the C-terminal polybasic domain was necessary for Ist2 to tether the ER and PM, we tested whether the polybasic domain was sufficient for PM targeting when expressed on its own. A previous study suggested it has weak, if any, affinity for the PM (Juschke et al., 2005). To increase the binding affinity for its target at the PM, we generated a tandem polybasic domain GFP construct (GFP-2xIst2$^{928-946}$). Strikingly, the tandem Ist2 polybasic domain (GFP-2xIst2$^{928-946}$) tightly associated with the PM (Figure 3.10A) compared to a single polybasic domain (Figure 3.10B), and still localized to the PM in Δtether cells (Figure 3.10C).

The VAP protein Scs2 contains a single transmembrane domain (TMD) and a cytoplasmic MSP domain (Figures 3.1C and 3.9C). As expected, expression of full-length Scs2 in Δtether cells was sufficient to restore cER (Figures 3.9C, 3.10E) and lower cellular PI4P levels (Figure 3.9D). A truncated form of Scs2 lacking the TMD (GFP-Scs2$^{1-225}$) did not localize to the ER and instead was in the nucleus, and weakly at the PM at sites of polarized growth (Figures 3.9C, 3.10E; Loewen et al., 2007). The mutant Scs2 protein lacking its TMD failed to reduce PI4P levels in the Δtether mutant cells (Figure 3.9D), suggesting Scs2 must be anchored in the ER to function as a tether. A mutant form of Scs2 (Kx6) bearing substitutions in basic

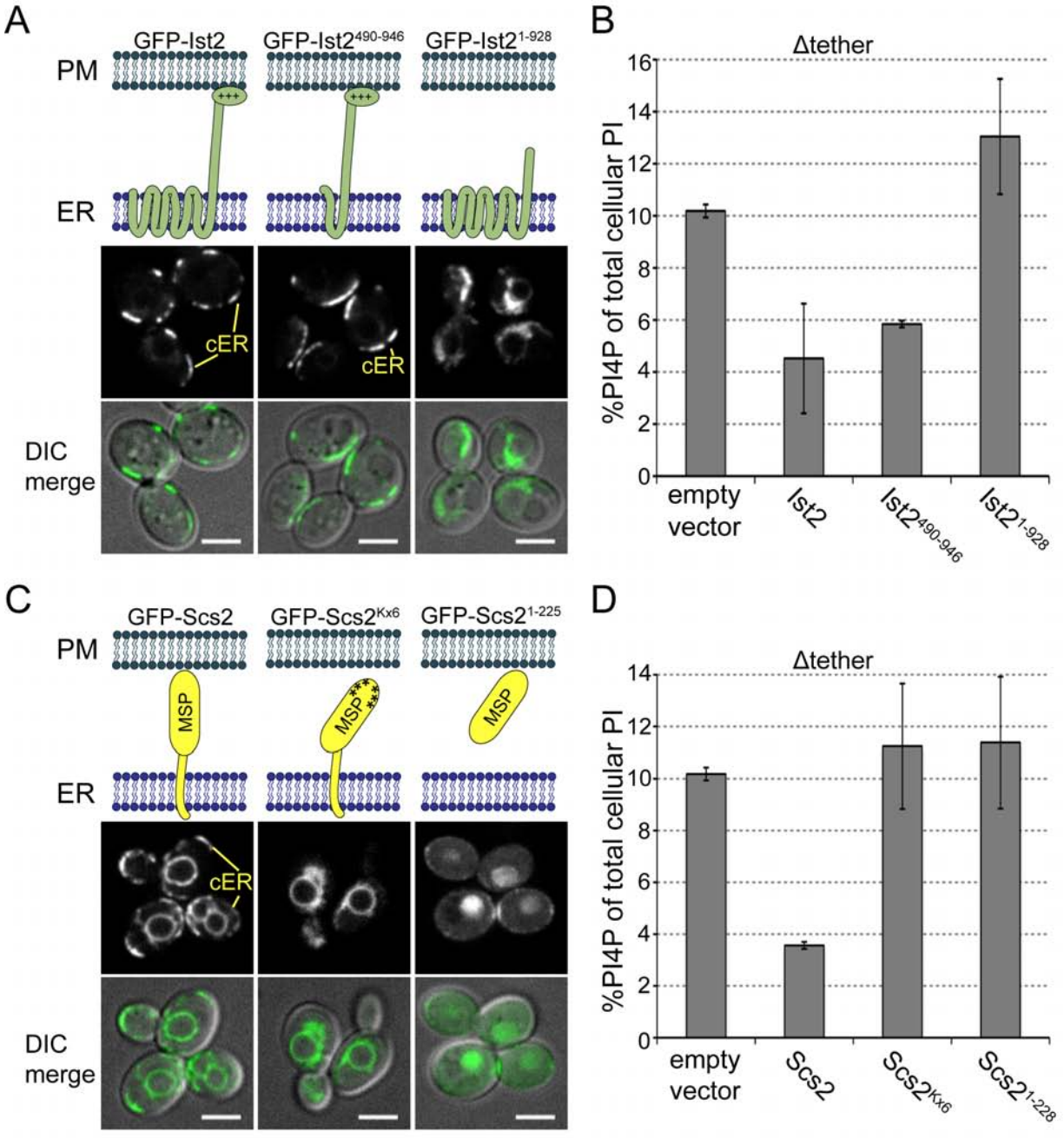
A
GFP-Ist2
GFP-Ist2490-946
GFP-Ist21-928
PM
ER
cER
cER
DIC
merge
B
Δtether
%PI4P of total cellular PI
16
14
12
10
8
6
4
2
0
empty vector
Ist2
Ist2490-946
Ist21-928
C
GFP-Scs2
GFP-Scs2Kx6
GFP-Scs21-225
PM
MSP
MSP***
MSP
ER
cER
DIC
merge
D
Δtether
%PI4P of total cellular PI
14
12
10
8
6
4
2
0
empty vector
Scs2
Scs2Kx6
Scs21-228

**Figure 3.9. Ist2 C-terminus is required for tethering and association with the PM.**

(A) Localization and models of GFP-Ist2, GFP-Ist2$^{490\text{-}946}$, and GFP-Ist2$^{1\text{-}928}$ constructs expressed in Δtether cell. Scale bar, 3 μm.

(B) PI4P levels in Δtether cells expressing GFP-Ist2, GFP-Ist2$^{490\text{-}946}$, or GFP-Ist2$^{1\text{-}928}$. Error bars show StdDev (n=2). See Table 3.3.

(C) Localization of GFP-Scs2, GFP-Scs2$^{Kx6}$, and GFP-Scs2$^{1\text{-}225}$ in Δtether cells. Scale bar, 3 μm. See also Table 3.4.

(D) PI4P measurements in Δtether cells carrying empty vector or expressing *SCS2*, *scs2*$^{Kx6}$, or *scs2*$^{1\text{-}225}$. Error bars show StdDev (n=2). See also Table 3.3.

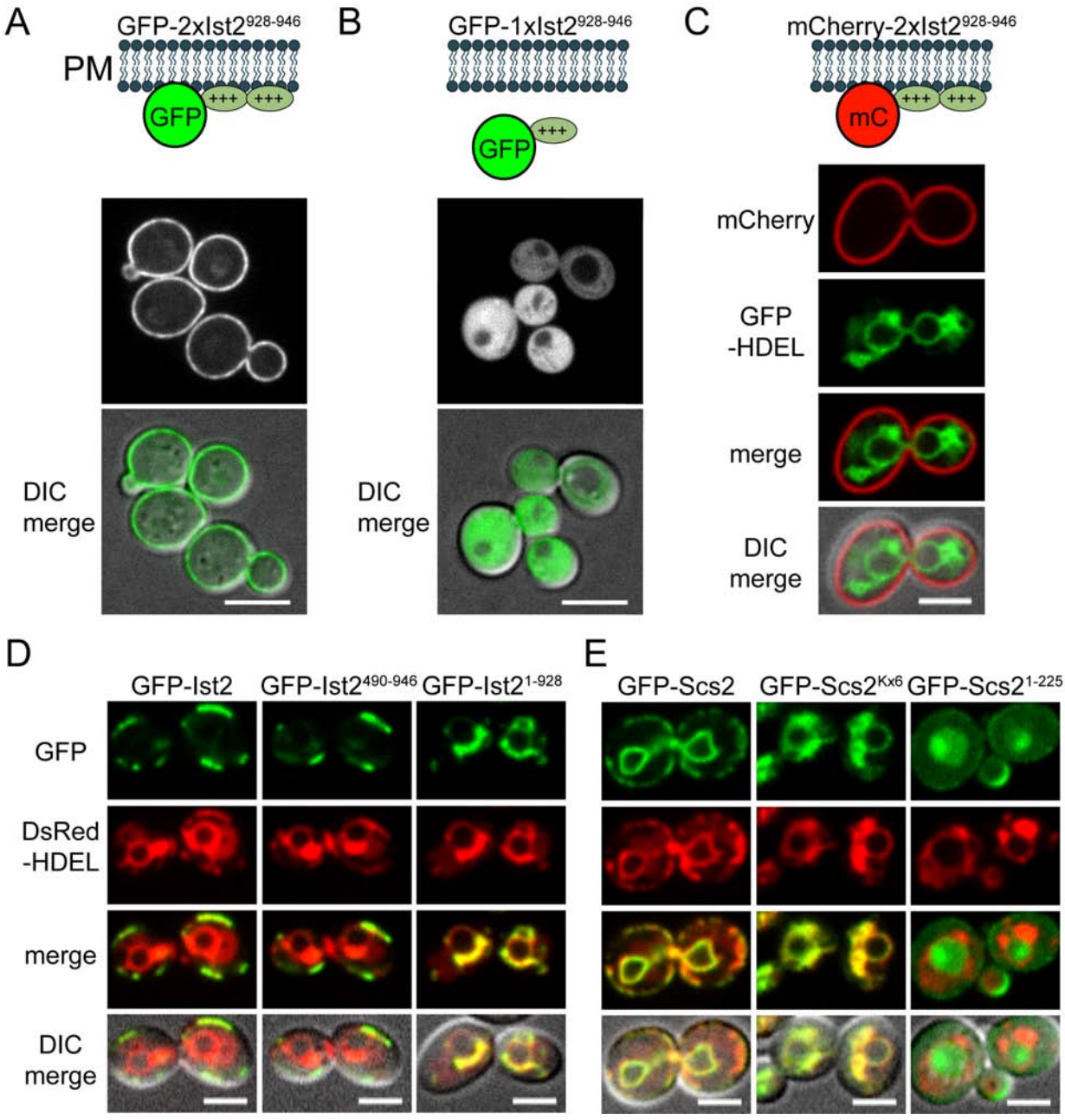
A
GFP-2xIst2928-946
PM
GFP
+++
+++
DIC
merge
B
GFP-1xIst2928-946
GFP
+++
DIC
merge
C
mCherry-2xIst2928-946
mC
+++
+++
mCherry
GFP
-HDEL
merge
DIC
merge
D
GFP-Ist2
GFP-Ist2490-946
GFP-Ist21-928
GFP
DsRed
-HDEL
merge
DIC
merge
E
GFP-Scs2
GFP-Scs2Kx6
GFP-Scs21-225

**Figure 3.10. The C-terminus of Ist2 is sufficient to target to the PM and additional images of tether constructs.**

(A) Localization of the tandem Ist2 polybasic domain (GFP-2xIst2$^{928-946}$) expressed in wild type cells. Scale bar, 5μm.

(B) Localization of GFP-1xIst2$^{928-946}$ in wild type cells. Scale bar, 5μm.

(C) Localization of mCherry-2xIst2$^{928-946}$ in Δtether cells expressing the ER marker GFP-HDEL Scale bar, 3μm.

(D) ER-PM contact site rescue and localization of GFP-Ist2, GFP-Ist2$^{490-946}$, and GFP-Ist2$^{1-928}$ in Δtether cells expressing the ER marker DsRED-HDEL. Scale bar, 3μm.

(E) ER-PM contact site rescue and localization of GFP-Scs2, GFP-Scs2$^{Kx6}$, and GFP-Scs2$^{1-225}$ in Δtether cells expressing the ER marker DsRED-HDEL. Scale bar, 3μm.

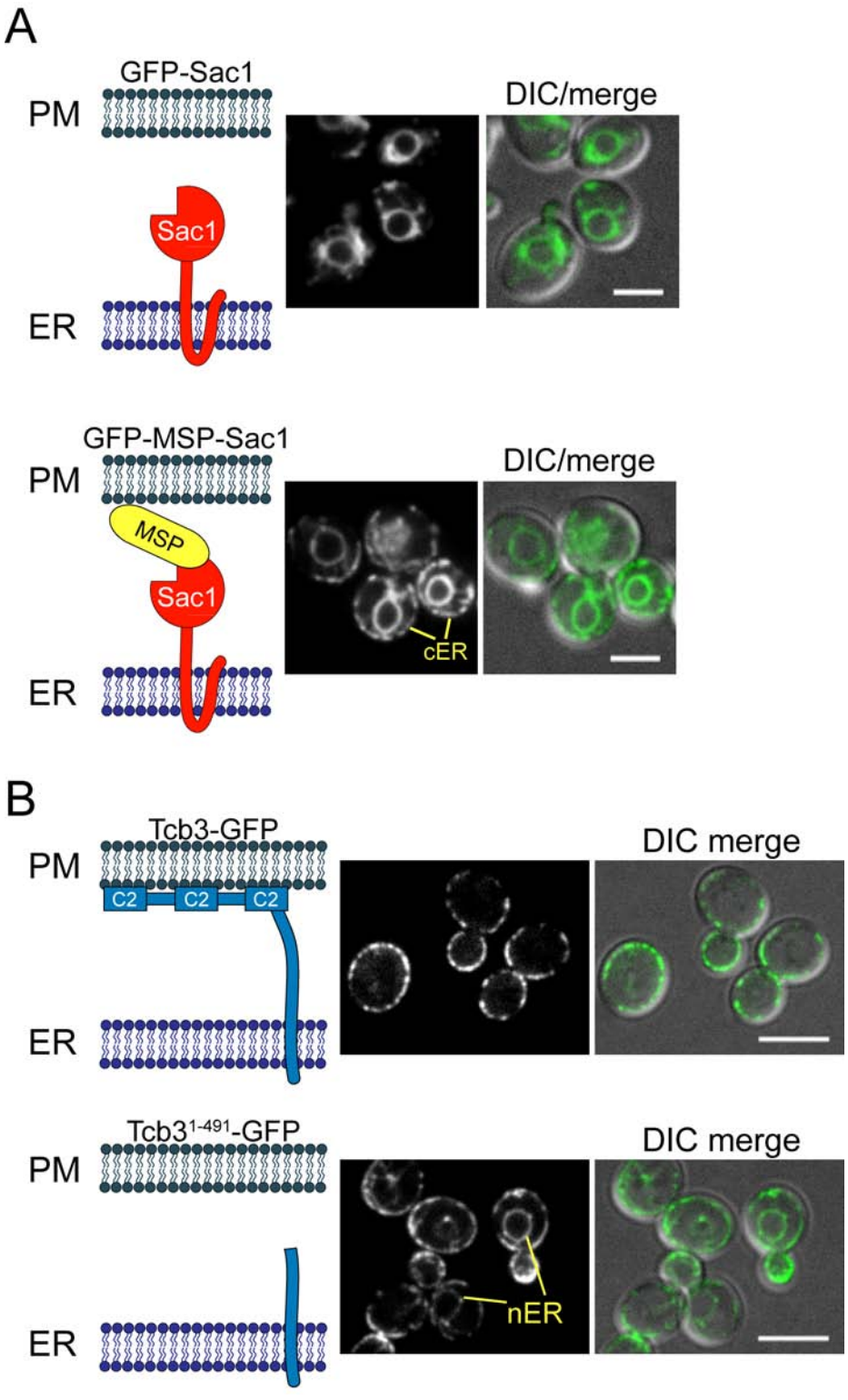
A
GFP-Sac1
PM
Sac1
ER
DIC/merge
GFP-MSP-Sac1
PM
MSP
Sac1
ER
cER
DIC/merge
B
Tcb3-GFP
PM
C2
C2
C2
ER
DIC merge
Tcb3$^{1-491}$-GFP
PM
ER
nER
DIC merge

**Figure 3.11. The MSP domain is sufficient for ER-PM tethering.**

(A) Localization and models of GFP-Sac1 and GFP-MSP-Sac1 (GFP-Scs2$^{1-129}$-Sac1) expressed in Δtether cells. Scale bar, 3μm.

(B) Localization of Tcb3-GFP and Tcb3$^{1-491}$-GFP (Lacking C2 domains) in *tcb3*Δ cells, nER is indicated. Scale bar, 5μm.

lysine residues within the MSP domain involved in binding to FFAT peptides and potentially to PI lipids (Kagiwada and Hashimoto, 2007) failed to restore cER (Figures 3.9C, 3.10E) or lower PI4P levels in Δtether mutant cells (Figure 3.9D). In addition to the Kx6 mutant, we also tested several other substitutions within the MSP domain of Scs2 (Table 3.4). The Scs2 mutant proteins showed a wide range of activity, including full wild type function (*e.g.* L86A), partial activity (*e.g.* K84A, L86A), and complete loss of function (*e.g.* the T41A, T42A and P44S, P51S mutant proteins; Table 3.4). We also tested whether the MSP domain was sufficient for ER-PM tethering when fused to another ER membrane protein. Expression of a GFP-MSP-Sac1 fusion protein in Δtether cells was sufficient to restore cER (Figure 3.11A). Taken together, these results implicate the MSP domain in Scs2 tethering function, consistent with previous findings (Loewen et al., 2007).

Our results showed that the tricalbins are sufficient for cER formation and that Tcb3-GFP remained localized to ER-PM contacts in cells lacking Ist2 and Scs2/22 (Figure 3.3C). The tricalbins contain multiple lipid-binding C2 domains (Figure 3.1C) that could be involved in ER-PM targeting. Interestingly, a mutant form of Tcb3 lacking the C2 domains ($Tcb3^{1-419}$-GFP) was observed in both nuclear and cortical ER structures, in contrast to full-length Tcb3-GFP that localized exclusively to the peripheral ER (Figure 3.11B). Thus, the C2 domains may serve in stabilizing the tricalbin proteins at ER-PM junctions, consistent with previous findings (Toulmay and Prinz, 2012).

**Cells lacking PM-ER contacts require the UPR for survival**

Due to the dramatic changes in ER morphology, we reasoned that ER functions might be affected in the Δtether cells. We first examined if there was a defect in protein trafficking from

the ER. However, glycosylation and delivery of the cargo protein carboxypeptidase Y (CPY) to the vacuole appeared normal, implying that ER export is unaffected by the change in ER morphology in Δtether cells (Figure 3.13A). We then tested whether the Δtether cells were sensitive to ER stress induced by tunicamycin. Tunicamycin blocks N-linked protein glycosylation in the ER leading to misfolding of both luminal and integral membrane proteins. Interestingly, the Δtether strain was hypersensitive to tunicamycin-induced ER stress as compared to wild type cells and *sac1* mutant cells (Figure 3.12A). Thus, the growth defect of Δtether cells under ER stress conditions was not simply due to loss of Sac1 function.

The sensitivity of Δtether cells to an ER stress suggested a potential impairment of the unfolded protein response (UPR). The UPR detects misfolded proteins in the ER and relays this signal to the nucleus, resulting in increased expression of ER chaperones, lipid synthesis enzymes, ER-associated degradation machinery (ERAD), and membrane trafficking protein (Travers et al., 2000). To determine if ER-PM contacts are required for the UPR, we measured induction of an UPRE-LacZ reporter in wild type and Δtether cells (Cox and Walter, 1996). Untreated wild type cells displayed low levels of UPRE-LacZ activity under basal conditions, but UPRE-LacZ activity was increased approximately 10-fold when wild type cells were exposed to an ER stress, the reducing agent DTT (Figure 3.12B). Unexpectedly, Δtether cells displayed constitutive UPR signaling, as there was a surprisingly high level of UPRE-LacZ activity (comparable to DTT-induced levels in wild type cells) even without the addition of DTT. The UPRE-LacZ activity further increased when Δtether cells were treated with DTT (Figure 3.12B). To determine if the constitutive induction of the UPR correlated with defects in cER formation, we measured basal UPR activity in each of the tether mutants. Interestingly, only mutants with cER defects constitutively induced the UPR and basal activity increased with

decreased cER formation (Figure 3.13B). The Δtether cells displayed significantly higher basal UPR signaling than *sac1* mutants (Figure 3.13B), implying ER stress in the Δtether cells was not entirely due to loss of Sac1 function. As an independent test, basal expression of Kar2 (yeast BIP, a protein induced during UPR) were moderately elevated in Δtether cells as compared to wild type cells in the absence of ER stress (Figure 3.13C). Both wild type and Δtether cells increased Kar2 expression in response to tunicamycin, indicating that Δtether cells possess an intact UPR signaling pathway (Figure 3.13C).

The Δtether cells undergo continuous UPR signaling even in the absence of exogenous ER stress-inducing agents (*e.g.* tunicamycin or DTT), implying that the loss of PM-ER contacts disrupts one or more processes in the ER. While Δtether cells grew normally under non-stress conditions, Δtether cells were hypersensitive to tunicamycin, as if they cannot overcome additional ER stress. These results suggested that the change in ER morphology and increased ER stress experienced by Δtether cells is compensated by the UPR (Figure 3.12C). We then predicted that loss of UPR signaling would compromise the viability of Δtether cells. To test if the UPR was critical, we deleted the *IRE1* gene that encodes kinase and RNAse activities required for UPR signaling. Compared to wild type, Δtether, and *ire1* cells, the growth of *ire1* Δtether mutant cells was severely impaired in both serial dilution plating assays and liquid cultures (Figures 3.12D, 3.12E). Loss of Hac1, a transcription factor downstream of Ire1 (Cox and Walter, 1996), also resulted in a severe synthetic growth defect in Δtether mutant cells (Figure 3.13D). The synthetic relationship between loss of PM-ER contacts and the UPR was not due to impaired protein trafficking out of the ER, as CPY was efficiently sorted in the *ire1* Δtether mutant (Figure 3.13E). Thus, the Δtether cells are defective for critical ER functions that are compensated by up-regulation of the UPR.

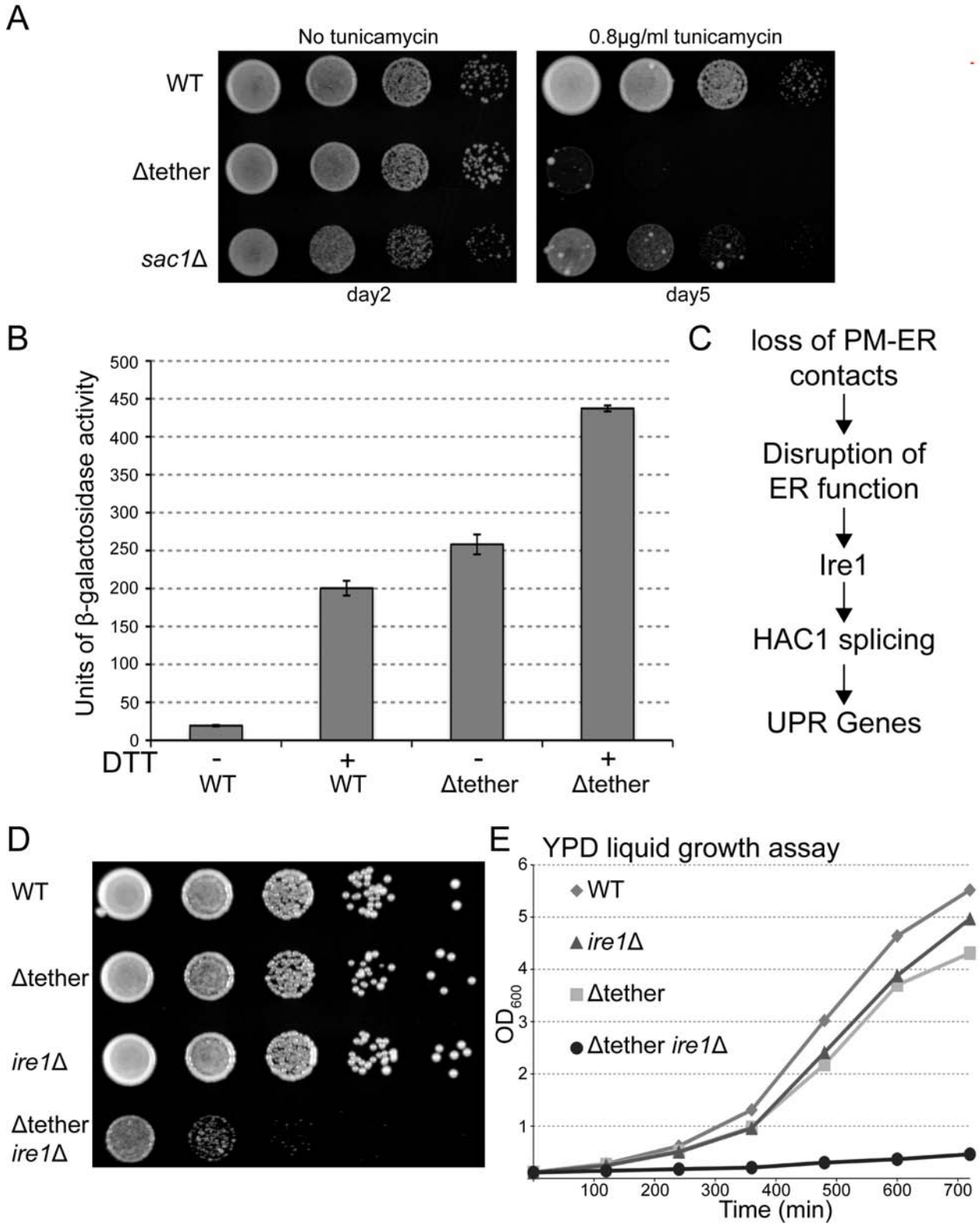
A
No tunicamycin
0.8µg/ml tunicamycin
WT
Δtether
sac1Δ
day2
day5
B
Units of β-galactosidase activity
500
450
400
350
300
250
200
150
100
50
0
DTT
-
+
-
+
WT
WT
Δtether
Δtether
C
loss of PM-ER contacts
Disruption of ER function
Ire1
HAC1 splicing
UPR Genes
D
WT
Δtether
ire1Δ
Δtether ire1Δ
E
YPD liquid growth assay
WT
ire1Δ
Δtether
Δtether ire1Δ
OD600
6
5
4
3
2
1
100
200
300
400
500
600
700
Time (min)

**Figure 3.12. The UPR is critical for the growth of cells lacking PM-ER contacts**

(A) Serial dilutions of wild type, Δtether, and *sac1*Δ cells grown for indicated times at 26°C on YNB or YNB + 0.8mg/ml tunicamycin.

(B) UPR assay using UPRE-LacZ reporter. Induction of the UPR was measured by b-galactosidase activity in indicated strains treated with or without 8mM DTT for 1 hour. Error bars show StdDev (n=3 assays performed in duplicate).

(C) Diagram of the UPR pathway and a potential link to disruption of PM-ER contacts. Loss of PM-ER contacts results in ER dysfunction that is sensed by Ire1, which induces the UPR.

(D) Serial dilutions of wild type, Δtether, *ire1*Δ, and Δtether /*ire1*Δ mutant cells grown on YPD plates at 26°C.

(E) Liquid growth assays of wild type, Δtether, *ire1*Δ, and Δtether/*ire1*Δ mutant cells. Cells were grown in YPD at 26°C and $OD_{600}$ measurements were taken at indicated time points.

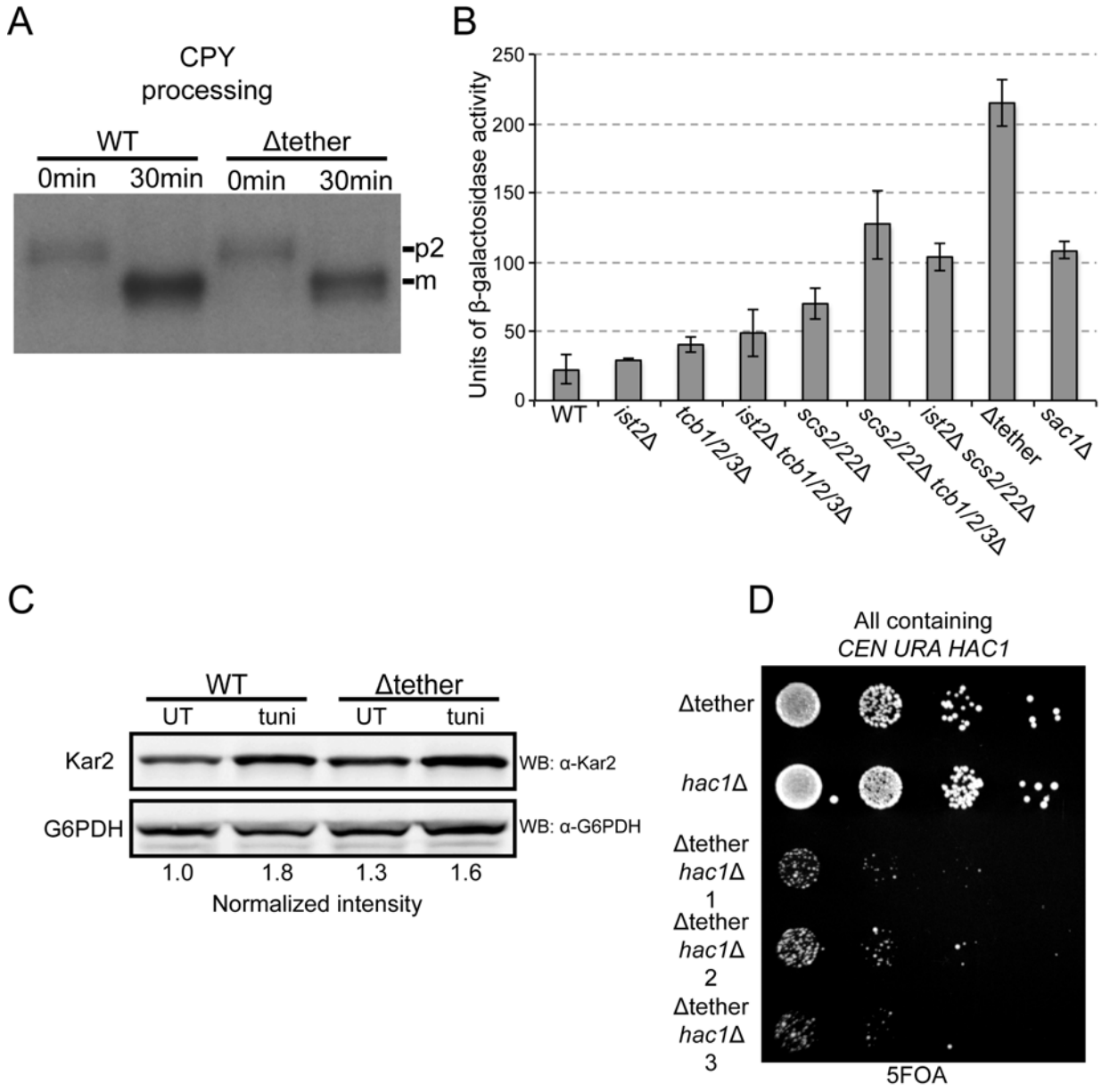
A
CPY
processing
WT
Δtether
0min
30min
0min
30min
p2
m
B
Units of β-galactosidase activity
250
200
150
100
50
0
WT
ist2Δ
tcb1/2/3Δ
ist2Δ tcb1/2/3Δ
scs2/22Δ
scs2/22Δ tcb1/2/3Δ
ist2Δ scs2/22Δ
Δtether
sac1Δ
C
WT
Δtether
UT
tuni
UT
tuni
Kar2
WB: α-Kar2
G6PDH
WB: α-G6PDH
1.0
1.8
1.3
1.6
Normalized intensity
D
All containing
CEN URA HAC1
Δtether
hac1Δ
Δtether hac1Δ 1
Δtether hac1Δ 2
Δtether hac1Δ 3
5FOA
E
WT
Δtether
ire1Δ
Δtether ire1Δ
Chase (min)
0
30
0
30
0
30
0
30
CPY
processing
p2
m

**Figure 3.13. The UPR is critical for growth of cells lacking cER, but trafficking out of the ER is normal.**

(A) CPY processing in wild type and Δtether mutant cells. Cells were pulsed with $^{35}$S methionine and cysteine for 10 min and chased for 0 and 30min. p2 (Golgi) and m (mature) forms are indicated.

(B) UPR reporter assay using UPRE-LacZ (pJC104). Induction of the UPR was measured by β-galactosidase activity from indicated strains with no treatment. Error bars are StdDev (n=3).

(C) Whole cell lysates of wild type and Δtether cells treated with or with out (UT) 1ug/ml tunicmycin for 90 minutes. Samples were probed for Kar2, a protein whose levels increase upon ER stress, and G6PDH as a loading control. Normalized intensity of Kar2 (normalized to G6PDH) ratio to untreated wild type is indicated.

(D) Serial dilutions of the following strains harboring a *CEN URA HAC1* plasmid were plated on 5FOA plates to select for loss of the HAC1 plasmid: Δtether, *hac1*Δ and three independent isolates Δtether/*hac1*Δ double mutants.

(E) CPY processing in wild type, Δtether, *ire1*Δ, and Δtether/*ire1*Δ double mutants. . Cells were pulsed with $^{35}$S methionine and cysteine for 10 min and chased for 0 and 30min. p2 (Golgi) and m (mature) forms are indicated.

## Discussion

### Multiple conserved tethering proteins form ER-PM junctions

PM-ER membrane contact sites are major sites for calcium and lipid signaling in eukaryotic cells. Yet, relatively little is known about the structural components of membrane junctions between these organelles. We have identified Ist2 (related to the mammalian TMEM16 family of ion channels) and the tricalbins (C2 domain-containing proteins similar to the extended synaptotagmin-like proteins E-Syt1/2/3) as ER tether proteins that function with the VAP orthologs Scs2 and Scs22 to establish junctions between the ER and PM. Upon loss of all six ER tether proteins, the morphology of the cortical ER was drastically altered from a network of sheets and tubes attached to the PM in wild type cells, to a near total loss of PM-ER contacts and accumulations of ER in the cytoplasm. Importantly, our results suggest critical roles for PM-ER contacts in regulating phosphoinositide signaling at the PM and ER morphology and homeostasis (Figure 3.14).

Of the PM-ER tethering proteins analyzed in our study, Scs2 appeared to be the most important. Loss of Scs2 alone resulted in a clear reduction in cER compartments (Loewen et al., 2007; Figure 3.4A). Though Scs2 has a critical role in PM-ER tethering, Scs2 and other VAP family members may function as general tethers for several ER-organelle connections. VAP proteins have been implicated in ER-Golgi and ER-endosome contacts in mammalian cells (Peretti et al., 2008; Rocha et al., 2009). Scs2 is not enriched at specific ER-organelle contact sites and instead localizes throughout the ER (Figure 3.2A). These results suggest that the VAP proteins may cycle between at least two states: an active tethering state at organelle junctions and an inactive state diffuse throughout the ER network. This idea is consistent with VAP localization and may allow the VAP proteins to make contacts with several organelles as needed

through regulated interactions with additional tethering factors. How the VAP protein Scs2 is regulated and the mechanisms by which Scs2 facilitates ER tethering are unclear. One possibility is that Scs2 binds to specific FFAT-containing ORP (oxysterol-binding protein related proteins) family members at membrane contact sites. Several ORP family members have been observed at ER-organelle contact sites (Peretti et al., 2008; Rocha et al., 2009; Schulz et al., 2009; Stefan et al., 2011). However ORPs (*e.g.* the Osh proteins in yeast) do not appear to be required for PM-ER tethering *in vivo* (Loewen et al., 2007; Schulz et al., 2009; Stefan et al., 2011). The Scs2 MSP domain has been suggested to bind negatively charged lipids such as PI4P (Kagiwada and Hashimoto, 2007). However, PI4P is not sufficient for Scs2 localization, as the MSP domain targets to sites of polarized growth and it was not observed at Golgi compartments that are enriched in PI4P (Loewen et al., 2007; Figure 3.9). Thus, Scs2 may interact with as yet unidentified proteins or lipids on target organelles to facilitate tethering.

Unlike the VAP orthologs Scs2/22, Ist2 and the tricalbins exclusively localized to the cortical ER where they likely function as specific tethers between the cER and PM (Figure 3.1D; Fischer et al., 2009; Toulmay and Prinz, 2012). Their restricted localization to the cER implies that both Ist2 and the tricalbins make extensive contacts with the PM. The tricalbins may bind directly to PM lipids as each contains lipid-binding C2 and SMP domains (Schulz and Creutz, 2004; Toulmay and Prinz, 2012). The C-terminus of Ist2 bound to PI(4,5)$P_2$ containing liposomes *in vitro* and was both necessary and sufficient for PM interaction (Figure 3.9; Fischer et al., 2009). Interestingly, a recent study found that Ist2 regulates the close association of cER with the PM (within 30 nm; Wolf et al., 2012), consistent with the idea that Ist2 directly contacts the PM.

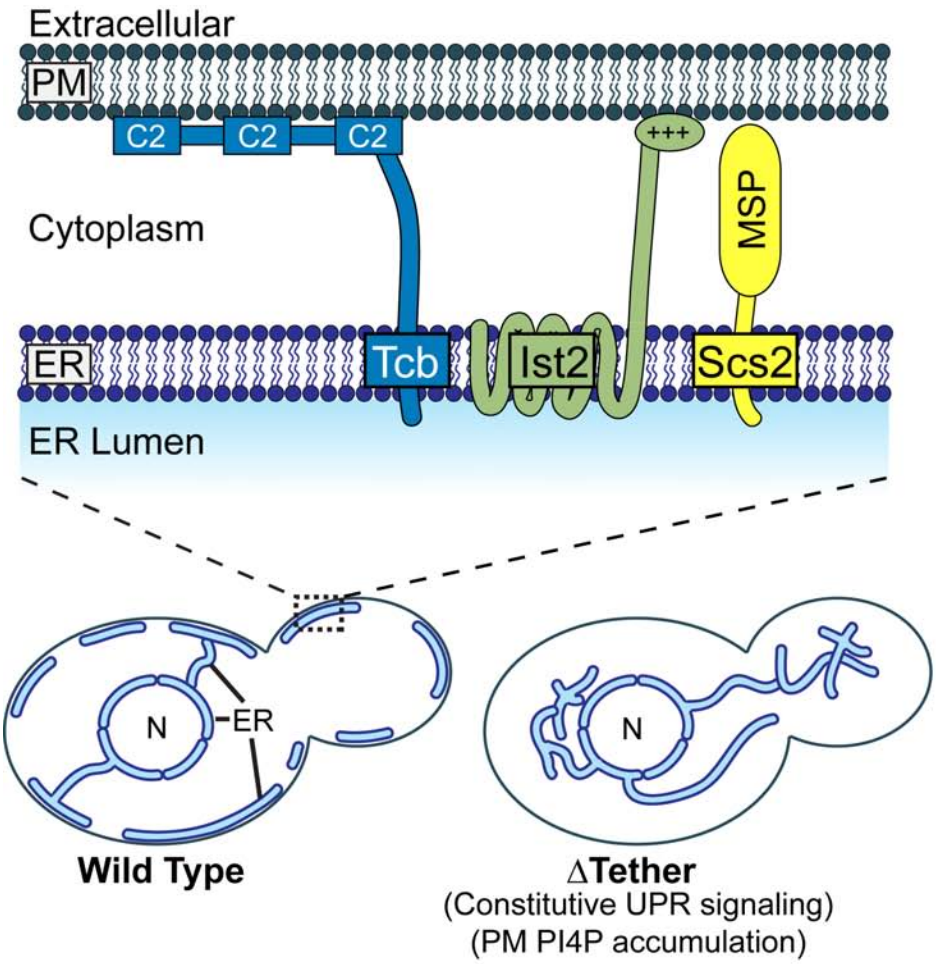


**Figure 3.14. Model for PM-ER tethering in yeast**

Three families of integral ER proteins tether the cortical ER to the PM: the VAP proteins Scs2/22, Ist2, and the tricalbins. Loss of ER-PM tethers results in dramatic changes in ER morphology, elevated PI4P levels at the PM, and activation of the unfolded protein response (UPR).

Similar to Scs2, Ist2 and the tricalbins are conserved in higher eukaryotes, including mammals. Ist2 is related to the TMEM16/anoctamin proteins, some of which are calcium-activated chloride channels (Caputo et al., 2008; Yang et al., 2008). Interestingly TMEM16a contains a cytoplasmic region that binds $PI(4,5)P_2$ *in vitro* and targets to cER-PM junctions in yeast cells (Fischer et al., 2009). The tricalbins are related to the mammalian extended synaptogamin proteins (E-Syt1/2/3), which share a similar architecture of N-terminal membrane-anchoring domains followed by cytoplasmic SMP and C2 domains. Although some PM-ER tethers in higher eukaryotes are known (*e.g.* STIM proteins and junctophilin), we propose Ist2 and the tricalbin orthologs have conserved roles as ER-organelle tethers in other eukaryotes.

**ER inheritance and establishment of the cortical ER in daughter cells**

It is worth noting that Ist2, Tcb2, and Tcb3, each of which are exclusively localized to the cER, are encoded by mRNAs that are transported into the growing bud by the myosin motor protein Myo4, the mRNA-binding protein She2, and the Myo4 adaptor protein She3 (Shepard et al., 2003). Myo4 and She3 are also required for the efficient inheritance of cER, which is derived from nuclear ER and is carried by Myo4 into the bud along actin cables (Estrada et al., 2003). Thus Myo4 transports ER into the bud and delivers mRNAs that encode ER-PM tethering proteins for cortical ER formation. This system likely evolved because pre-existing cER membrane proteins in the mother cell, such as Ist2 and the tricalbins that localize exclusively to the cER, are unable to enter the bud due to the proposed diffusion barrier created by the septin ring at the mother-bud neck. In contrast, Scs2 localizes to nuclear and cytoplasmic ER structures, in addition to the cER, and thus pre-existing Scs2 protein can be inherited from the mother cell. Cells lacking Scs2 have cER defects that are more pronounced in the bud (Loewen et al., 2007).

Thus Scs2 may initially establish the cER in the newly forming bud. Subsequently, Ist2 and the tricalbins further stabilize cER-PM contacts following their translation and insertion into the newly formed cER.

**Roles for PM-ER junctions**

The identification of proteins that function in the establishment of PM-ER junctions provides a foundation for future investigations into the roles for ER-PM contacts. We found that loss of PM-ER connections resulted in the dramatic accumulation of PI4P at the PM, consistent with previous work indicating that Sac1 functions at PM-ER junctions (Stefan et al., 2011). PI 4-kinase activity has been implicated in several important cellular processes at the PM, including signaling responses to numerous stimuli in both yeast and metazoan cells (Audhya and Emr, 2002; Balla et al., 2008; Jesch et al., 2010; Hammond et al., 2012; Yavari et al., 2010). ER-PM contacts serve as important sites for the modulation of PI4P levels and may contribute to the regulation of cell signaling pathways controlled by PI4P. It will also be interesting to determine whether processes regulated by PM-ER junctions in metazoan cells (*e.g.* lipid and $Ca^{2+}$ transport) are affected in Δtether yeast cells.

Unexpectedly, cells lacking cER exhibited continuous UPR signaling and required the UPR for viability, suggesting one or more critical processes in the ER require PM-ER contacts for full function. In the absence of PM-ER connections these processes are perturbed–resulting in imbalances in the ER and induction of the UPR. Thus, constitutive UPR signaling may be necessary as a protective mechanism to compensate for the disruption of ER homeostasis upon loss of PM-ER tethers. The compromised ER function in the Δtether cells and synthetic growth defect of Δtether cells lacking *IRE1* was not due to impaired protein trafficking out of the ER, as

biosynthetic sorting and processing of the cargo protein CPY were normal. In addition, even with strong constitutive UPR signaling in Δtether cells, expression levels of the UPRE-LacZ reporter and the ER chaperone Kar2 (BIP) were further induced when Δtether cells were treated with a protein folding stress. These results suggest that the constitutive UPR signaling in Δtether cells is not the accumulation of unfolded proteins, but mis-regulation of additional processes in the ER. Consistent with this, cells impaired in several ER processes (*e.g.* protein glycosylation and folding; the ERAD pathway, ion transport, and lipid metabolism) exhibit elevated UPR signaling (Jonikas et al., 2009), as well as synthetic growth defects upon inactivation of the UPR (Thibault et al., 2011).

Altogether, our study has (1) revealed a complex system composed of multiple tethering factors involved in the formation of PM-ER membrane junctions, (2) provided a more detailed understanding of phosphoinositide signaling at the PM, and (3) uncovered an unexpected role for ER-PM contacts in ER organization and function. In addition, the ER tether proteins possess lipid-binding domains and may serve as sensors of membrane composition to transmit signals between the ER and PM. Upon loss of PM-ER signaling, cells may become dependent on other cell signaling and stress response systems, such as the UPR, to maintain organelle homeostasis and integrity.

## Acknowledgments

We thank A. Chang, P. Walter, and J. Nunnari for plasmids and antibodies. We are grateful to M. Smolka for assistance with the mass spectrometry experiments, B. Judson for microscopy support, and G. Bai, D. Frasheri, and S. Griffin for assistance with strain construction. We also thank members of the Emr lab for the helpful discussions and comments. J.A.M. is supported by

a Fleming Research Fellowship. This work was supported by funds from a Cornell University Research Grant (S.D.E.).

## Tables

**Table 3.1. Sac1 SILAC**

| ORF | Total peptides(H/L) | Xpress | Process |
|---|---|---|---|
| Sac1* | 179(177/2) | 123.01 | Bait |
| MNN11 | 10(10/0) | 31.89 | Protein glycosylation (Golgi) |
| MNN5 | 10(10/0) | 23.47 | |
| ALG2 | 11(11/0) | 38.51 | Protein glycosylation (ER) |
| DPM1* | 25(24/1) | 25.06 | |
| OST1* | 11(11/0) | 22.36 | |
| OST3 | 10(10/0) | 61.1 | |
| PMT1* | 18(18/0) | 68.2 | |
| PMT2* | 12(12/0 | 24.59 | |
| WBP1* | 17(17/0) | 24.3 | |
| CHO2 | 16(16/0) | 21.39 | Lipid metabolism |
| ERG2* | 10(10/0) | 23.1 | |
| ERG9* | 14(14/0) | 26.19 | |
| LCB1 | 25(25/0) | 137.91 | |
| LCB2 | 32(32/0) | 93.11 | |
| OLE1* | 10(10/0) | 25.33 | |
| SCS2* | 18(17/1) | 39.26 | |
| SLC1 | 10(9/1) | 37.56 | |
| ERV25* | 10(10/0) | 50.53 | Protein trafficking and modification |
| GSF2* | 12(12/0 | 90.56 | |
| SEC63* | 27(27/0) | 27.66 | |
| RTN1* | 25(25/0) | 30.54 | ER Shape |
| IST2* | 16(16/0) | 79.17 | Other/Unknown |
| MSC7 | 15(15/0) | 22.47 | |
| SPF1* | 42(40/2) | 45.92 | |
| TCB3* | 14(14/0) | 24.2 | |
| TYW1 | 12(12/0) | 63.26 | |

*denotes overlapping protein in Sac1 and Scs2 interactomes

Proteins highlighted in red are candidate tethers.

**Table 3.2. Scs2 SILAC**

| ORF | Total peptides(H/L) | Xpress | Process |
|---|---|---|---|
| SCS2* | 86(83/3) | 163.4 | Bait |
| DPM1* | 33(33/0) | 83.33 | Protein glycosylation |
| PMT2* | 14(14/1) | 56.59 | |
| PMT1* | 27(27/0) | 49.48 | |
| OST1* | 12(11/1) | 45.72 | |
| STT3 | 12(11/1) | 82.3 | |
| WBP1* | 13(13.0) | 40.32 | |
| ERG2* | 15(15/0) | 43.25 | |

| | | | |
|---|---|---|---|
| ERG9* | 12(12/0) | 29.34 | Lipid metabolism |
| ERG11 | 13(13/0) | 40.73 | |
| OLE1* | 21(21/0) | 101.41 | |
| OSH1 | 14(14/0) | 32.94 | |
| SAC1* | 34(31/3) | 25.06 | |
| YET1 | 11(11/0) | 37.51 | |
| EMC1 | 10(10/0) | 33.49 | Protein trafficking and modification |
| EMP24 | 14(14/0) | 68.17 | |
| ERP1 | 16(14/2) | 32.67 | |
| ERV25* | 16(16/0) | 99.3 | |
| GPI17 | 10(10/0) | 34.09 | |
| GSF2* | 22(22/0) | 48.8 | |
| PGA3 | 10(10/0) | 48.19 | |
| SEC63* | 19(19/0) | 30.4 | |
| STE24 | 11(11/0) | 81.04 | |
| RTN1* | 33(30/3) | 80.84 | ER shape |
| RTN2 | 10(10/0) | 71.12 | |
| SEY1 | 43(43/0) | 63.49 | |
| IST2* | 24(23/1) | 70.23 | Other/Unknown |
| PEP4 | 36(31/5) | 50.25 | |
| PEX30 | 20(20/0) | 83.69 | |
| PHO88 | 14(14/0) | 108.11 | |
| SPF1* | 41(40/1/) | 43.63 | |
| TCB1 | 24(23/1) | 30.54 | |
| TCB3* | 30(30/0) | 52 | |
| *denotes overlapping protein in Sac1 and Scs2 interactomes | | | |
| Proteins highlighted in red are candidate tethers. | | | |

**Table 3.3. Phosphoinositide levels in all strains examined.**

| | PI levels (% of the total $^{3}$H-labeled PtdIns + PIPs) | | | |
|---|---|---|---|---|
| **Strain** | **PI3P** | **PI4P** | **PI(3,5)$P_2$** | **PI(4,5)$P_2$** |
| Wild type | 1.16±0.26 | 1.39±0.41 | 0.11±0.04 | 0.87±0.17 |
| *ist2*Δ | 1.46±0.36 | 2.44±0.51 | 0.11±0.07 | 0.92±0.50 |
| *tcb1*Δ *tcb2*Δ *tcb3*Δ | 1.66±0.40 | 1.82±0.70 | 0.14±0.07 | 1.00±0.34 |
| *ist2*Δ *tcb1*Δ *tcb2*Δ *tcb3*Δ | 1.28±0.26 | 2.60±0.63 | 0.19±0.16 | 1.56±1.16 |
| *scs2*Δ *scs22*Δ | 1.42±0.22 | 3.23±1.03 | 0.27±0.18 | 1.86±0.66 |
| *scs2*Δ *scs22*Δ *tcb1*Δ *tcb2*Δ *tcb3*Δ | 1.48±0.47 | 3.39±1.04 | 0.16±0.08 | 1.48±0.70 |
| *ist2*Δ *scs2*Δ *scs22*Δ | 1.09±0.15 | 5.79±0.51 | 0.24±0.07 | 1.70±0.65 |
| Δtether: *ist2*Δ *scs2*Δ *scs22*Δ *tcb1*Δ *tcb2*Δ *tcb3*Δ | 1.23±0.18 | 10.1±0.68 | 0.12±0.03 | 0.61±0.03 |
| N=3 | | | | |
| | | | | |
| Δtether: *ist2*Δ *scs2*Δ *scs22*Δ *tcb1*Δ *tcb2*Δ *tcb3*Δ | | | | |
| + [*CEN* GFP-*IST2*] | 1.82±0.65 | 4.52±2.11 | 0.22±0.11 | 1.46±0.69 |
| + [*CEN* GFP-*ist2*$^{490-946}$] | 2.08±0.20 | 5.84±0.13 | 0.31±0.13 | 1.70±0.64 |
| + [*CEN* GFP-*ist2*$^{1-928}$] | 2.16±0.63 | 13.1±2.21 | 0.14±0.03 | 0.63±0.18 |
| + [*CEN SCS2*] | 2.00±0.04 | 3.57±0.13 | 0.16±0.04 | 1.22±0.50 |
| + [*CEN scs2*$^{K80A, K84A, K119A, K120A, K122A, K124A}$] | 2.00±0.72 | 11.3±2.41 | 0.21±0.02 | 0.91±0.10 |
| + [*CEN scs*$^{1-225}$] | 1.69±0.45 | 11.4±2.54 | 0.11±0.02 | 0.57±0.28 |
| + [empty vector] | 2.14±0.10 | 10.2±0.25 | 0.14±0.01 | 0.65±0.01 |
| N=2 | | | | |
| | | | | |

| All 38°C | | | | |
|---|---|---|---|---|
| wild type | 1.75±0.38 | 1.58±0.22 | 0.22±0.02 | 2.02±0.77 |
| *ist2*Δ *scs2*Δ *scs22*Δ | 1.68±0.41 | 6.47±1.60 | 0.21±0.04 | 0.94±0.13 |
| *sac1*Δ [*CEN sac1*$^{ts}$] | 1.80±0.05 | 11.6±2.53 | 0.20±0.04 | 0.92±0.26 |
| *ist2*Δ *scs2*Δ *scs22*Δ *sac1*Δ[*CEN sac1*$^{ts}$] | 1.52±0.17 | 13.5±1.01 | 0.12±0.02 | 0.39±0.08 |
| N=3 | | | | |

Yeast strains incubated at the indicated temperatures were labeled and processed as described in our Extended Experimental Procedures. The mean peak area (cpm) of each PI species is reported as a percentage of the total $^{3}$H-labeled lipids. The values reported are the mean (± standard deviation) of at least two independent experiments.

**Table 3.4. Tethering function of variant Scs2 proteins.**

| Scs2 Substitution | Cortical ER Formation[a] | Growth on Tunicamycin[b] | Growth on (–)inositol[c] |
|---|---|---|---|
| Scs2 (wild type) | ++ | ++ | ++ |
| M226Stop (ΔTMD) | - | - | - |
| P44S, P51S | - | - | - |
| T41A, T42A | - | - | - |
| K80A, K84A, K119A, K120A, K122A, K124A | - | - | - |
| K119A, K120A, K122A, K124A | -/+ | -/+ | + |
| K80A, K84A | ++ | ND | ND |
| L86A | ++ | ++ | ++ |
| K84A, L86A | + | + | + |
| K84D, L86D | -/+ | - | - |
| P44S | ++ | ND | ND |
| P51S | + | -/+ | + |

[a]Mutant Scs2 proteins bearing the indicated substitutions were expressed in Δtether cells co-expressing Sec61-GFP, and cortical ER formation was assessed as none/weak/partial/strong (-, -/+, +, ++).

[b,c]Also shown are the growth phenotypes on media containing 0.8 μg/ml tunicamycin and media lacking inositol (scored as -, -/+, +, ++). No growth (-) indicates the loss of Scs2 function. ND, not determined.

[b]Growth on tunicamycin correlates with cortical ER formation; see Figures 3.12 and 3.13.

[c]Growth on media lacking inositol monitors interaction with FFAT motifs (see Kaiser et al., 2005; Loewen and Levine, 2005; Loewen et al., 2007; Kagiwada and Hashimoto, 2007; Nakamichi et al., 2011).

**Table 3.4. Strains used in this study**

| Strain | Genotype | Reference |
|---|---|---|
| SEY6210 | *MATα leu2-3,112 ura3-52 his3-Δ 200 trp1-Δ901 lys2-801 suc2-Δ9* | Robinson et al., 1988 |
| SEY621 | *MATa leu2-3,112 ura3-52 his3-Δ 200 trp1-Δ901 lys2-801 suc2-Δ9* | Robinson |

| | | |
|---|---|---|
| 0.1 | | et al., 1988 |
| MFY62 | SEY6210.1 *sac1*Δ::*TRP1* | Foti et al., 2001 |
| DBY354 | SEY6210.1 *scs2*Δ::*TRP1* | This study |
| DBY356 | SEY6210.1 *scs2*Δ::*TRP1 scs22*Δ:: *HISMX6* | Stefan et al., 2011 |
| JMY556 | SEY6210 *arg4*Δ::*KANMX6* | Macgurn et al., 2011 |
| ANDY149 | SEY6210 *SAC1*-6xHIS-TEV-3xFLAG::*TRP1 arg4*Δ::*KANMX6* | This Study |
| ANDY250 | SEY6210.1 *scs2*Δ::*TRP1 arg4*Δ::*KANMX6* | This Study |
| ANDY121 | SEY6210 *tcb3*Δ*::HISMX6* | This Study |
| ANDY113 | SEY6210.1 ist2Δ::HISMX6 | This Study |
| ANDY129 | SEY6210.1 ist2Δ::HISMX6 scs2Δ::TRP1 scs22Δ:: HISMX6 | This Study |
| ANDY151 | SEY6210 SAC1-6xHIS-TEV-3xFLAG::TRP1 ist2Δ::HISMX6 | This Study |
| ANDY153 | SEY6210.1 SEC61-GFP::TRP1 ist2Δ::HISMX6 scs2Δ::TRP1 scs22Δ::HISMX6 | This Study |
| ANDY157 | SEY6210.1 SEC61-GFP::KANMX6 | This Study |
| ANDY161 | SEY6210.1 SEC61-GFP::KANMX6 ist2Δ::HISMX6 | This Study |
| ANDY163 | SEY6210.1 ist2Δ::HISMX6 scs2Δ::TRP1 scs22Δ::HISMX6 sac1Δ::TRP1 and harboring pRS416sac1ts-23 | This Study |
| ANDY173 | SEY6210.1 SEC61-GFP::TRP1 ist2Δ::HISMX6 tcb1Δ::KANMX6 tcb2Δ::KANMX6 tcb3Δ::HISMX6 | This Study |
| ANDY176 | SEY6210.1 ist2Δ::HISMX6 tcb1Δ::KANMX6 tcb2Δ::KANMX6 tcb3Δ::HISMX6 | This Study |
| ANDY185 | SEY6210 SEC61-GFP::KANMX6 tcb1Δ::KANMX6 tcb2Δ::KANMX6 tcb3Δ::HISMX6 | This Study |
| ANDY188 | SEY6210.1 SEC61-GFP::KANMX6 scs2Δ::TRP1 scs22Δ::HISMX6 | This Study |
| ANDY196 | SEY6210.1 scs2Δ::TRP1 scs22Δ::HISMX6 tcb1Δ::KANMX6 tcb2Δ::KANMX6 tcb3Δ::HISMX6 | This Study |
| ANDY198 | SEY6210.1 ist2Δ::HISMX6 scs2Δ::TRP1 scs22Δ::HISMX6 tcb1Δ::KANMX6 tcb2Δ::KANMX6 tcb3Δ::HISMX6 | This Study |
| ANDY200 | SEY6210.1 SEC61-GFP::TRP1 scs2Δ::TRP1 scs22Δ::HISMX6 tcb1Δ::KANMX6 tcb2Δ::KANMX6 tcb3Δ::HISMX6 | This Study |
| ANDY201 | SEY6210.1 SEC61-GFP::TRP1 ist2Δ::HISMX6 scs2Δ::TRP1 scs22Δ::HISMX6 tcb1Δ::KANMX6 tcb2Δ::KANMX6 tcb3Δ::HISMX6 | This Study |
| ANDY214 | SEY6210.1 tcb1Δ::KANMX6 tcb2Δ::KANMX6 tcb3Δ::HISMX6 | This Study |
| ANDY215 | SEY6210.1 TCB1-GFP::TRP1 | This Study |
| ANDY217 | SEY6210.1 TCB2-GFP::TRP1 | This Study |
| ANDY219 | SEY6210.1 TCB3-GFP::TRP1 | This Study |
| ANDY222 | SEY6210.1 TCB3-GFP::KANMX6 ist2Δ::HISMX6 scs2Δ::TRP1 scs22Δ::HISMX6 | This Study |

| | | |
|---|---|---|
| ANDY233 | SEY6210.1 ist2Δ::HISMX6 scs2Δ::TRP1 scs22Δ::HISMX6 tcb1Δ::KANMX6 tcb2Δ::KANMX6 tcb3Δ::HISMX6 ire1Δ::NATMX and harboring pRS416IRE1 | This Study |
| ANDY236 | SEY6210.1 ist2Δ::HISMX6 scs2Δ::TRP1 scs22Δ::HISMX6 tcb1Δ::KANMX6 tcb2Δ::KANMX6 tcb3Δ::HISMX6 ire1Δ::NATMX | This Study |
| ANDY242 | SEY6210.1 ist2Δ::HISMX6 scs2Δ::TRP1 scs22Δ::HISMX6 tcb1Δ::KANMX6 tcb2Δ::KANMX6 tcb3Δ::HISMX6 hac1Δ::NATMX and harboring pRS416HAC1 | This Study |

**Table 3.5. Plasmids used in this study**

| Plasmid | Description | Source |
|---|---|---|
| pAM20 | pRS416-$P_{IST2}$-3xHA-*IST2* | This study |
| pAM21 | pRS415-$P_{IST2}$-GFP-*IST2* | This study |
| pAM22 | pRS416-$P_{IST2}$-GFP-*IST2* | This study |
| pAM23 | pRS416-$P_{IST2}$-GFP-$ist2^{1-928}$ | This study |
| pAM24 | pRS416-$P_{IST2}$-GFP-$ist2^{490-946}$ | This study |
| pAM25 | pRS416-$P_{IST2}$-GFP-$ist2^{928-946}$ | This study |
| pAM26 | pRS416-$P_{IST2}$-GFP-2x$ist2^{928-946}$ | This study |
| pAM27 | pRS415-$P_{GPD}$-mCherry-2x$ist2^{928-946}$ | This study |
| pAM28 | pRS416-$P_{SCS2}$-3xFLAG-*SCS2* | This study |
| pAM29 | pRS415-$P_{SCS2}$-GFP-*SCS2* | This study |
| pAM30 | pRS416-$P_{SCS2}$-GFP-*SCS2* | This study |
| pAM31 | pRS416-$P_{SCS2}$-GFP-$scs2^{K80A, K84A, K119A, K120A, K122A, K124A}$ | This study |
| pAM32 | pRS416-$P_{SCS2}$-GFP-$scs2^{1-225}$ | This study |
| pHY5 | pRS416-*SCS2* | This study |
| pHY6 | pRS416-$scs2^{K80A, K84A, K119A, K120A, K122A, K124A}$ | This study |
| pHY7 | pRS416-$scs2^{1-225}$ | This study |
| pHY8 | pRS416-$scs2^{P44S, P51S}$ | This study |
| pHY9 | pRS416-$scs2^{T41A, T42A}$ | This study |
| pHY10 | pRS416-$scs2^{K119A, K120A, K122A, K124A}$ | This study |
| pHY11 | pRS416-$scs2^{K80A, K84A}$ | This study |
| pHY12 | pRS416-$scs2^{L86A}$ | This study |
| pHY13 | pRS416-$scs2^{K84A, L86A}$ | This study |
| pHY14 | pRS416-$scs2^{K84D, L86D}$ | This study |
| pHY15 | pRS416-$scs2^{P44S}$ | This study |
| pHY16 | pRS416-$scs2^{P51S}$ | This study |
| pAM36 | pRS416-*IRE1* | This study |
| pAM37 | pRS415-$P_{ADH1}$-GFP-*SAC1* | This study |
| pAM38 | pRS415-$P_{ADH1}$-GFP-$SCS2^{1-129(MSP)}$-*SAC1* | This study |
| pAM39 | pRS416-HAC1 | This study |
| pYL95 | pRS415- $P_{GPD}$-mCherry-2xPHPlcδ | This study |
| pAM40 | pRS306-DsRED-HDEL | This study |
| pAM41 | pRS305-DsRED-HDEL | This study |
| pAM42 | pRS306-GFP-HDEL | This study |
| | pRS416-DsRED-HDEL | (Audhya and Emr, 2003) |
| pCS276 | pRS426-PCPY-GFP-2xPHOsh2 | (Stefan et al., 2011) |
| MFB65 | pRS416-sac1ts-23 | (Foti et al., 2001) |
| pJC104 | 4xUPRE-PCYC1-lacZ | (Cox et al., 1996) |
| pAM43 | pRS415-*TCB3*-GFP | This study |
| pAM44 | pRS415-$TCB3^{1-491}$-GFP | (This study |

## References


Audhya, A., and Emr, S.D. (2002). Stt4 PI 4-kinase localizes to the plasma membrane and functions in the Pkc1-mediated MAP kinase cascade. Dev Cell *2*, 593-605.

Audhya, A., and Emr, S.D. (2003). Regulation of PI4,5P2 synthesis by nuclear-cytoplasmic shuttling of the Mss4 lipid kinase. EMBO J *22*, 4223-4236.

Balla, A., Kim, Y.J., Varnai, P., Szentpetery, Z., Knight, Z., Shokat, K.M., and Balla, T. (2008). Maintenance of hormone-sensitive phosphoinositide pools in the plasma membrane requires phosphatidylinositol 4-kinase IIIalpha. Mol Biol Cell *19*, 711-721.

Breslow, D.K., Collins, S.R., Bodenmiller, B., Aebersold, R., Simons, K., Shevchenko, A., Ejsing, C.S., and Weissman, J.S. (2010) Orm family proteins mediate sphingolipid homeostasis. Nature *463*, 1048-1053.

Caputo, A., Caci, E., Ferrera, L., Pedemonte, N., Barsanti, C., Sondo, E., Pfeffer, U., Ravazzolo, R., Zegarra-Moran, O., and Galietta, L.J. (2008). TMEM16A, a membrane protein associated with calcium-dependent chloride channel activity. Science *322*, 590-594.

Carrasco, S., and Meyer, T. (2011). STIM proteins and the endoplasmic reticulum-plasma membrane junctions. Annu Rev Biochem *80*, 973-1000.

Cox, J.S., and Walter, P. (1996). A novel mechanism for regulating activity of a transcription factor that controls the unfolded protein response. Cell *87*, 391-404.

Creutz, C.E., Snyder, S.L., and Schulz, T.A. (2004). Characterization of the yeast tricalbins: membrane-bound multi-C2-domain proteins that form complexes involved in membrane trafficking. Cell Mol Life Sci *61*, 1208-1220.

Estrada, P., Kim, J., Coleman, J., Walker, L., Dunn, B., Takizawa, P., Novick, P., and Ferro-Novick, S. (2003). Myo4p and She3p are required for cortical ER inheritance in Saccharomyces cerevisiae. J Cell Biol *163*, 1255-1266.

Faulhammer, F., Konrad, G., Brankatschk, B., Tahirovic, S., Knodler, A., and Mayinger, P. (2005). Cell growth-dependent coordination of lipid signaling and glycosylation is mediated by interactions between Sac1p and Dpm1p. J Cell Biol *168*, 185-191.

Fischer, M.A., Temmerman, K., Ercan, E., Nickel, W., and Seedorf, M. (2009). Binding of plasma membrane lipids recruits the yeast integral membrane protein Ist2 to the cortical ER. Traffic *10*, 1084-1097.

Foti, M., Audhya, A., and Emr, S.D. (2001). Sac1 lipid phosphatase and Stt4 phosphatidylinositol 4-kinase regulate a pool of phosphatidylinositol 4-phosphate that functions in the control of the actin cytoskeleton and vacuole morphology. Mol Biol Cell *12*, 2396-2411.

Hammond, G.R., Fischer, M.J., Anderson, K.E., Holdich, J., Koteci, A., Balla, T., and Irvine, R.F. (2012). PI4P and PI(4,5)P2 are essential but independent lipid determinants of membrane identity. Science *337*, 727-730.

Hayashi, M., Raimondi, A., O'Toole, E., Paradise, S., Collesi, C., Cremona, O., Ferguson, S.M., and De Camilli, P. (2008). Cell- and stimulus-dependent heterogeneity of synaptic vesicle endocytic recycling mechanisms revealed by studies of dynamin 1-null neurons. Proc Natl Acad Sci USA *105*, 2175-2180.

Hepler, P.K., Palevitz, B.A., Lancelle, S.A., Mccauley, M.M., and Lichtscheidl, I. (1990). Cortical Endoplasmic-Reticulum in Plants. Journal of Cell Science *96*, 355-373.

Hu, J., Shibata, Y., Zhu, P.P., Voss, C., Rismanchi, N., Prinz, W.A., Rapoport, T.A., and Blackstone, C. (2009). A class of dynamin-like GTPases involved in the generation of the tubular ER network. Cell *138*, 549-561.

Jesch, S.A., Gaspar, M.L., Stefan, C.J., Aregullin, M.A., and Henry, S.A. (2010) Interruption of inositol sphingolipid synthesis triggers Stt4p-dependent protein kinase C signaling. J Biol Chem *285*, 41947-41960.

Jonikas, M.C., Collins, S.R., Denic, V., Oh, E., Quan, E.M., Schmid, V., Weibezahn, J., Schwappach, B., Walter, P., Weissman, J.S. (2009). Comprehensive characterization of genes required for protein folding in the endoplasmic reticulum. Science *323*, 1693-1697.

Juschke, C., Wachter, A., Schwappach, B., and Seedorf, M. (2005). SEC18/NSF-independent, protein-sorting pathway from the yeast cortical ER to the plasma membrane. J Cell Biol *169*, 613-622.

Kagiwada, S., and Hashimoto, M. (2007). The yeast VAP homolog Scs2p has a phosphoinositide-binding ability that is correlated with its activity. Biochem Biophys Res Commun *364*, 870-876.

Kaiser, S.E., Brickner, J.H., Reilein, A.R., Fenn, T.D., Walter, P., and Brunger, A.T. (2005). Structural basis of FFAT motif-mediated ER targeting. Structure *13*, 1035-1045.

Kopec, K.O., Alva, V., and Lupas, A.N. (2010) Homology of SMP domains to the TULIP superfamily of lipid-binding proteins provides a structural basis for lipid exchange between ER and mitochondria. Bioinformatics *26*, 1927-1931.

Liou, J., Kim, M.L., Heo, W.D., Jones, J.T., Myers, J.W., Ferrell, J.E., Jr., and Meyer, T. (2005). STIM is a Ca2+ sensor essential for Ca2+-store-depletion-triggered Ca2+ influx. Curr Biol *15*, 1235-1241.

Loewen, C.J., Roy, A., and Levine, T.P. (2003). A conserved ER targeting motif in three families of lipid binding proteins and in Opi1p binds VAP. EMBO J *22*, 2025-2035.

Loewen, C.J., and Levine, T.P. (2005). A highly conserved binding site in vesicle-associated membrane protein-associated protein (VAP) for the FFAT motif of lipid-binding proteins. J Biol Chem *280*, 14097-14104.

Loewen, C.J., Young, B.P., Tavassoli, S., and Levine, T.P. (2007). Inheritance of cortical ER in yeast is required for normal septin organization. J Cell Biol *179*, 467-483.

Longtine, M.S., McKenzie, A., 3rd, Demarini, D.J., Shah, N.G., Wach, A., Brachat, A., Philippsen, P., and Pringle, J.R. (1998). Additional modules for versatile and economical PCR-based gene deletion and modification in Saccharomyces cerevisiae. Yeast *14*, 953-961.

MacGurn, J.A., Hsu, P.C., Smolka, M.B., and Emr, S.D. (2011) TORC1 regulates endocytosis via Npr1-mediated Phosphoinhibition of a ubiquitin ligase adaptor. Cell *147*, 1104-1117.

Nakamichi, S., Yamanaka, K., Suzuki, M., Watanabe, T., and Kagiwada, S. (2011) Human VAPA and the yeast VAP Scs2p with an altered proline distribution can phenocopy amyotrophic lateral sclerosis-associated VAPB(P56S). Biochem Biophys Res Commun *404*, 605-609.

Park, C.Y., Hoover, P.J., Mullins, F.M., Bachhawat, P., Covington, E.D., Raunser, S., Walz, T., Garcia, K.C., Dolmetsch, R.E., and Lewis, R.S. (2009). STIM1 clusters and activates CRAC channels via direct binding of a cytosolic domain to Orai1. Cell *136*, 876-890.

Peretti, D., Dahan, N., Shimoni, E., Hirschberg, K., and Lev, S. (2008). Coordinated lipid transfer between the endoplasmic reticulum and the Golgi complex requires the VAP proteins and is essential for Golgi-mediated transport. Mol Biol Cell *19*, 3871-3884.

Pichler, H., Gaigg, B., Hrastnik, C., Achleitner, G., Kohlwein, S.D., Zellnig, G., Perktold, A., and Daum, G. (2001). A subfraction of the yeast endoplasmic reticulum associates with the plasma membrane and has a high capacity to synthesize lipids. Eur J Biochem *268*, 2351-2361.

Porter, K.R., and Palade, G.E. (1957). Studies on the endoplasmic reticulum. III. Its form and distribution in striated muscle cells. J Biophys Biochem Cytol *3*, 269-300.

Robinson, J.S., Klionsky, D.J., Banta, L.M., and Emr, S.D. (1988). Protein sorting in Saccharomyces cerevisiae: isolation of mutants defective in the delivery and processing of multiple vacuolar hydrolases. Mol Cell Biol *8*, 4936-4948.

Rocha, N., Kuijl, C., van der Kant, R., Janssen, L., Houben, D., Janssen, H., Zwart, W., and Neefjes, J. (2009). Cholesterol sensor ORP1L contacts the ER protein VAP to control Rab7-RILP-p150 Glued and late endosome positioning. J Cell Biol *185*, 1209-1225.

Roy, A., and Levine, T.P. (2004). Multiple pools of phosphatidylinositol 4-phosphate detected using the pleckstrin homology domain of Osh2p. J Biol Chem *279*, 44683-44689.

Schulz, T.A., Choi, M.G., Raychaudhuri, S., Mears, J.A., Ghirlando, R., Hinshaw, J.E., and Prinz, W.A. (2009). Lipid-regulated sterol transfer between closely apposed membranes by oxysterol-binding protein homologues. J Cell Biol *187*, 889-903.

Schulz, T.A., and Creutz, C.E. (2004). The tricalbin C2 domains: lipid-binding properties of a novel, synaptotagmin-like yeast protein family. Biochemistry *43*, 3987-3995.

Shepard, K.A., Gerber, A.P., Jambhekar, A., Takizawa, P.A., Brown, P.O., Herschlag, D., DeRisi, J.L., and Vale, R.D. (2003). Widespread cytoplasmic mRNA transport in yeast: identification of 22 bud-localized transcripts using DNA microarray analysis. Proc Natl Acad Sci USA *100*, 11429-11434.

Shibata, Y., Voeltz, G.K., and Rapoport, T.A. (2006). Rough sheets and smooth tubules. Cell *126*, 435-439.

Stefan, C.J., Manford, A.G., Baird, D., Yamada-Hanff, J., Mao, Y., and Emr, S.D. (2011). Osh proteins regulate phosphoinositide metabolism at ER-plasma membrane contact sites. Cell *144*, 389-401.

Suzuki, E., and Hirosawa, K. (1994). Immunolocalization of a Drosophila phosphatidylinositol transfer protein (rdgB) in normal and rdgA mutant photoreceptor cells with special reference to the subrhabdomeric cisternae. J Electron Microsc *43*, 183-189.

Thibault, G., Ismail, N., and Ng, D.T. (2011) The unfolded protein response supports cellular robustness as a broad-spectrum compensatory pathway. Proc Natl Acad Sci USA *108*, 20597-20602.

Toulmay, A., and Prinz, W.A. (2011). Lipid transfer and signaling at organelle contact sites: the tip of the iceberg. Curr Opin Cell Biol *23*, 458-463.

Toulmay, A., and Prinz, W.A. (2012). A conserved membrane-binding domain targets proteins to organelle contact sites. J Cell Sci *125*, 49-58.

Travers, K.J., Patil, C.K., Wodicka, L., Lockhart, D.J., Weissman, J.S., and Walter, P. (2000). Functional and genomic analyses reveal an essential coordination between the unfolded protein response and ER-associated degradation. Cell *101*, 249-258.

Voeltz, G.K., Prinz, W.A., Shibata, Y., Rist, J.M., and Rapoport, T.A. (2006). A class of membrane proteins shaping the tubular endoplasmic reticulum. Cell *124*, 573-586.

West, M., Zurek, N., Hoenger, A., and Voeltz, G.K. (2011). A 3D analysis of yeast ER structure reveals how ER domains are organized by membrane curvature. J Cell Biol *193*, 333-346.

Wilson, J.D., Thompson, S.L., and Barlowe, C. (2011).Yet1p-Yet3p interacts with Scs2p-Opi1p to regulate ER localization of the Opi1p repressor. Mol Biol Cell *22*, 1430-1439.

Wolf, W., Kilic, A., Schrul, B., Lorenz, H., Schwappach, B., and Seedorf, M. (2012) Yeast Ist2 recruits the endoplasmic reticulum to the plasma membrane and creates a ribosome-free membrane microcompartment. PLoS One *7*, e39703.

Yang, Y.D., Cho, H., Koo, J.Y., Tak, M.H., Cho, Y., Shim, W.S., Park, S.P., Lee, J., Lee, B., Kim, B.M.*, et al.* (2008). TMEM16A confers receptor-activated calcium-dependent chloride conductance. Nature *455*, 1210-1215.

Yavari, A., Nagaraj, R., Owusu-Ansah, E., Folick, A., Ngo, K., Hillman, T., Call, G., Rohatgi, R., Scott, M.P., and Banerjee, U. (2010) Role of lipid metabolism in smoothened derepression in hedgehog signaling. Dev Cell *19*, 54-65.

# Chapter V

## Conclusions and future directions

ER-PM contacts are important platforms for direct intracellular communication between the ER and PM. However, despite being first described in the 1950s, the research on these conserved structures in many systems had remained mostly limited to $Ca^{2+}$ signaling in muscle cells. In the last decade, research on the functions of ER-PM contact sites has expanded, yet how these junctions are formed in many systems is not known. Through the work presented in my thesis focusing on understanding the paradox of how ER localized Sac1 regulates PI4P on the PM, we have uncovered both the mechanism of Sac1 function and ER-PM contact site formation in yeast. Our work has identified conserved families of ER-PM tethering proteins in yeast that mediate ER-PM junction formation and are required for Sac1 regulation of PM PI4P. Notably we uncovered a novel function for ER-PM contacts in maintaining ER homeostasis and function. In addition we discovered an important new and shared role for the yeast oxysterol binding proteins in regulating Sac1 and PI4P metabolism at ER-PM contact sites. Hopefully our studies will serve as a foundation for future work on ER-PM contacts in other systems.

Since we started the initial investigations on PI4P regulation at ER-PM contacts, the field of ER-PM and ER-organelle contacts has expanded, with a large amount of exciting research being published. These new studies, together with our work, have increased the understanding of ER-PM contact site formation and function. However, new questions and puzzles have arisen that will drive future research in this area. In the following section the culmination of this exciting recent work on ER-PM contacts will be highlighted and the important next questions will be discussed.

**ER-PM tethering proteins**

In chapter four, we elucidated the mechanism for ER-PM tethering in yeast. Out of the six proteins identified, the VAP protein Scs2 was the most critical component of ER-PM tethering. Scs2 was first implicated in ER-PM contacts by the Levine group and our subsequent work found that deletion of Scs2 was required to reveal the additive phenotypes of deletion mutants of the other tethering genes (Loewen et al., 2007; Manford et al., 2012). However, unlike Ist2 and the tricalbins, the mechanism of how VAP proteins tether organelles is still an outstanding question. Scs2 is critical for ER-PM tethering in yeast and is sufficient to rescue many of the ER-PM defects in the Δtether cells (Manford et al., 2012). In addition, in another critical difference from the other tethers identified, Scs2/VAP localize to all of the ER in yeast and mammalian cells (Alpy et al., 2013; Loewen et al., 2003). This suggests a regulated mechanism for the VAP tethering function, where it's tethering is activated at ER-organelle junctions. One simple mechanism for this localized tethering activation is through specific interactions with FFAT containing proteins. In yeast and mammalian cells the VAP proteins have been shown to bind lipid transfer proteins that contain the VAP binding FFAT motif, but also PH domains that would bind phosphoinositides on another organelle (Kawano, 2006; Lehto et al., 2005; Loewen et al., 2003; Mesmin et al., 2013; Peretti et al., 2008; Rocha et al., 2009). In addition, recent work in mammalian cells has identified transmembrane proteins on endosomes that contain FFAT motifs that interact with the VAP proteins (Alpy et al., 2013). However, in many of these mammalian experiments both a VAP protein and an FFAT containing proteins are over expressed, resulting in large induced ER-Golgi or ER-Endosome contacts. Determining whether these proteins mediate these contacts at endogenous expression levels is difficult, but is

needed to address whether these are important for tethering complexes or simply recruiting proteins to these junctions. In support of this, at least for ER-PM tethering in yeast, no FFAT containing proteins can recapitulate the *scs2* ER-PM tethering mutant phenotype (Loewen et al., 2007). Thus, it is still an open question for how the VAP proteins mediated tethering in yeast and in other systems. Whether there are unidentified PM localized FFAT containing proteins that mediate the Scs2 tethering function or a completely FFAT independent mechanism are questions that remain to be addressed. In addition, if FFAT interactions are independent of VAP tethering function, elucidating how lipid transfer protein recruitment and ER-organelle tethering are integrated together is an important question. Taking advantage of Scs2 phenotypes that are dependent on FFAT binding (inositol auxotrophy) and tethering (sensitivity to tunicamycin) could be used to screen for separation of function alleles of *SCS2*. In addition, identifying potential PM binding partners of Scs2 could provide a mechanism for ER-PM tethering. As we have generated an Scs2 interactome, candidate tests for ER-tethering defects could be done for all PM proteins identified by our Scs2 mass spec analysis.

In addition to the yeast VAP proteins, two other families of tethering proteins mediate ER-PM contacts in yeast (Manford et al., 2012; Toulmay and Prinz, 2012; Wolf et al., 2012). These proteins are conserved in mammalian cells and likely facilitate ER-organelle tethering other systems. While the VAP proteins discussed above have known roles in tethering in higher eukaryotes, it was not known if relatives of Ist2 or tricalbins (mammalian extended synaptotagmin (E-Syt)) function as tethers. In fact the E-Syts had been shown to be PM proteins (Min et al., 2007). A recent paper reexamined the localization of these proteins, in part due to the recent observations in yeast. Consistent with the yeast work, E-Syt2 and E-Syt3 localized to the cortex of cells, but also colocalized with ER markers (Giordano et al., 2013). This indicates that

although E-Syt2 and E-Syt3 appear to be a PM proteins, overexpression actually induces massive cER formation. Interestingly expression of E-Syt1 did not induce cER and it localized throughout the ER network, but upon increased cytoplasmic $Ca^{2+}$ E-Syt1 dramatically induced ER-PM contacts. Importantly, knock down of all three E-Syts was shown to significantly reduced the levels of ER-PM contact, confirming that the E-Syts at endogenous expression levels is required for a portion of the ER-PM contacts in the cell (Giordano et al., 2013). Surprisingly, the triple knock down cells still could induce a STIM1 translocation and store operated calcium entry (SOCE see below), indicating that though reduced, ER-PM contacts were still present.

Another recent study uncovered a role for E-Syt1 induced ER-PM contacts in linking two established ER-PM contact site functions, lipid transfer and SOCE $Ca^{2+}$ signaling. As reviewed in the introduction chapter, upon activation PLC, large amounts of PIP2 is hydrolyzed on the PM releasing $IP_3$. $IP_3$ binds to the $IP_3$ receptor, triggering the release of the Ca2+ stores in the ER. This drop in ER $Ca^{2+}$ stores induces STIM oligomerization and translocation to ER-PM contacts, where the STIM proteins subsequently activate the PM $Ca^{2+}$ channel ORAI (reviewed in Carrasco and Meyer, 2011). Using a genetically encoded fluorescent ER-PM reporter and TIRF microscopy, this new study found that upon the increase cytoplasmic pool of $Ca^{2+}$ from SOCE, there was an increase in the number ER-PM junctions and the distance of the ER to the PM became smaller (Chang et al., 2013). Consistent with the findings of the study described in the previous paragraph, the increase in number and tightening of ER-PM contacts was mediated by the calcium regulated extended synaptotagmin, E-Syt1. The authors reasoned that a likely function for increasing the number and shortening the distance of ER-PM contacts was for lipid transfer of phosphatidylinositol for the regeneration of $PI(4,5)P_2$. This is a similar to function rdgB PI transfer protein and the specialized ER-PM contacts in the fly eye. Consistent with this

hypothesis, the mammalian homolog of rdgB, Nir2, was recruited to ER-PM junctions after $Ca^{2+}$ elevation in an E-Syt1 dependent manner. Nir2 also contains a FFAT motif and its localization to the ER-PM junction requires interaction with VAPA, which was also recruited to these sites after $Ca^{2+}$ elevation. Notably, $PI(4,5)P_2$ regeneration for subsequent rounds of signaling was impaired in cells treated with siRNAs to Nir2 or E-Syt1 (Chang et al., 2013).. Taken together both of theses recent studies identify a conserved role for the tricalbin/E-Syts in ER-PM tethering in mammalian cells and integrate them into two important functions for ER-PM contacts. In addition the SOCE signaling pathway now possess a phosphoinositide cycle, with $PI(4,5)P_2$ hydrolysis at the beginning of the cycle and $PI(4,5)P_2$ generation at the end.

As indicated in both of these studies, the E-Syts are not the only ER-PM tethers in mammalian cells. It is still unknown what additional proteins facilitate the stable ER-PM contacts in mammalian cells and identifying these factors is an important next step for future work. Intriguingly, the other tethering protein identified in yeast, Ist2, has at least 10 family members of the TMEM16/anoctamin family of proteins in mammalian cells and it is unknown if whether any of these function as tethers (Duran et al., 2012). As highlighted in yeast, redundancy may play a major role in ER-PM tethering in higher eukaryotes. Thus siRNA screens that have identified components of SOCE, may have missed the ER-PM tethering proteins. Similar proteomic approaches to the ones described in chapter 4, using proteins that function at these sites as baits, could be helpful to identify additional mammalian tethering proteins.

**The mechanism of ORP PI4P regulation**

In chapter three we uncovered a role for the yeast *o*xy*s*terol-binding *h*omology (OSH) family of lipid transfer proteins as key regulators of PI4P metabolism. *OSH* mutants,

where all seven family members are deleted, exhibit a massive accumulation of PI4P in cells, which can be mitigated by expression of any one of the Osh proteins. This indicates that a shared and likely essential function of all of the Osh proteins is in PI4P regulation. The accumulation of PI4P in *osh* mutants was through regulation of Sac1 PI4P phosphatase function, as *osh/sac1* double mutants do not have a further increase in PI4P levels beyond that of Osh alone. Consistent with this the conserved ORD domain of the Osh proteins can stimulate Sac1 phosphatase activity *in vitro*. However the details of the Osh-Sac1 regulation mechanism is unclear. We proposed that the Osh proteins could bind and present PI4P substrate to Sac1 that was acting *in trans* from the ER to the PI4P on the PM. The presentation model for a lipid-modifying enzyme has been suggested for Sec14 PI transfer proteins that bind PI and stimulate PI4-kinase activity (Schaaf et al., 2008). Interestingly, recent studies have provided new structural details into the Osh-PI4P interaction. Although all of the Osh proteins were assumed to bind sterols in their conserved *o*xysterol binding protein *r*elated *d*omain (ORD), complexes of ORD domains of Osh3 and Osh4 bound to PI4P have been recently solved (de Saint-Jean et al., 2011; Tong et al., 2013). These structures revealed that Osh4 binds PI4P and sterol in the same conserved pocket, while Osh3's ORD cannot bind sterol at all, consistent with the low sterol transfer activity of Osh3. Intriguingly, the structure of the ORD domain of Osh3 bound to PI4P demonstrate that the residues which facilitate PI4P binding are conserved amongst ORD domains and those specifically involved in sterol binding in Osh4 are not. This is consistent with PI4P metabolism being a shared function of the Osh proteins.

These structures raise new questions on how PI4P binding by the Osh protein integrates into Sac1 PI4P turnover. It has been proposed for the mammalian oxysterol binding protein (OSBP) and Osh4 that sterol and PI4P transfer is coupled, where sterol delivery to the Golgi

would result in PI4P transfer back to the ER for Sac1 turnover *in cis* (de Saint-Jean et al., 2011; Mesmin et al., 2013). A reconstitution of this process was recently published and the ORD domains of Osh4 and OSBP can transfer PI4P *in vitro* (Mesmin et al., 2013). However, as highlighted in the introduction, the evidence of PI4P transfer specifically *in vivo* is lacking. Whether this is the primary mechanism for Sac1 PI4P regulation *in vivo,* especially at the PM, remains to be addressed. To complicate the Osh family even further, Osh6 and Osh7 have recently been shown to primarily bind phosphatidylserine (PS) *in vivo* and mediate transfer of PS from the ER to the PM (Maeda et al., 2013). In the most convincing demonstration of an *in vivo* transfer activity by an Osh protein, retargeting Osh6 to the ER-vacuole contacts result in the detection of PS on the vacuole membrane. This mix of various lipid transfer substrates of the Osh family, but a shared function in PI4P regulation provides ample opportunity for future investigation. In the short term, direct *in vivo* tests for *trans* and *cis* activities of Sac1 would shed light on the primary mechanism of Sac1 PI4P regulation. We have generated Sac1 mutants that may function only in *cis* which could be used to address this question.

**Identifying new functions for ER-PM contacts**

An important and novel phenotype of yeast cells lacking ER-PM contacts is the induction of the unfolded protein response (UPR). In chapter four we reasoned that this constitutive UPR signaling and the requirement for this signaling to maintain viability of Δtether cells, indicated that the UPR was compensating the disruption to pathways or process in the ER that require these contacts for function. However, we were unable to determine the pathways or processes that were affected in this mutant, and therefore could not identify potential new functions for ER-PM contacts. Although we have tested specific pathways directly in chapter 4, more global

approaches, such as expression profiling, would be more comprehensive in identifying all the perturbation in Δtether cells. This approach has been a successful in identifying specific subsets of UPR regulated genes that are induced in mutants that rely on UPR signaling for viability (Thibault et al., 2011; 2012). This analysis helped determine which pathways are upregulated by the UPR to compensate for the ER dysfunction in these mutants. In addition, as the UPR counteracts defects Δtether cells, assaying Δtether cells with a crippled or conditional UPR system would reveal more potent phenotypes. Alternatively, isolating suppressors of Δtether/UPR double mutants could identify pathways linked to ER-PM contact phenotypes. In addition to identifying more functions in yeast, as more is understood about the proteins that tether ER and PM in other systems, additional phenotypes will likely be discovered in higher eukaryotes. Furthermore, testing if the functions identified in yeast are conserved or whether ER-PM contacts have a role in development are exciting questions to be addressed.

**References**

Alpy, F., Rousseau, A., Schwab, Y., Legueux, F., Stoll, I., Wendling, C., Spiegelhalter, C., Kessler, P., Mathelin, C., Rio, M.-C., et al. (2013). STARD3/STARD3NL and VAP make a novel molecular tether between late endosomes and the ER. Journal of Cell Science.

Carrasco, S., and Meyer, T. (2011). STIM Proteins and the Endoplasmic Reticulum-Plasma Membrane Junctions. Annu. Rev. Biochem. *80*, 973–1000.

Chang, C.-L., Hsieh, T.-S., Yang, T.T., Rothberg, K.G., Azizoglu, D.B., Volk, E., Liao, J.-C., and Liou, J. (2013). Feedback Regulation of Receptor-Induced Ca2+ Signaling Mediated by E-Syt1 and Nir2 at Endoplasmic Reticulum-Plasma Membrane Junctions. CellReports 1–28.

de Saint-Jean, M., Delfosse, V., Douguet, D., Chicanne, G., Payrastre, B., Bourguet, W., Antonny, B., and Drin, G. (2011). Osh4p exchanges sterols for phosphatidylinositol 4-phosphate between lipid bilayers. The Journal of Cell Biology *195*, 965–978.

Duran, C., Qu, Z., Osunkoya, A.O., Cui, Y., and Hartzell, H.C. (2012). ANOs 3-7 in the anoctamin/Tmem16 Cl- channel family are intracellular proteins. AJP: Cell Physiology *302*, C482–C493.

Giordano, F., Saheki, Y., Idevall-Hagren, O., Colombo, S.F., Pirruccello, M., Milosevic, I., Gracheva, E.O., Bagriantsev, S.N., Borgese, N., and Pietro De Camilli (2013). PI(4,5)P2-Dependent and Ca2+-Regulated ER-PM Interactions Mediated by the Extended Synaptotagmins. Cell *153*, 1494–1509.

Kawano, M. (2006). Efficient Trafficking of Ceramide from the Endoplasmic Reticulum to the Golgi Apparatus Requires a VAMP-associated Protein-interacting FFAT Motif of CERT. Journal of Biological Chemistry *281*, 30279–30288.

Lehto, M., Hynynen, R., Karjalainen, K., Kuismanen, E., Hyvärinen, K., and Olkkonen, V.M. (2005). Targeting of OSBP-related protein 3 (ORP3) to endoplasmic reticulum and plasma membrane is controlled by multiple determinants. Experimental Cell Research *310*, 445–462.

Loewen, C.J.R., Young, B.P., Tavassoli, S., and Levine, T.P. (2007). Inheritance of cortical ER in yeast is required for normal septin organization. The Journal of Cell Biology *179*, 467–483.

Loewen, C.J.R., Roy, A., and Levine, T.P. (2003). A conserved ER targeting motif in three families of lipid binding proteins and in Opi1p binds VAP. Embo J *22*, 2025–2035.

Maeda, K., Anand, K., Chiapparino, A., Kumar, A., Poletto, M., Kaksonen, M., and Gavin, A.-C. (2013). Interactome map uncovers phosphatidylserine transport by oxysterol-binding proteins. Nature *501*, 257–261.

Manford, A.G., Stefan, C.J., Yuan, H.L., Macgurn, J.A., and Emr, S.D. (2012). ER-to-Plasma Membrane Tethering Proteins Regulate Cell Signaling and ER Morphology. Developmental Cell *23*, 1129–1140.

Mesmin, B., Bigay, J., Filseck, von, J.M., Lacas-Gervais, S., Drin, G., and Antonny, B. (2013). A Four-Step Cycle Driven by PI(4)P Hydrolysis Directs Sterol/PI(4)P Exchange by the ER-Golgi Tether OSBP. Cell *155*, 830–843.

Min, S.-W., Chang, W.-P., and Südhof, T.C. (2007). E-Syts, a family of membranous Ca2+-sensor proteins with multiple C2 domains. Proc. Natl. Acad. Sci. U.S.a. *104*, 3823–3828.

Peretti, D., Dahan, N., Shimoni, E., Hirschberg, K., and Lev, S. (2008). Coordinated lipid transfer between the endoplasmic reticulum and the Golgi complex requires the VAP proteins and is essential for Golgi-mediated transport. Molecular Biology of the Cell *19*, 3871–3884.

Rocha, N., Kuijl, C., van der Kant, R., Janssen, L., Houben, D., Janssen, H., Zwart, W., and Neefjes, J. (2009). Cholesterol sensor ORP1L contacts the ER protein VAP to control Rab7-RILP-p150Glued and late endosome positioning. The Journal of Cell Biology *185*, 1209–1225.

Schaaf, G., Ortlund, E.A., Tyeryar, K.R., Mousley, C.J., Ile, K.E., Garrett, T.A., Ren, J., Woolls, M.J., Raetz, C.R.H., Redinbo, M.R., et al. (2008). Functional Anatomy of Phospholipid Binding and Regulation of Phosphoinositide Homeostasis by Proteins of the Sec14 Superfamily. Molecular Cell *29*, 191–206.

Thibault, G., Ismail, N., and Ng, D.T.W. (2011). The unfolded protein response supports cellular

robustness as a broad-spectrum compensatory pathway. Proceedings of the National Academy of Sciences *108*, 20597–20602.

Thibault, G., Shui, G., Kim, W., McAlister, G.C., Ismail, N., Gygi, S.P., Wenk, M.R., and Ng, D.T.W. (2012). The Membrane Stress Response Buffers Lethal Effects of Lipid Disequilibrium by Reprogramming the Protein Homeostasis Network. Molecular Cell *48*, 16–27.

Tong, J., Yang, H., Yang, H., Eom, S.H., and Im, Y.J. (2013). Structure of Osh3 Reveals a Conserved Mode of Phosphoinositide Binding in Oxysterol-Binding Proteins. Structure/Folding and Design *21*, 1203–1213.

Toulmay, A., and Prinz, W.A. (2012). A conserved membrane-binding domain targets proteins to organelle contact sites. Journal of Cell Science *125*, 49–58.

Wolf, W., Kilic, A., Schrul, B., Lorenz, H., Schwappach, B., and Seedorf, M. (2012). Yeast Ist2 Recruits the Endoplasmic Reticulum to the Plasma Membrane and Creates a Ribosome-Free Membrane Microcompartment. PLoS ONE *7*, e39703.

# Appendix

## Crystal Structure of the Yeast Sac1: Implications for Its Phosphoinositide Phosphatase Function

Andrew Manford, Tian Xia, Ajay Kumar Saxena, Christopher Stefan, Fenghua Hu, Scott D. Emr, Yuxin Mao

Weill Institute for Cell and Molecular Biology and Department of Molecular Biology and Genetics, Cornell University, Ithaca, NY 14853, USA

Appendix was originally published in The EMBO Journal 29, 1489–1498, (2010)

Andrew Manford major contribution was Figure A1.10.

Data deposition: Coordinates for the Sac phosphoinositide phosphatase domain structure have been deposited in the Protein Data Bank with the PDB ID: 3LWT.

## Abstract

Sac family phosphoinositide phosphatases are an essential family of $CX_5R(T/S)$ based enzymes, involved in numerous aspects of cellular function such as phosphoinositide homeostasis, cellular signaling, and membrane trafficking. Genetic deletions of several Sac family members result in lethality in animal models and mutations of the Sac3 gene have been found in human hereditary diseases. Here we report the crystal structure of a founding member of this family, the Sac phosphatase domain of yeast Sac1. The 2.0 Å resolution structure reveals that the Sac domain is comprised of two closely packed sub-domains, a novel N-terminal sub-domain and the phosphoinositide phosphatase catalytic sub-domain. The structure further reveals a striking conformation of the catalytic P-loop and a large positively charged groove at the catalytic site. These findings suggest an unusual mechanism for its dephosphorylation function. Homology structural model of human Fig4/Sac3 allows the mapping of several disease related mutations and provides a framework for the understanding of the molecular mechanisms of human diseases.

## Introduction

Phosphoinositides (PIs) control numerous cellular processes such as cell signaling, proliferation, cytoskeleton organization, membrane trafficking, ion channel activity, transcription and mRNA trafficking (De Matteis and Godi, 2004; Di Paolo and De Camilli, 2006; Odorizzi et al., 2000). PIs localize at membrane-cytoplasmic interfaces and achieve their functions through the binding of proteins to their cytoplasmic-exposed phosphorylated inositol head groups, which can be reversibly phosphorylated at the 3', 4', and 5' positions to generate an ensemble of seven biological active derivatives. Each PI isoform has a specific intracellular distribution, which provides spatial and temporal cues within the cell for PI-binding proteins. The recruitment of specific PI-binding proteins promotes the assembly of macromolecular complexes to initiate a series of physiological events including membrane trafficking and cytoskeletal dynamics. Moreover, in response to extracellular stimuli, PIs also serve as precursors for second messagers to initiate downstream intracellular signaling pathways. To maintain the selective concentration of specific PI species, as well as to generate the dynamic PI composition changes in response to acute signaling inputs, eukaryotic cells encode a large number of PI metabolizing enzymes: including PI kinases and PI phosphatases. Despite their physiological importance, the properties of many of these enzymes remain poorly characterized.

One class of these enzymes contains a conserved PI phosphatase module termed the Sac domain. The Sac phosphatase domain comprises approximately 500 amino acids and contains seven highly conserved motifs including the conserved catalytic $CX_5R(T/S)$ motif, which is essential for catalytic activity (Hughes et al., 2000a). There are five Sac phosphatase domain-containing proteins in human, which appear to fall into two subfamilies. Members of the first subfamily, including the transmembrane protein Sac1, cytosolic proteins Sac2/INPP5f, and

Sac3/Fig4, have an N-terminal Sac phosphatase and no other recognizable structural domains. The second subfamily comprises two synaptojanin homologues, which have a PI 5-phosphatase domain immediately after the N-terminal Sac phosphatase module (Figure A1.1). In yeast, there are also five Sac domain-containing enzymes including Sac1, Fig4 and three synaptojanin like proteins (Sjl1,2,3)

Sac1 is a 67kD type II membrane protein that localizes to the endoplasmic reticulum (ER) and Golgi apparatus (Nemoto et al., 2000; Whitters et al., 1993). It was originally identified by two independent genetic screens searching for modifiers of actin cytoskeleton defects and of trans-Golgi network exocytic failure caused by inactivation of Sec14p, the major yeast phosphatidylinositol/phosphatidylcholine transfer protein (Bankaitis et al., 1990; Cleves et al., 1989; Novick et al., 1989). In yeast, loss of Sac1 function has been implicated in a broad range of cellular defects (Strahl and Thorner, 2007), such as disorganization of the actin cytoskeleton (Novick et al., 1989), inositol auxotrophy (Whitters et al., 1993), cold sensitivity for growth (Novick et al., 1989), multiple drug sensitivities (Hughes et al., 1999), abnormal vacuolar morphology (Foti et al., 2001; Tahirovic et al., 2005), cell wall defects (Schorr et al., 2001), and unbalanced sphingolipid synthesis (Brice et al., 2009). Sac1 mutants in *Drosophila* die as embryos with defects in dorsal closure (Wei et al., 2003). Mouse strains deficient in Sac1 are embryonic lethal (Liu et al., 2009; Liu et al., 2008). Knock-down of Sac1 expression in mammalian cell lines results in disorganization of Golgi membranes and mitotic spindles (Liu et al., 2009; Liu et al., 2008). These findings suggest essential roles for Sac1 mediated PI metabolism in multicellular organisms.

*In vitro* studies have demonstrated that Sac1 dephosphorylates a number of PIs, including PI(3)P, PI(4)P, and PI(3,5)$P_2$ (Guo et al., 1999). *In vivo*, genetic ablation of Sac1 activity in yeast

results in a 10-fold increase in the steady state levels of PI(4)P with little effect on PI(4,5)$P_2$ and modest increases in the levels of the 3-OH PIP species (Guo et al., 1999; Nemoto et al., 2000; Rivas et al., 1999), suggesting that yeast Sac1 is a major pathway for PI(4)P dephosphorylation *in vivo*.

While Sac1 primarily dephosphorylates PI(4)P, other Sac phosphatase members have been shown to regulate other PI isoforms in vivo. Fig4 (Sac3 in mammal) was originally identified in a screen for genes induced by mating pheromone in *S. cerevisiae* (Erdman et al., 1998). Sac3 is a phosphoinositide 5-phosphatase that specifically hydrolyzes PI(3,5)$P_2$ to generate PI(3)P both *in vitro* and *in vivo* (Duex et al., 2006a; Duex et al., 2006b; Rudge et al., 2004). Interestingly, Sac3/Fig4p forms a complex with a PI(3)P-5-kinase Fab1p and a scaffold protein Vac14p. This complex is also conserved in mammals and is responsible for the acute regulation of subcellular levels of PI(3,5)$P_2$ (Botelho et al., 2008; Jin et al., 2008; Sbrissa et al., 2008). Genetic mutations affecting the function of Sac3/Fig4 lead to neurological diseases, including Charcot-Marie-Tooth (CMT) disease Type 4J, a subset of Amyotrophic Lateral Sclerosis (ALS) in human, and neurodegeneration in the pale tremor mouse (Chow et al., 2009; Chow et al., 2007).

Despite considerable attention on Sac domain-containing proteins, a lack of structural information of this unique Sac phosphatase domain has left large gaps in our knowledge of this protein family. For example, each Sac phosphatase prefers a specific subgroup of PIs as substrates, but how the substrate specificity is determined by the otherwise homologous phosphatase region is unresolved. Mutations have been mapped to Sac3/Fig4 in patients with CMT 4J and ALS, but how the function of the enzyme is impaired in disease mutants is still not understood. Hence, we performed structural studies on the Sac phosphatase. Here we report the

first crystal structure of a Sac phosphatase, the yeast Sac1. The structure reveals a strikingly different configuration of the catalytic motif compared to protein tyrosine phosphatases and a large positively charged groove at the catalytic site which is surrounded by flexible loops enriched with hydrophobic and anionic residues. Our results further provide insights into the molecular mechanism for the enzymatic function of Sac phosphatases and suggest how mutations in Sac3/Fig4 affect its normal function in two human neuronal degeneration diseases (CMT4J and ALS).

## Materials and Methods

### Protein expression and purification

The DNA sequence encoding a variety portions of the cytoplasmic Sac domain of wild type yeast Sac1 were PCR amplified and subcloned into a pET28 based bacterial expression vector in frame with an N-terminal His-sumo tag. The constructs were confirmed by DNA sequencing. Recombinant proteins were over expressed in *E.coli.* BL21 cells. The selenomethionine substituted proteins were expressed in M9 minimum media supplied with Drop-out mix synthetic minus methionine powder (USBiological) and selenomethionine powder was added upon induction. Recombinant proteins were purified with metal affinity beads (Clontech). The His-sumo tag was removed by the sumo specific protease Ulp1 during over night dialysis in a buffer of 20 mM hepes, pH 7.3, 20 mM NaCl, 5 mM β-mercaptoethanol. The cutting mixture was further purified by Hi-trap Q column followed by gel filtration. The peak corresponding to Sac1 was pooled and concentrated to 10 mg/ml in a buffer containing 20 mM Hepes, pH 7.3, 20 mM NaCl, 10 mM DTT.

**Crystallization and preliminary X-ray crystallographic analysis**

Crystallization trials were set up with a PHENIX liquid handling system (Art Robbins Instruments). The construct containing residues 1-503 of ySac1 yielded crystals and thus was pursued for further structural analysis. Sac1 crystals used for native data set were grown by hanging drop vapor diffusion at 4 $^0$C by mixing protein (10 mg/ml) with reservoir solution containing 1.5 M NaCl, 0.1 M Na Citrate pH 7.5, 0.45 M Na Citrate in 1:1 ratio (v/v). Crystals were quite sensitive to pH and obtained in the pH range of 5.5-5.9. SeMet-Sac1 crystals were grown under similar conditions. Crystals were transferred into the same solution supplemented with 20% glycerol before cooling to 100K in a nitrogen stream. The crystal diffracted up to 1.97 Å at the Cornell synchrotron light source, MacCHESS beam line A1. The crystal belongs to space group I222 with *a=86.16* Å*; b=94.7* Å *3; c=155.44* Å*;* $\alpha=\beta=\gamma=90$ with the calculated Matthews coefficient $V_m$= 2.88 and with 57.3% of solvent in the crystal and one protein molecule in an asymmetric unit (Matthews, 1968). All the X-ray diffraction data were processed by using *hkl2000* (Otwinowski and Minor, 1997).

**Structure determination and refinement**

A complete three wavelength data set was collected at wavelengths around the selenium K edge. However, due to crystal decay during data collection, only the data collected at the peak wavelength (0.9794 Å) was used for phasing. The initial phase was calculated by single wavelength anomalous diffraction method (SAD) using the program HKL2MAP (Pape and Schneider, 2004). Since there are only a total of 4 methionine sites (including the NH2-terminal starting codon) in the 503-residue Sac1 domain, the anomalous signal contributed by selenium atoms was relatively weak and the initial electron density is not of quality expected for a 2.2 Å

resolution anomalous data set. The *ab initio* protein model was built manually in Xtalview (McRee, 1999) with the aid of automatic modeling building by using program ARP/wARP 7.0 (Perrakis et al., 1999) in the CCP4 program suite (Collaborative Computational Project, 1994). The model was completed by iterative model building with COOT (Emsley and Cowtan, 2004) refinement with CNS (Brunger et al., 1998). The amino acids beyond 456 were not visible in electron density maps and presumed to be disordered. The final Sac1 structure consists of 1-456 amino acids with excellent stereochemistry and good crystallographic statistics (Table A1.1).

**Homology structure modeling**

For Sac3 homology modeling, the Sac1 crystal structure was used as the template for modeling. Secondary structure prediction on the Sac3 sequence was done using the PSIPRED program (McGuffin et al., 2000). The CLUSATLW2 program (Labarga et al., 2007) was used to get the best sequence alignment between Sac3 and Sac1 using secondary structures as constraints. The Sac3 homology model was built using the computational Modeler 9V4 program (Sali et al., 2008). The Sac3 structure was further refined and validated using Ramachandran plot analysis indicating no residues in disallowed regions.

**Yeast in vivo experiments and PI analysis**

*SAC1* was cloned into pGOGFP N-terminal GFP vector (Odorizzi et al., 1998) with *BglII* and *Sal1*. Point mutants were constructed from the pGOGFP-SAC1 template by site directed mutagenesis and confirmed by sequencing. The resultant constructs were transformed into *sac1Δ* yeast cells (strain MFY62) (Foti et al., 2001). For the cold sensitive growth assay, transformants were grown to midlog ($OD_{600}$=0.5), adjusted to 1OD/ml, serially diluted 1:10 3 times, spotted

onto selection plates, and left at 15°C for 6 days. For Western blot, 5 $OD_{600}$ of midlog cells were harvested, precipitated in 10% Trichloroacetic acid, washed 2x in Acetone, and bead beated in sample buffer. 1 $OD_{600}$ equivalent of the samples were run on an 8% SDS PAGE and immunoblotted against GFP (Santa Cruz Biotechnology sc-9996) and G6PDH (Sigma A-0251). Intracellular PI level analysis was performed as previously described (Botelho et al., 2008). Briefly, cells transformed with control empty vector or vector harboring WT or mutant Sac1 were grown to log phase. Cells (5 $OD_{600}$) were harvested, washed in media lacking inositol, and labeled with *myo*-[2-3H] inositol for 1 hour. Lipids were deacylated, glycerophospholipids were extracted, and $10^7$ cpm of samples were separated by HPLC.

## Results

### Structure Determination and Overall Structure

The cytosolic portion of yeast Sac1 (residues 1-503) was expressed as an N-terminal His-sumo-tagged fusion protein. Crystals were obtained by using hang drop vapor diffusion method with the reservoir solution containing 0.55 M Na Citrate (pH 7.0) and 1.5 M NaCl. The crystals formed in space group I222 with unit cell dimensions of a=86.16 Å; b=94.73 Å; c=155.44 Å and one molecule in the asymmetric unit. The structure was solved by selenomethionine single wavelength anomalous diffraction method (SAD) using the program HKL2MAP (Pape and Schneider, 2004). The final structure was refined against a 1.97 Å resolution data to a crystallographic $R_{work}$ = 20.1% and $R_{free}$ = 24.2% (Table A1.1).

The crystal structure of the Sac domain of yeast Sac1p represents the first atomic structure of the approximate 500-residue Sac domain family. Figure A1.2 displays the ribbon diagram of the Sac phosphatase domain of yeast Sac1p. The overall structure has a dimension of about 65 x 35 x 70 Å, which can be divided into two domains, an N-terminal domain (residue 1-182 shown in blue and referred as the SacN domain thereafter) and a roughly 320-residue C-terminal catalytic domain (shown in yellow), which contains the $CX_5R(T/S)$ catalytic motif. It is also worth noting that in the Sac1 structure, there is a peptide stretch of about 40 residues at the COOH-terminus lacking any electron density, suggesting a flexible nature of this region.

### The SacN domain of Sac1 has a unique fold

The SacN domain is comprised of three layers of β sheets and one long and three short α helices. The first layer of β sheet contains anti-parallel β1 to β5. The second layer consists of β6 and half of the long and twisted β7 to β8. The first and second β sheet layers stack on each other

| A. Data collection and phasing | | |
|---|---|---|
| Space group | I222 | |
| Cell dimensions | a = 86.2 Å, b = 94.7 Å, c = 155.4 Å, $\alpha = 90^0$, $\beta = 90^0$, $\gamma = 90^0$ | |
| | Se SAD phasing data | Refinement data |
| Wavelength (Å) | 0.9788 | 0.9789 |
| Resolution (Å) | 50-2.20 (2.28-2.20) | 50-1.97 (2.04-1.97) |
| Observed reflections | 469,908 | 649,170 |
| Unique reflections | 32,111 | 45,940 |
| Completeness (%)[a] | 100 (100) | 99.7 (100) |
| <I>/< >[a] | 14.5 | 15.3 |
| $R_{sym}$[a,b] | 0.068(0.371) | 0.065(0.729) |
| Se-SAD FOM | 0.184 | |
| Se-SAD FOMDM | 0.30 | |
| B. Refinement | | |
| Resolution (Å)[a] | 33-1.97(2.00-1.97) | |
| $R_{crys}$ / $R_{free}$ (%)[a,c] | 20.1/24.2 (25.5/25.9) | |
| Rms bond length (Å) | 0.01 | |
| Rms bond angles (°) | 1.2 | |
| Ramachandran plot | | |
| Most favored/Additional (%) | 94/6 | |
| Generous/Disallowed (%) | 0.0/0.0 | |

[a]Values in parenthesis are for the highest resolution shell.
[b]$R_{sym} = \sum_h \sum_i |I_I(h) - \langle I(h)|/ \sum_h \sum_i I_I(h)$.
[c]$R_{crys} = (||F_{obs}|-k|F_{cal}||)/ |F_{obs}|$. $R_{free}$ was calculated for 5% of reflections randomly excluded from the refinement.

**Table A1.1 Data collection, phasing and structural refinement statistics**

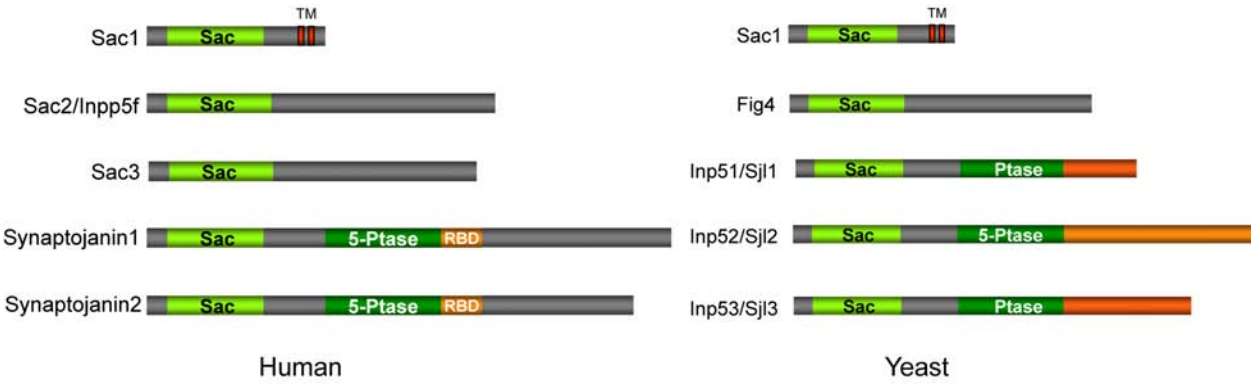


**Figure A1.1. Domain Structures of members of the Sac phosphoinositide phosphatase family.** Both in human and yeast, there are five proteins contain the Sac phosphatase module. (TM: transmembrane motif; RBD: RNA binding domain)

through extensive hydrophobic interactions. The third layer contains the other half of β7 and β8 and a short strand β9. This layer directly contacts with the catalytic domain. The α1 helix and its preceding loop between β8 and β9 are partially aligned with the region that was previously predicted to have a leucine zipper motif in mammalian Sac1 (Blagoveshchenskaya and Mayinger, 2009). The SacN domain of Sac1 has a novel fold and structural homology search by DALI server (Holm and Sander, 1995) did not reveal any significant hits. The SacN domain is closely opposed to the catalytic domain, occluding a surface area of about 1300 $Å^2$ on each domain. The function of the SacN domain is still unknown. A likely role of this domain is to control the enzymatic function through the interactions with other unknown factors.

**The Catalytic Domain of Sac1**

The catalytic domain of Sac1 consists of a nine-stranded and partially split β sheet that is flanked by five alpha helixes with two on one side, and three on the other. The β sheet starts with four long anti-parallel strands (β10 to β13) and then splits with three short parallel strands (β14, β15, and β18) in one branch and two anti-parallel strands (β16 and β17) in the other (Figure A1.2C). The P-loop (shown in red in Figure A1.2A, A1.2B), which contains the catalytic $CX_5R(T/S)$ motif (residue 392-399), extends from the end of β18, across the entire connecting loop, to the first turn of α8.

Interestingly, the P loop is surrounded by five flexible loops (labeled from L1 to L5 and colored in green in Figure A1.2A, A1.2B, and Figure A1.3). Three longer loops (L1, L2, and L5), side chains of which are partially invisible in our crystal structure, protrude out from the catalytic surface and form part of the edge of a large groove (see below). Although the primary sequences in these loop region are not as conserved as other regions across Sac domain family members,

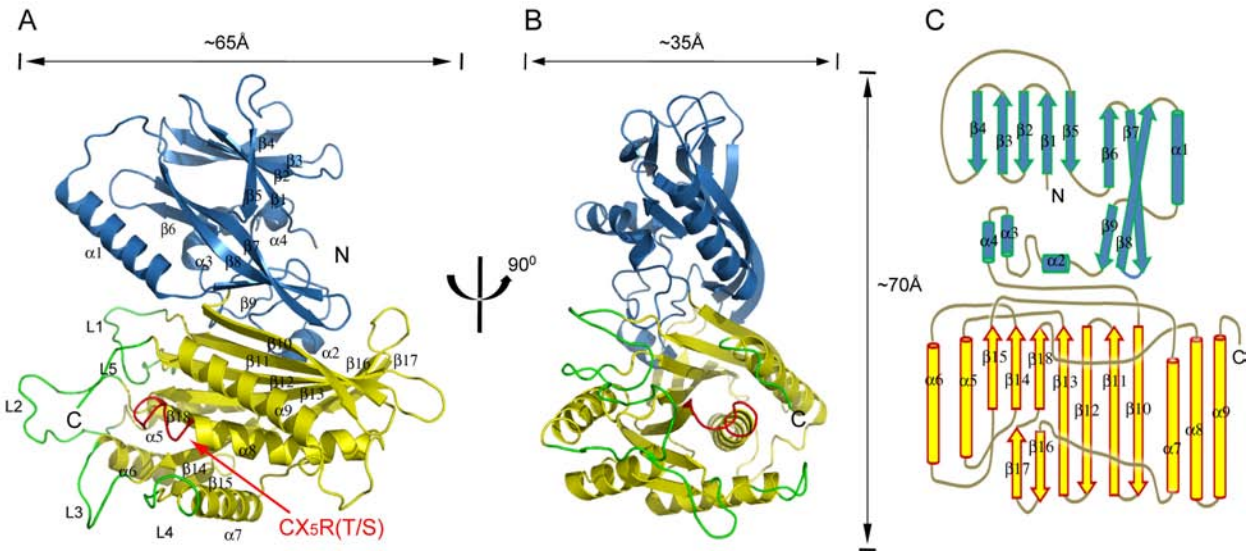


**Figure A1.2. Overall crystal structure of Sac1.**

(A) Ribbon diagram of the Sac phosphoinositide phosphatase. The SacN domain is colored blue and the catalytic domain yellow. The secondary structure elements (strand β1-β18 and helices α1-α9) are labeled. The catalytic $CX_5R(T/S)$ motif (P-loop) is colored red and labeled. Five protruding loops (L1 to L5) surrounding the catalytic site are colored green.

(B) a $90^0$ rotated view of (A).

(C) Schematic diagram of the secondary structure topologies of Sac1.

these loops are enriched with positively charged and hydrophobic residues (Figure A1.3), the physicochemical nature of which is ideal to support interfacial membrane binding (Cho and Stahelin, 2005). These structural properties suggest that the catalytic site may be protected by the surrounding loops and upon activation, the surrounding loops, particularly the three long protruding loops, may directly interact with or insert into the lipid bilayer.

**Structure comparison of Sac1 with other phosphatases**

Comparison of the structure of the catalytic domain of Sac1 with other $CX_5R(T/S)$-based phosphatases reveals that the topology of the catalytic core of Sac1 is conserved with other PTPs, including two lipid phosphatases MTMR2 and PTEN. They all share a common architecture of a central β sheet consisting of four parallel β strands flanked by antiparallel ones. This sheet is sandwiched by a variable number of α helices on each side (Barford et al., 1994; Stuckey et al., 1994). We further searched the Protein Data Bank for structural similarities to the catalytic domain of Sac1 using the Dali server (Holm and Sander, 1995). The structure found to have the highest Z-score (7.4) is human PRL-1 (PDB ID: 1XM2) (Jeong et al., 2005). The overall structure of the two catalytic domains can be superimposed on that of PRL-1 with a rmsd of 3.5 Å over 128 Cα residues (Figure A1.4A). Despite the limited similarity of the catalytic core topology, the catalytic domain of Sac1 is unique with its large and split central β sheet compared to other PTPs, including the low molecular weight phosphotyrosyl phosphatase and canonical PTP1B (Figure A1.4A and A1.4B, and Figure A1.2C). Furthermore, structural comparison with the dual specific phosphatase, PTEN, reveals the difference of the interactions between the catalytic domain and other regulatory domains. When the catalytic domain of Sac1 is superimposed with

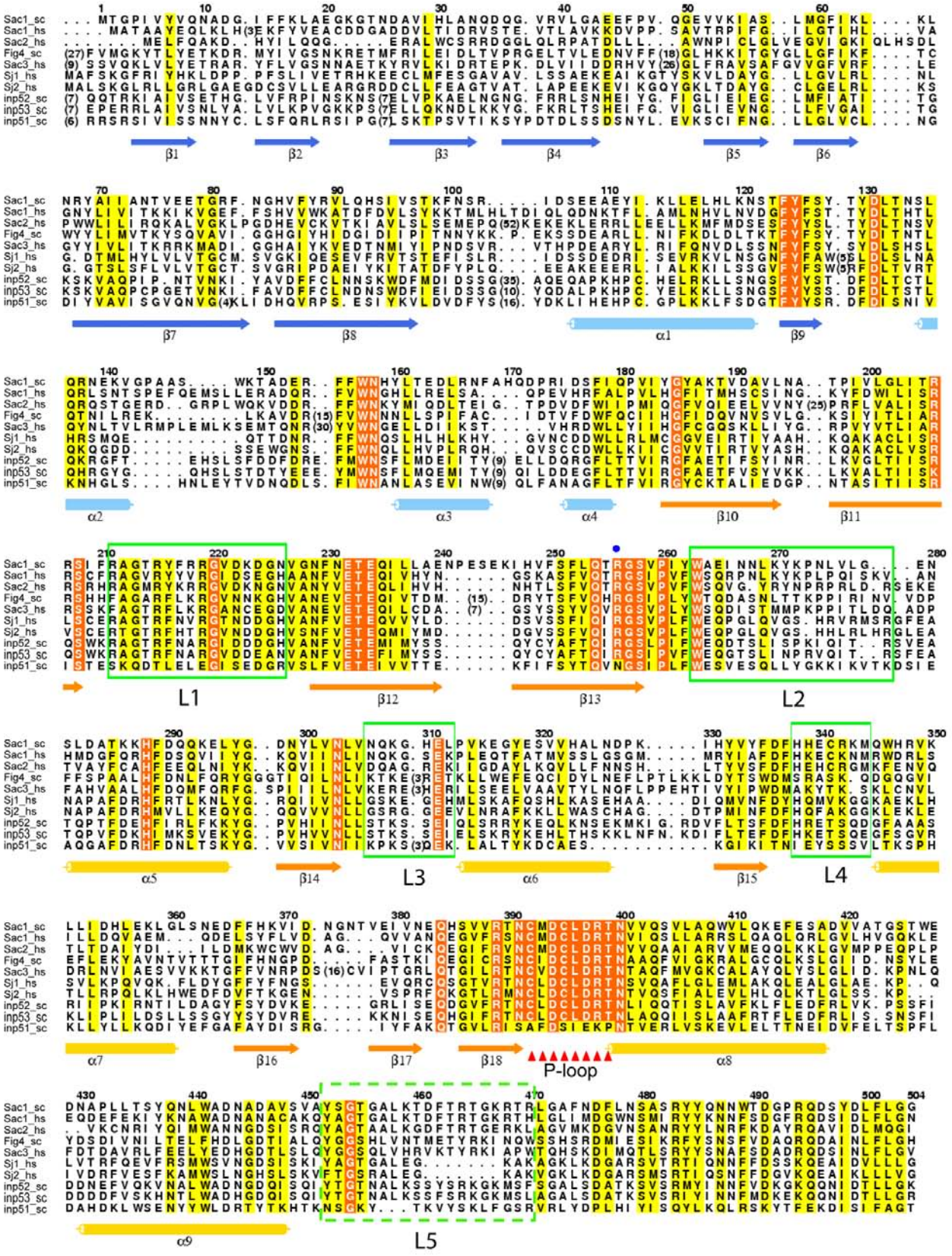
Sac1_sc
Sac1_hs
Sac2_hs
Fig4_sc
Sac3_hs
Sj1_hs
Sj2_hs
inp52_sc
inp53_sc
inp51_sc
β1
β2
β3
β4
β5
β6
β7
β8
α1
β9
α2
α3
α4
β10
β11
L1
β12
β13
L2
α5
β14
L3
α6
β15
L4
α7
β16
β17
β18
P-loop
α8
α9
L5

**Figure A1.3. Sequence alignment of the Sac domain region of all Sac phosphatases in human and yeast.**

The sequences corresponding to the Sac domain region were aligned by ClustalW 2 (Labarga et al., 2007) and colored by ALSCRIPT (Barton, 1993). The conserved residues are shaded yellow and identical residues are shaded red. Secondary elements are drawn under the alignment. The catalytic site is marked by triangles. Regions that correspond to the five protruding loops (colored green in Figure A1.3A and B) are indicated with green boxes. Entrez database accession numbers are as follow: Sac1_sc: gi: 486379; Inp51_sc, gi: 6322189; Fig4_sc, gi: 6324005; Inp52_sc, gi: 6324224; Inp53_sc, gi: 6324683; Sac3_hs, gi: 7662034; Sac2_hs, gi: 7662414; Sac1_hs, gi: 190014578; Sj1_hs, gi: 223460134; Sj2_hs, gi: 26190608;

A

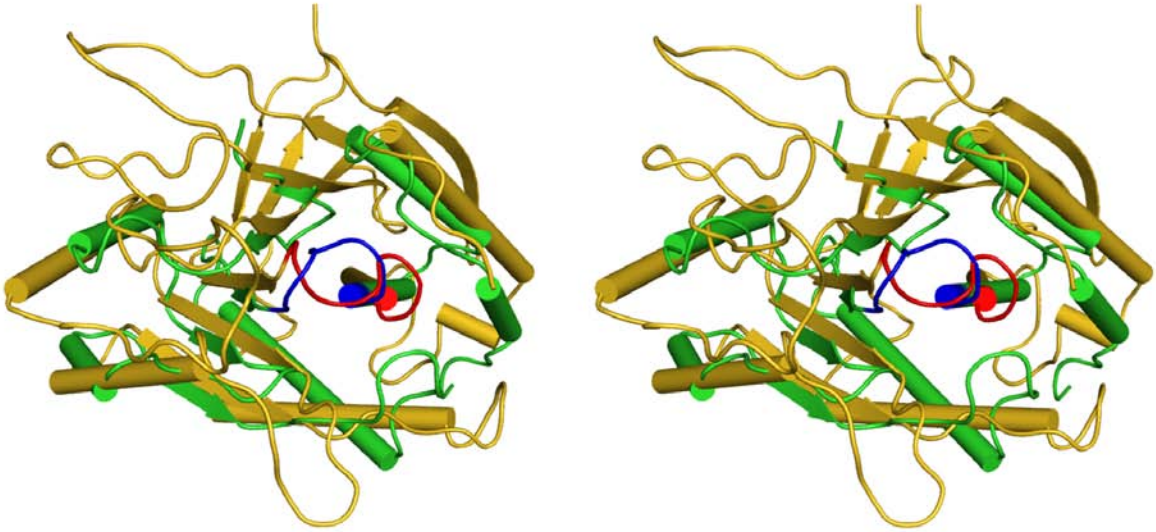

B

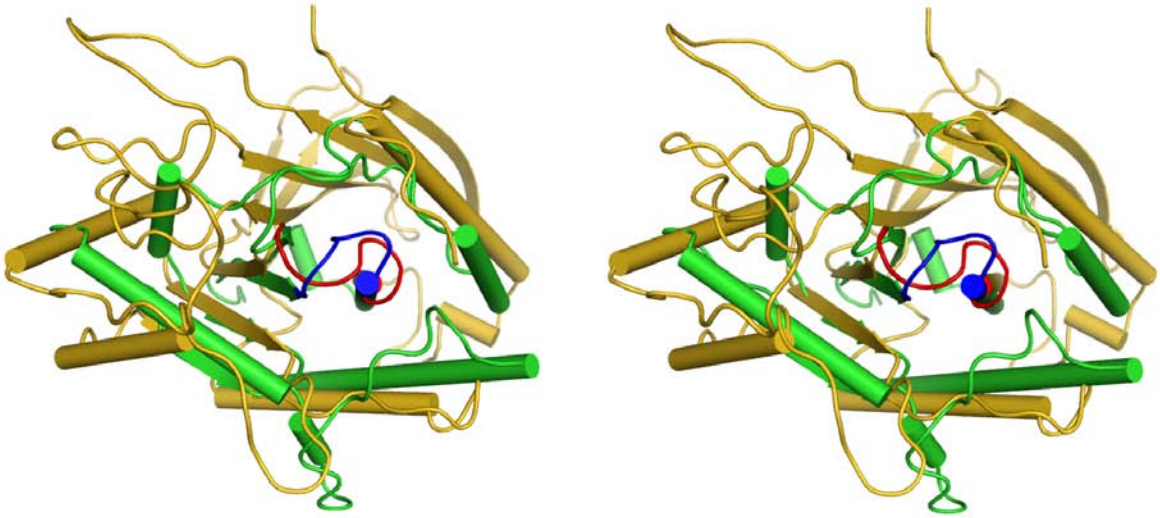

**Figure A1.4. Superimposition of the Sac1 phosphatase domain with human PRL-1 phosphatase and HPTP-B.**

(A) Stereo view of the two overlayed structures of the catalytic domain of Sac1 (yellow) and human PRL-1 (green, PDB ID: 1xm2).

(B) Stereo view of the structural superimposition of Sac1 (yellow) and HPTP-B, a human B-form low molecular weight PTP (green, PDB ID: 1XWW). The catalytic P-loops are colored in red for Sac1 and blue for both PRL-1 and HPTP-B.

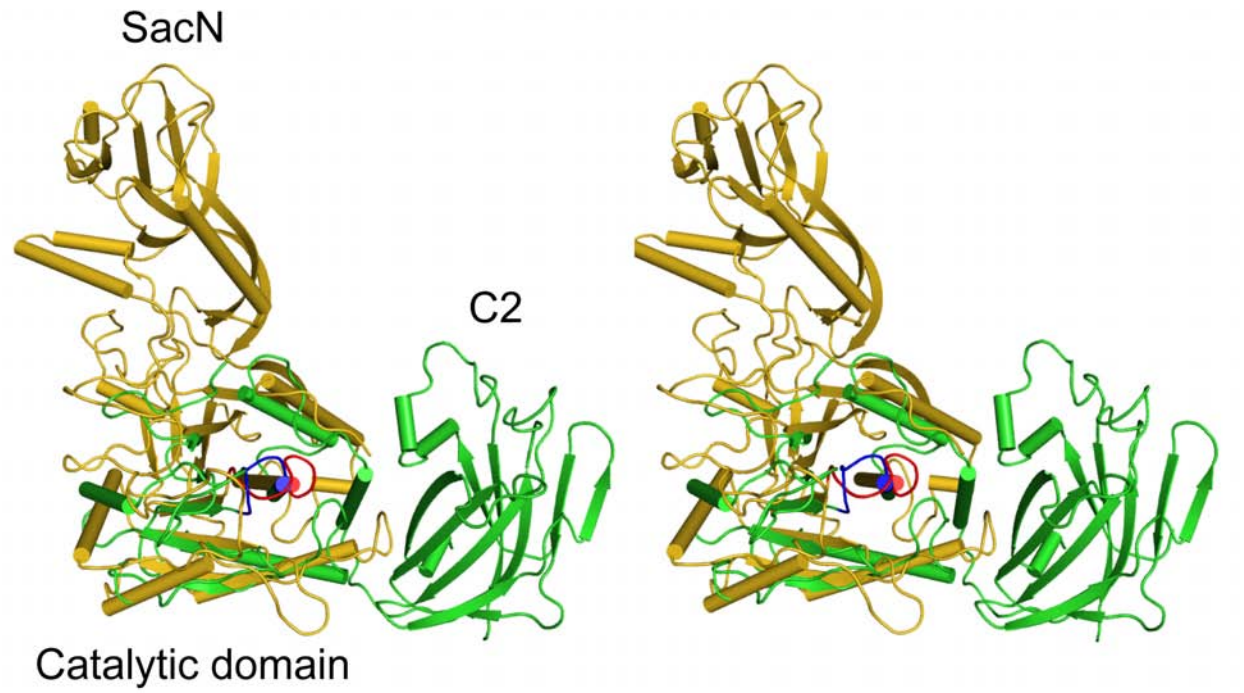


**Figure A1.5. Structural comparison of Sac1 with PTEN.**

Sac1 is colored in yellow and PTEN is in green. These two structures are superimposed based in structural homology on the catalytic domain. The catalytic P-loops of Sac1 and PTEN are colored in red and blue, respectively. Note that the SacN domain of Sac1 is located on the opposite side of the central β sheet compared to the C2 domain of PTEN

that of PTEN (Lee et al., 1999), the SacN domain of Sac1 ends up on the opposite side of the central β sheet in contrast to the C2 domain in PTEN (Figure A1.5).

Another major difference is the unique conformation of the catalytic P-loop of the Sac phosphatase (Figure A1.6A). Among all PTPs, the P-loops in PTPs are strictly superimposable, and a consecutive seven main-chain amide groups in this loop all face inward for the binding of a phosphate group of the substrate (Barford et al., 1998). The conformation of the P-loop is fairly stable, as evidenced by the fact that Cα tracing superimposition of P-loops from different PTPs (in the presence or absence of binding ligands) yields a minor standard deviation of less than 1 Å (Tabernero et al., 2008). However, this conserved P-loop configuration is disrupted in Sac1. Moreover, within the $CX_5R(T/S)$ motif, the distance between the γ-thiol group of C392 and the guanidinium group of R398 is 14 Å apart in Sac1, while the corresponding distance is only about 5 Å in other PTPs, including MTMR2 and PTEN (Figure A1.6B and A1.6C). Conformational deviation of the P-loop, resulting from the exposure of the enzyme to oxidants has been reported (Salmeen et al., 2003; van Montfort et al., 2003; Yang et al., 2007). In PTP1B, formation of cyclic sulphenamide of the catalytic cysteine causes a significant change in conformation. However, oxidation is not likely the cause of the conformational variation in Sac1 since high amount of reducing reagent, DTT is present in Sac1 protein stock and crystallization solutions. Furthermore, the electron density map around the P-loop does not reveal any extra density supporting the presence of oxidized forms of the thiol group of the catalytic C392 (Figure A1.7). Structural comparison of the catalytic domain of Sac1 with reduced [PDB ID: 1AAX; (Puius et al., 1997)] and oxidized [in the cyclic sulphenamide state; PDB ID: 1OEM; (Salmeen et al., 2003)] forms of PTP1B reveals that the P-loop conformation of Sac1 is strikingly different from that of either form of PTP1B (Figure A1.8A and A1.8B). Particularly, the catalytic C392 and the

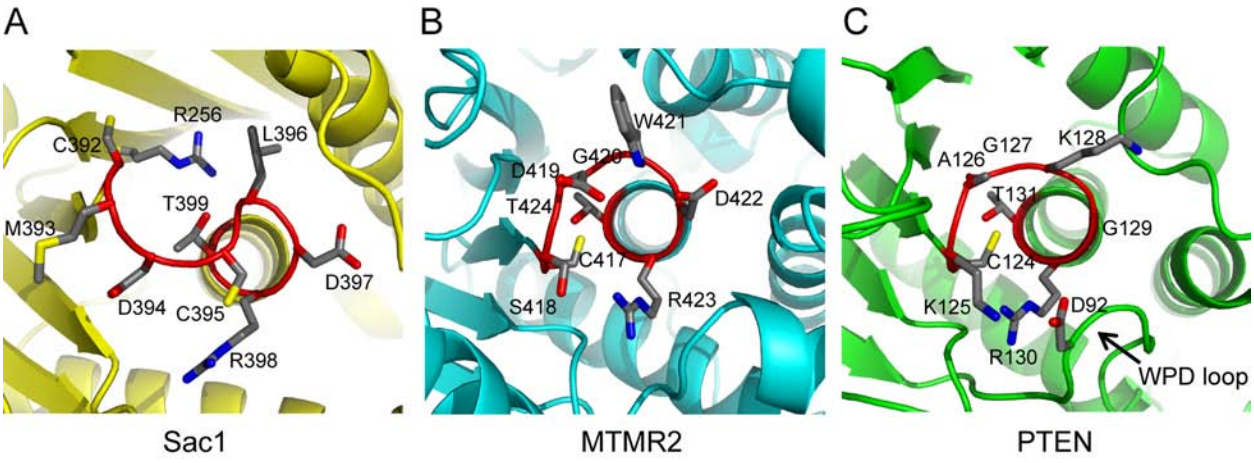


**Figure A1.6. Structural comparison of the catalytic site P-loop between Sac1, MTMR2, and PTEN.**

(A) The P-loop configuration in Sac1. This loop, which comprises the $CX_5R(T/S)$ motif, is colored in red and residues in this loop are shown as sticks. This figure is generated in the same orientation as in Figure A1.3B.

(B) The P-loop of MTMR2, and PTEN (C). The WPD loop in PTEN is indicated by an arrow.

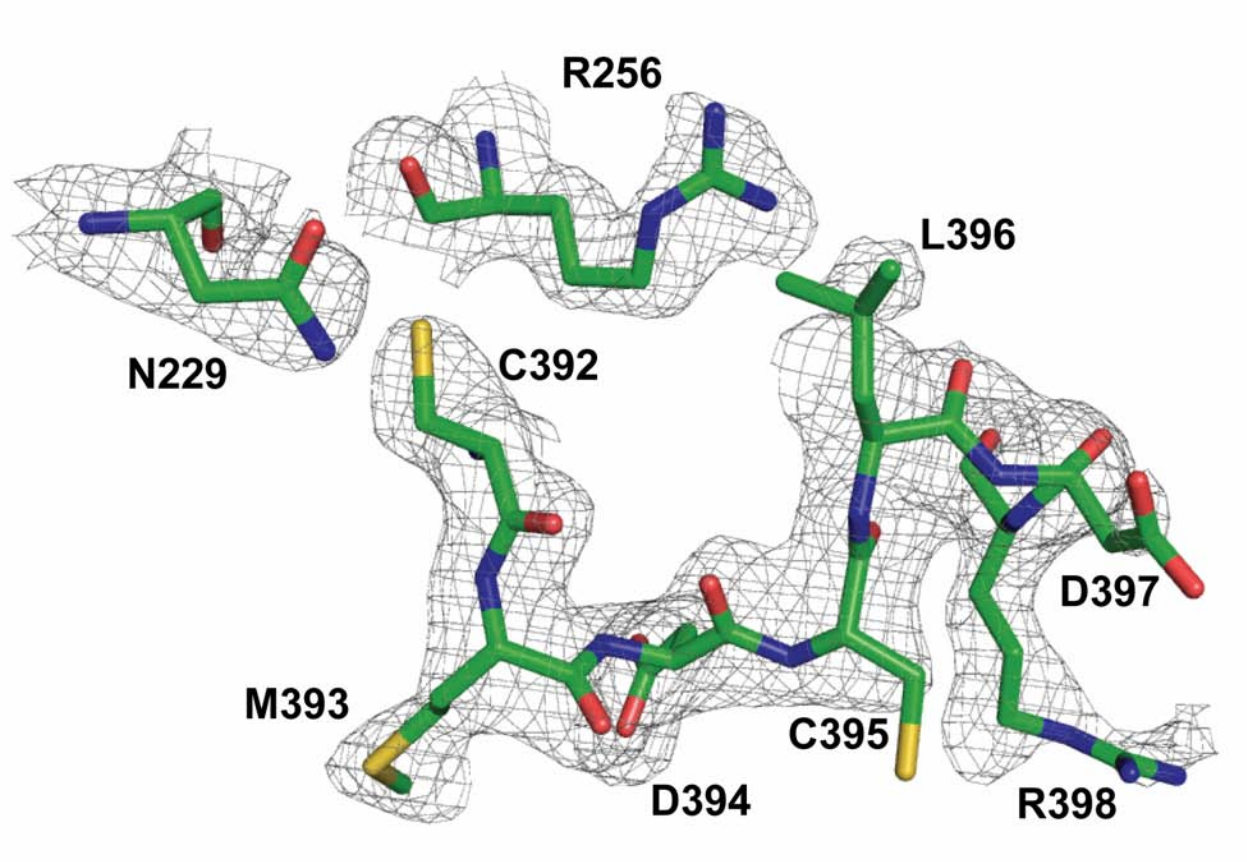


**Figure A1.7. Electron density map (2fo-fc) of the P-loop and residues in close vicinity with the catalytic C392.**

The map is contoured at 1σlevel. The electron density for the thiol group of the catalytic residue, C392 is well defined.

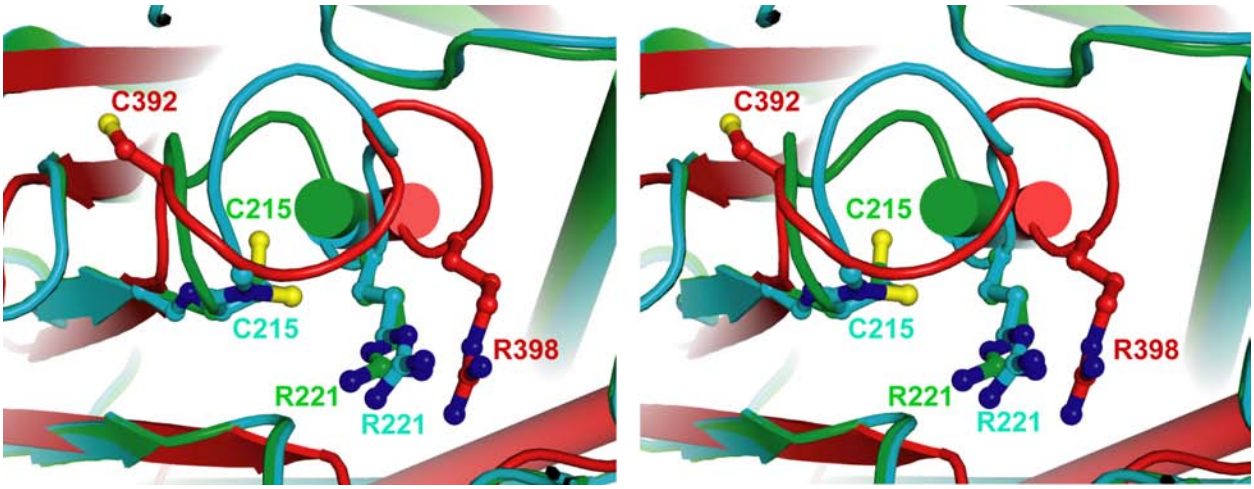


**Figure A1.8. Structural comparison of Sac1 with canonical PTP1Bs at both reduced and oxidized state.**

Stereo view of the superimposition of the catalytic region of Sac1 (red) with reduced form of PTP1B (green, PDB ID: 1AAX) and oxidized (cyclic sulphenamide state) PTP-1B (cyan, PDB ID: 1OEM). Note that the conformation of the catalytic P-loop of Sac1 is strikingly different from that of both reduced and oxidized forms of PTP1B. The side chains of the catalytic C392 and the conserved R398 residues in Sac1 are located on the opposite side of the P-loop; while in both reduced and oxidized PTP1Bs, these two residues are on the same side relative to the P-loop.

conserved R398 residues in Sac1 are located on the opposite side of the P-loop; while in both reduced and oxidized PTP1Bs, these two residues are on the same side. Thus this unique P-loop conformation of Sac1 may implicate an unusual mechanism for its catalytic function.

**Surface characteristics of Sac1**

Interestingly, the Sac domain is an electrostatically bipolar protein with one surface negatively charged (Figure A1.9A) and the opposite surface enriched with positive charges (Figure A1.9B). The bipolar charge distribution has been observed in other membrane interacting protein modules, such as PH domains (DiNitto and Lambright, 2006; Ferguson et al., 1994; Ferguson et al., 1995). The positively charged face of the Sac domain is likely to interface with the lipid bilayer which is concentrated with negatively charged phospholipids. In agreement with this notion, the catalytic $CX_5R(T/S)$ motif is localized on this positively charged surface.

The other striking surface feature of the Sac domain is the presence of a deep canyon-like groove on the positively charged surface (Figure A1.9B and A1.9C). This groove is formed by both the SacN domain and the catalytic domain and travels a distance about 40 Å long at an average depth of more than 10 Å. There is a highly conserved positively charged residue, R256 (labeled in Figure A1.9B and marked by a blue dot in Figure A1.3) aligned at the bottom of the groove. This arginine residue, together with some other positively charged residues, contributes to the electrostatic surface potential property in the groove.

**Mutagenesis of catalytic site residues**

Previous studies have revealed several interesting Sac1 mutant alleles. The catalytic cysteine to serine mutation (C392S) has been shown to be catalytically dead and fails to

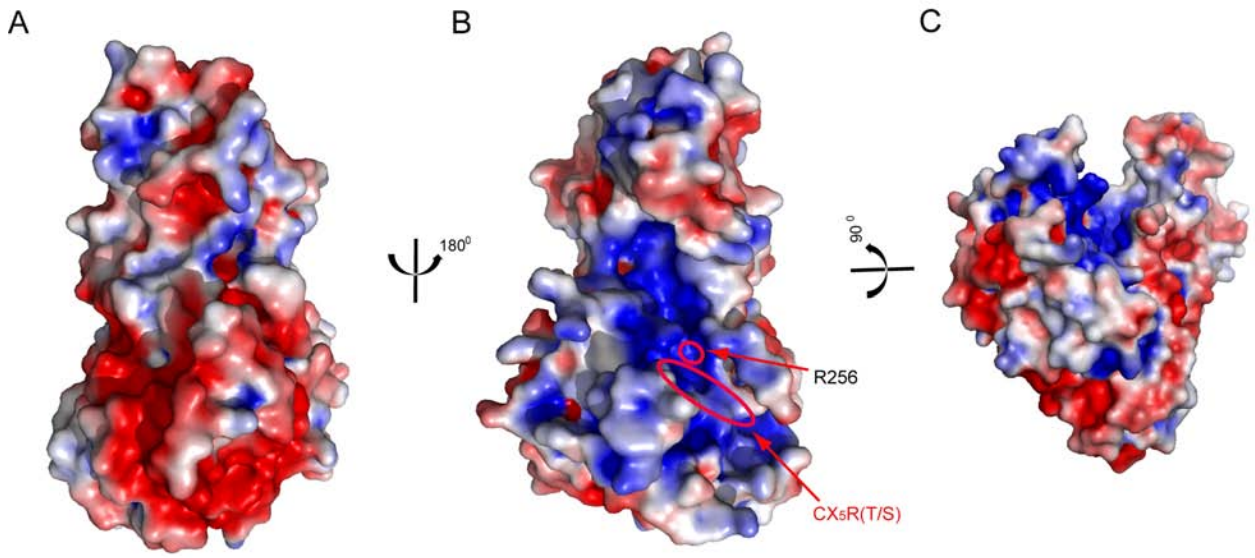


**Figure A1.9. Surface representative of Sac1 phosphatase.**

The surfaces were colored based on electrostatic potential with positively charged regions in blue (+3 kcal/electron) and negatively charged surface in red (-3 kcal/electron).

(A) is rotated $180^0$ about the perpendicular axis relative to (B).

(B) has the same orientation as in Figure A1.2B. The position of R256 is pinpointed by a red circle. (C) is rotated about ~$90^0$ around the horizontal axis of (B) and then slightly tilted left for a view of the deep cleft. The catalytic $CX_5R(T/S)$ motif is highlighted with an oval shape. Note that the catalytic site is located at the bottom of the positively charged groove.

complement the *sac1Δ* phenotype in yeast (Rohde et al., 2003). The yeast D394N and A445V mutants (the product of the *sac1-8* and *sac1-10* alleles, respectively) have been shown to confer phenotypes consistent with the loss of phosphatase activity as reported previously (Kearns et al., 1997; Liu et al., 2008; Nemoto et al., 2000). The L304P mutation has some puzzling effects in that it has normal *in vivo* functions when the cells were grown on YPD medium, but displayed *sac1* mutant phenotypes including elevated PI(4)P levels when grown on synthetic minimal medium (Hughes et al., 2000b). Interestingly, all these mutations are either located within or adjacent to the P-loop as revealed by the Sac1 structure (Figure A1.10A). The carboxyl group of D394 is 2.10 Å away from the amide group of L304 and forms a hydrogen bond with the main chain amide proton of L304. This hydrogen bond would then be disrupted in the L304P mutant due to the lack of an amide proton in the proline residue, and thus may cause conformational changes of the P-loop that may affect the catalytic activity in the end.

In order to gain insight into the role of other conserved residues near the catalytic site, we generated several GFP-tagged Sac1 mutants in the vicinity of the catalytic site and introduced them into *sac1Δ* yeast cells. *Sac1Δ* yeast cells are viable when grown at permissive temperature, but with elevated PI(4)P level (6-8 fold greater than wild type cells) and fail to grow at 15 $^{0}$C (Foti et al., 2001). These defects can be rescued by the re-introduction of functional Sac1. Based on these observations, the ability of our mutants to rescue the growth defects of *sac1Δ* cells at 15 $^{0}$C and the intracellular PI levels were analyzed by HPLC (Figure A1.10B and A1.10C). Immunoblotting experiments showed that GFP-tagged wild-type and mutant forms of Sac1 were expressed as stable proteins at a roughly similar level (Figure A1.10D). R256 in Sac1 is conserved among the Sac family members except for the catalytically inactive yeast sjl1 (Figure

A1.3). This conserved arginine contributes significantly to the positive electrostatic potentials at the catalytic

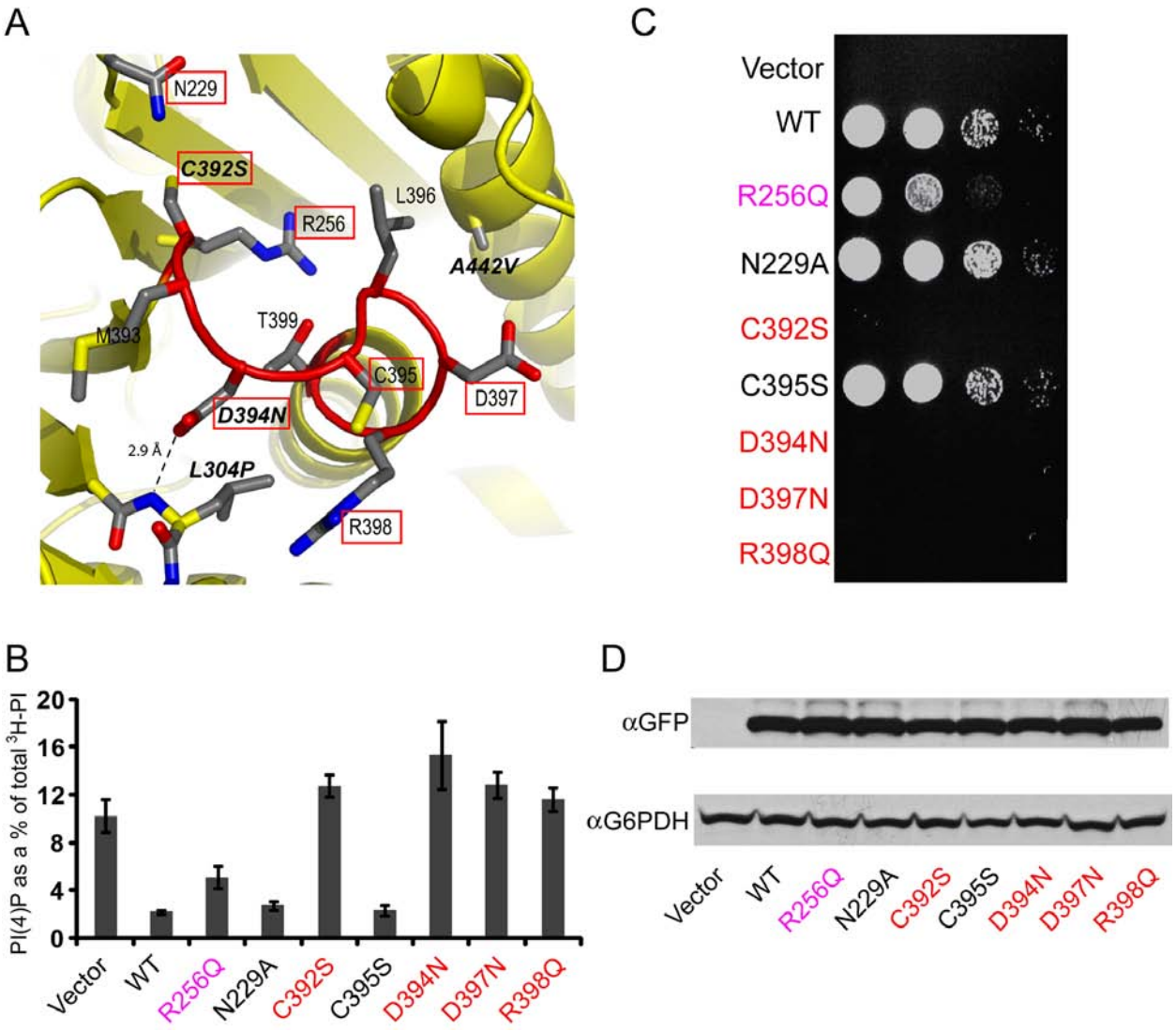

**Figure A1.10. In vivo characterization of Sac1 mutants.**

(A) A close view of the catalytic P-loop of Sac1. Reported Sac1 mutant alleles are labeled in italic. Residues tested in this study are highlighted with red squares.

(B) Quantitative analysis of PI(4)P is shown from *sac1Δ* cells transformed with empty vector control, N-term GFP tagged WT Sac1, and Sac1 mutants. The error bars represent ± SEM of three independent experiments.

(C) *In vivo* growth rescue assay of *sac1* cold sensitivity. *Sac1Δ* cells were transformed with indicated Sac1 constructs or vector control. The cells were spotted onto plates with three serial of dilutions from left to right, and grown at restrictive temperature at 15 °C for 6 days.

(D) Western blots of samples prepared from the transformed cell show that the exogenously introduced Sac1 wild type or mutants are expressed as stable proteins and at a comparable level (G6PDH is shown as a loading control).

site. In *sac1Δ* cells transformed with the R256Q mutant, the $^{3}H$ incorporated PI(4)P represents ~5% of total newly synthesized PI, which is nearly double that of cells transformed with wild type Sac1 (Figure A1.10B). In agreement with this result, the R256Q mutant can only partially rescue the growth defect of *sac1Δ* cell at 15 $^{0}C$ (Figure A1.10C). We also tested several P-loop residues. As reported previously, the catalytically dead C392S or D394N mutants completely fail to rescue the growth phenotype and the PI(4)P level is about 6-8 fold greater than that of *sac1Δ* cells transformed with wild type Sac1. Similar to MTMR2, the Sac domain does not have the conserved aspartic acid residue (D92 in PTEN, Figure A1.9C) on its corresponding WPD loop. It has been suggested that in MTMR2, D422 within the P-loop may serve as the general acid and base during catalysis (Begley et al., 2003). This aspartic acid residue (D397 in yeast Sac1) is also conserved in Sac family phosphatases (Figure A1.3) and the D397N mutation has similar phenotypes as catalytically dead mutants. The only conserved basic residue within the catalytic P-loop, R398, seems also critical for the phosphatase function, as the R398Q mutant also has similar effects as catalytic dead mutants. Residues N229 is conserved among Sac phosphatases and is in the vicinity to the catalytic cysteine (C392), however, N229A has no apparent effect on the *in vivo* function of Sac1. Mutation of another conserved P-loop reside C395S also behaves like wild type Sac1 (Figure A1.10B and A1.10C).

Collectively, these observations suggest that selective substitutions of some anionic residues near the catalytic site impair the normal function of Sac1, which may be due to direct impact on phospholipid binding. Both of the aspartic residues at the catalytic site are critical for the catalytic function by either serving as the general acid or maintaining proper P-loop conformation.

**Missense disease mutations in human Sac3/Fig4**

Several missense mutations of the human Sac3 are responsible for the genetic neurological disorders CMT4J and ALS. To understand how these single amino acid substitutions can affect the function of the protein, we computationally modeled the structure of the Sac phosphatase domain of human Sac3 based on the crystal structure of Sac1 (Figure A1.11). We then mapped five known missense mutations to the modeled structure of the Sac domain of Sac3. The I41T is a recessive mutation found in patients with CMT4J. This residue localizes at the C-terminal end of β3 in the SacN domain and is about 40 Å away from the catalytic site. The hydrophobic side chain of this isoleucine is buried in a hydrophobic core between the first two layers of β sheets in the SacN domain. Thus, the I41T substitution may not directly affect the catalytic activity of the Sac3, but likely may affect the local folding or the stability of the protein. In agreement with this prediction, yeast Fig4 carrying with a corresponding I59T mutation was able to produce normal levels of $PI(3,5)P_2$ and corrected the vacuolar enlargement phenotype when this mutant was expressed in *fig4Δ* cells (Chow et al., 2007). Two other mutations, D48G and D53Y, which have been predicted to be responsible for a subset of ALS disease, are located at two ends of the β4 strand (Figure A1.11 inset). These two mutations are likely to affect protein folding or stability since both of these residues are surface exposed and located in flexible loop regions. Interestingly, these two residues, together with I41, are clustered in a surface area on the top of the SacN domain. This finding indicates that the SacN domain may be involved in protein-protein interaction through a surface area on the first layer of the β sheet. Human disease mutations in Sac3 may displace the binding with other proteins, which may cause defective regulation on its enzymatic activity. The last two mutations, R388G and I411V, are located in the catalytic domain. The R388G is in the close vicinity of the catalytic P loop, thus it may have a

direct impact on its enzymatic function. The I441V is away from the catalytic P-loop and on the opposite side of the catalytic domain. Although I441 forms part of a hydrophobic core, substitution by a hydrophobic valine residue at this position may not be deleterious. Consistent with this prediction, the I441V variant has an activity close to the wild-type (Chow et al., 2009).

## Discussion

The structure of the Sac domain of yeast Sac1, the first atomic structure of the Sac family phosphoinositide phosphatase, reveals that the previous predicted Sac domain contains two modules, the SacN and the catalytic sub-domains. Sequence and structure homology analysis suggests that the SacN domain has a unique sequence and a novel structural fold, both of which are only conserved in the Sac phosphatase family. Interestingly, several disease-related mutations found in Sac3/Fig4 form a cluster on the SacN domain, indicating that the SacN domain may mediate the interactions with other unknown factors. Recent results also show that mammalian Sac1 orthologs contain a leucine zipper motif within the SacN domain region and that this motif is required for Sac1 oligomerization. The predicted leucine zipper region is not conserved in yeast Sac1. However, this region partially overlaps with the α1 helix in the SacN domain (Figure A1.3). It has been further shown that the leucine zipper-dependent oligomerization of Sac1 is required for its shuttling to the Golgi complex (Blagoveshchenskaya et al., 2008; Blagoveshchenskaya and Mayinger, 2009). These results suggest that the regulatory function of the SacN domain might also be mediated by Sac1 oligomerization and translocation.

The $CX_5R(T/S)$ catalytic motif of Sac1 is located between the C-terminus of a β-strand and the first turn of an α-helix. Despite the sequence variability of the $X_5$ segment, the conformation of the P loop is strictly superimposable among different PTPs. Strikingly, seven

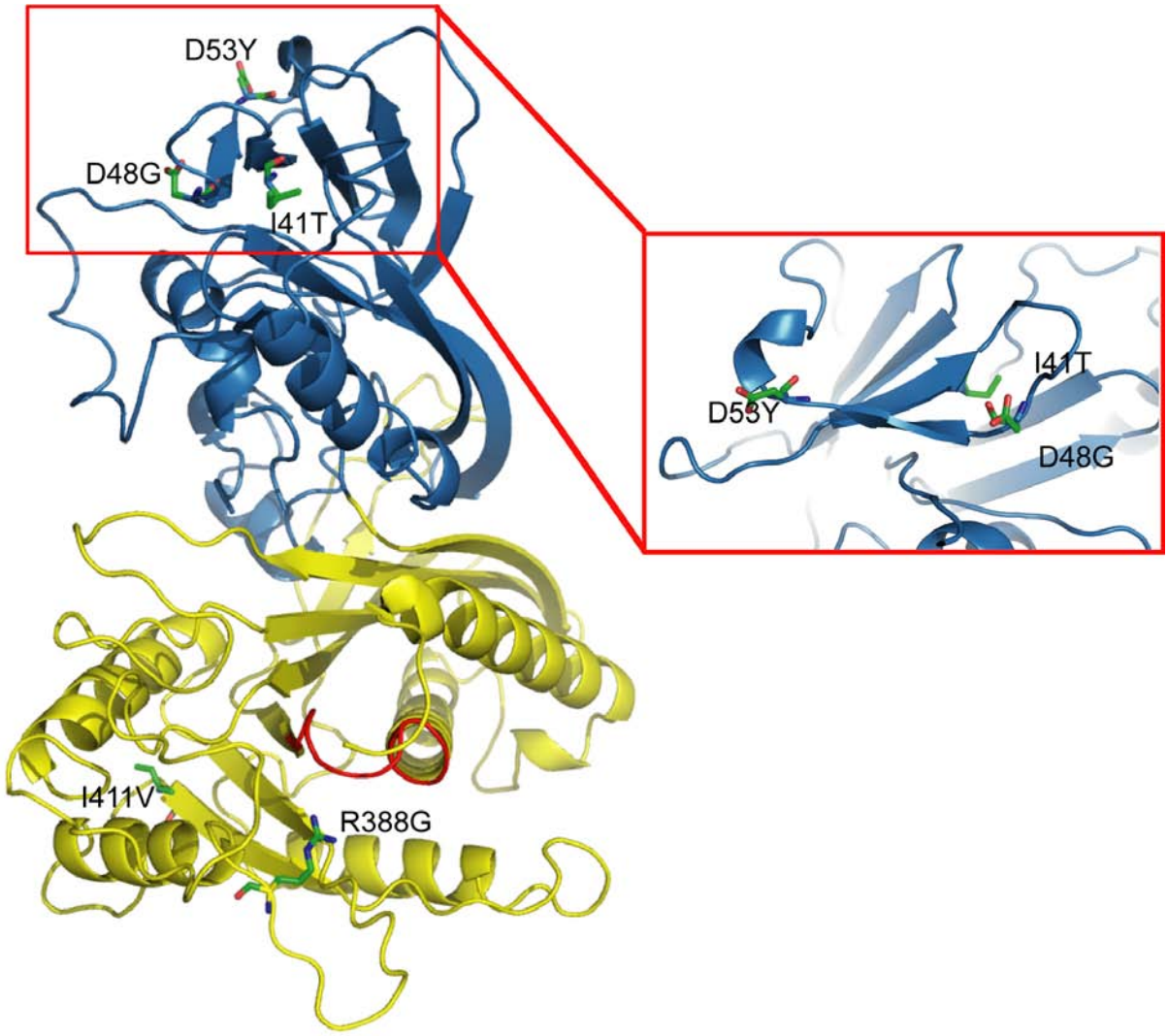


**Figure A1.11. Homology structural modeling and missense disease mutations in human Sac3.** The modeled Sac domain of Sac3 has a similar two domain structure: the SacN domain (blue) and the catalytic domain (yellow). The catalytic P-loop is colored red. Genetic mutations that have been implicated in CMT4J or ALS are labeled and illustrated with sticks. The inset is a zoomed view of a region with a clustering of three mutations in the SacN domain.

successive main-chain amide groups in this loop all face inward, together with the guanidinium group of the $CX_5R(T/S)$ arginine, to coordinate the phosphate group of the substrate in place for nucleophilic attack by the S$\gamma$-atom of the catalytic cysteine (Figure A1.6B and A1.6C). Surprisingly, the conformation of the P-loop of the catalytic domain of Sac1 is different from all known PTP structures. These dissimilarities between Sac and other phosphatases suggest that the Sac domain family phosphatases utilize an unusual mechanism for phosphoinositide dephosphorylation. However, it may also be possible that the structure we crystallized is in an inactive conformation; it requires a conformational change that flips the P-loop into the consensus P-loop confirmation for its full activity. A complex structure of Sac1 with its substrate analogues would resolve this ambiguity. We have intensively tried the co-crystallization of wild type or catalytically dead C392S mutant Sac domain with inositol head groups [Ins(1,4)$P_2$ and Ins(1,3)$P_2$], but without success so far. Further structural studies are warranted for the delineation of the catalytic mechanisms and substrate specificity determinants of Sac phosphatases.

Since the substrates of lipid phosphatases are embedded in membrane bilayers, Sac1 must bind to the membrane-water interface in order to hydrolyze its substrates on membranes. Unlike enzymatic reactions that occur in solution, interfacial enzymatic reactions have their own unique kinetic features. The enzyme first needs to be adsorbed to the lipid interface for activation. Once the enzyme is tightly bound to the membrane surface, it may catalyze the reaction with high processivity in a so called "scooting" mode (Jain et al., 1986). Under the "scooting" model, the enzyme hydrolyzes many phosphoinositide lipids without dissociating from the membrane surface. The crystal structure of Sac1 reveals that the catalytic P-loop is surrounded by five flexible loops. Interestingly, some of these loops are enriched with cationic and hydrophobic

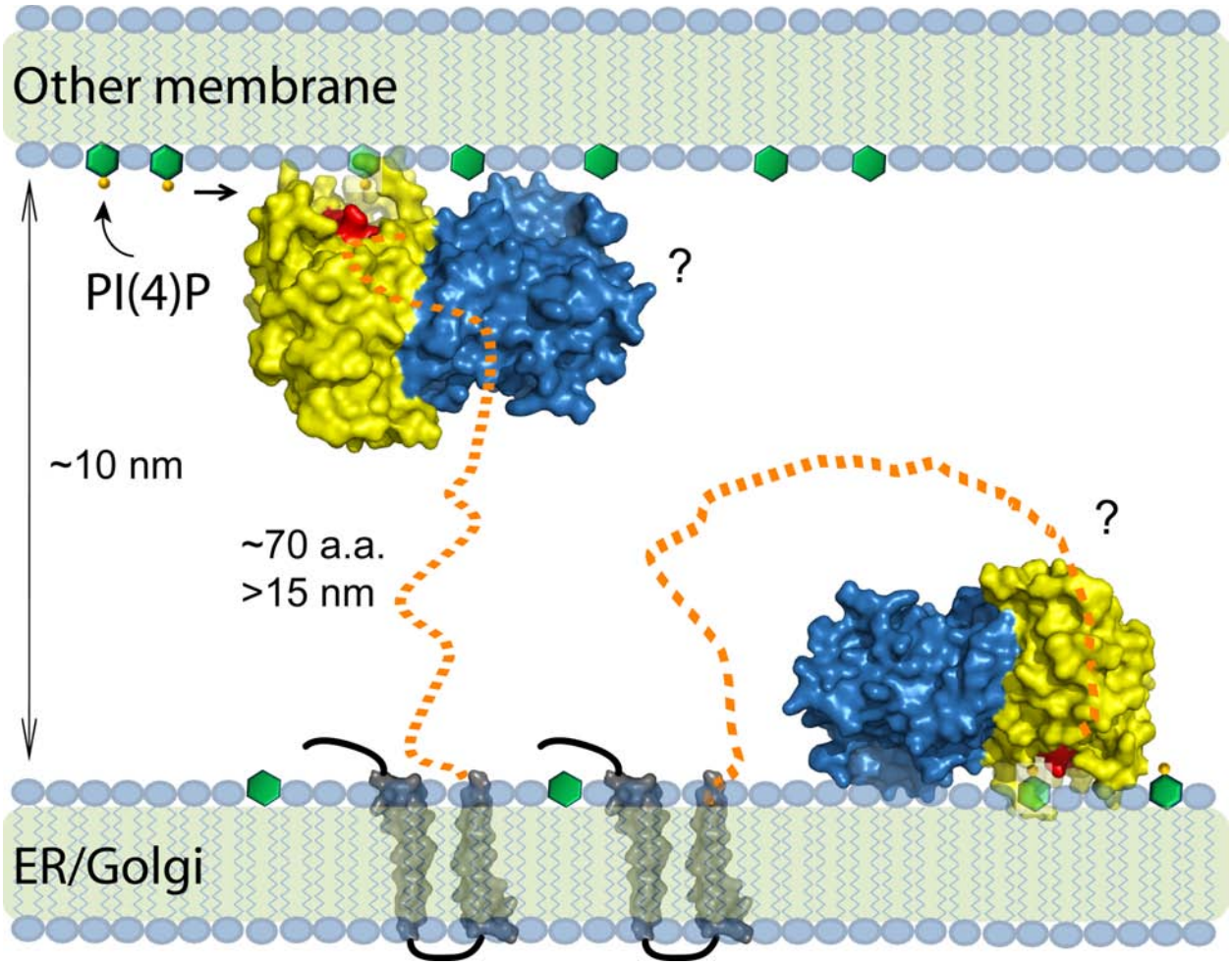


**Figure A1.12. Functional model of Sac1 at the membrane interface.**

The Sac domain of Sac1 is shown by molecular surfaces colored cyan (the SacN sub-domain) and yellow (the catalytic sub-domain). The catalytic site P-loop is colored red. The polarized charge distribution controls the membrane docking of the Sac domain by orienting the catalytic site to its membrane embedded substrates. Several loops surrounding the catalytic site may directly interact or insert into the lipid bilayer and may facilitate the hydrolysis of phosphoinositides processively. The long flexible linker between the catalytic domain and the membrane anchors allows Sac1 to hydrolyze its substrates either in a *trans* or *cis* mode.

residues, the physicochemical nature of which is ideal to support interfacial membrane binding (Cho and Stahelin, 2005; Gelb et al., 1999). The structure further reveals a deep long groove on the catalytic surface of Sac1 (Figure A1.9B and A1.9C). This groove has its ends both open, which makes it possible for the enzyme to load its substrates from one end of the groove to the catalytic site for hydrolysis and to release the products through the other opening of the groove while the Sac domain remains "scooting" on the membrane. Thus Sac1 may function in an efficient processive manner at the membrane-water interface.

Sac1 is a type II membrane protein that localizes to both the ER and Golgi apparatus (Nemoto et al., 2000; Whitters et al., 1993). A question that remains is whether its substrate is localized on the same membrane where Sac1 resides (*cis*) or on a different membrane (*trans*). Studies in yeast have demonstrated that PI(4)P is concentrated on the Golgi and the plasma membrane. Inactivation of Sac1p leads to a specific increase in the cellular level of PI(4)P and the bulk of accumulated PI(4)P is generated by the phosphoinositol-4 kinase Stt4 at the plasma membrane (Foti et al., 2001; Tahirovic et al., 2005). These findings suggest that Sac1 has the ability to hydrolyze its substrate in *trans*. Thus Sac1, and hence the ER, must be in close proximity to the plasma membrane. Indeed, ER membranes in close proximity to the PM (< 100 Å) are often seen in ER images of both yeast and mammalian cells. In the Sac domain structure, there is a peptide stretch of 50 residues (residues 453-503) at the C-terminus lacking any electron density, suggesting a flexible nature of this region. Given an additional nearly 20-residue long spacer (residues 504-522, between the Sac domain and the first transmembrane motif), presumably also adopts a linear unfolded state, the Sac domain could extend far away from the membrane (A completely extended peptide of about 70 residues can reach a distance of 20 nm). This structural feature of Sac1 certainly allows it to overcome the space restriction to act in *trans*

on the pool of PI(4)P generated by Stt4 at the plasma membrane, although we cannot rule out Sac1 may also function in a *cis* mode.

The structural properties of Sac1 lead us to propose a membrane interaction model for this phosphoinositide phosphatase (Figure A1.12). In this model, the cationic surface mediates the membrane association. On this surface, the catalytic P-loop is surrounded by several flexible loops that are enriched with cationic and hydrophobic residues. Once the Sac domain gets adsorbed to membrane bilayer, the deep open groove at the catalytic site would allow Sac1 to hydrolyze phosphoinositides in a processive manner. The long linker region between the catalytic domain and the first transmembrane motif allows the endoplasmic reticulum anchored Sac1 to reach its substrates embedded in the plasma membrane.

In conclusion, the structure of the Sac domain of yeast Sac1 provides the first representative structure of the Sac phosphatase family. The structure reveals a large positively charged groove at the catalytic site and a strikingly different configuration of the catalytic P-loop of the Sac domain. These findings suggest a novel catalytic mechanism for Sac1. The structure also provides a three dimensional framework for the understanding of disease mechanisms of the missense mutations found in human Sac3. Further structural and functional studies of enzyme substrate complexes and of other Sac family members will lead to a full understanding of the structural determinants for substrate recognition and specificity.

## Acknowledgment:

We thank Dr. Anthony Bretscher, Linda Nicholson and Volker Vogt for critical discussion and suggestions, Adam Brady for comments on the manuscript. This work is supported by the start

up fund for YM from Weill Institute for Cell and Molecular Biology, Cornell University. The X-ray data were collected at MacChess beamline A1 and F2. CHESS is supported by the NSF & NIH/NIGMS via NSF award DMR-0225180, and the MacCHESS resource is supported by NIH/NCRR award RR-01646.

## Reference:

Bankaitis, V.A., Aitken, J.R., Cleves, A.E. and Dowhan, W. (1990) An essential role for a phospholipid transfer protein in yeast Golgi function. Nature, 347, 561-562.

Barford, D., Das, A.K. and Egloff, M.P. (1998) The structure and mechanism of protein phosphatases: insights into catalysis and regulation. Annu Rev Biophys Biomol Struct, 27, 133-164.

Barford, D., Flint, A.J. and Tonks, N.K. (1994) Crystal structure of human protein tyrosine phosphatase 1B. Science, 263, 1397-1404.

Barton, G.J. (1993) ALSCRIPT: a tool to format multiple sequence alignments. Protein Eng, 6, 37-40.

Begley, M.J., Taylor, G.S., Kim, S.A., Veine, D.M., Dixon, J.E. and Stuckey, J.A. (2003) Crystal structure of a phosphoinositide phosphatase, MTMR2: insights into myotubular myopathy and Charcot-Marie-Tooth syndrome. Mol Cell, 12, 1391-1402.

Blagoveshchenskaya, A., Cheong, F.Y., Rohde, H.M., Glover, G., Knodler, A., Nicolson, T., Boehmelt, G. and Mayinger, P. (2008) Integration of Golgi trafficking and growth factor signaling by the lipid phosphatase SAC1. J Cell Biol, 180, 803-812.

Blagoveshchenskaya, A. and Mayinger, P. (2009) SAC1 lipid phosphatase and growth control of the secretory pathway. Mol Biosyst, 5, 36-42.

Botelho, R.J., Efe, J.A., Teis, D. and Emr, S.D. (2008) Assembly of a Fab1 phosphoinositide kinase signaling complex requires the Fig4 phosphoinositide phosphatase. Mol Biol Cell, 19, 4273-4286.

Brice, S.E., Alford, C.W. and Cowart, L.A. (2009) Modulation of sphingolipid metabolism by the phosphatidylinositol-4-phosphate phosphatase Sac1p through regulation of phosphatidylinositol in Saccharomyces cerevisiae. J Biol Chem, 284, 7588-7596.

Brunger, A.T., Adams, P.D., Clore, G.M., DeLano, W.L., Gros, P., Grosse-Kunstleve, R.W., Jiang, J.S., Kuszewski, J., Nilges, M., Pannu, N.S., Read, R.J., Rice, L.M., Simonson, T. and

Warren, G.L. (1998) Crystallography & NMR system: A new software suite for macromolecular structure determination. Acta Crystallogr D Biol Crystallogr, 54, 905-921.

Cho, W. and Stahelin, R.V. (2005) Membrane-protein interactions in cell signaling and membrane trafficking. Annu Rev Biophys Biomol Struct, 34, 119-151.

Chow, C.Y., Landers, J.E., Bergren, S.K., Sapp, P.C., Grant, A.E., Jones, J.M., Everett, L., Lenk, G.M., McKenna-Yasek, D.M., Weisman, L.S., Figlewicz, D., Brown, R.H. and Meisler, M.H. (2009) Deleterious variants of FIG4, a phosphoinositide phosphatase, in patients with ALS. Am J Hum Genet, 84, 85-88.

Chow, C.Y., Zhang, Y., Dowling, J.J., Jin, N., Adamska, M., Shiga, K., Szigeti, K., Shy, M.E., Li, J., Zhang, X., Lupski, J.R., Weisman, L.S. and Meisler, M.H. (2007) Mutation of FIG4 causes neurodegeneration in the pale tremor mouse and patients with CMT4J. Nature, 448, 68-72.

Cleves, A.E., Novick, P.J. and Bankaitis, V.A. (1989) Mutations in the SAC1 gene suppress defects in yeast Golgi and yeast actin function. J Cell Biol, 109, 2939-2950.

Collaborative Computational Project, N. (1994) The CCP4 suite: programs for protein crystallography. Acta Cryst., D, 760-763.

De Matteis, M.A. and Godi, A. (2004) PI-loting membrane traffic. Nat Cell Biol, 6, 487-492.

Di Paolo, G. and De Camilli, P. (2006) Phosphoinositids in cell regulation and membrane dynamics. Nature.

DiNitto, J.P. and Lambright, D.G. (2006) Membrane and juxtamembrane targeting by PH and PTB domains. Biochim Biophys Acta, 1761, 850-867.

Duex, J.E., Nau, J.J., Kauffman, E.J. and Weisman, L.S. (2006a) Phosphoinositide 5-phosphatase Fig 4p is required for both acute rise and subsequent fall in stress-induced phosphatidylinositol 3,5-bisphosphate levels. Eukaryot Cell, 5, 723-731.

Duex, J.E., Tang, F. and Weisman, L.S. (2006b) The Vac14p-Fig4p complex acts independently of Vac7p and couples PI3,5P2 synthesis and turnover. J Cell Biol, 172, 693-704.

Emsley, P. and Cowtan, K. (2004) Coot: model-building tools for molecular graphics. Acta Crystallogr D Biol Crystallogr, 60, 2126-2132.

Erdman, S., Lin, L., Malczynski, M. and Snyder, M. (1998) Pheromone-regulated genes required for yeast mating differentiation. J Cell Biol, 140, 461-483.

Ferguson, K.M., Lemmon, M.A., Schlessinger, J. and Sigler, P.B. (1994) Crystal structure at 2.2 A resolution of the pleckstrin homology domain from human dynamin. Cell, 79, 199-209.

Ferguson, K.M., Lemmon, M.A., Schlessinger, J. and Sigler, P.B. (1995) Structure of the high

affinity complex of inositol trisphosphate with a phospholipase C pleckstrin homology domain. Cell, 83, 1037-1046.

Foti, M., Audhya, A. and Emr, S.D. (2001) Sac1 lipid phosphatase and Stt4 phosphatidylinositol 4-kinase regulate a pool of phosphatidylinositol 4-phosphate that functions in the control of the actin cytoskeleton and vacuole morphology. Mol Biol Cell, 12, 2396-2411.

Gelb, M.H., Cho, W. and Wilton, D.C. (1999) Interfacial binding of secreted phospholipases A(2): more than electrostatics and a major role for tryptophan. Curr Opin Struct Biol, 9, 428-432.

Guo, S., Stolz, L.E., Lemrow, S.M. and York, J.D. (1999) SAC1-like domains of yeast SAC1, INP52, and INP53 and of human synaptojanin encode polyphosphoinositide phosphatases. J Biol Chem, 274, 12990-12995.

Holm, L. and Sander, C. (1995) Dali: a network tool for protein structure comparison. Trends Biochem Sci, 20, 478-480.

Hughes, W.E., Cooke, F.T. and Parker, P.J. (2000a) Sac phosphatase domain proteins. Biochem J, 350 Pt 2, 337-352.

Hughes, W.E., Pocklington, M.J., Orr, E. and Paddon, C.J. (1999) Mutations in the Saccharomyces cerevisiae gene SAC1 cause multiple drug sensitivity. Yeast, 15, 1111-1124.

Hughes, W.E., Woscholski, R., Cooke, F.T., Patrick, R.S., Dove, S.K., McDonald, N.Q. and Parker, P.J. (2000b) SAC1 encodes a regulated lipid phosphoinositide phosphatase, defects in which can be suppressed by the homologous Inp52p and Inp53p phosphatases. J Biol Chem, 275, 801-808.

Jain, M.K., Rogers, J., Jahagirdar, D.V., Marecek, J.F. and Ramirez, F. (1986) Kinetics of interfacial catalysis by phospholipase A2 in intravesicle scooting mode, and heterofusion of anionic and zwitterionic vesicles. Biochim Biophys Acta, 860, 435-447.

Jeong, D.G., Kim, S.J., Kim, J.H., Son, J.H., Park, M.R., Lim, S.M., Yoon, T.S. and Ryu, S.E. (2005) Trimeric structure of PRL-1 phosphatase reveals an active enzyme conformation and regulation mechanisms. J Mol Biol, 345, 401-413.

Jin, N., Chow, C.Y., Liu, L., Zolov, S.N., Bronson, R., Davisson, M., Petersen, J.L., Zhang, Y., Park, S., Duex, J.E., Goldowitz, D., Meisler, M.H. and Weisman, L.S. (2008) VAC14 nucleates a protein complex essential for the acute interconversion of PI3P and PI(3,5)P(2) in yeast and mouse. Embo J, 27, 3221-3234.

Kearns, B.G., McGee, T.P., Mayinger, P., Gedvilaite, A., Phillips, S.E., Kagiwada, S. and Bankaitis, V.A. (1997) Essential role for diacylglycerol in protein transport from the yeast Golgi complex. Nature, 387, 101-105.

Labarga, A., Valentin, F., Anderson, M. and Lopez, R. (2007) Web services at the European

bioinformatics institute. Nucleic Acids Res, 35, W6-11.

Lee, J.O., Yang, H., Georgescu, M.M., Di Cristofano, A., Maehama, T., Shi, Y., Dixon, J.E., Pandolfi, P. and Pavletich, N.P. (1999) Crystal structure of the PTEN tumor suppressor: implications for its phosphoinositide phosphatase activity and membrane association. Cell, 99, 323-334.

Liu, Y., Boukhelifa, M., Tribble, E. and Bankaitis, V.A. (2009) Functional studies of the mammalian Sac1 phosphoinositide phosphatase. Adv Enzyme Regul, 49, 75-86.

Liu, Y., Boukhelifa, M., Tribble, E., Morin-Kensicki, E., Uetrecht, A., Bear, J.E. and Bankaitis, V.A. (2008) The Sac1 phosphoinositide phosphatase regulates Golgi membrane morphology and mitotic spindle organization in mammals. Mol Biol Cell, 19, 3080-3096.

Matthews, B.W. (1968) Solvent content of protein crystals. J Mol Biol, 33, 491-497.

McGuffin, L.J., Bryson, K. and Jones, D.T. (2000) The PSIPRED protein structure prediction server. Bioinformatics, 16, 404-405.

McRee, D.E. (1999) XtalView/Xfit--A versatile program for manipulating atomic coordinates and electron density. J Struct Biol, 125, 156-165.

Nemoto, Y., Kearns, B.G., Wenk, M.R., Chen, H., Mori, K., Alb, J.G., Jr., De Camilli, P. and Bankaitis, V.A. (2000) Functional characterization of a mammalian Sac1 and mutants exhibiting substrate-specific defects in phosphoinositide phosphatase activity. J Biol Chem, 275, 34293-34305.

Novick, P., Osmond, B.C. and Botstein, D. (1989) Suppressors of yeast actin mutations. Genetics, 121, 659-674.

Odorizzi, G., Babst, M. and Emr, S.D. (1998) Fab1p PtdIns(3)P 5-kinase function essential for protein sorting in the multivesicular body. Cell, 95, 847-858.

Odorizzi, G., Babst, M. and Emr, S.D. (2000) Phosphoinositide signaling and the regulation of membrane trafficking in yeast. Trends Biochem Sci, 25, 229-235.

Otwinowski, Z. and Minor, W. (1997) Processing of X-ray diffraction data collected in oscillation mode. Methods Enzymol., 276, 307-326.

Pape, T. and Schneider, T.R. (2004) HKL2MAP: a graphical user interface for macromolecular phasing with SHELX programs. J. Appl. Cryst., 37, 843-844.

Perrakis, A., Morris, R. and Lamzin, V.S. (1999) Automated protein model building combined with iterative structure refinement. Nat Struct Biol, 6, 458-463.

Puius, Y.A., Zhao, Y., Sullivan, M., Lawrence, D.S., Almo, S.C. and Zhang, Z.Y. (1997)

Identification of a second aryl phosphate-binding site in protein-tyrosine phosphatase 1B: a paradigm for inhibitor design. Proc Natl Acad Sci U S A, 94, 13420-13425.

Rivas, M.P., Kearns, B.G., Xie, Z., Guo, S., Sekar, M.C., Hosaka, K., Kagiwada, S., York, J.D. and Bankaitis, V.A. (1999) Pleiotropic alterations in lipid metabolism in yeast sac1 mutants: relationship to "bypass Sec14p" and inositol auxotrophy. Mol Biol Cell, 10, 2235-2250.

Rohde, H.M., Cheong, F.Y., Konrad, G., Paiha, K., Mayinger, P. and Boehmelt, G. (2003) The human phosphatidylinositol phosphatase SAC1 interacts with the coatomer I complex. J Biol Chem, 278, 52689-52699.

Rudge, S.A., Anderson, D.M. and Emr, S.D. (2004) Vacuole size control: regulation of PtdIns(3,5)P2 levels by the vacuole-associated Vac14-Fig4 complex, a PtdIns(3,5)P2-specific phosphatase. Mol Biol Cell, 15, 24-36.

Sali, A., Webb, B., Madhusudhan, M.S., Shen, M.-Y., Marti-Renom, M.A., Eswar, N., Alber, F., Topf, M., Oliva, B., Fiser, A., Snchez, R., Yerkovich, B., Badretdinov, A., Melo, F., Overington, J.P. and Feyfant, E. (2008) MODELLER. A program for protein structure modeling, version 9v4. University of California: San Francisco, CA,.

Salmeen, A., Andersen, J.N., Myers, M.P., Meng, T.C., Hinks, J.A., Tonks, N.K. and Barford, D. (2003) Redox regulation of protein tyrosine phosphatase 1B involves a sulphenyl-amide intermediate. Nature, 423, 769-773.

Sbrissa, D., Ikonomov, O.C., Fenner, H. and Shisheva, A. (2008) ArPIKfyve homomeric and heteromeric interactions scaffold PIKfyve and Sac3 in a complex to promote PIKfyve activity and functionality. J Mol Biol, 384, 766-779.

Schorr, M., Then, A., Tahirovic, S., Hug, N. and Mayinger, P. (2001) The phosphoinositide phosphatase Sac1p controls trafficking of the yeast Chs3p chitin synthase. Curr Biol, 11, 1421-1426.

Strahl, T. and Thorner, J. (2007) Synthesis and function of membrane phosphoinositides in budding yeast, Saccharomyces cerevisiae. Biochim Biophys Acta, 1771, 353-404.

Stuckey, J.A., Schubert, H.L., Fauman, E.B., Zhang, Z.Y., Dixon, J.E. and Saper, M.A. (1994) Crystal structure of Yersinia protein tyrosine phosphatase at 2.5 A and the complex with tungstate. Nature, 370, 571-575.

Tabernero, L., Aricescu, A.R., Jones, E.Y. and Szedlacsek, S.E. (2008) Protein tyrosine phosphatases: structure-function relationships. Febs J, 275, 867-882.

Tahirovic, S., Schorr, M. and Mayinger, P. (2005) Regulation of intracellular phosphatidylinositol-4-phosphate by the Sac1 lipid phosphatase. Traffic, 6, 116-130.

van Montfort, R.L., Congreve, M., Tisi, D., Carr, R. and Jhoti, H. (2003) Oxidation state of the

active-site cysteine in protein tyrosine phosphatase 1B. Nature, 423, 773-777.

Wei, H.C., Sanny, J., Shu, H., Baillie, D.L., Brill, J.A., Price, J.V. and Harden, N. (2003) The Sac1 lipid phosphatase regulates cell shape change and the JNK cascade during dorsal closure in Drosophila. Curr Biol, 13, 1882-1887.

Whitters, E.A., Cleves, A.E., McGee, T.P., Skinner, H.B. and Bankaitis, V.A. (1993) SAC1p is an integral membrane protein that influences the cellular requirement for phospholipid transfer protein function and inositol in yeast. J Cell Biol, 122, 79-94.

Yang, J., Groen, A., Lemeer, S., Jans, A., Slijper, M., Roe, S.M., den Hertog, J. and Barford, D. (2007) Reversible oxidation of the membrane distal domain of receptor PTPalpha is mediated by a cyclic sulfenamide. Biochemistry, 46, 709-719.